CRYSTALLIZATION BEHAVIOR OF BISPHENOL-A POLYCARBONATE: EFFECTS OF CRYSTALLIZATION TIME, TEMPERATURE, AND MOLAR MASS

by

Seungman Sohn

Dissertation Submitted to the Faculty of the
Virginia Polytechnic Institute and State University
in partial fulfillment of the requirements for the degree of
DOCTOR OF PHILOSOPHY
in
Materials Science and Engineering

Dr. Hervé Marand, Chairman
Dr. Garth L. Wilkes
Dr. Ronald G. Kander
Dr. Richey M. Davis
Dr. William T. Reynolds

April, 2000
Blacksburg, Virginia

Key words: Crystallization, Bisphenol-A polycarbonate, Multiple melting behavior, Secondary crystallization kinetics

CRYSTALLIZATION BEHAVIOR OF BISPHENOL-A POLYCARBONATE: EFFECTS OF CRYSTALLIZATION TIME, TEMPERATURE, AND MOLAR MASS

by

Seungman Sohn

Hervé Marand, Chairman

Materials Science and Engineering

(Abstract)

Crystallization and multiple melting behavior of bisphenol-A polycarbonate (PC) was investigated using differential scanning calorimetry (DSC) for the monitoring of thermal behavior and atomic force microscopy (AFM) for the morphology study. The exceedingly slow crystallization kinetics of PC and the feasibility of obtaining near monodisperse fractions provide distinct advantages for the elucidation of the effects of crystallization time, temperature, and molar mass on crystallization kinetics.

The effects of molar mass on the glass transition temperature (T_g) and heat capacity change at T_g, and the amorphous density of PC were investigated.

Similar to many semicrystalline polymers, PC exhibits a multiple melting behavior upon heating. While for each PC sample, the coexistence of low and high temperature endothermic regions in the DSC heating traces is explained by the melting of populations of crystals with different stabilities, melting-recrystallization-remelting effects are observed only for the lowest molar mass samples.

The effects of crystallization temperature and molar mass distribution on overall crystallization kinetics were studied for some of the fractions, including the commercial PC-28K (M_w = 28,000 g.mol^{-1}) sample. Regarding the kinetics of secondary

crystallization, particular attention was placed on understanding the effects of molar mass, initial degree of crystallinity prior to the secondary crystallization, and secondary crystallization time and temperature. The secondary crystallization of PC follows the same laws discovered in previous studies of PEEK, PET, it-PS and ethylene copolymers, and the results are discussed in the context of a bundle-like secondary crystallization model.

During isothermal annealing of semicrystalline PC-28K around the high melting endotherm, a significant increase of melting temperature along with peak broadening with time was observed. Independently, morphological studies using AFM showed that mean lamellar thickness increases with time during isothermal annealing. These results are discussed in light of isothermal thickening of lamellar crystals.

Lastly, almost 200 DSC melting traces of varying molar mass PC samples thermally treated under various conditions were analyzed to calculate crystallinity (X_c), rigid fraction (RF), and rigid amorphous fraction (RAF). The correlation between RAF *vs* X_c, T_g, and T_g broadening are discussed.

To

my lovely family

Yeunjung Doe, Hyuckjoon Sohn, and

my parents

Nanchan Sohn, Guinam Jung, Junhoei Doe, Myungsuk Yang

Without whose sacrifices none of this would have been possible

Acknowledgements

My first appreciation must go to my great advisor Prof. Hervé Marand, who showed me an incessant love and enthusiasm about polymer science, and who also showed me a clear and satisfactory way of being a good scientist. He is my friend, teacher, and further, the learning from him will be a corner stone in my future career. Without his guidance, I never would have seen the beauty of polymer science.

I wish to acknowledge the guidance, helpful discussions for my work as provided during the last five years by:

- Prof. Garth L. Wilkes, who is a great teacher with broad knowledge and enthusiasm, and who knows how to help students.
- Prof. William T. Reynolds, who is extremely generous and thoughtful.
- Prof. Ronald G. Kander, Prof. Richey M. Davis, who gave me helpful suggestions for my research.
- Dr. Azar Alizadeh, with whom I spent numerous nights in the lab. Her critical discussions were essential ingredient in the completion of this work.
- Prof. Darrell H. Iler and Mr. L. C. Shank for their help in preparation of polycarbonate fractions.
- Dr. Qing Ji for more than 100 runs of GPC analysis and helpful discussions.
- The fellow students in Prof. Marand's group, old and new, especially Mr. Sean M. Christian for his good friendship.
- The fellow students in Prof. Ward's and Prof. McGrath's labs, who helped me in several ways for my experiments.

Special thanks are due to my senior alumnus Dr. Ojin Kwon, who encouraged me when I was in difficulty. His scientific knowledge and enthusiasm towards science were good justifications why I wanted to be a scientist. Dr. Taigyu Park also deserves my appreciation for his critical discussions and timely help.

Lastly, the never-ending sacrifice of my wife, Yeunjung, will be the heart of my appreciation for the last five years of my research.

Table of Contents

List of Figures

List of Tables

Chapter 1

Introduction

Polymers are widely used in many important everyday applications such as clothing, household appliances, automotive products, and even aerospace. Recently, some specialty polymers expanded their realms into the electronics industry for packaging, dielectric, and display purposes. Various kinds of thermoplastic polymers, such as poly(aryl ether ether ketone) (PEEK) and poly(phenylene sulfide) (PPS), have been introduced in the last two decades. These thermoplastic materials have been the subjects of extensive studies due to their potential use as high performance engineering plastics in many applications, such as a matrix for advanced composite material.

One of the most important features of these various polymers is that they are always used as semicrystalline materials. Therefore, crystallinity, along with polymer morphology, plays an important role in determining their critical material properties such as modulus, toughness, permeability, and chemical resistance. Broadly speaking, above T_g, with a crystallinity increase, modulus tends to increase at the expense of toughness. Similarly, crystallinity would enhance chemical resistance and decrease permeability.

A crystallization process is largely divided into two regimes: primary and secondary[1]. Primary crystallization can be defined as the succession of primary nucleation of a crystal phase and growth of three-dimensional semicrystalline structures (such as spherulites and hedrites, etc.) from an unconstrained metastable melt. The end of primary crystallization can be associated with the impingement of the three-dimensional structures. Secondary crystallization is identified with phenomenon leading to an increase of crystallinity after the completion of the primary crystallization stage.

Although the extent of secondary crystallization may, in certain instances, be relatively small, its impacts on fundamental material properties, such as glass transition temperature and shear or tensile modulus, are thought to be profound. As secondary crystallization proceeds, it often increases the glass transition temperature of a given polymer, and it enhances shear or tensile modulus at the expense of toughness. A possible reason is that secondary crystallization imposes conformational constraints on the amorphous fraction between lamellar structures[2]. These constraints will increase as secondary crystallization proceeds. In other words, material properties will change as a function of time. Therefore, an understanding of the kinetics of secondary crystallization is necessary to predict the evolution of material's properties. This information will be invaluable in designing polymeric materials, especially for long time use.

While the kinetics of primary crystallization is relatively well documented for many polymers, secondary crystallization kinetics is not. This is because the increase of crystallinity in this stage is significantly smaller than in the primary crystallization stage, this secondary crystallization phenomenon was thought to be relatively unimportant and thus has not been seriously investigated. Again, the author argue that the study of secondary crystallization kinetics is important because time-dependent material property changes are not governed by the primary crystallization, but by secondary crystallization processes.

The main goal of this study is to further the understanding of secondary crystallization. For this specific purpose, bisphenol-A polycarbonate (PC) was chosen as a model system. The distinctive advantage of PC lies in its extremely slow crystallization kinetics. This material, therefore, was a good candidate to follow the various steps of the

crystallization process whether primary or secondary, and further, it allowed to examine each stage, independently. In Table 1.1, the chemical structure and some important physical parameters of PC are summarized.

Overview of this study:

Chapter 2 is devoted to a review of a few subjects that are relevant to this study:

1) The two-phase and three-phase models
2) Secondary crystallization
3) Multiple melting behavior
4) Previous studies of crystallization of PC

Chapter 3 describes materials, including sample preparation and characterization, and experiments. In the section on materials, sample preparation and characterization will be offered. Sample preparation includes fractionation (carried out by Dr. Iler and Mr. Shank at Eastern Mennonite University, Harrisonburg, VA) and purification processes followed by GPC analysis (carried out by Dr. Ji, Virginia Tech, Blacksburg, VA). Amorphous samples have also been characterized in terms of glass transition temperature (T_g), (isobaric) heat capacity change at T_g (ΔC_P at T_g) and room temperature amorphous density (ρ_a). The experimental section describes all the experimental techniques utilized in this study.

Chapter 4 focuses on the elucidation of the origin of multiple melting behavior observed from the DSC heating traces of semicrystalline PC. The feasibility of reorganization by melting-recrystallization-remelting will be thoroughly examined by heating rate studies performed on PC crystallized under various conditions.

In Chapter 5, primary and secondary crystallization kinetics of PC are presented. The effects of crystallization temperature, time, and molar mass on the kinetics of primary and secondary crystallization are offered. Some of the results from the kinetics of secondary crystallization are explained in the light of a newly proposed secondary crystallization model. The study of the crystallization time and temperature dependencies of the melting behavior suggests the existence of a crossover temperature, T_{co}, separating two different secondary crystallization regimes.

Chapter 6 provides some evidences, from calorimetry, suggesting the existence of isothermal lamellar thickening, above the cross over temperature discussed in Chapter 5. To further support the existence of isothermal lamellar thickening in PC, AFM is employed to determine the mean lamellar thickness and its distribution as a function of annealing time. These results are analyzed using the Gibbs-Thomson equation, allowing to propose values for the magnitude of the equilibrium melting point (T_m^o) and the interfacial surface free energy (σ_e).

In Chapter 7, the existence of a rigid amorphous fraction (RAF) in semicrystalline PC is presented. To evaluate crystallinity more precisely, the temperature dependence of the theoretical heat of fusion and surface enthalpic contributions were accounted for. It is shown that the calculated RAF is associated with both the T_g broadening and T_g increase during secondary crystallization.

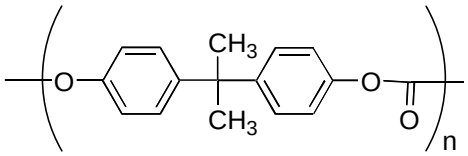

IUPAC Nomenclature:

Poly (oxycarbonyloxy-1,4 phenylene isopropylidene-1,4 phenylene)

Molecular weight of repeating unit [g/mol]	254.1
Glass transition temperature[3], (at 10°C/min, M_w =37,000 g.mol^{-1})	145 °C
Apparent melting temperature	220-230 °C
Equilibrium melting temperature[4,12]	310-327°C
Crystal unit cell[5]	Monoclinic
Space group[6]	D_2 3
Room temperature unit cell dimensions[5]	
a	~ 12.3 Å
b	~ 10.1 Å
c	~ 20.8 Å
γ	84°
Density [g/cm^3]	
Amorphous[5,7-10]	1.196-1.200
Crystal[5]	1.3022
Heat of fusion, ΔH_m^o [J/g][9,11]	109.6 – 142.3

Table 1.1 Chemical structure and some physical properties of bisphenol-A polycarbonate (PC).

References

1. J. M. Schultz, *Polymer Materials Science*, **1974**, Prentice-Hall, Inc., New Jersey.
2. H. Marand, A. Alizadeh, R. Farmer, R. Desai, V. Velikov, *Macromolecules* in press; *Bull. Am. Phys. Soc*., **1999**, *44(1)*, 608.
3. Polymer Handbook 3rd edition, VI-258.
4. R. Legras, J. P. Mercier, J. Polym Sci., Polym.Phys., **1977**, *15*, 1283.
5. R. Bonart, Makromolekular Chem., **1966**, *92*, 149.
6. Hermann Schnell, "Chemistry and Physics of Polycarbonates", 1964, John Wiley & Sons, Inc.
7. B. Falkai, W. Rellensmann, Makromolekular Chem., **1964**, *75*, 112.
8. K.-H. Hellwege, J. Hennig, W. Knappe, Kolloid-Zeitschrift und Zeitschrift für Polymere, 1962, 186, 29.
9. J.P. Mercier, R. Legras, J. Polym Sci., Polym.Lett., **1970**, *8*, 645.
10. G. E. Wissler, B. Crist. Jr, J. Polym Sci., Polym.Phys., **1980**, *18*, 1257.
11. L. D. Jones, F. E. Karasz, J. Polym Sci., Polym.Lett., **1966**, *4*, 803.
12. J. M. Jonza, R. S. Porter, *J. Polym. Sci. Polym. Phys*., **1986**, *24*, 2459.

Chapter 2

Review

The long chain nature of macromolecules distinguishes them from small molecular substances. It is because of their long chain nature that polymers can not crystallize completely. Crystallizable polymers can then exist in two states: a liquid amorphous state above the melting point and a semicrystalline state at lower temperatures. In the amorphous state, polymer chains are randomly arranged and the overall conformational state of the individual chain is in random coil state, although locally there could be some degree of order. In the crystalline state, all chains have the same conformation, which favors packing into an ordered structure. As indicated above, unlike small molecular solids such as metals, polymers do not crystallize completely. That is to say, their morphology is controlled by kinetics not by thermodynamics. Therefore, the morphological structure of any semicrystalline polymer must be represented by both an amorphous and crystalline phases. In the first section of this chapter, a description of semicrystalline polymer morphology will be offered in the context of conventional two-phase and the three-phase models.

Another important consequence of the semicrystalline nature of polymers is that under proper conditions, virtually all semicrystalline polymers may undergo a secondary crystallization process. This can be readily understood from the viewpoint that thermodynamically semicrystalline polymers are in a metastable state; therefore, under proper conditions such as in the presence of enough thermal energy, further crystallization can occur. This phenomenon, along with several proposed models, will be discussed in the second section of this chapter.

Secondary crystallization process is often related to a multiple melting behavior observable by calorimetry. Despite the numerous studies of this subject, controversies still exist regarding the origin of the multiple melting behavior. In the third section of this chapter, general aspects and competing mechanisms for multiple melting behavior will be considered.

The last section will be devoted to an overview of crystallization and melting behavior of bisphenol-A polycarbonate (PC). This will further explain some unique features of PC crystallization such as its extremely slow crystallization kinetics. The multiple melting behavior of semicrystalline PC will be also discussed.

2.1 The Two-phase and Three-phase Models

In this section, a brief review of the two-phase and the three-phase models will be presented. In the context of the two-phase model, well-defined amorphous and crystalline phases will be assumed; for the three-phase model, besides these two phases, an interphase will be introduced. This interphase can be described as an intermediate phase similar to either the amorphous (rigid amorphous phase) or crystalline (para-crystalline phase) phases.

2.1.1 *The Two-phase Model*

Historically, semicrystalline polymer morphology has been described by a simple two-phase model consisting of amorphous and crystalline phases. In early times, the "fringed-micelle" model[1] fully adopted these two clear phases. The essential features of this model are schematically presented in Figure 2.1. The main characteristics of this "ideal" model lie in two folds. First, this model does not intrinsically consider the existence of interphase or transition zones, because immediately outside of the ordered

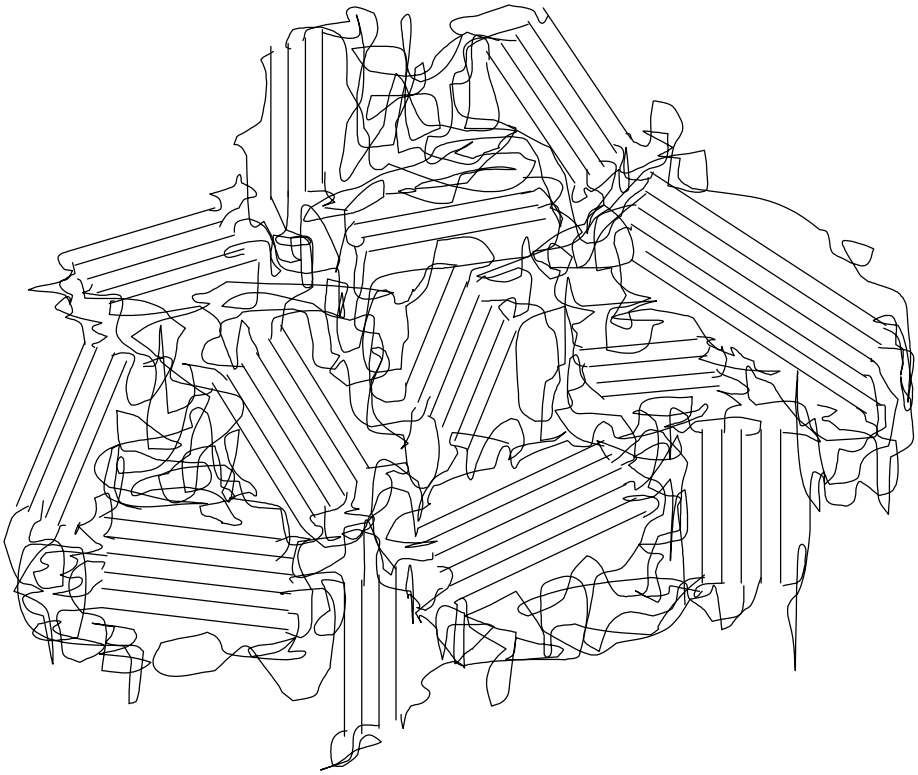

Figure 2.1 The fringed-micelle model for the morphology of semicrystalline polymers (from reference 1).

crystalline phase is a randomly oriented amorphous phase and vice versa. Without sacrificing any main features of this model, one can describe the transition zones as infinitesimally thin; therefore, as originally proposed, only two sharp phases: disordered amorphous and ordered crystalline phases. Second, theses two distinguished phases allow the assumption that any partial properties associated with each phase can be represented by the fraction of the equilibrium properties of each phase. This statement is significant in material property determination. One good example is that, in the calculation of crystallinity from calorimetry study, if the above premise is truly acceptable, the answer will be given as the ratio of measured heat of fusion to equilibrium heat of fusion (i.e., $X_c = \Delta H_m^{exp}/\Delta H_m^o$). This relationship is widely used, and in most circumstances and within a certain degree of uncertainty, this equation is fairly acceptable*. This fringed micelle model has been successfully applied to describe the morphology and structure-property relationship of rubber, cellulose, and polymers with low crystallinity[2]. For example, in the explanation of the observed increase of strength of elastomer with crystallinity, this model may suggest that the pinning effect of embedded crystalline phase will increase the strength; if so, as crystallinity increases so does the modulus.

2.1.2 *The Three-phase Model*

---

* Despite the simplicity of this equation, an accurate determination of ΔH_m^o is not an easy task. This is mainly because an extrapolation is mandatory regardless of the type of methods to set the proper value of ΔH_m^o. This extrapolation could be subject to large uncertainty, especially when crystallinity is low. It also needs to be noted that for more accurate crystallinity determination, the surface enthalpy term (ΔH_m^s) and temperature corrections for heat of fusion must be included. This will be especially important when the crystals are not all lamellar-type crystals and when the apparent melting temperature is far below the equilibrium melting temperature. This issue will be further discussed in Chapter 7.

Since the discovery of the chain folding nature of semicrystalline polymers, the validity of the two-phase model has often been challenged by more complicated, yet more realistic, models[3]. Figure 2.2 illustrates, some of the models assuming specific description of the crystal/liquid interphase. These various models have important features. First, chain folding is required to form three-dimensional crystals; therefore, the surface property, such as surface energy in the basal plane (σ_e) where chain folding takes place will be different from that in lateral plane (σ_s). Largely speaking, σ_e is in the range of 40 to 100 mJ/m^2, and σ_s is in the vicinity of 5 to 20 mJ/m^2. Second, the existence of various types of chain folds such as tight folds (adjacent reentry, (a)), loose loops (non-adjacent reentry, (b)), tie molecules and free ends (chain cilia, (b)) will give rise to a transition zone, or an interphase between lamellar crystals and disordered free melt. The formation of an interphase is a clear deviation from the simple two-phase model, in which the physical nature of the interphase is not questioned because it is assumed to be infinitesimally thin.

Numerous experimental observations suggested the existence of interphase:

In calorimetry study, the lower intensity of relaxation strength at T_g (ΔC_p at T_g) even after considering the effect of crystallinity, e.g., poly(oxymethylene) (POM)[4], polyethylene (PE)[5], isotactic polypropylene (it-PP)[6], poly(caprolactone)[7], isotactic polystyrene (it-PS)[8], poly(butylene terephthalate) (PBT)[9], poly(ethylene terephthalate) (PET)[7,10], poly(phenylene sulfide) (PPS)[11,12], poly(ether ether ketone) (PEEK)[13], and thermoplastic polyimide (TPI)[14];

In dielectric measurement, the unexpected decrease of α-relaxation intensity in the presence of crystals, e.g., TPI[14], PEEK[17];

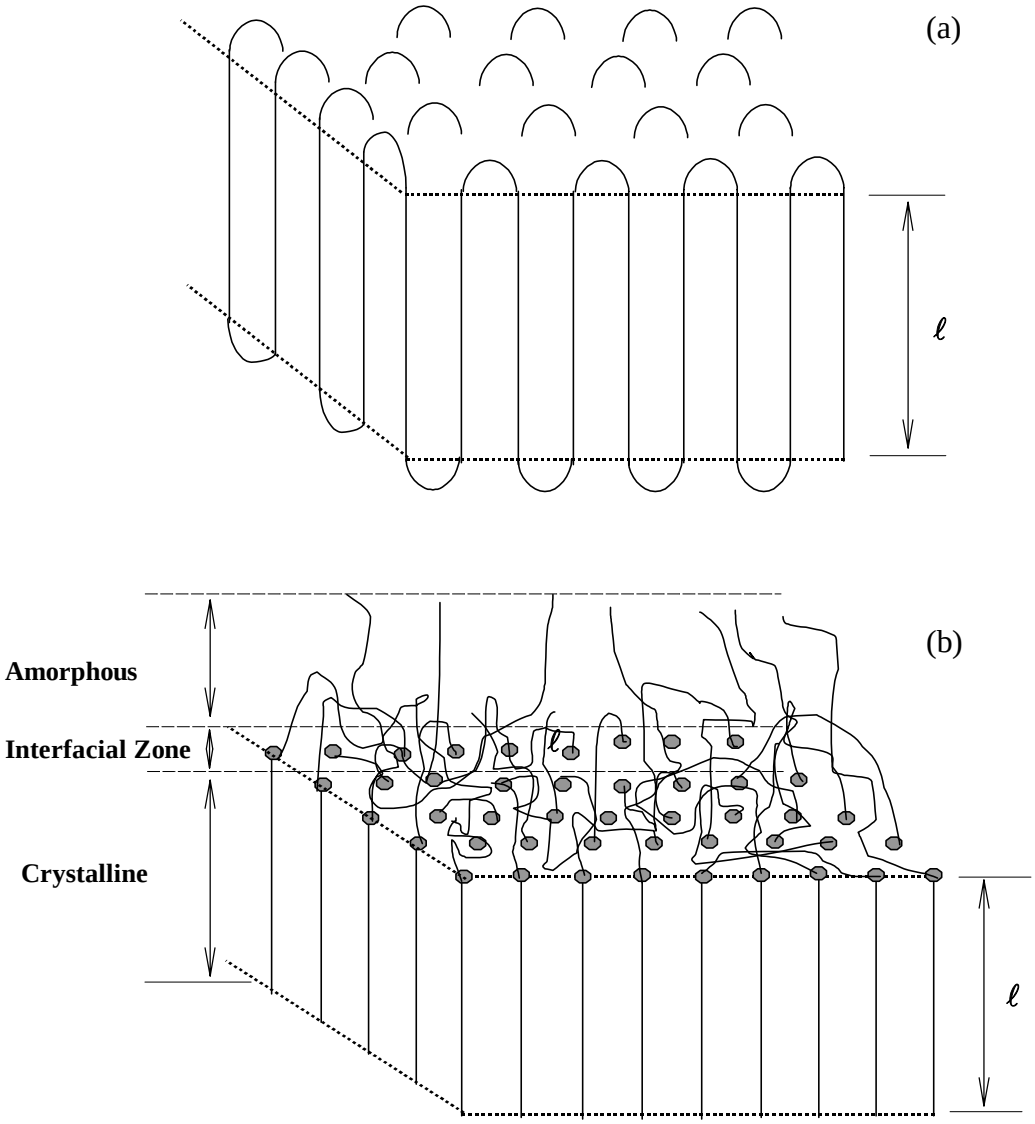

Figure 2.2 Two typical models considering the nature of chain folding: (a) regular folds (adjacent reentry); (b) irregular folds (non-adjacent reentry) (from reference 3).

In dynamic mechanical analysis, the broadening and shifting of T_g in semicrystalline polymers, e.g., TPI[15], Bisphenol-A polycarbonate (PC)[18];

In SAXS study, direct measurement of the interphase thickness, e.g., PPS[11], TPI[14].

Again, all of these diverse and independent techniques unanimously agree on the existence of the interphase. However, despite these numerous observations suggesting the presence of interphase, fundamental questions regarding its physical nature remain open. In the following review of this section, two types of interphase will be discussed: 1) a rigid amorphous phase that assumes this interphase is more akin to the amorphous phase, and 2) para-crystalline phase that treats the interphase as pseudo-crystalline phase. Based on some experimental observations, the nature of interphase will be discussed.

2.1.2.1 *Rigid Amorphous Phase*

All amorphous polymers are in a single equilibrium phase above T_g, as are the semicrystalline polymers above T_m. These completely mobile chains will be gradually hindered in their motions by a decrease in temperature; upon reaching T_g, all the chains become virtually frozen, exhibiting very restricted local motions such as bond rotation. By several experimental methods, such as calorimetry and volume dilatometry, this glass transition behavior can be accurately monitored. From calorimetry, for instance, T_g is often defined as the inflection point of the heat capacity step. Another important parameter characterizing the amorphous state is heat capacity change at T_g *per se*. In principle, the *change in heat capacity at T_g (ΔC_p at T_g) must reveal the relaxation strength of all the amorphous chains undergoing glass transition*. Therefore, the intensity of ΔC_p step, or the relaxation strength at T_g for semicrystalline polymers, will be diminished because the fraction of amorphous chains participating in glass transition has

been reduced. Under the strict application of the two-phase model, the heat capacity change at T_g can be used to determine the crystallinity of a given semicrystalline system through a simple relationship, if the ΔC_p associated with the fully amorphous state can be measured:

$$X_c = 1 - f_{maf} = 1 - \Delta C_p^{sc} / \Delta C_p^{am} \qquad [2.1]$$

Where X_c is crystallinity, f_{maf} is a fraction of mobile amorphous phase, and ΔC_p^{sc} and ΔC_p^{am} are the heat capacity changes at T_g in the semicrystalline and completely amorphous polymers, respectively. Equation (2.1) assumes that all the amorphous polymer chains relax at T_g and that polymer chains in the crystalline phase do not.

In reality, many authors, including Wunderlich *et al.*[4,6,7,9,10,12,13] and Cebe *et al.*[11,14], often observed that the right side of equation (2.1) is greater than the measured crystallinity either from calorimetry study or from other independent methods such as WAXS. These results strongly suggest that in the case of semicrystalline polymers, *not all the amorphous chains relax at the normal glass transition temperature*. Based on this observation, Wunderlich *et al.*[6,19,20] introduced the concept of *rigid amorphous fraction* (RAF), which is the fraction of amorphous chains that does not relax at the normal glass transition temperature. Accordingly, equation (2.1) should be reformulated as follows.

$$f_r = 1 - \Delta C_p^{sc} / \Delta C_p^{am} \qquad [2.2]$$

$$f_r = X_c + f_{raf} \qquad [2.3]$$

Where f_r is the total rigid fraction, the summation of crystallinity (X_c) and rigid amorphous fraction (f_{raf}).

Equations (2.2) and (2.3) clearly demonstrate that the existence of a RAF will lead to the inequality of equation (2.1). More importantly, the inapplicability of equation (2.1) is a clear deviation of a simple two-phase model, since the conventional two-phase model strictly assumes two distinctive phases, not the third phase that does not follow the characteristic behavior of either the amorphous or the crystalline phase. The existence of RAF was originally proposed based on calorimetric measurement, yet other methods, such as dielectric measurement, DMA, and SAXS, pointed out similar results (for proper references, see above).

The introduction of a RAF helped significantly, at least conceptually, in the development of the three-phase model composed of mobile amorphous (liquid-like), rigid amorphous (non-liquid like), and crystalline phases. Although the existence of RAF (also called non-liquid like amorphous phase) has been suggested by various techniques, some questions regarding its fundamental nature are still open: the location of RAF, difference between RAF and mobile amorphous, and the description of the relaxation behavior of RAF.

Regarding the first question, at least three "geographical" locations could be assigned. They are 1) the interspherulitic amorphous region, where non-crystallized chains may be accumulated after spherulites impingement; 2) interlamellar stacks (liquid pocket zone); and 3) interlamellar amorphous layer. Among these possibilities, the last two locations have recently been proposed to be the most probable. Sauer and Hsiao[27] calculated the total rigid fraction (RF) from SAXS measurements, assuming that the RAF

formed in the interlamellar amorphous layer *does not* contribute to the glass transition, and that the rigid amorphous between the lamellar stacks will increase and broaden normal T_g. They showed that, based on these two hypotheses, the measured RAF value from SAXS is close to the value from DSC. Recently, Srinivas and Wilkes[15], based upon the observed decrease of lamellar thickness with time, used the "lamellar insertion model" for the mechanism of secondary crystallization, in which thinner lamellae form in the region of lamellar stacks. These authors also adopted the assumption that the amorphous fraction in the interlamellar layer may not contribute to T_g due to the thinness of amorphous layer. This "dual lamellar thickness" model, originally proposed by Keller[21] and later by Bassett *et al*.[22] as a plausible mechanism of multiple melting behavior often observed for semicrystalline materials, intrinsically assumes the development of rigid fraction in the region of interlamellar stacks and interlamellar amorphous layer. Various secondary crystallization models will be further considered in the next section. Cebe *et al*. provided evidence suggesting that RAF develops in the amorphous layer, which could be either the interlamellar region or the interlamellar stacks, from various techniques such as DSC[11,14,23], MDSC[23,24], dielectric[16,17], DMA[16] and SAXS[11,14,23]. These studies of RAF suggest that interlamellar stacks and/or interlamellar amorphous layer could be the possible locations of rigid amorphous fraction; however, their results do not rule out the possibility that the interspherulitic amorphous zone may contribute to the formation of RAF.

The next question is how the properties of RAF differ from those of the pure amorphous phase. The presence of crystals will constrain the neighboring amorphous phase and may prevent it from relaxing at the normal T_g. This constrained amorphous

interphase would be composed of chain cilia, tight or loose loops, which may or may not have the same average chain conformation as mobile amorphous since they have a constrained conformation[70]. Intuitively speaking, this interphase will have an intermediate chain conformation somewhere between well-ordered crystals and that of a completely disordered amorphous. These intermediate chain conformation would be reflected in the density of the RAF (ρ_{raf}); accordingly, if measured properly, the expected RAF density would be somewhere between the crystal density (ρ_c) and amorphous density (ρ_a). Cebe *et al.*[11] calculated ρ_{raf} of PPS crystallized from the glassy and melt by the combination of DSC and WAXS techniques. In addition, from SAXS, under the assumption of a well-defined one dimensional step-wise electron density distribution along a direction normal to the lamellar stacks, they estimated the thickness of lamellae, amorphous and rigid amorphous phases. From this study, they concluded that ρ_{raf} being equal to 1.325 g/cc is very close to the pure amorphous density (ρ_a = 1.3195 g/cc) but considerably far from the density of the crystal (ρ_c = 1.430 g/cc). The thickness of the RAF layer is reported to be approximately 40Å, and the mobile amorphous layer is *ca*. 30 -50Å. It also needs to be noted that in case of PPS, Cebe *et al.*[11,23] consistently reported a very high value for RAF bigger than 0.4 in case of cold crystallization, and this is, compared with PEEK[17] (0.24-0.32) or TPI[17] (0.10-0.15), the largest value ever reported.

The measured density of RAF qualitatively agrees with the prediction that it would be between ρ_a and ρ_c, and more importantly, that the value is quite close to the amorphous density. This result may indicate that within a limited uncertainty, conventional two-phase model may suffice at least from the standpoint of density variation, although for an accurate description of semicrystalline polymer morphology

the three-phase model will be necessary. Based upon these observations, the RAF can be envisaged as *a constrained amorphous phase existing between the crystals exhibiting slightly higher macroscopic density compared with mobile amorphous phase.*

Lastly, the relaxation behavior of the RAF will be considered. One of the important consequences of the existence of the RAF is the upward shift and broadening of T_g. This is mainly because, as described earlier, the constrained amorphous will not completely relax at the normal T_g. Several experimental observations have been made showing the T_g increase and broadening upon crystallization in various polymers[9,11-17,23-26]. Equations (2.2) and (2.3) allow the quantitative determination of the amount of rigid fraction, yet it does not consider the relaxation behavior itself. For this, it is necessary to know the characteristic relaxation time and its distribution in RAF, which is, however, substantially complicated since a rigid amorphous phase may relax in the whole temperature range between T_g and T_m[28-30]. To simplify this problem of broad overlap, Sauer *et al.*[27] and Srinivas *et al.*[15] formed the hypothesis that RAF in the interlamellar region does not contribute to T_g shift, but the RAF residing in the interlamellar stacks does (see above). The premise of this critical hypothesis lies in the relative thinness (~ 50Å) of the observed interlamellar amorphous layer thickness from SAXS measurement in many semiflexible polymers[14,27,30-33], compared with the gap between the interlamellar stacks[27] (300 –800Å). However, Cebe *et al.*[11] reported that in the case of PPS exhibiting the largest RAF ever reported, the interphase thickness is about 40Å. Based on this result, one can postulate that other semicrystalline polymers such as PET, PEEK and TPI will have a thinner interphase than PPS since these polymers are known to have lower levels of RAF than PPS. Actually, Cebe *et al.*[14] reported 20±5Å of interphase thickness

for TPI. These studies indicate that the above hypothesis– RAF in the interlamellar region does not contribute to T_g– may not reflect the true nature of RAF since the interphase thickness seems thinner than the entire interlamellar amorphous layer thickness. Mobile amorphous chains remaining in the interlamellar amorphous layer may relax at normal T_g. To elucidate the precise nature of the RAF, especially the "retarded" relaxation behavior, fundamental research is needed.

2.1.2.2 *Pseudo-Crystalline Phase*

Until now, the interphase between crystals was understood in light of the rigid amorphous phase, which can be depicted as a less mobile amorphous phase due to the constraints imposed by surrounding crystals. This type of approach is based on the hypothesis that the nature of the interphase is akin to an amorphous phase rather than a crystalline phase. Supporting this premise is the observation that RAF density is noticeably close to that of amorphous[11] (see above).

However, recently it has been claimed that the nature of interphase is closer to the crystalline phase based on TMDSC, DMA, and TMA measurements[34]. For example, Petermann *et al*.[34] used this "pseudo-crystalline" or "para-crystalline" concept to interpret the low endotherm in multiple melting behavior in PET. Again, this concept is basically the same as the RAF in the sense of introducing the existence of an interphase, yet it treats the interphase closer to crystalline phase. As with RAF, various questions regarding the para-crystalline phase remain unanswered.

In summary, despite the simplicity and usefulness of the conventional two-phase model, the more precise nature of semicrystalline polymer morphology may be better understood in the context of the three-phase model consisting of crystalline, free melt,

and interphase. From various techniques, including but not limited to DSC, SAXS, dielectric and thermo-mechanical measurements, this interphase has been interpreted as a rigid amorphous phase that does not relax at the normal glass transition but at higher temperatures due to the constraints imposed by surrounding crystals. While the quantity of RAF can be readily determined from the known crystallinity and heat capacity change at T_g, its physical nature, such as its exact relaxation behavior, is far from being completely understood. As an alternative for the explanation of interphase, the concept of pseudo-crystalline phase has recently been introduced.

2.2 Secondary Crystallization

2.2.1 *Overall Crystallization Kinetics*

Largely speaking, crystallization is a type of phase transformation, in which a thermodynamic driving force results from the decrease of Gibbs free energy by formation of the more stable crystalline phase. In the case of polymer crystallization, complete transformation, thus the achievement of 100% crystallinity, is seldom possible for kinetic reasons. The overall isothermal transformation kinetics, initially formulated by Göler *et al.*[35], can be effectively described by the Avrami theory[38], which was originally formulated for metals. Later this was modified by Evans[36] and Morgan[37] for different growth geometry. The Avrami equation relates the fraction or amount of *uncrystallized material* (θ) that persists in the system after some time t at the crystallization temperature to its growth rate parameter *k* and the nucleation parameter *n*.

$$\theta = \exp(-k \cdot t^n) \qquad [2.4]$$

The overall transformation rate *k* embodies both nucleation and growth rates, assumed by Avrami to take place under *isovolume* conditions, where a change from amorphous to a fully crystallized state occurs. The equation was further modified by Mandelkern[39] to include some aspects of incomplete crystallization encountered in polymer crystallization. It is important to remember that the idea of a *distinct phase transformation from amorphous to crystalline* is implicit in this model wherein the value of the *n* exponent is an integer generally varying from 2 to 4 depending on the geometry, dimensionality of the growth process, and mode of nucleation. For example, if *n* is 4, growth is three-dimensional spherulitic and occurs from nucleated centers created sporadically in location and time (i.e., homogeneous or thermal nucleation). For $n = 3$ nucleation is predetermined in time (heterogeneous or athermal nucleation) and the form of growth of spherulites.

In polymer crystallization, however, a non-integral value of *n* is often encountered because of the complexity of the phase transformation. These complexities are, to name a few, volume shrinkage upon crystallization, variable crystallinity within the spherulite, and possible mixing of thermal and athermal nucleation.

Equation (2.4) can be rewritten in terms of crystallinity (X_c), which is often determined from calorimetry or volume dilatometry.

$$\theta = 1 - X_c(t)/X_c^{\infty} = \exp(-k \cdot t^n)$$

or
$$X_c(t)/X_c^{\infty} = 1 - \exp(-k \cdot t^n) \qquad [2.5]$$

Where $X_c(t)$ is a crystallinity at a given time and temperature, and X_c^{∞} represents the maximum crystallinity for a given crystallization temperature.

After taking a double logarithm on both sides and proper manipulation, equation (2.5) can be linearized to give the exponent *n* and the growth parameter *k* from the slope and calculated intercept, respectively.

$$\ln[-\ln(1-X_c(t))] = \ln k + n\ln t \qquad [2.6]$$

Experimentally, it has long been known that in polymer crystallization, equation (2.6) is a good approximation up to a certain period of time, yet at longer times negative deviations from Avrami behavior is observed. A typical behavior is illustrated in Figure 2.3, which presents the double logarithmic plot of crystallinity as a function of crystallization time measured from dilatometry and calorimetry for polyethylene fraction (M_w = 85,000 g/mol), crystallized from the melt at 127.5^oC[40]. While the initial part of the plots is indeed linear, being the slope (*n*) equal to 2.5, after a certain period of time (40 to 50 minutes) the slope of the line starts to decrease to approximately 0.5.

This type of observation for PE and other polymers has led to the formal breakup of the crystallization process into two processes: *primary* and *secondary*. As noted earlier, the primary crystallization kinetics can be dealt with using the Avrami equation, while the secondary crystallization cannot. Although often, primary and secondary crystallization overlap, the secondary crystallization process is generally characterized as a slow process to complete the crystallization. Once again, it needs to be underscored that the time scale in Figure 2.3 is in logarithm; therefore, the increase of crystallinity

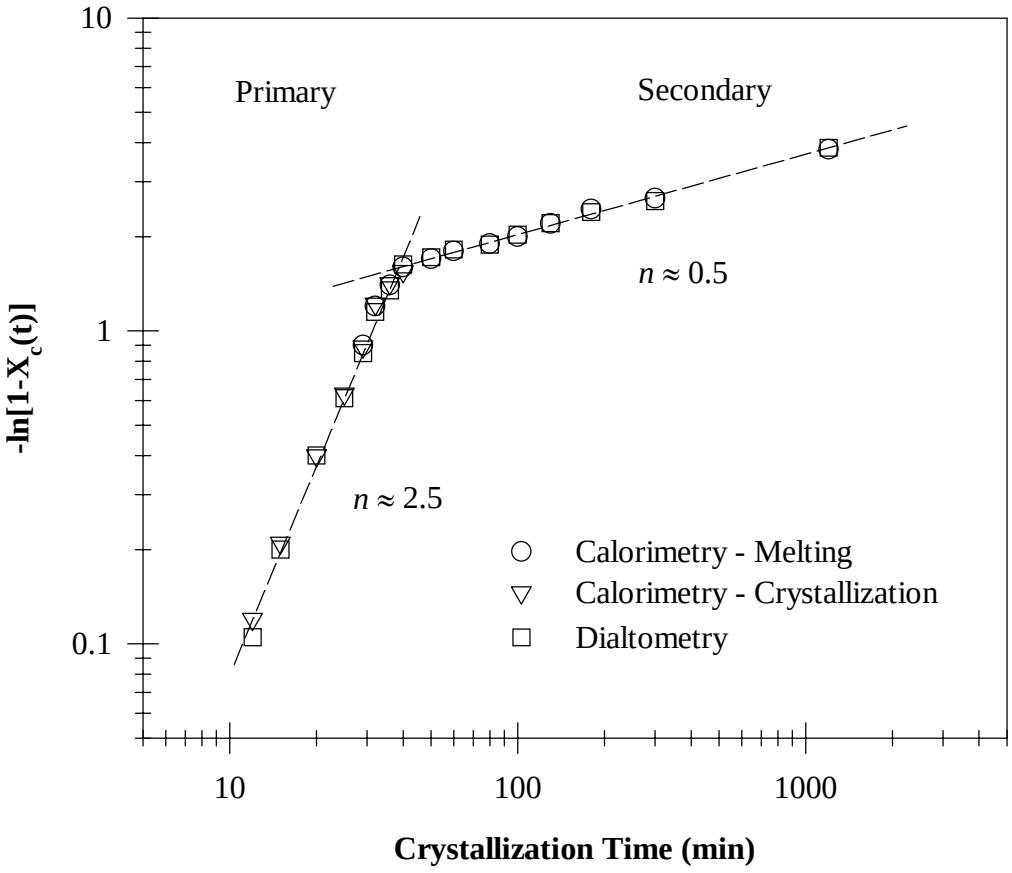

Figure 2.3 A typical example of primary and secondary crystallization in polyethylene. Sample has been crystallized at 127.5^{o}C from DSC and dilatometry (data from reference 40). Y-axis has been expressed in terms of negative logarithm of residual amorphous fraction upon crystallization so that the slope in this figure represents the Avrami exponent, *n*, (see equation 2.6 in the text). In this particular case, *n* for the primary and the secondary crystallization is close to 2.5 and 0.5, respectively.

during the secondary crystallization stage is substantially smaller and slower than during the primary crystallization.

2.2.2 *Secondary Crystallization Models*

In the literature, the long-time evolution of crystallinity through the secondary crystallization stage has often been associated with the lamellar thickening mechanism[41-43]. This conclusion has been reached by studying the effect of annealing on relatively high crystallinity linear PE. Fischer and Schmidt have reported, from SAXS experiments, that upon annealing, the long period of single crystals of linear PE linearly increases with the logarithm of annealing time[44,45]. Some other studies also showed similar log-time kinetics[46-49]. It is important to note that all of the studies quoted above have been more or less limited in scope, devoted to the annealing effects and lamellar thickening above α_c relaxation temperature of PE under relatively low undercooling, or even upon direct crystallization from the melt.

In polymers with medium to low levels of crystallinity, the effects of long-time annealing on crystallinity, morphology, and properties are far less understood, which could be due in part to the high number of polymers and a wider range of methodologies that can be applied. While these factors should be beneficial, the interpretation of results from different techniques or a combination of techniques can lead to conflicting conclusions. For instance, in contrast to PE[41-49] or it-PP[50-52], poly(ethylene terephthalate) (PET), whose T_g is above room temperature, has been studied over the entire range from T_g to T_m. Various mechanisms for the long-time annealing effect on the crystal structure and morphology have been suggested: lamellar thickening[53], evolution of a new population of lamellae[54], combination of thickening and recrystallization[53], and crystal

perfection[55,57,58]. The thermal transitions and morphological changes observed upon heating from the isothermal crystallization or annealing temperature have been attributed to melting and recrystallization[56] or the melting of separate populations of lamellae[53,54].

It is highly unlikely, however, that lamellar thickening is at the origin of secondary crystallization of semi-flexible polymers such as PET, PBT, PEEK, PPS and PC at lower temperatures. For these polymers, the chain rigidity is unfavorable to the reorganization at the lamellar fold surface, which is required if isothermal lamellar thickening is to occur. Although some of these polymers such as PET[59-62], PEEK[63] and PC[64], were proposed to exhibit an α_c relaxation, such a transition should only be observed, if at all, at temperatures much closer to the apparent melting temperature (this will be further detailed for PC in Chapter 6). Thus, isothermal lamellar thickening, if it exists, cannot be the dominant mechanism for the secondary crystallization of semiflexible polymers annealed at temperature close to T_g.

The above proposed secondary crystallization mechanisms in either flexible or semi-flexible polymers can be classified into two major processes: reorganization, including lamellar thickening and crystal perfection of pre-existing lamellae crystals; and formation of new crystals upon secondary crystallization. In the first hypothesis, lamellae initially formed during primary crystallization can be more stable through either lamellar thickening or crystal perfectioning by the diffusion of imperfections existing inside the crystals. Polyolefins such as PE[44-49,65,66] and it-PP[6,65,67,68,76] are good examples. Above the α_c-relaxation temperature, for example, PE can thicken during the secondary crystallization stage. This thickening mechanism, however, may not be the most feasible mechanism of secondary crystallization in other semi-flexible polymers such as PEEK,

PET, PPS and PC since, as noted previously, no α_c relaxation has been experimentally observed for these polymers. Therefore, commonly observed log-time dependent crystallinity increase during the secondary crystallization stage cannot be attributed to the lamellar thickening mechanism in the case of semi-flexible polymers. In this case, the second hypothesis, the formation of new crystals appears to be more appropriate.

Although this formation of new crystals is likely to be at the origin of secondary crystallization, there are considerable debates regarding the location and the nature of secondary crystals: 1) *lamellar insertion model*[93,96], in which secondary crystals are thinner lamellae formed in the interlamellar amorphous layer; 2) *stack insertion model*[15,32,33,106-108], in which stacks of thinner secondary lamellae form in the interlamellar stacks (or in the liquid pocket zone); and 3) *bundle-like secondary crystallization model*[64,70,75,110-111], in which bundle-like or fringed-micelle type crystals form in the amorphous layer between the preexisting crystals either in interlamellar or in stacks. The differences in these models are schematically presented in Figure 2.4. Although they contain the essential characteristics of each model, these graphical presentations should be taken with caution since the sizes of lamellae, either primary or secondary, and bundle-like crystals are not to scale.

The lamellar insertion model is primarily based upon SAXS data, from which the long spacing (L_p) can be assigned as either twice the first minimum or the first maximum. Further under the assumptions of two-phase and one dimensional stack plate models, lamellar thickness (ℓ_c) and amorphous layer thickness (ℓ_a) can be determined from the known crystallinity. Hsiao *et al*., from the morphology study of PEEK[93], observed the decrease of long spacing and lamellar thickness with crystallization time, but relatively

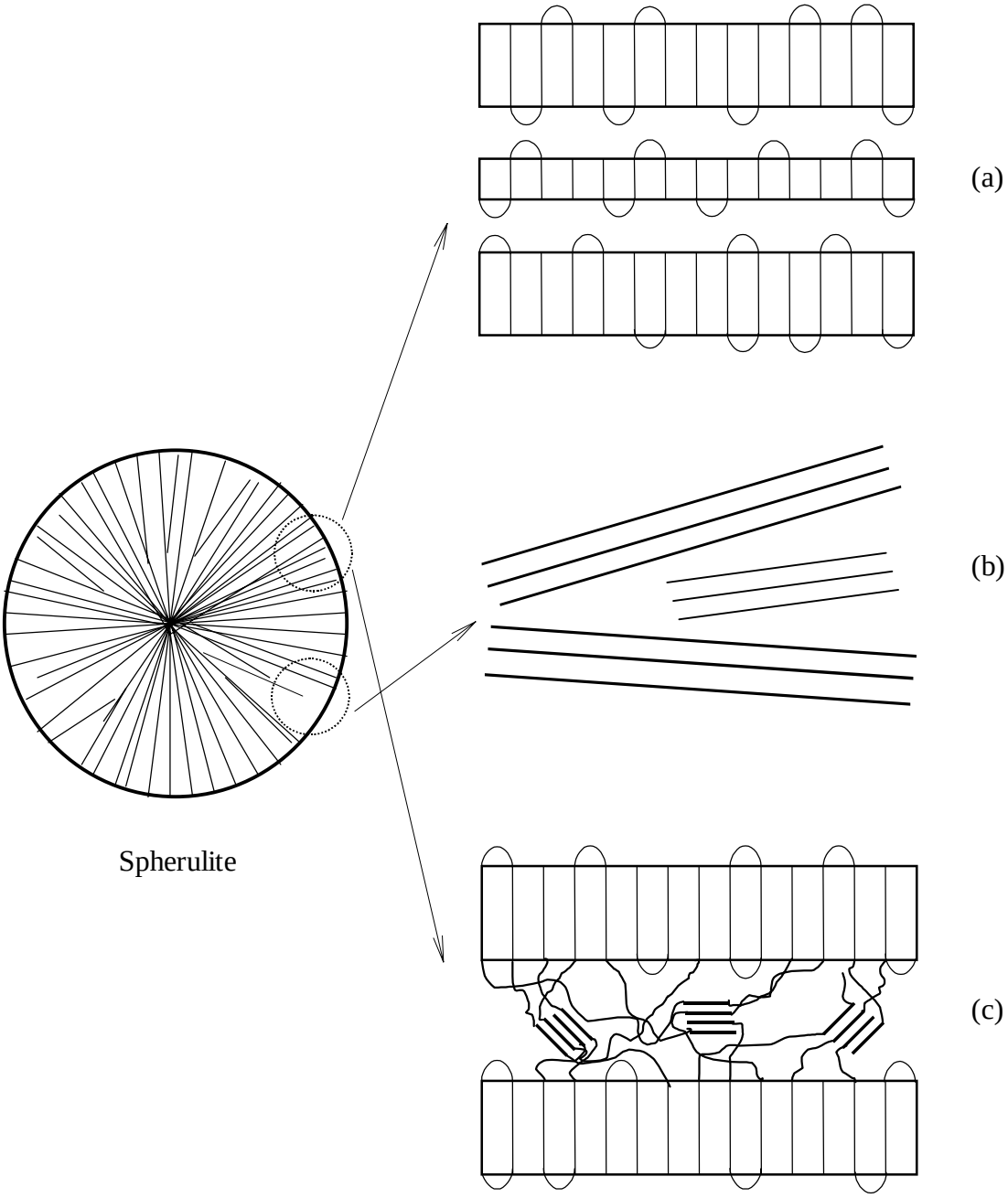

Figure 2.4 Various secondary crystallization models: (a) Lamellar insertion model; (b) Stack insertion model; (c) Bundle-like secondary crystallization model (for detailed description of each model, see the text).

constant ℓ_a; and they attributed theses results to the formation of new lamellae inserted between the interlamellar amorphous layer upon secondary crystallization (*lamellar insertion model*). Later, this model was seriously challenged by Verma *et al*. due to the inconsistent observation that the amorphous layer thickness does not decrease even after the new lamellae insertion[31]. Instead, Verma *et al*. claimed that thinner secondary lamellae form between the separate *lamellar stacks*, and further that these thinner lamellae grow simultaneously and independently with primary lamellae, not by the insertion mechanism.

Very recently, Hsiao *et al*., from the morphology study of PET[32] and PBT[33], discarded the previous lamellar insertion model, and claimed instead the *stack insertion model*, in which new lamellae form in the liquid pocket or interlamellar stacks. This model is similar to the mechanism proposed by Verma *et al*.[31], but with a difference in whether the formation is simultaneous or serial. Srinivas *et al*. observed the decrease of lamellar thickness with crystallization time from the study of TPI and claimed that this decrease is consistent with the stack insertion model[15]. Although this dual lamellar morphology model has been widely recognized in several independent studies, no unanimous agreement has been achieved regarding the sequence of formation, whether the two different lamellar populations grow simultaneously[31,112] or in series[15,22,32,33]. To avoid these complexities, some authors did not specify the sequence, although they did interpret the polymer morphology in terms of the dual lamellar population model[109].

This dual lamellar population model, regardless of the sequence of lamellar formation, is predominantly based on the interpretation of SAXS data. Morphological information from the SAXS is most often based on two-phase model and one-

dimensional correlation function analysis[113]. From these two simplified assumptions, the morphology of semicrystalline polymers is envisaged as alternating between two well-defined layers: lamellae and amorphous. Under this assumed morphology, the correlation function of SAXS intensity data yields two thicknesses, L_1 and L_2 (with $L_1>L_2$) the sum of which is equal to the long period (L_p). The assignment of the crystal thickness (ℓ_c) to either L_1 or L_2 has to be made on the basis of other information. In other words, SAXS data alone can not identify which length corresponds to either the lamellar or amorphous layer thickness. This intrinsic difficulty of SAXS data analysis has led to a controversy, as lamellar thickness was in some cases attributed to the shorter thickness[14,15,23,58,107-109], and in others, to the larger thickness[31-34,93,106,114]. Despite several studies devoted to this topic, the question has not been settled definitely.

It needs to be emphasized that the assumptions of the two-phase model and the linear correlation function in SAXS data analysis will lead to the detection of only well-defined layer thickness. The serious question is, what if the secondary crystals are not of the lamellar-type, making their electron density distribution unable to be interpreted by an idealized stacked plate model? This potential problem of SAXS was recently pointed out by Alizadeh *et al*. in the study of ethylene/1-octene copolymer[75]. They claimed that a lamellar morphology coexisting with fringed-micellar structure cannot be interpreted by an idealized stacked plate model used in classical analysis of SAXS data, since the fluctuation in electron density along the normal to the lamellar surface is far from matching the density expected for this idealized stack model.

Despite numerous investigations of secondary crystallization, no quantitative information regarding the size or orientation of secondary crystals has been gained, and

no quantitative analysis of calorimetric data has been reported to support the notion that the secondary crystals are indeed lamellar type crystals. For instance, in the literature, multiple melting behavior is often attributed to the existence of two different populations of lamellae, thinner lamellae for low endotherm and thicker lamellar for high endotherm based on combined calorimetric and SAXS data[31,32,107-109]. It needs to be underscored, however, that this conclusion was achieved through a more or less qualitative understanding of the evolution of the endothermic behavior, not by a systematic and quantitative analysis of each endotherm as a function of temperature, time, and molar mass. Marand and his coworkers extensively investigated the multiple melting behavior in several types of polymers, such as ethylene/α-olefin[75], PEEK[70], PET[115], PBT[115], nylon-6[115], and PC[64,110,111], and unambiguously showed that the characteristic of the low endotherm cannot be associated with chain-folded lamellar type structures except, possibly at the highest secondary crystallization temperatures. This conclusion was based on two major findings. First, at the initial stage of secondary crystallization, the Avrami exponent from the plot of heat of fusion associated with the low endotherm (ΔH_m^{low}) *vs* log[time] is 0.5, showing the kinetics of secondary crystals to be very different from that of lamellar type crystals. Second, the peak position of the low endotherm (T_m^{low}) increases linearly with logarithm of time over several decades, and more importantly, at a shorter time of secondary crystallization, the melting temperature of secondary crystals becomes very close to the crystallization temperature (i.e., $T_m \approx T_x$), suggesting that the formation of secondary crystals is reversible. It is necessary to remember that lamellar formation is not a reversible process, and even at a shorter time of crystallization, the melting temperature of lamellar crystals is always significantly higher than the

crystallization temperature. It also needs to be noted that the peak melting temperatures of the high endotherms of the above mentioned semiflexible polymers do not change during secondary crystallization unless they are annealed at very high temperature close to the apparent melting temperature. The kinetics of secondary crystallization will be further detailed in Chapter 5.

Based on these observations, a new model of secondary crystallization has been proposed, and is schematically presented in Figure 2.4 (c). The major characteristic that distinguishes this new model from the previous two models is that the secondary crystals are visualized as bundle-like or fringed-micellar type crystals at low temperatures and mosaic blocks at high temperatures, and lamellar crystals at the highest temperatures. Again this model is qualitative so that more quantitative information such as the size and the orientation of small secondary crystals can not be theoretically predicted. The thicknesses of lamellar and the interlamellar amorphous layer, in case of semicrystalline PC, are known[101] to be approximately 40 to 50Å, and 70 to 150Å, respectively. These numerical values must be taken with a caution that, depending on the crystallization and/ or annealing conditions and molar mass, there exist considerable variations.

In summary, the non-equilibrium nature of semicrystalline polymers leads to a secondary crystallization phenomenon, which occurs, more than likely, through a combination of multiple processes, such as reorganization and two or more populations of crystals with different thermal stabilities. In the case of rigid backbone polymers, such as PEEK, PET, and PC, however, reorganization such as isothermal lamellar thickening seems unlikely to be the main mechanism of secondary crystallization considering chain rigidity. As a secondary crystallization model for these systems, three models have been

proposed, namely, lamellar insertion, stack insertion, and bundle-like secondary crystallization models. The first two models propose, mainly based on the SAXS experiments, that secondary crystallization occurs through the formation of thinner lamellae inserted during crystallization, either in an interlamellar amorphous layer or in lamellar stacks. On the other hand, from the quantitative analysis of calorimetric data and morphology studies, the last model claims that secondary crystals do not have a lamellar nature but form through a non-chain folding process; it is thus more likely that they are bundle-like crystals grown between the preexisting main lamellae.

2.3 Multiple Melting Behavior

This review will be restricted to the investigation of multiple endothermic transitions resulting from isothermal crystallization and/or annealing of semicrystalline polymers from the glassy or from the melt states.

High molar mass linear PE, rigid backbone polymers such as PEEK, PET, PPS, PC, and polymers with regio-defects, and copolymers such as ethylene/α-olefin copolymers exhibit multiple melting endotherms upon heating in the DSC. Typical multiple melting traces in the case of PC is illustrated in Figure 2.5. Although the crystallization kinetics of PC is extremely slow, under proper temperature and time conditions it is crystallizable, and upon heating, it exhibits multiple melting endotherms, in which the high endotherm is around 230^{o}C and the low endotherm appears *ca*. 10 to 20^{o}C above the initial crystallization temperature. The exact position of the low endotherm is dependent on crystallization temperature and time. Although in this particular case we observe two endotherms, it has been reported that by step-wise crystallization methods, one can control the number of endotherms; for instance, Cebe *et*

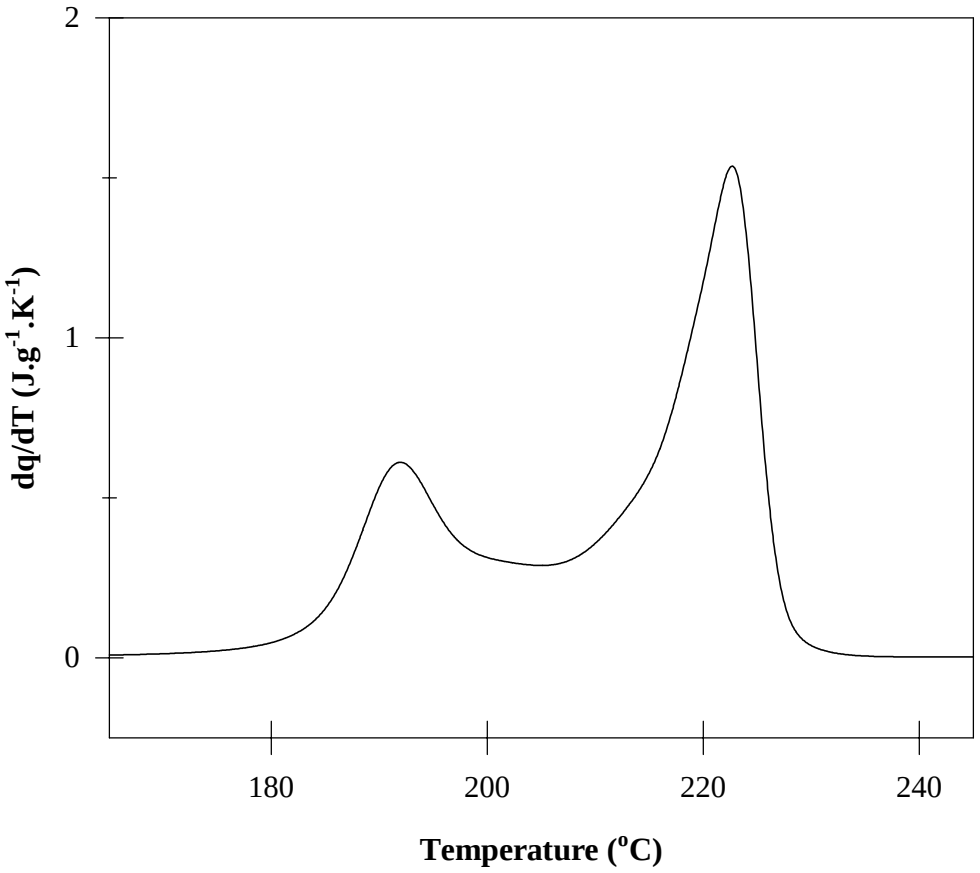

Figure 2.5 A multiple melting behavior of semicrystalline bisphenol-A polycarbonate (M_w = 18,800 g/mol, M_w/M_n =2.0). Sample has been crystallized at 170°C for 192 hours. Melting traces were recorded at 10°C/min heating rate. Temperature scale was properly calibrated using In-sandwich sample (for detail, see Chapters 3 and 4).

al. reported as many as 7 endotherms for PPS[69]. Similar results have been obtained for PEEK[70], PET[71,72].

More importantly, this multiple melting behavior is virtually a universal phenomenon, observed for many flexible or semi-flexible semicrystalline chain polymers. Among polymers known to exhibit this multiple melting behavior are:

- (high molar mass) polyethylene (PE)[74] and its copolymers with α-olefin[75]
- isotactic polypropylene (i-PP)[6,76]
- isotactic polystyrene (i-PS)[77-79]
- poly(vinyl chloride) (PVC)[80-82]
- polyamides (several even numbered nylons)[83-85]
- poly(ethylene terephthalate) (PET)[53,56,86,87]
- poly(butylene terephthalate) (PBT)[9]
- poly(phenylene sulfide) (PPS)[12,23,24,69,88]
- poly(arylene ether ether ketone) (PEEK)[13,91-94,97-99]
- thermoplastic polyimide (TPI)[14,15]
- bisphenol-A polycarbonate (PC)[18,101,102]

Of these polymers, PE and its copolymers, TPI, and semi-flexible polymers such as PET, PEEK, and PPS have been the subject of extensive study in attempts to understand this multiple melting behavior.

In case of PET, Holdsworth and Tuner-Jones[56] suggested that the multiple endotherms are the result of the melting of the lamellae originally formed at the crystallization temperature and their further recrystallization during heating followed by the final melting of the recrystallized lamellae. Groeninckx *et al*.[53] later challenged this

model. They investigated the effects of various thermal treatments on the crystallinity, melting behavior, and morphological features with the conclusion of the possibility of crystal perfection without thickening as well as the partial melting and recrystallization. Zhou and Clough[86] and Lin and Koenig[87] attributed the low endotherm to the melting of small imperfect lamellae formed during the secondary crystallization process.

Lemstra *et al.*[77], in a study of the triple endothermic melting behavior of isothermally crystallized it-PS, identified the upper two endotherms in the DSC scan as the process of melting-recrystallization-remelting, but fail to provide a well-supported model for the low endotherm. They suggested that one possible reason for the small annealing endotherm could be a process of "densification", possibly a secondary crystallization, without specifying the mechanism for the process.

In a study on multiple melting of Nylon 6,6, Bell *et al.*[84] suggested the coexistence of two different morphological forms of the polymer that melt correspondingly at different temperatures: one kinetically favored, the other thermodynamically favored.

In case of PEEK, like other polymers, despite a considerable amount of studies, controversies still exist regarding the interpretation of multiple melting endotherms in the DSC heating scan. Blundell and Osborn[89], two of the first authors to identify the multiple melting endotherms of PEEK, attributed these multiple endotherms to the melting-recrystallization-remelting process following the model proposed by Holdsworth and Turner-Jones for PET[56]. Later, Lee and Porter defined the high endotherm as the maximum of the combined endothermic melting and exothermic recrystallization peaks of the continuously reorganizing crystalline regions[90]. In contrast to these interpretations,

which are largely based on a reorganization model, the dual lamellae population model was discussed by Cebe and Hong[91] and Bassett *et al.*[22], and was further expanded with morphological evidences by other authors[92-94]. Cebe and Hong studied the melting behavior of PEEK by applying a cyclic thermal treatment in the DSC on a previously crystallized sample[91]. They demonstrated that the upper melting endotherm remained unchanged as a result of successive heating above the temperature of the previous treatment, followed by immediate cooling down of the sample. The only feature of the DSC heating scans that changed during this particular treatment was the position and the heat of fusion of the low endotherm, which appeared just above the highest previous thermal treatment temperature. Based on this observation, it was suggested that the low endotherm represents the melting of a secondary population of less perfect, thus less stable, lamellae that melt just above the isothermal crystallization temperature.

Additional evidence against the melting-recrystallization-remelting model has been provided in a work on the thermal properties of PEEK by Cheng *et al.*[13], and by the morphology study of Bassett *et al.*[22]. A sequence of DSC heating scans of samples that were isothermally melt-crystallized for various times showed unequivocally that the high endotherm develops first and should, therefore, be associated with the melting of primary PEEK lamellae. However, Cheng *et al.*[13] did not completely exclude the possibility of partial reorganization during the heating scan.

Bassett *et al.*[22] suggested that the two peaks in the typical double melting scan of PEEK represent the melting of different components within the spherulitic morphology; these components are formed at different stages of the crystallization process and situated at physically different locations within the spherulitic structure. At the earlier stage of

primary crystallization, primary lamellae develop to occupy but not fill the spherulitic structure. Upon heating in the DSC, the melting of these primary lamellae occurs at the high endotherm. At the later stage, secondary crystallization, a population of secondary lamellae develops from the melt *between the primary ones*. These secondary lamellae are smaller and stable only up to a temperature slightly above the crystallization temperature. The constraining effect of the primary lamellae is named as the reason for the slowing down of the secondary stage of crystallization. The authors are cautious in assigning a specific molecular mechanism for the secondary crystallization. Rather, they assign its name according to the time factor: it represents the development of new lamellae *after* the formation of the dominant primary ones. Finally they point out that such a model of sequential crystallization would be applicable to the crystallization mechanism of other chain folding polymers of intermediate crystallinity, namely it-PS and PET.

Very recently Marand *et al*.[70] studied the crystallization and melting behavior of PEEK crystallized from both the glassy and from the melt. From the quantitative analysis of calorimetric data, they concluded that indeed the low endotherm is dominantly a melting of separate populations of crystals, yet 1) at a relatively low temperature of crystallization temperature ($T_x < 320^oC$), secondary crystals are not of the lamellar type but appear to be bundle-like crystals grown between the primary lamellae; 2) at higher temperature ($T_x > 320^oC$), the crystallization kinetics of secondary crystals approaches that of lamellar type crystals.

In summary, despite the numerous investigations for various semiflexible polymers mentioned above, the true nature of multiple melting behavior has yet to be completely understood. The two most competing explanations are 1) the reorganization

process during heating scan, and 2) the existence of two or more crystal populations with different thermal stabilities. As noted earlier, in a particular temperature range of crystallization and/or isothermal annealing, either one of these processes could be dominant, nonetheless, a single mechanism seems unlikely to be fully responsible for the multiple melting behavior occurring in the whole temperature between T_g and T_m. Therefore, in general, multiple endotherms occurring between T_g and T_m of given semicrystalline polymers upon heating should be understood as a consequence of the combination of the above two mechanisms.

2.4 Crystallization and Melting Behavior of PC

2.4.1 *Crystallization*

Since the commercialization of bisphenol-A polycarbonate (PC), in the mid 1950s, there has been diverse research into this material. Among them, crystallization studies are relatively few, since its crystallization kinetics are extremely slow, especially for the commercially applicable molar mass range (> 15,000 g/mol); also in most applications, amorphous PC is generally used. High molar mass PC (> 60,000 g/mol) used for coatings, films, and filaments processed from the solution due to its high melt viscosity, can be readily crystallized up to the extent of 25 to 30 %[116]. In other processing conditions such as high pressure during injection molding, PC can develop a small extent of crystallinity (~8%)[127].

Falkai and Rellensmann[117,118] measured the spherulite growth rate from the bulk at different temperatures and concluded that PC (M_v = 33,000 g/mol) shows a maximum growth rate at 190^{o}C. In addition, from volumetric dilatometry, they reported that the primary crystallization kinetics follow the classical nucleation and growth mechanism

with the Avrami exponent of 3, regardless of the crystallization temperature between 175^{o}C and 205^{o}C[118].

Bonart[124], based on X-ray data, reported that PC has a monoclinic crystal structure of density equal to 1.3022 g/cm^{3}. Kämpf concluded from a morphology study of bulk crystallized PC (M_v =33,000 g/mol) that PC crystallizes slowly (190^{o}C for 8 days) and forms spherulitic structures[119].

Due to PC's extremely slow bulk crystallization kinetics, the majority of later PC crystallization studies adopted other methods of crystallization. These are:

- solvent induced crystallization (SINC)[128,129,131,132,134]

- vapor induced crystallization (VINC)[18,101,102,126]

- plasticizer and/or nucleating agent (organic or inorganic)[104,105,130,133]

Some of these methods enhance the crystallization kinetics by the factor of 200 times over that of conventional bulk crystallization[130]. According to Mercier *et al.*[104,105,133], the final crystallinity could be increased up to 76 %, and the apparent melting temperature of nucleated PC could be as high as 295^{o}C, which approaches one of reported equilibrium melting temperature (~ 327^{o}C)[98]. Considering that bulk crystallized PC seldom exceeds 25 to 30% crystallinity with 230^{o}C apparent melting temperature[18,101,102,117,131,132], these remarkable results demonstrate the critical effect of nucleating agents. Legras and Mercier suggested that this exceptionally high apparent melting temperature of nucleated PC might be due to the extended chain morphology[104,133].

Although the above methods can enhance the crystallization kinetics of PC, there are some crucial drawbacks. When PC is crystallized in the presence of plasticizer and/or organic or inorganic nucleating agents a considerable degradation may occur. Mercier *et*

al. reported that in some cases, molar mass has been decreased by as much as 50% of its initial value in the presence of nucleating agents[130]. The decrease of molar mass in the presence of nucleating agents is rare because in general nucleating agents serve as a physical nucleating sites leading to the increase of number density for potential nuclei. To explain this somewhat peculiar behavior, Mercier *et al*. proposed the "chemical nucleation model", in which they claimed that nucleating agents chemically react with PC through chain scission[104,105]. These chemically modified ionic chain-ends may enhance the crystallization kinetics. Based on this observation, they concluded that at least some portion of the increased crystallinity should be ascribed to the decrease of molar mass.

In cases of SINC or VINC, the difficulty lies in the complete removal of the residual solvent. Even after a prolonged drying, approximately 0.5% of solvent still exists and may act as plasticizer, which may decrease the glass transition temperature of the sample considered[132], although some authors claimed that these residual solvents should not affect the crystallization kinetics[18,102,103].

To avoid these undesirable molar mass decreases or plasticizer effects upon crystallization, bulk crystallization is preferred. Another reason for bulk crystallization is that the potential effects of plasticizers, nucleating agents, and residual solvents on secondary crystallization and multiple melting behavior are not known. However, even in the case of bulk crystallization, there is still a possibility of molar mass decrease through thermal degradation, since bulk crystallization requires a relatively high temperature (180-190^{o}C) and prolonged crystallization time (on the order of days)[117-119]. To minimize thermal degradation, PC samples must be thoroughly dried under vacuum

above the glass transition temperature of the given sample; they also must be crystallized under an inert atmosphere. Prolonged crystallization (at 190^{o}C for 504 hours) without degradation has been reported even under these careful experimental conditions[131].

2.4.2 *Multiple Melting Behavior of PC*

The bulk of earlier investigations on semicrystalline PC relied primarily on methodologies such as optical microscopy[117,119,126], dilatometry[118], WAXS[124,125] and mechanical testing[120,123]. Although these various techniques revealed some valuable aspects of semicrystalline PC, such as spherulitic morphology, crystal structure, and modulus, other information obtainable only by calorimetry was not provided. Calorimetry studies on semicrystalline PC started to appear rather recently. Gallez *et al*. studied the effect of plasticizer (in this particular case, trimellitic acid) on the kinetics of PC crystallization; they provided a DSC thermogram exhibiting a small but distinguishable shoulder as well as a main melting peak at 245^{o}C[130]. Later, Wissler and Crist studied the relationship of heat capacity increase at T_g (i.e., ΔC_p at T_g) with the degree of primary crystallization[131]. In this work they crystallized PC (M_w =30,000 g/mol) both from the solution and from the bulk, yet they only reported DSC thermogram from the solution, in which a single peak was observed although the peak became broadened with crystallinity. Jonza and Porter also reported a similar broad single peak with high endotherm shoulder[101]. They crystallized PC (M_w =37,000 g/mol) initially in the presence of acetone vapor and further annealed at two different temperatures, 197^{o}C and 230^{o}C, for various times between 4 and 125 hours. Di Filippo *et al*.[132] studied the relaxation behavior of semicrystalline PC (M_v =32,000 g/mol) crystallized by VINC, and their thermograms are similar to those of Jonza and Porter.

Recently Laredo *et al*. studied the influence of aging and crystallinity on the molecular motion of PC (M_w =33,000 g/mol), and in this work they reported that two well-separated peaks appear around 180^{o}C and 220^{o}C, respectively upon acetone vapor induced crystallization[18]. Mendez *et al*. studied the effects of annealing temperature and time on the melting behavior of PC (M_w =33,000 g/mol), and in this work they clearly showed the multiple melting behavior of semicrystalline PC upon heating[102]. They crystallized the samples in the presence of acetone vapor and then further annealed them at different temperatures and times.

These several independent investigations on the melting behavior of semicrystalline PC fail to show consistent results in DSC melting traces. Considering the fact that in all above studies, the authors used similar molar mass commercial samples (M_w =30,000 to 37,000 g/mol) crystallized by the same vapor-induced crystallization technique, these inconsistencies in the DSC thermograms are difficult to understand. The reason might be due to the possibility that upon VINC, the sample may not be homogeneously crystallized; this heterogeneity may result in sometimes broad and otherwise clear multiple melting behavior upon heating. It is highly unlikely that molar mass distribution is at the origin of these different behaviors since all studies mentioned used commercial PC samples not fractions. This observation may suggest a potential problem in the VINC technique of polymer crystallization. To prevent this erratic behavior, sample thickness should be precisely determined based upon the time- and crystallinity- dependent diffusion behavior of the solvent or vapor used. Ware *et al*. reported a non-Fickian diffusion behavior from the study of acetone-induce crystallization of PC[128]. In the present work, as will be shown later, multiple melting

behavior was consistently observed regardless of molar mass, molar mass distribution, crystallization temperature, and time. This consistency indirectly shows sample homogeneity upon bulk crystallization.

Laredo *et al*. attributed the multiple melting behavior of PC to reorganization, without providing any evidence for it[18]. Mendez *et al*. drew the same conclusion based on the temperature dependent shift of low endotherm[102]. Again, they did not pay attention to the quantitative analysis of the low endotherm, but rather interpreted the data from the viewpoint of reorganization process based on qualitative observations of thermograms. If the multiple melting behavior is truly arising from reorganization, then low and high endotherm should both be dependent on heating rates. A detailed discussion of the reorganization process will be offered in Chapter 4. Neither of the above two investigations provided this heating rate dependent behavior of semicrystalline PC; therefore, the conclusions from previous studies must be verified in the light of more systematic and quantitative calorimetric studies.

In summary, compared with other widely investigated multiple melting behavior of semi-flexible polymers such as PEEK, PET, PPS, and TPI, a relatively small number of studies have been reported for PC. To further complicate the situation, the results from these limited studies are not consistent in terms of the multiple melting behavior and did not provide a precise mechanism for the multiple melting behavior. In this regard, systematic and quantitative calorimetry study will be necessary to clearly resolve the issue of multiple melting behavior in PC.

References

1. J. Schultz, "Polymer Materials Science", **1974**, Prentice-Hall, Inc, Englewood Cliffs, New Jersey.
2. J. H. Magill, "Morphogenesis of Solid Polymer Microstructure", in "*Treaties on Materials Science and Technology, Volume 10, Properties of Solid Polymeric Materials, Part A,*" ed. J. M. Schultz, 1977 Academic Press, New York.
3. L. Mandelkern, "The Crystalline State", in "Physical Properties of Polymers", **1984**, ed. J. E. Mark, ACS Washington D.C.
4. H. Suzuki, J. Grebowicz, B. Wunderlich, *Brittish Polym. J.*, **1985**, *17*, 11.
5. C. L. Beatty, F. E. Karasz, *J. Macromol. Sci.-Rev. Macromol. Chem.*, **1979**, *C17*, 37.
6. J. Grebowicz, S. F. Lau, B. Wunderlich, *J. Polym. Sci.:Polym. Symp.*, **1984**, *71*, 19.
7. J. Menczel, B. Wunderlich, *J. Polym Sci. Polym. Lett. Ed.*, **1981**, *19*, 265.
8. F. E. Karasz, H. E. Bair, J. M. O'Reilly, *J. Phys. Chem.*, **1965**, *69(8)*, 2657.
9. S. Z. D. Cheng, R. Pan, B. Wunderlich, *Macromol. Chem.*, **1988**, *189*, 2443.
10. B. Wunderlich, "Thermal Analysis", **1990**, Academic Press: Sandiego, CA.
11. P. Huo, P. Cebe, *Colloid Polym. Sci.*, **1992**, *270*, 840.
12. S. Z. D. Cheng, Z. Q. Wu, B. Wunderlich, *Macromolecules*, **1987**, *20*, 2802.
13. S. Z. D. Cheng, M. Y. Cao, B. Wunderlich, *Macromolecules*, **1986**, *19*, 1868.
14. P. P. Huo, J. B. Friler, P. Cebe, *Polymer*, **1993**, *34*, 4387.
15. S. Srinivas, G. L. Wilkes, *Polymer*, **1998**, *39*, 5839.
16. P. P. Huo, P. Cebe, *Polymer*, **1993**, *34*, 696.
17. P. Cebe, P. P. Huo, *Thermochimica Acta*, **1994**, *238*, 229.
18. E. Laredo, M. Grimau, A. Muller, A. Bello, N. Suarez, *J. Polym. Sci. Polym. Phys.*, **1996**, *34*, 2863.
19. S. F. Lau, B. Wunderlich, *J. Polym Sci. Polym. Phys.*, **1984**, *22*, 379.
20. H. Suzuki, J. Grebowicz, B. Wunderlich, *Macromol. Chem.*, **1985**, *186*, 1109.
21. A. Keller, *IUPAC Int. Symp., Macromol. Proc.*, Florence, **1980**, p 135.
22. D. C. Bassett, R. H. O'Relley, I. A. M. Al Raheil, *Polymer*, **1988**, *29*, 1945.
23. S. X. Lu, P. Cebe, M. Capel, *Macromolecules*, **1997**, *30*, 6243.
24. S. X. Lu, P. Cebe, *Polymer*, **1996**, *37*, 4857.
25. J. C. Coburn, R. H. Boyd, *Macromolecules*, **1986**, *19*, 2238.

26. D. S. Kalika, R. K. Krishnaswamy, *Macromolecule*s, **1993**, *26*, 4252.
27. B. B. Sauer, B. S. Hsiao, *Polymer*, **1995**, *36*, 2553.
28. P. Huo, P. Cebe, *Mat. Res. Soc. Symp. Proc*., **1991**, *215*, 93.
29. P. Huo, P. Cebe, *J. Polym. Sci. Polym. Phys*., **1992**, *30*, 239.
30. P. Huo, P. Cebe, *Macromolecule*, **1992**, *25*, 902.
31. R. K. Verma, V. Velikov, R. G. Kander, H. Marand, B. Chu, B. S. Hsiao, *Polymer*, **1996**, *37*, 5357.
32. Z. G. Wang, B. S. Hsiao, B. B. Sauer, W. G. Kampert, *Polymer*, **1999**, *40*, 4615.
33. B. S. Hsiao, Z. G. Wang, F. Yeh, Y. Gao, K. C. Sheth, *Polymer*, **1999**, *40*, 3515.
34. M. Bonnet, K. D. Rogausch, J. Petermann, *Colloid Polym. Sci*., **1999**, *277*, 513; C. D. Breach, X. Hu, *J. Mater. Sci. Lett*., **1996**, *15*, 1416; J. J. Scobbo, C. R. Hwang, *Polym. Engr. Sci*., **1994**, *34*, 1744.
35. V. Göler, F. Sacks, G. Sacks, *Z. Phys*., **1932**, *77*, 281.
36. U. R. Evans, *Trans. Faraday Soc*., **1945**, *41*, 365.
37. L. B. Morgan, Phil. *Trans. Phys. Soc*., **1954**, *A247*, 13.
38. M. Avrami, *J. Chem. Phys*., **1939**, *7*, 1103; **1940**, *8*, 212; **1941**, *9*, 177.
39. L. Mandelkern, " Crystallization of Polymers", **1964**, Ch. 8, McGraw Hill, New York.
40. A. Booth, J. H. Hay, *Polymer*, **1969**, *10*, 95.
41. J. M. Schultz, R. D. Scott, *J. Polym. Sci*., **1969**, A-2, *7*, 659.
42. J. D. Hoffman, J. J. Weeks, *J. Chem. Phys*., **1965**, *42*, 4301.
43. B Wunderlich, J. Mellilo, *Macromol. Chem*., **1968**, *118*, 250.
44. E. W. Fischer, G. F. Schmidt, *Angew. Chem*. **1962**, *1*, 488.
45. E. W. Fischer, *Pure Appl. Chem*., **1972**, *31(1)*, 113.
46. W. Banks, M. Gordon, R. J. Roe, A. Sharples, *Polymer*, **1963**, *4*, 61.
47. S. Buckser, L. H. Tung, *J. Phys. Chem*., **1959**, *63*, 763.
48. F. Rybnikar, *J. Polym Sci*., **1960**, *44*, 517.
49. D. T. Grubb, J. H. Liu, M. Caffrey, D. H. Blderback, *J. Polym. Sci. Polym. Phys*., **1984**, *22*, 367.
50. L. C. E. Struik, *Polymer*, **1987**, *28*, 1521.
51. R. H. Boyd, *Polymer*, **1985**, *26*, 323.

52. D. Schaeter, H. W. Spiess, U. W. Suter, W. W. Fleming, *Macromolecules*, **1990**, *23*, 3431.
53. G. Groeninckx, H. Reynaers, H. Berghmans, G. Smets, *J. Polym. Sci. Polym Phys*., **1980**, *18*, 1311; G. Groeninckx, H. Reynaers, *J. Polym. Sci. Polym Phys*., **1980**, *18*, 1325.
54. J. P. Bell, T. Murayama, *J. Polym. Sci*., part A-2, **1969**, *7*, 1059.
55. R. C. Roberts, *Polymer*, **1969**, *10*, 117.
56. P. J. Holdsworth, A. Tuner-Jones, *Polymer*, **1971**, *12*, 195.
57. S. Fakirov, E. W. Fischer, R. Hoffmann, G. F. Schmidt, *Polymer*, **1977**, *18*, 1121.
58. E. W. Fischer, S. Fakirov, *J. Mat. Sci*., **1976**, *11*, 1041.
59. A. Lovinger, D. Davis, F. Padden, *Polymer*, **1985**, *26*, 1594.
60. K. O'Leary, P. H. Geil, *J. Macromol. Sci*., **1967**, *B1*, 147.
61. P. Zoller, P. Bolli, *J. Macromol. Sci. Phys*., **1980**, *B18*, 55.
62. K. Iler, H. Bruer, *J. Colloid Sci*., **1963**, *18*, 1.
63. J. Rault, *J. Macromol Sci. Rev. Macromol. Chem. Phys*., **1997**, *C37*(2), 335.
64. A. Alizadeh, S. Sohn, L. C. Shank, H. D. Iler, H. Marand, submitted to *Macromolecules*.
65. J. Enns, R. Simha, *J. Macromol. Sci*., **1977**, *B13*, 25.
66. J. Enns, R. Simha, *J. Macromol. Sci*., **1977**, *B13*, 11.
67. J. Blais, R. S. Manley, *J. Macromol. Sci*., **1967**, *B1*, 525.
68. P. Törmala, *J. Macromol Sci. Rev. Macromol. Chem. Phys*., **1970**, *C17*, 297.
69. J. S. Chung, P. Cebe, *Polymer*, **1992**, *33*, 2325.
70. H. Marand, A. Alizadeh, R. Farmer, R. Desai, V. Velikov, *Macromolecules*, in print.
71. F. J. M. Rodriguez, P. J. Phillips, J. S. Lin., *Macromolecules*, **1996**, *29*, 7491.
72. E. M. Woo, T. Y. Ko, *Colloid Polym Sci*., **1996**, *274*, 309.
73. R. G. H. Lammertink, M. A. Hempenius, I. Manners, G. J. Vancso, *Macromolecules*, **1998**, *31*, 795.
74. F. Sakaguchi, L. Mandelkern, J. Maxfield, *J. Polym. Sci., Polym Phys*, **1976**, *14*, 2137.
75. A. Alizadeh,L. Richardson, J. Xu, S. McCartney, H. Marand, Y. W. Cheung, S. Chum, *Macromolecules*, **1999**, *32*, 6221; *Bull.Am. Phys. Soc*.,**1999**, *44*(1), 1562.

76. W. K. Busfield, C. S. Blake, *Polymer*, **1980**, *21*,35.
77. P. J. Lemstra, T. Kooistra, G. Challa, *J. Polym. Sci*. Part A-2, **1972**, *10*, 823.
78. Z. Pelzbauer, R. St. J. Manley, *J. Macromol. Sci- Phys*, **1973**, *B7*, 345.
79. J. Vivirito, H. D. Iler, H. Marand, unpublished results.
80. K. H. Illers, *Makromol. Chem*., **1969**, *127*, 1.
81. H. E. Bair, P. C. Warren, *Macromol. Sci.-Phys*., **1981**, *B20*, 381.
82. A. Gray, M. Gilbert, *Polymer*, **1976**, *17*, 44.
83. P. Weigel, R. Hirte, C. Ruscher, *Faserforsch. Textiletech*., **1974**, *25*, 283.
84. J. P. Bell, P. E. Slade,J. H. Dumbleton, *J. Polym. Sci*. Part A-2, **1968**, *6*, 1773.
85. F. Shuren, Z. Guanguha, T Qun, Y. Yuqin, *J. Thermal Anal*., **1993**, *39*, 875.
86. C. Zhou, S. B. Clough, *Polym. Eng. Sci*., **1988**, *28*, 65.
87. S. B. Lin, J. L. Koenig, , *J. Polym Sci. Polym. Symp*., **1984**, *71*, 121.
88. J. S. Chung, P. Cebe, *Polymer*, 1992, 33, 2312.
89. D. J. Blundell, B. A. Osborn, *Polymer*, **1983**, *24*, 953.
90. Y. Lee, R. S. Porter, *Macromolecules*, **1987**, *20*, 1336.
91. P. Cebe, S.-D. Hong, *Polymer*, **1986**, *27*, 1183.
92. M. P. Lattimer, J. K. Hobs, M. J. Hill, P. J. Barham, *Polymer*, **1992**, *33*, 3971.
93. B. S. Hsiao, K. H. Gardner, D. Q. Wu, B. Chu, *Polymer*, 1993, 34, 3986; B. S. Hsiao, K. H. Gardner, D. Q. Wu, B. Chu, *Polymer*, 1993, 34, 3996.
94. J. Wang, M. Alvarez, W. Zhang, Z. Wu, Y. Li, B. Chu, *Macromolecules*, **1992**, *25*, 6943.
95. A. Jonas, R. Legras, J.-P. Issi, *Polymer*, **1991**, *32*, 3364.
96. A. M. Jonas, T. P. Russel, D. Y. Yoon, *Macromolecules*, **1995**, *28*, 8491.
97. S.-S. Chang, *Polymer*, **1988**, *29*, 138.
98. A. J. Lovinger, S. D. Hudson, D. D. Davis, *Macromolecules*, **1992**, *25*, 1752.
99. H. Marand, A. Prasad, *Macromolecules*, **1992**, *25*, 1731.
100. K.-N. Kruger, H. G. Zachmann, *Macromolecules*, **1993**, *26*, 5202.
101. J. M. Jonza, R. S. Porter, *J. Polym. Sci. Polym. Phys*., **1986**, *24*, 2459.
102. G. Mendez, A. J. Müller, *J. Thermal Analysis*, **1997**, *50*, 593.
103. R. P. Kambour, F. E. Karasz, J. H. Daane, *J. Polym. Sci*. part A-2, **1966**, *4*, 327.

104. C. Bailly, *M. Daumerie, R. Legras, J. P. Mercier, J. Polym. Sci. Polym. Phys.*, ***1985***, 23, 343; C. Bailly, R. Legras, J. P. Mercier, *J. Polym. Sci. Polym. Phys*., **1985**, *23*, 355; C. Bailly, M. Daumerie, R. Legras, J. P. Mercier, *J. Polym. Sci. Polym. Phys*., **1985**, *23*, 493.
105. R. Legras, C. Bailly, M. Daumerie, J. M. Dekoninck, J. P. Mercier, V. Zichy, E. Nield, *Polymer*, **1984**, *25*, 835.
106. B. S. Hsiao, B. B. Sauer, *J. Polym Sci. Polym Phys*., **1993**, *31*, 901.
107. A. M. Jonas, T.P. Russel, D. Y. Yoon, *Macromolecules*, **1995**, *28*, 8491.
108. A. M. Jonas, T.P. Russel, D. Y. Yoon, *Colloid Polym. Sci*., **1994**, *272*, 1344.
109. C. Fougnies, P. Damman, D. Villers, M. Dosiere, M. H. J. Koch, *Macromolecules*, **1997**, *30*, 1385; C. Fougnies, P. Damman, M. Dosiere, M. H. J. Koch, *Macromolecules*, **1997**, *30*, 1392; C. Fougnies, M. Dosiere, M. H. J. Koch, J. Roovers, *Macromolecules*, **1998**, *31*, 6266.
110. S. Sohn, A. Alizadeh, H. Marand, L. C. Shank, H. D. Iler, *American Chemical Soc. Polym. Preprint*, **1999**, *81*, 250.
111. S. Sohn, A. Alizadeh, H. Marand, *Polymer* in print.
112. M. P. Lattimer, J. K. Hobbs, M. J. Hill, P. J. Barham, *Polymer*, **1992**, *33*, 3971.
113. G. R. Stroble, M. J. Schneider, *J. Polym. Sci. Polym. Phys*., **1980**, *18*, 1343; G. R. Stroble, M. J. Schneider, I. G. Voigt-Martin, *J. Polym. Sci. Polym. Phys*., **1980**, *18*, 1361.
114. G. Konard, H. G. Zachmann, *Kolloid Z. Z. Polym*., **1971**, *247*, 851.
115. A. Alizadeh, S. Sohn, H. Marand to be published.
116. Hermann Schnell, "Chemistry and Physics of Polycarbonates", **1964**, John Wiley & Sons, Inc.
117. B. Falkai, W. Rellensmann, *Makromolekular Chem*., **1964**, *75*, 112.
118. B. Falkai, W. Rellensmann, *Makromolekular Chem*., **1965**, *88*, 38.
119. G. Kämpf, *Kolloid-Zeitschrift*, **1960**, *172*, 50.
120. J. P. Mercier, J. J. Aklonis, M. Litt, A. V. Tobolsky, *J. Appl. Polym. Sci*., **1965**, *9*, 447.
121. F. Gallez, R. Legras, J. P. Mercier, *Polym Engr. Sci*., **1976**, *16*, 276.

122. K.-H. Hellwege, J. Hennig, W. Knappe, *Kolloid-Zeitschrift und Zeitschrift für Polymere*, **1962**, *186*, 29.
123. K.-H. Hellwege, J. Hennig, W. Knappe, *Kolloid-Zeitschrift und Zeitschrift für Polymere*, **1964**, *188*, 121.
124. R. Bonart, *Makromol. Chem*., **1966**, *92*, 149.
125. A. Prietzschk, *Kolloid Z*., **1958**, *156(1)*, 8.
126. R. E. J. Fryer, *J. Appl. Polym. Sci*., **1974**, *18*, 2261.
127. K. Djurner, J-A. Manson, M. Rigdahl, *J. Polym Sci., Polym. Lett*., **1978**, *16*, 419.
128. R. A. Ware, S. Tirtowidjojo, C. Cohen, *J. Appl. Polym. Sci*., **1981**, *26*, 2975.
129. E. Turska, W. Benecki, *J. Appl. Polym. Sci*., **1979**, *23*, 3489.
130. F. Gallez, R. Legras, J. P. Mercier, *Polym Engr. Sci*.,**1976**, *16*, 276.
131. G. E. Wissler, B. Crist. Jr, *J. Polym Sci., Polym.Phys*., **1980**, *18*, 1257.
132. Giuseppe V. Di Filippo, Maria E. Gonzalez, Maria T. Gasiba, A.V. Müller, *J. Appl. Polym. Sci*., **1987**, *34*, 1959.
133. F. Gallez, R. Legras, J. P. Mercier, *J. Polym Sci. Polym. Phys*., **1976**, *14*, 1367; R. Legras, J. P. Mercier, *J. Polym Sci. Polym. Phys*., **1977**, *15*, 1283; R. Legras, J. P. Mercier, *J. Polym Sci. Polym. Phys*., **1979**, *17*, 1171.
134. J. Parlapiano, G. L. Wilkes, *Polymer preprint*, **1976**; J. Parlapiano, M.S Thesis, **1976**, Virginia Tech., Blacksburg, Virginia.

Chapter 3

Materials and Experimental

This chapter is composed of three main parts: first, a description of the fractionation and purification procedures, and few words about sample preparation; second, the description of experimental techniques used in the present study; and lastly, amorphous sample characterization. The result of amorphous sample characterization will be included in this Chapter, as a precursor to the study of semicrystalline polycarbonate, which will be offered in Chapters 4 to 7.

Commercial materials and fractions have been characterized in terms of molar mass distribution, glass transition temperature (T_g), heat capacity change at T_g (ΔC_p at T_g), and room temperature amorphous density (ρ_a).

Most widely used polycarbonates are bisphenol-A based polycarbonate (i.e., aromatic polycarbonates), yet aliphatic polycarbonates do exist[1]. In the present study, however, only bisphenol-A polycarbonates have been utilized, so without any further complication, sample nomenclature can be abbreviated as PC for bisphenol-A polycarbonate.

3.1 Sample Preparation

Two types of materials were used for this study: commercial samples and fractions from one of the higher molar mass commercial PC. Two different molar mass commercial PC's were supplied from GE under the trade name of "Lexan" in the form of pellets. NMR analysis revealed these two commercial PCs to be chemically identical, and from the results of GPC (solvent $CHCl_3$, at 30^oC), their molar masses and molar mass distributions were characterized. To obtain the absolute molar mass of PC samples, a

universal calibration methods was used in GPC analysis. To remove the unknown effects of additives in these commercial PCs on crystallization, both were purified. Actual GPC traces of "as is" samples are shown in Figure 3.1, and molecular characteristics before and after purification are listed in Table 3.1.

3.1.1 *PC Fractionation*

For this study, Dr. H. D. Iler (Eastern Mennonite Univ., VA 22802) kindly fractionated one commercial PC (PC-28K, M_w = 28,000 g/mol) into 11 different molar mass fractions ranging from approximately 4,300 to 55,000 g/mol. GPC traces of these fractions and molar masses and distributions are presented in Figure 3.2 and in Table 3.2, respectively. Detailed procedures of the fractionation are given below.

A solvent/non-solvent fractionation method similar to that described by Schnell[2] and Sitaramaiah[3] was used. The procedure involved stepwise addition of methanol (non-solvent) to a 0.5% w/v solution of the polymer (PC-28K) in methylene chloride at 25.0±0.1°C. The fractionation flask was a 5L round bottom flask modified through the addition of a 3cm diameter x 5cm extension designed to amass the denser polymer rich phases resulting from each stage of the fractionation. For a given fraction, methanol was added drop-wise* with vigorous stirring until the solution developed a slight haze indicating a liquid/liquid phase separation**. After complete settling of the polymer rich phase into the flask extension, the solvent rich phase was siphoned off into a catch flask submerged in a 30°C water bath. The polymer fraction was then collected by shocking with methanol and drying in a vacuum oven under a reduced pressure of 29.9 inches of

---

* Flow rate of non-solvent was about 12.5 ml/min.

** For the first fraction, about 1000 ml of methanol was necessary, for the second or later fractions, however, only 40 to 50 ml of methanol was sufficient.

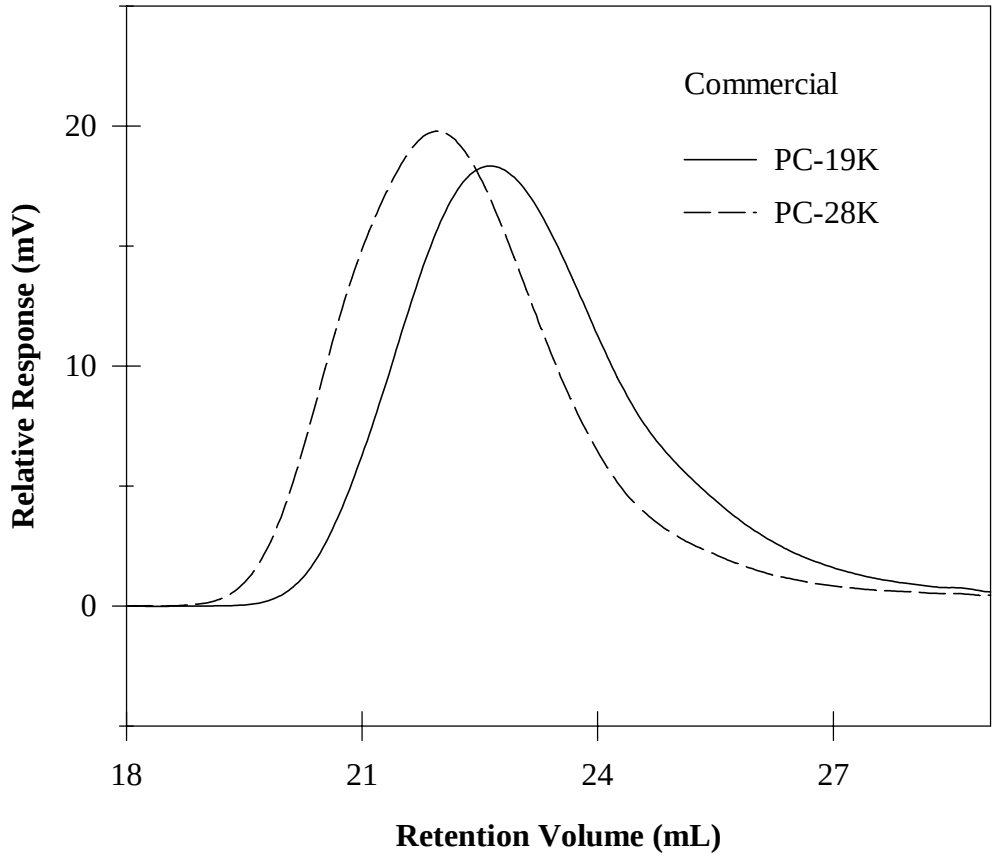

Figure 3.1 GPC traces of two commercial PC samples

Sample	Purification	M_w (g.mol^{-1})	M_w/M_n
PC-19K	*Before*	18,800	*1.99*
	After	19,300	*2.01*
PC-28K	*Before*	28,400	*1.95*
	After	28,600	*2.05*

Table 3.1 Results from the molar mass characterization by GPC for two commercial PC samples before and after purification.

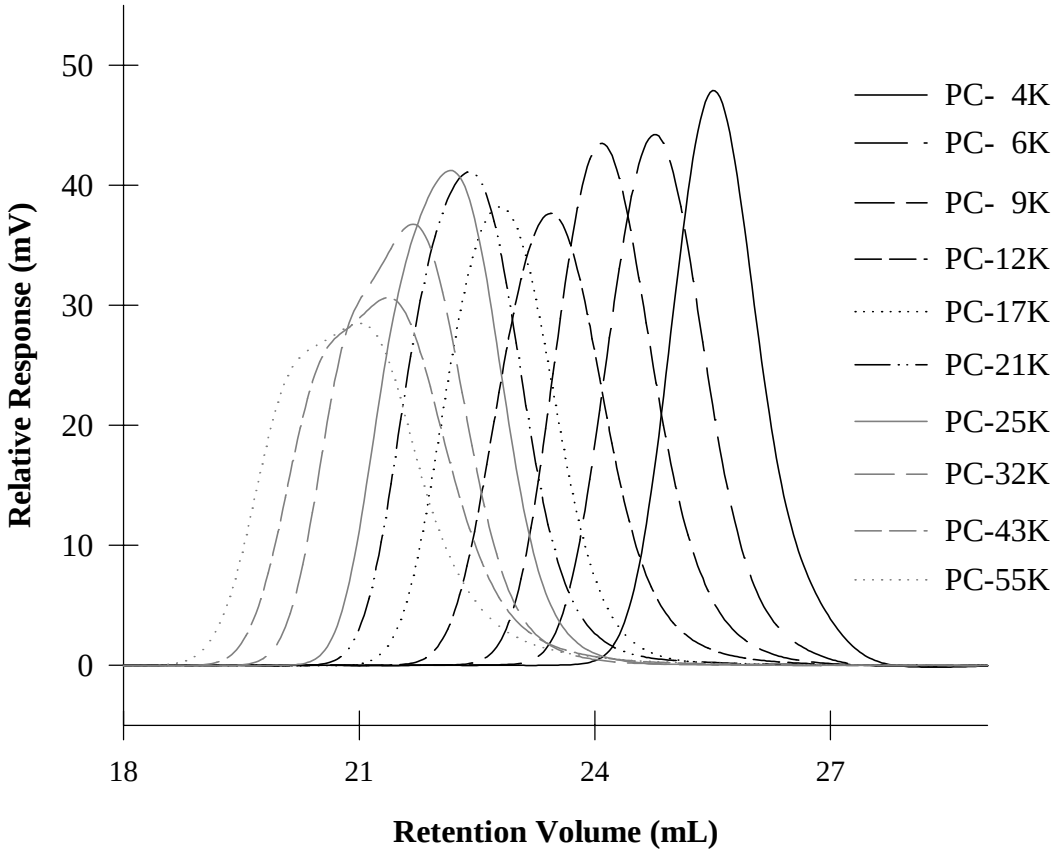

Figure 3.2 GPC traces of PC fractions (see also Table 3.2).

Sample	M_w (g.mol^{-1})	M_n (g.mol^{-1})	M_w/M_n
PC-4K	4,270	4,170	*1.02*
PC-6K	6,390	6,110	*1.05*
PC-8K	8,710	8,180	*1.07*
PC-12K	12,400	11,300	*1.10*
PC-17K	17,100	15,600	*1.10*
PC-21K	21,400	18,800	*1.14*
PC-25K	25,200	21,900	*1.15*
PC-30K	29,800	24,900	*1.20*
PC-32K	32,400	25,900	*1.25*
PC-43K	43,200	31,600	*1.37*
PC-55K	55,000	37,000	*1.49*

Table 3.2 Results from the molar mass characterization by GPC for PC fractions.

Hg at ambient temperature. Eleven fractions were obtained from 3L of initial polymer solution by repeating these procedures. The fractionation apparatus is schematically illustrated in Figure 3.3.

It should be noted that although the initial phase separation for a fraction appeared to be liquid-liquid in nature, the polymer would crystallize from the polymer rich phase during the time allotted for settling. This actually made polymer collection easier and did not appear to adversely affect the fraction polydispersity. Also, the reported potential for degradation of polycarbonate with this particular solvent/non-solvent system[4,5] was minimized by using HPLC grade solvents stored under dry nitrogen blankets and drying the polymer fractions under vacuum at temperatures below 25^{o}C.

GPC was used for the characterization of fractions, and molecular characteristics are presented in Table 3.2 along with weight average molar masses and molar mass distributions (polydispersity = $<M_w>/<M_n>$). Actual GPC traces are also plotted in Figure 3.2. From Tables 3.1 and 3.2, it is clear that the polydispersity of fractions has been reduced considerably upon fractionation almost up to the theoretical limit of 1.0, especially in the case of low molar mass fractions. These more narrow samples will provide an excellent opportunity for the study of molar mass distribution effect on the crystallization kinetics, which is one of the main goals of this study. With molar mass increase, polydispersity tends to increase although the value is still lower than that of commercial samples. Also of interest, as seen in Figure 3.2, small shoulder starts to appear around 32,000 g/mol fraction. Although the exact nature of this GPC peak broadening at higher molar mass fractions is not completely understood, it might be due to the presence of ring-type oligomers connecting polymer chains and thus hampering

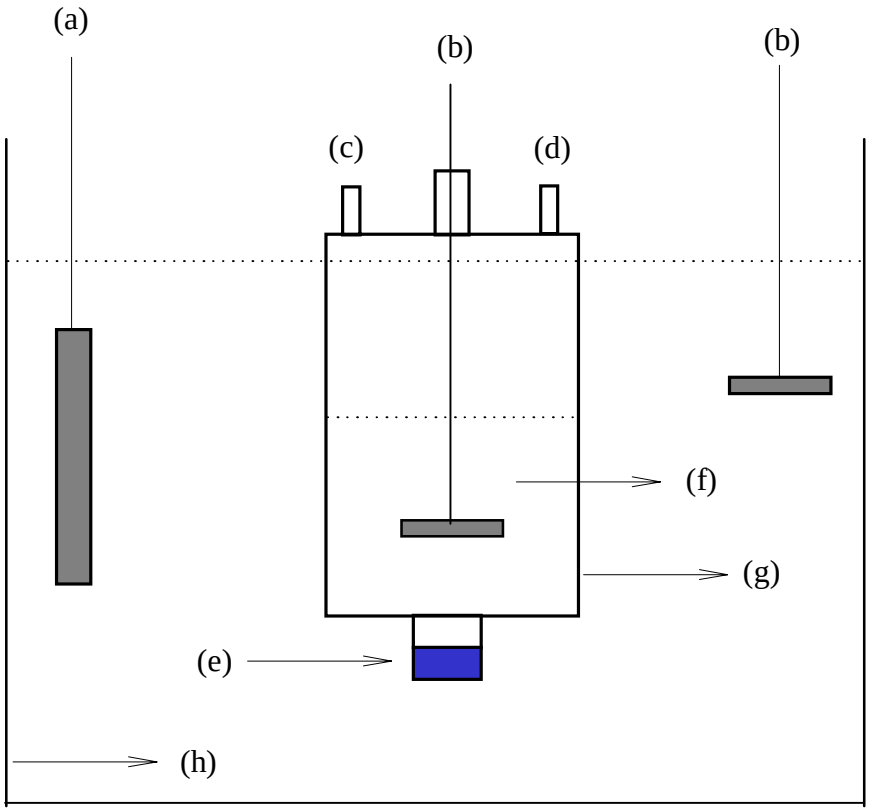

Figure 3.3 A schematic diagram of fractionation apparatus.
(a) heater; (b) stirrer; (c) non-solvent injection hole;
(d) Siphoning hole; (e) polymer-rich phase; (f) solvent-rich phase;
(g) 5L fractionation flask; (h) isothermal bath

narrower fractionation. The present study, however, does not pursue the molecular nature of these shoulders due to the extremely sluggish crystallizability of these high molar mass fractions even under optimum conditions (see Chapter 5).

Once the molar masses of fractions are known, one can use the Stockmayer-Fixman analysis[6] to obtain the (normalized) unperturbed dimensions ($<R_o^2>/<M>$) and the chain stiffness factor (C_∞). The reliability of the molar masses determined by GPC can be ensured by comparing these values with reported ones. Indeed, this analysis confirmed that the molar masses of fractions from this study are quite acceptable. Detail of the procedures and results of the Stockmayer-Fixman analysis are given in Appendix A.1. Briefly, the reported values of unperturbed dimensions[19] and C_∞[19] of PC are, respectively, 0.93 and 2.0. From the analysis of the Stockmayer-Fixman plot using the molar masses from the GPC, they have been found as equal to 0.84 and 1.83.

3.1.2 *Purification*

To remove the potential effects of impurities and of some additives on the crystallization behavior of PC, commercial samples have been purified. The procedure involved dissolving approximately 10 grams of PC in 100 ml of HPLC grade chloroform and precipitating that solution very slowly in the excess amount of HPLC grade methanol under vigorous stirring. Upon completion, precipitated PC was filtered and subsequently washed with methanol (HPLC grade) several times. This was further dried under vacuum for 24 hours at 150^{o}C, which is above the glass transitions of two commercial PCs, to ensure the complete removal of residual solvent and non-solvent. After drying, GPC analysis was employed to check the molar mass change during the purification step.

Molar mass and molar mass distribution did not appear to change during the purification step. GPC results are given in Figure 3.1 and Table 3.1.

3.2 Experimental

In the present study, various techniques have been used to characterize amorphous and semicrystalline PC. These are differential scanning calorimetry (DSC) for the monitoring of thermal behavior, density gradient column (DGC) for macroscopic density measurement, and atomic force microscopy (AFM) and optical microscopy (OM) for morphological studies. This section will describe general experimental methods involved in these techniques. Before introducing these techniques, sample moulding method after fractionation or purification will be offered. While this chapter deals only with amorphous characterization, the methodologies used for the study of semicrystalline PC are similar unless otherwise specified.

3.2.1 *Sample Moulding*

The fractions and purified commercial samples became porous and white (i.e., partially crystallized) solids after drying. To remove all thermal histories and to prepare appropriate samples for various measurements, samples were reshaped into films using a platen-heated Carver Laboratory press. For this procedure, an appropriate amount of material was hot pressed at 250^{o}C and 150 psi under a nitrogen atmosphere for 5 minutes, and subsequently cooled down to room temperature. These fresh moulded samples were shown to be amorphous by DSC and density measurements. These amorphous samples were further characterized using various techniques described in the following section. For bulk crystallization from the glassy state, amorphous films were wrapped in aluminum foil and placed in an oven at the desired crystallization temperature

under an inert atmosphere. Specific crystallization conditions are detailed in the following chapters.

3.2.2 *Calorimetric Study*

Differential scanning calorimetry (DSC) was used for the monitoring of thermal behavior in amorphous or semicrystalline PC. A DSC-2 Perkin-Elmer calorimeter operated with an ice and water bath was used. In order to reduce differences among samples, discoid samples of 120±20 μm thickness and 11.0±1.0 mg weight were employed. A linear horizontal baseline of the DSC signal was obtained before and after a few series of DSC scans. This baseline corrects for the difference between the heat flow output of a blank DSC pan and the reference pan to zero or a constant. The heat flow output for the sample was obtained after subtraction of the baseline heat flow from the recorded output for that sample. In the ΔC_P measurement, sapphire calibration was done for each sample and scan rate. Both heating and cooling experiments were performed at different scan rates ranging from 0.3 to 40°C/min, although the majority of DSC melting traces were recorded at 10^{o}C/min heating rate. Temperature calibration during cooling scans was achieved by recording the isotropic-to-nematic phase transition of *p*-azoxyanisole. The theoretical value for the reversible isotropic to nematic phase transition of this liquid crystal is equal to 136.0°C (see below).

Temperature calibration during heating scans was accomplished by recording the melting transition of an indium standard sandwiched between two amorphous PC films. This step was necessary for the correct temperature calibration in the experiments with different heating rates, since polymers have lower thermal conductivity than metal standards. Figures 3.4 (a) and (b) show typical examples of temperature calibrations

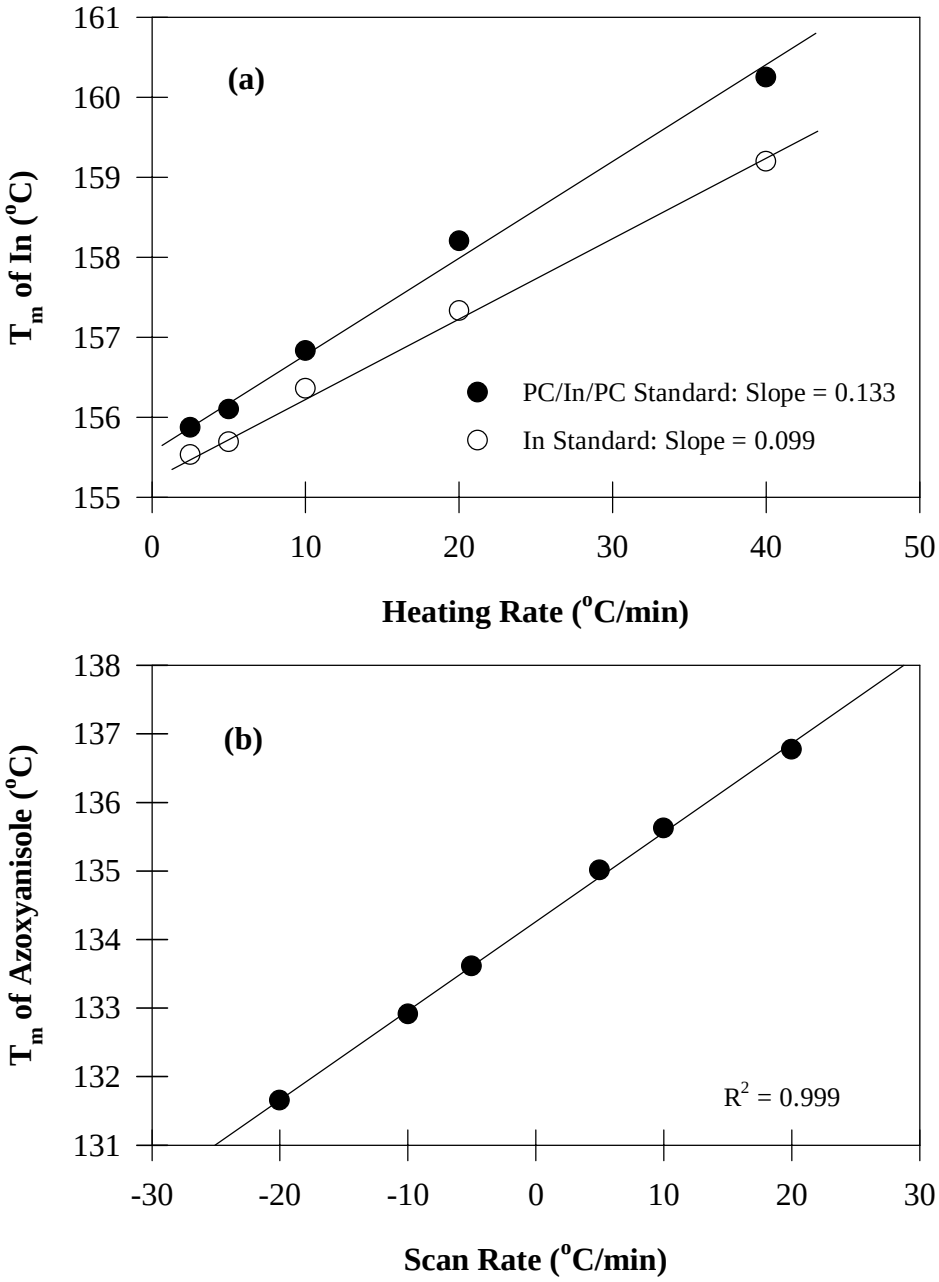

Figure 3.4 Typical examples of DSC temperature scale calibrations upon heating (a) and cooling (b). Note about 30% higher slope in In-sandwich sample showing the thermal lag effect (for detail, see the text).

using In-sandwiched sample and normal metal standard upon heating (a) and *p*-azoxyanisole upon cooling (b). In general, *p*-azoxyanisole is used only for the temperature correction upon cooling, but even upon heating, it can serve as a good standard material without thermal lag correction. The approximately 30% steeper slope from the In-sandwiched sample suggests the existence of a considerable degree of thermal lag due to the instrument as well as the low thermal conductivity of polymers.

An increase in heating rate and thus an increased thermal lag leads not only to a shift in the peak melting temperature but also to a broadening of the melting endotherm. The peak melting temperature can be effectively corrected using this In-sandwiched sample, yet the broadening of the melting endotherm requires other calibration methods. Gray's procedure[7,8] was used as a first approximation in the calibration of melting endotherm peak broadening. Figure 4.2 (Chapter 4) shows a typical example of these corrections. Some important features of Gray's model have been briefly discussed in Appendix A.2. Finally, instrument temperatures (resolution $\leq 0.2^{o}C$) during isothermal experiments were calibrated by extrapolating the melting temperatures of standards (tin, lead and indium) to zero heating rate.

3.2.3 *Density Measurement*

Amorphous and semicrystalline PC densities were measured from the density gradient column. The column was constructed from NaBr aqueous solution with a resolution of 0.0003 g/cc. The calibration curve is shown in Fig 3.5. To remove the surface effects such as impurities and bubbles, samples have been carefully moulded between clean Kapton film. This PC film was cut to approximately 5mm $\times$ 5mm and dropped into the column. The actual column reading was done after 8 hours of

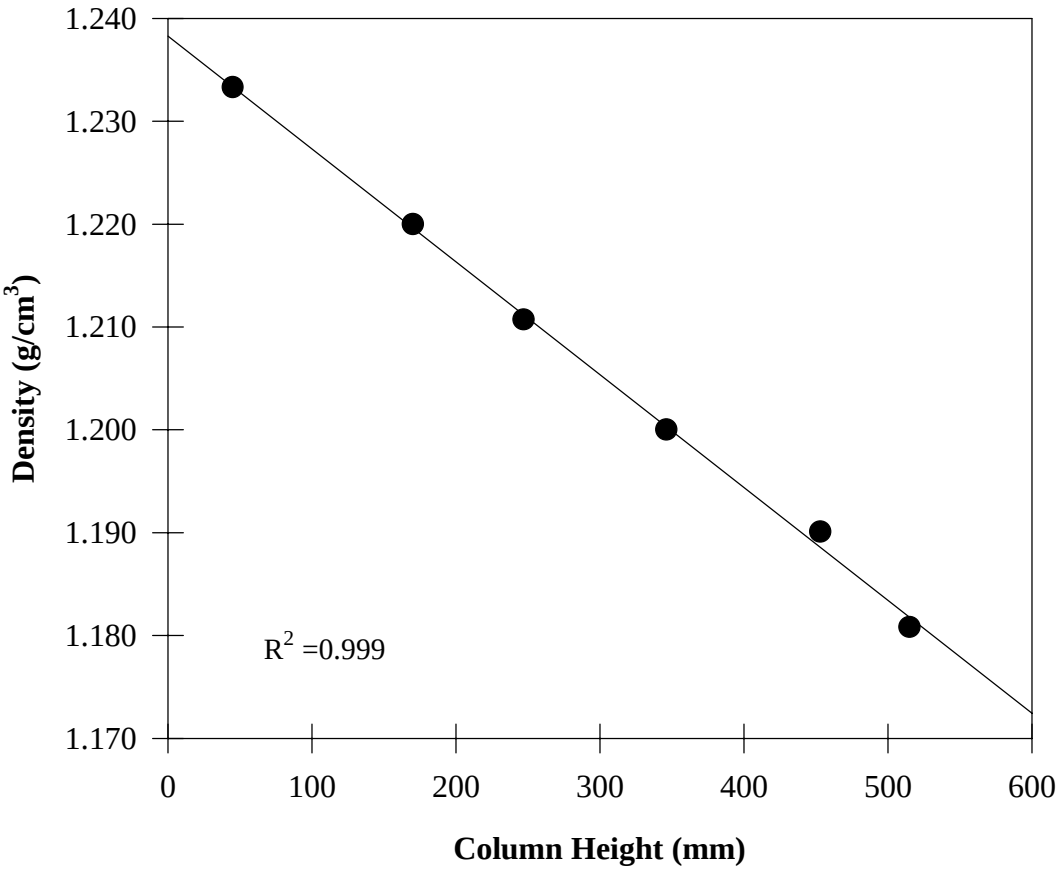

Figure 3.5 A typical example of calibration curve for density gradient column

equilibration, and 5 or more samples were used and averaged. The positions of standard bead were checked every 48 hours, and whenever the bead heights varied more than the resolution of column, 10^{-4} g/cc, the column was discarded. The lifetime of the density gradient column was approximately 4 weeks.

3.2.4 *Atomic Force Microscopy*

Lamellar structures in spherulites from the cold-crystallized samples and structures resulting from possible epitaxy of PC on calcite substrate were examined using AFM. Details of sample preparation will be offered in the appropriate sections; however, this section will present a general description of AFM used in this study. An atomic force microscopy (Digital Instrument, Dimension 3000) was operated in tapping mode at room temperature using nanosensor TESP (tapping etched silicon probe) type single beam cantilevers. The resolution in Z-axis (i.e., vertical direction) was better than 0.1nm, and in the plane of sample (i.e., x- and y- axis), the resolution was *ca*. 0.5nm. To minimize the potential artifacts from tip broadening, the tip has been replaced whenever the image was not reproducible. To enhance the image resolution, 1 Hz or slower scan rate was used. Images were collected in both height and phase modes.

3.2.5 *Optical Microscopy*

The spherulitic structure of semicrystalline PC morphology has been examined using polarized light optical microscopy (Zeiss, Axioplan) equipped with a Linkam heating stage with temperature controller and camera. Temperature control in this heating stage was better than $\pm 1^{o}$C, and the temperature scale was calibrated using the onset melting temperatures of Indium and Tin standards.

Optical microscopy is usually used for morphology study; however in the present investigation, it has also been applied to the determination of thin film melting temperature. For this purpose, a photo diode detector and a light intensity analyzer were connected to an OM equipped with heating stage. With this set of equipment, the change in the polarized light intensity of the sample during heating could be monitored as a function of temperature for a given heating rate. The distinct advantage of this technique lies in being able to measure the melting temperature of very thin film crystallized on transparent but inseparable substrate such as glass. This will be further described in Chapter 6 along with the results.

3.3 Amorphous characterization

After fractionation and purification, amorphous samples were characterized in terms of their glass transition temperature (T_g), heat capacity change at T_g (ΔC_p at T_g) and amorphous density (ρ_a). The first two properties were measured from calorimetry, and the last, from density measurements. This characterization step is an important precursor to crystallization study since the amorphous state can serve as "zero" crystallinity state. In general, one of the most important phenomena representing the amorphous state is the glass transition behavior. Before presenting the results, therefore, some general features of glass transition behavior will be offered along with the introduction of several important parameters characterizing glass transition region.

3.3.1 *General Features of Glass transition Behavior*

Glass transition can be defined as the change in relaxation behavior of polymer chains from the long-range cooperative chain motions to short-range restricted chain motions such as bond rotation. Below the glass transition temperature (T_g), polymer

chains are virtually frozen and act like a stiff spring (glassy state); however, above T_g, polymer chains achieve enough thermal energy to move more freely (rubbery state) like a weak spring. From the definition of Ehrenfest classification[9] of phase transitions, glass transition exhibits the characteristics of the second-order phase transition: continuity in the first derivative of Gibbs free energy, such as enthalpy, entropy, and volume, but discontinuity in the second order derivative of Gibbs free energy, such as thermal expansion coefficient and heat capacity.

Phenomenologically, the glass transition temperature is defined as the inflection point of heat capacity increase (decrease) upon heating (cooling) in a calorimetry study. Figure 3.6 shows a schematic diagram of DSC traces around the glass transition region. Five temperatures characterize the glass transition region[10]. The first perceptible beginning of the glass transition, T_b, is judged by the first increase in heat capacity from that of the solid glassy state. The extrapolated beginning and end of the glass transition, T_1 and T_2, are indicative of the breadth of the major portion of the glass transition. The major portion of T_g broadening will be reflected in ΔT_g (= T_2-T_1), which will be one of the main subjects of Chapter 7. When judged by heat capacity increase, the glass transition temperature, T_g, is chosen at half-devitrification. Finally, T_e, the end of glass transition, is reached when the heat capacity meets the liquid heat capacity.

Before applying this general description of glass transition from DSC, one important caution needs to be mentioned. The precise shape of Figure 3.6 and T_g depends on the scan rate. Therefore, whenever the glass transition temperature is specified, the scan rate must be specified. Largely speaking, the more time is allowed in the vicinity of the glass transition region (i.e., lower scan rates), the more time the

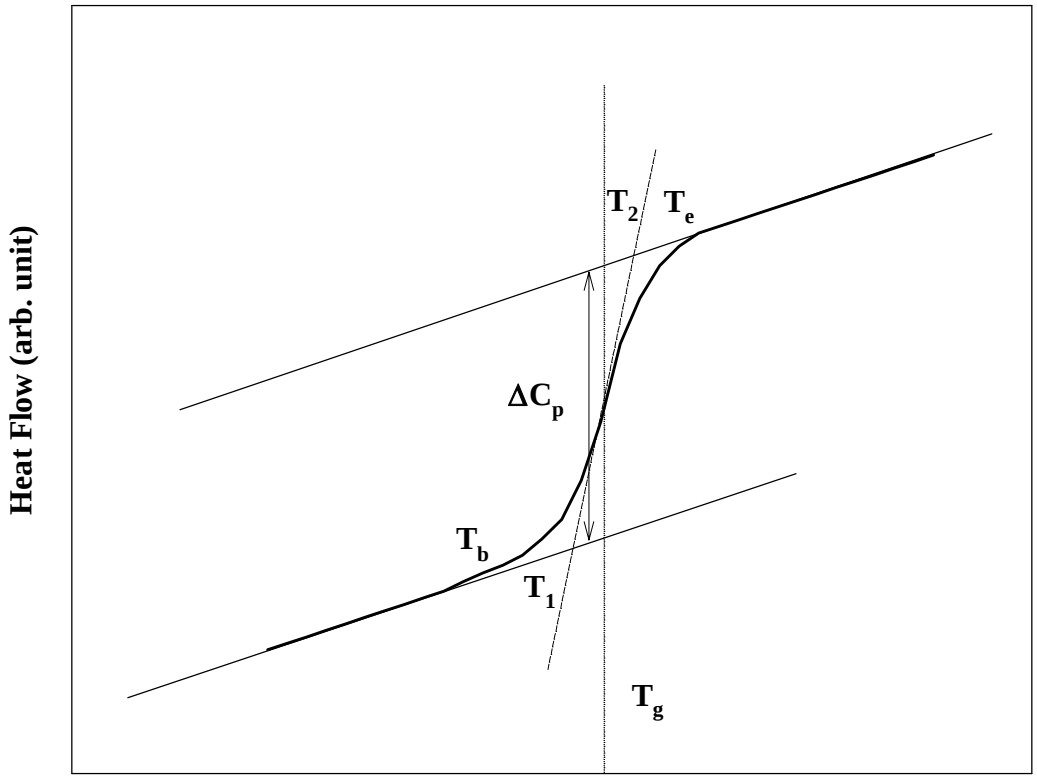

Figure 3.6 A schematic DSC traces in the glass transition region (For detailed description, see the text).

polymer chains will have to adjust themselves to an energetically favorable chain conformation. Thus, upon decreasing the cooling rate, the departure from equilibrium occurs at a lower temperature leading to the decrease of T_g.

Another important parameter in Figure 3.6 is the heat capacity difference between the glassy and liquid states, i.e., ΔC_p at T_g. At the glass transition temperature, because of chain mobility change, the heat capacity will undergo a jump, and this magnitude directly reveals the intensity of relaxation of the amorphous phase for a given polymer. This was discussed briefly in Chapter 2 and will be further discussed in Chapter 7.

3.3.2 *Glass Transition Temperature in Amorphous PC*

In this study, three different scan rates were used (-20, -10, -5^{o}C/min) to observe the effect of cooling rate on the glass transition temperature of PC fractions. The necessary temperature scale corrections were done for each scan rate following the procedures described in the previous section. After proper temperature correction, the variation of T_g with the logarithm of cooling rate became almost linear, and by the extrapolation to zero cooling rate for each fraction, T_g^{o} could be determined. This value was designated as the T_g for each fraction. The results are plotted in Figures 3.7 and 3.8 where, respectively, T_g is presented as a function of cooling rate and as a function of $<M_n>^{-1}$ and $<M_w>$. Figure 3.8 includes the data from the literature to compare with the results from this study. Since the glass transition temperature is sensitive to the method employed for its measurement, literature data[11-14] obtained calorimetrically under similar conditions are only included.

Figure 3.7 clearly shows the increase of T_g with molar mass. The variation of T_g is over 25^{o}C for the number average molar mass ranging between *ca*. 4,200 to 37,000

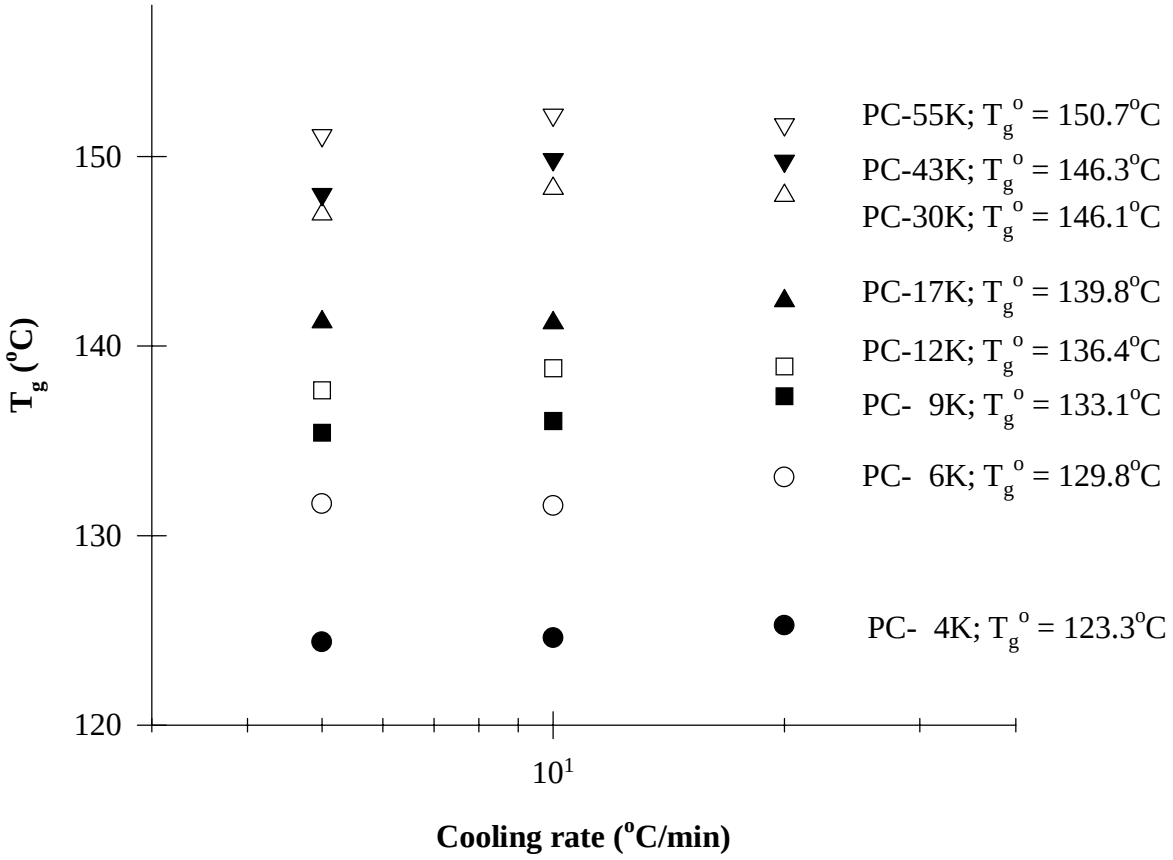

Figure 3.7 Glass transition temperatures of PC fractions as a function of logarithm of cooling rate for different molar mass samples. T_g^o is the linear extrapolation value to zero cooling rate. Temperature scale has been properly calibrated using In-sandwich sample.

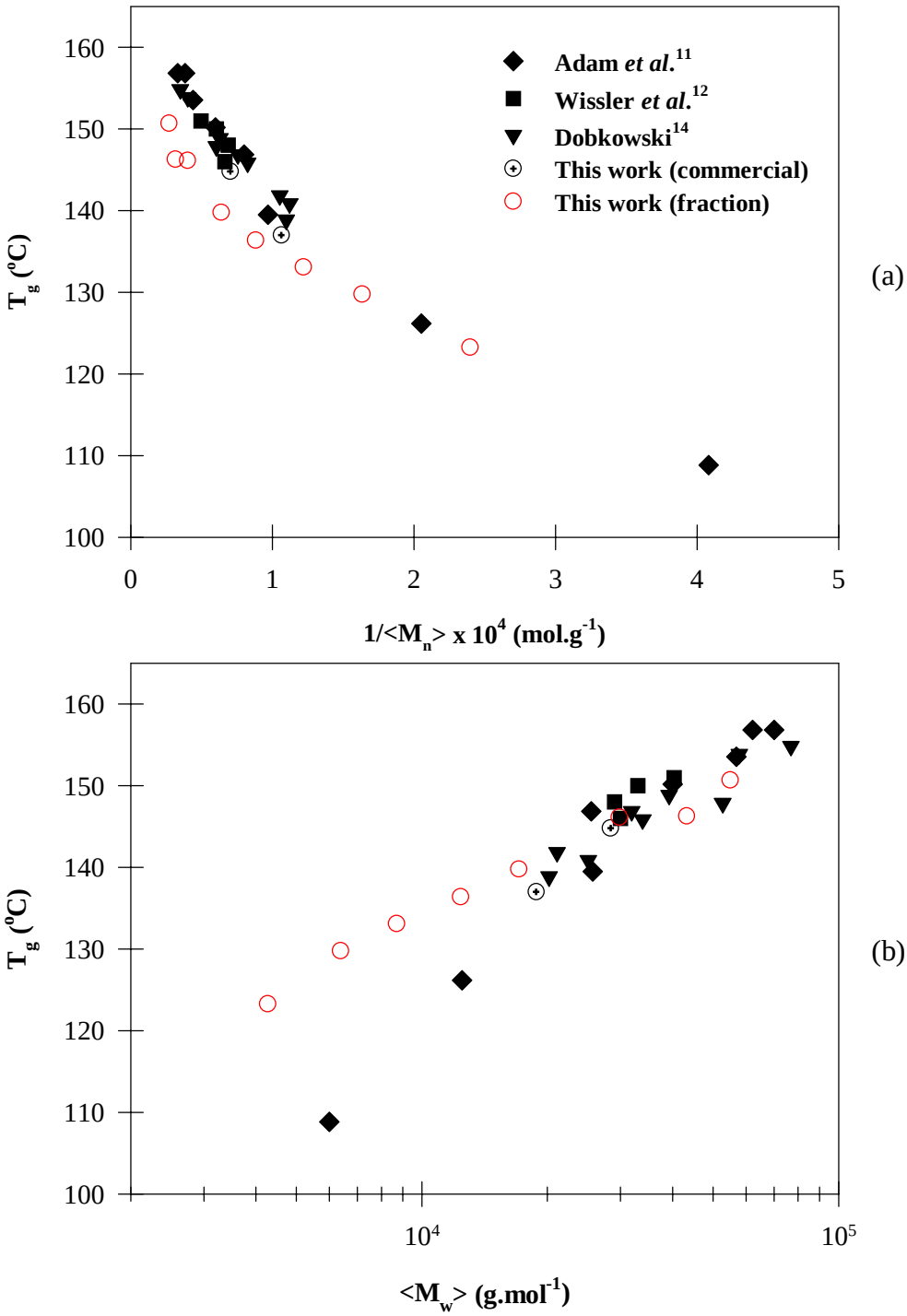

Figure 3.8 A variation of amorphous PC glass transition temperature as a function of $\langle M_n \rangle^{-1}$(a) and as a function of $\langle M_w \rangle$ (b).

The polydispersity of fractions used in the present study was in the range of 1.02 to 1.49 and the polydispersity for the literature data including the commercials in this work is in the range of 2.0 to 3.5

$g.mol^{-1}$.

The particular way of presenting T_g with molar mass shown in Figure 3.8 (a), follows the Fox-Flory equation[15], in which the variation of T_g has been empirically approximated as a linear function of $<M_n>^{-1}$.

$$T_g = T_g^{\infty} - K \cdot <M_n>^{-1} \qquad [3.1]$$

Where T_g^{∞} is the glass transition temperature of infinite molar mass, K is a material constant related to the free volume of the given polymer, and $<M_n>$ is a number average molar mass. Overall, the agreement between the data from this study and from the literature is acceptable, with the exception of somewhat lower T_gs of high molar mass fractions in this study. Similar results have been reported from the study of polystyrene. Monodisperse and polydisperse samples of polystyrene are indistinguishable when their glass transition temperature is expressed as a function of M_n[16].

However, when T_g is plotted as a function of M_w, the effect of molar mass distribution becomes apparent. Results shown in Figure 3.8 (b) corroborate the strong effect of polydispersity on the glass transition temperature. The samples from the literature have a much broader molar mass distribution ($M_w/M_n \approx 2.0$-3.5) than the fractions investigated here. Note the systematic and significant deviation between the narrower and broader molar mass distribution samples for $M_w < 20{,}000$ $g.mol^{-1}$, when the glass transition temperature is plotted as a function of weight average molar mass.

From the glass transition study of near monodisperse polystyrene, Lin claimed that the plot of T_g *vs* $<M_n>$ will show three characteristic regimes in which above M_T (≈

$10\pm2M_e$, M_e is an entanglement molar mass), glass transition temperature reaches a plateau value[17]. In the case of PC, M_e has been known to be around 1,300 to 1,600 g/mol[18,19], and thus the molar mass for the upper bound is *ca*. 20,000 g.mol^{-1}. As shown in Figure 3.8 (a), Lin's claim appears to not apply to PC fractions, since the glass transition of T_g continuously increases with molar mass. This discrepancy is not completely understood at present; however, the reason might be found in the relatively broad molar mass distribution in higher molar mass PC fractions, although the polydispersity indices of these samples are still smaller than those of commercial materials.

These comparisons strongly suggest that for accurate studies of glass transition and crystallization behaviors, near mono-disperse samples will be necessary to eliminate the potential effect of the polydispersity. From this point of view, the fractions utilized in the present investigation, especially for lower molar mass PC fractions, are expected to reveal more precise effects of molar mass on the crystallization behaviors.

3.3.3 *Heat Capacity Change at T_g*

The difference of heat capacity change at T_g ($\Delta C_p = C_p^l - C_p^g$) is an important parameter in describing chain relaxation behavior around the glass transition. For example, semicrystalline polymers often exhibit a smaller magnitude of ΔC_p as compared to the complete amorphous state because the chain molecules in the crystalline phase do not exhibit segmental relaxation at nominal T_g. This well-known phenomenon has been further developed and expanded to introduce the concept of rigid amorphous phase by many authors (see Chapter 2 for proper references).

The variation of ΔC_p (HR = 10°C/min) of amorphous PC as a function of molar mass is shown in Figure 3.9. The main feature is that with a decrease of molar mass, ΔC_p at T_g increases. Similar results have been reported for other polymers[20]. Of more interest, above a certain molar mass* (≈15,000 g/mol), ΔC_p seems to be constant being equal to 0.25 $J \cdot g^{-1} \cdot K^{-1}$. In the similar range of molar mass, ΔC_p of amorphous PC has been reported[20] as 0.3 $J \cdot g^{-1} \cdot K^{-1}$. Cheng and Wunderlich[21] and Wunderlich and Jones[22] reported ΔC_p of amorphous PC as 0.22 and 0.25 $J \cdot g^{-1} \cdot K^{-1}$, respectively. Adam and Hay[11] reported it as 0.17 $J \cdot g^{-1} \cdot K^{-1}$. DiMarzio and Dowell[23], Kim and Burns[24], and Wissler and Crist[12] reported it as 0.24, 0.22 and 0.29 $J \cdot g^{-1} \cdot K^{-1}$, respectively. In these various studies, molar masses were in the range of 25,000 to 45,000 g/mol. The average value (see Figure 3.9) of 0.25 $J \cdot g^{-1} \cdot K^{-1}$ from this study agrees with previous reports.

3.3.4 *Amorphous Density*

As a last step in amorphous PC characterization, the densities of PC fractions have been measured. The results are presented in Figure 3.10. Except for two relatively low molar mass fractions (PC-9K and PC-12K), all the other fractions showed an essentially constant value, an average being equal to 1.1977 ± 0.0002 (g/cm^3). This value is in agreement with the reported values, being from 1.196 to 1.200 (g/cm^3) of amorphous PC[12,13,26-28].

In the case of relatively low molar mass fractions**, there could be some crystallinity developed during air cooling due to the relatively fast crystallization kinetics.

---

* Interestingly, the mechanical property of amorphous PC has been shown to change rather abruptly around this molar mass, and Wilkes has attributed this to the *formation of the effective entanglements* at or above this critical molar mass[25].

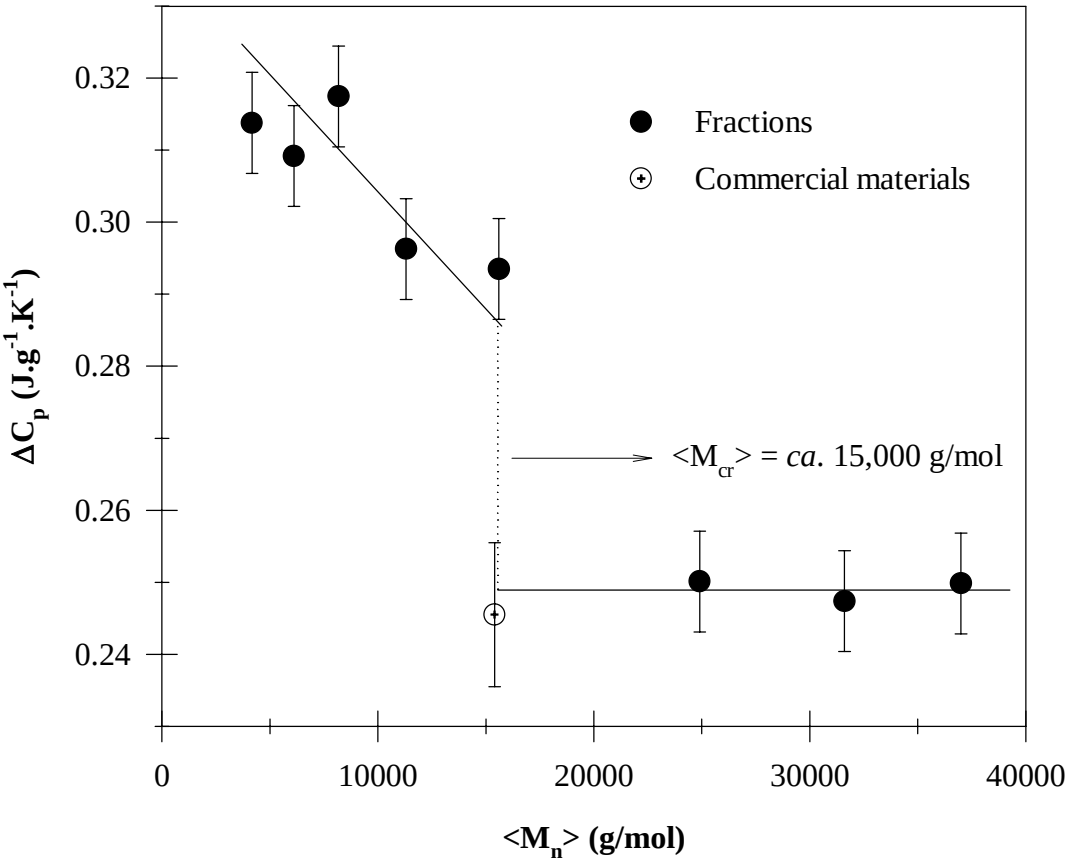

Figure 3.9 Heat capacity change at T_g as a function of number average molar mass of amorphous PC.

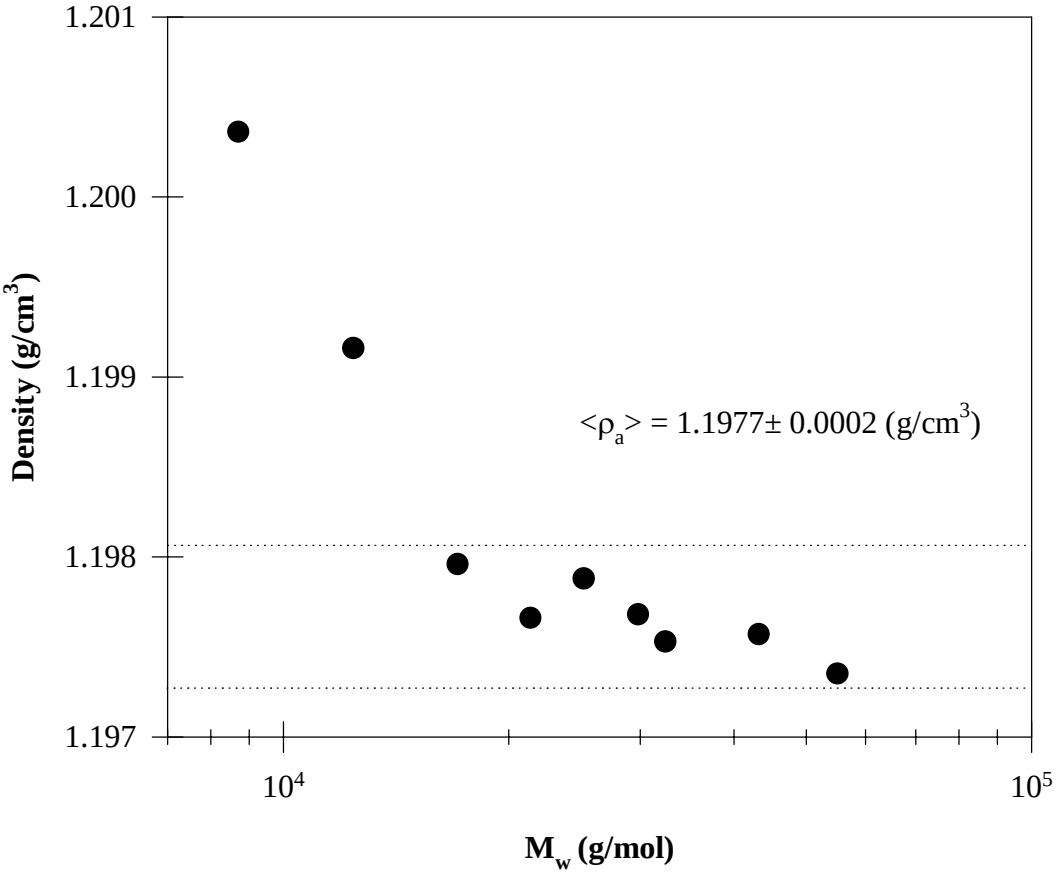

Figure 3.10 Room temperature amorphous densities of PC fractions as a function of weight average molar mass.

For example, in case of PC-12K, based on the density measurement, it could be said that the amorphous sample has been crystallized to the extent of *ca*. 1% upon cooling. It should be noted that even this small amount of crystallinity may give rise to the variation of density in its third decimal point. This is a good justification for the sensitive measurement of crystallinity from the density measurement. On the other hand, however, extreme caution must be used when defining the absolute values of amorphous and 100% crystalline phase densities for the accurate determination of crystallinity. In this regard, the reported amorphous PC density range is too broad to be used for the exact calculation of crystallinity from the density measurement. From now on, 1.1977 g/cc is assigned as pure amorphous density and 1.294 g/cc for 100% crystalline phase density from the study of WAXS for semicrystalline PC[29]. The latter value is in agreement with previous studies by Bonart[26] and Prietzschk[30].

** (see Page 73) Several attempts to measure the densities of two lowest molar mass fractions (PC-4K and PC-6K) have been discouraged because the films with reasonable size and stability for density measurement could not be achieved due to the brittleness of the films.

References

1. Hermann Schnell, "Chemistry and Physics of Polycarbonates", **1964**, John Wiley & Sons, Inc.
2. H. Schnell, *Angew. Chem*., **1956**, *68*, 633.
3. G. Sitaramaiah, *J. Polym. Sci*. Part-A, **1965**, *3*, 2743.
4. G. V. Schulz, A. Horbach, *Makromol. Chem*., **1959**, *29*, 93.
5. G. C. Berry, H. Nomura, K. G. Mayhan, *J. Polym. Sci*. Part-A, **1967**, *5*, 1.
6. L. Trosasarelli, D. Campi, G. Saini, *J. Polym. Sci*., **1959**, *34*, 205.
7. A. Gray, in "Analytical Chemistry", Plenum Press, New York, **1963**, *V1*, p 322.
8. V. Berstein, V. M. Ergov, in "Differential Scanning Calorimetry of Polymers: Physics, Chemistry, Analysis, Technology", **1994**, Ellis Horwood, U. K.
9. P. W. Atkins, "Physical Chemistry", Fifth ed. **1994**, W. H. Freeman & Co., New York. P 200.
10. S. Z. D. Cheng, M. Y. Cao, B. Wunderlich, *Macromolecules*, **1986**, *19*, 1868.
11. G. A. Adam, J. N. Hay, I. W. Parsons, R. N. Haward, *Polymer*, **1976**, *17*, 51.
12. G. E. Wissler, B. Crist, *J. Polym. Sci. Polym Phys*., **1980**, *18*, 1257.
13. B. Falkai, W. Rellensmann, *Makromol. Chem*., **1964**, *75*, 112.
14. Z. Dobkowski, *Eur. Polymer J*., **1982**, *18*, 563.
15. P. J. Flory, *J. Appl. Phys*., **1950**, *21*, 581; *J. Polym. Sci*., Part C, **1968**, *16*, 3373.
16. P. L. Kumler, S. E. Keinath, R. F. Boyer, *J. Macromol. Sci. Phys*., **1977**, *B13*, 631.
17. Y. H. Lin, *Macromolecules*, **1990**, *23*, 5292.
18. L. J. Fetters, D. J. Lohse, S. C. Milner, W. W. Graessley, *Macromolecules*, **1999**, *32*, 6847.
19. L. J. Fetters, D. J. Lohse, D. Richter, T. A. Witten, A. Zirkel, *Macromolecules*, **1994**, *27*, 4639.
20. R. F. Boyer, *J. Macromol. Sci. Phys*., **1973**, *B7*, 487.
21. S. Z. D. Cheng, B. Wunderlich, *J. Polym. Sci. Polym. Phys*., **1986**, *24*, 1755.
22. B. Wunderlich, L. D. Jones, *J. Macromol. Sci. Phys*., **1969**, *B3*, 67.
23. E. A. DiMarzo, F. Dowell, *J. Appl. Phys*., **1979**, *50*, 6061.
24. W. Kim, C. M. Burns, *J. Appl. Polym. Sci*., **1987**, *34*, 945.

25. G. L. Wilkes, in “Encyclopedia of Physical Science and Technology”, **1988**, *11*, p 61.
26. R. Bonart, *Makromol. Chem*., **1966**, *92*, 149.
27. K. H. Hellwege, J. Hennig, W. Knappe, *Kolloid. Z. Z. Polym*., **1962**, *186*, 29.
28. J. P. Mercier, R. Legras, *J. Polym. Sci. Polym. Lett*., **1970**, *8*, 645.
29. A. Alizadeh, R. Farmer, S. Sohn, H. Marand, in preparation.
30. A. Prietzschk, *Kolloid Z*., 1958, *156(1)*, 8.

Chapter 4

On the Origin of Multiple Melting Behavior of Semicrystalline PC

4.1 Introduction

As previously discussed in Chapter 2, semicrystalline bisphenol-A polycarbonate exhibits a multiple melting behavior upon heating, similar to many other polymers such as poly(ethylene terephthalate)[1-4], poly(butylene terephthalate)[5], poly(ether ether ketone)[6-13], poly(phenylene sulfide)[14-17], isotactic polystyrene[18-20], aliphatic polyamides[21-23], and ethylene/α-olefin copolymers[24], to name a few. The most common concepts used to explain the multiple melting behavior of semicrystalline polymers are 1) the melting of crystals of different thermal stability[13,17,18,20,24], and 2) a reorganization process (a melting-recrystallization-remelting process)[2,10,11]. Besides these two competing mechanisms, the existence of different crystal structures may give rise to a multiple melting behavior, yet, it has been shown that PC has only one type of crystalline structure –monoclinic[25]. Therefore, the multiple melting behavior in semicrystalline PC must be ascribed to either one of the above two hypotheses. It is fair to state, however, that this apparently universal behavior is not completely understood since controversies still exist between the first and the second hypotheses. In many cases, these controversies are due to the complicated nature of melting behavior possibly involved in both of these two mechanisms. It will be necessary, therefore, to establish the proper conditions under which either one of these two mechanisms dominates. In this respect, the exceedingly slow crystallization kinetics of PC will be beneficial since it allows us to effectively separate the high endotherm from the low endotherm and thus allows the pursuit of a precise kinetics study of low endotherm in a controlled morphological environment. This

low endotherm kinetic study will be essential in understanding the exact nature of low endotherm. The low and high endotherm kinetics will be further detailed in the following chapter.

Multiple melting behavior explained by the hypothesis of reorganization is often visualized through a heating rate dependent melting behavior[26,27]. The quantitative understanding of the reorganization process (melting-recrystallization-remelting) is still incomplete, yet qualitative experimental observations can be explained rather easily. As the heating rate increases, the peak temperature and heat of fusion associated with high endotherm should decrease, and eventually melting endotherms will show a single, possibly broad, peak at sufficiently high heating rate. A more detailed description of reorganization during heating will be offered in the following section. Because the effect of heating rate on the observed multiple melting behavior is generally used as a justification for the existence of reorganization effects, it is worthwhile to address this issue more thoroughly. Specifically, it is imperative to examine whether such heating rate dependence is consistent with the explanation of the multiple melting behavior in terms of a bimodal population of crystals of different morphological characteristics. In the context of the present work, we use loosely the term reorganization during heating as implying melting-recrystallization-remelting process, although we realize that reorganization can also occur through lamellar thickening or increase in crystal perfection.

4.2 Reorganization Process

Some essential features of the reorganization process during heating are presented schematically in Figure 4.1. At the lower heating rate (a), there is ample time for the

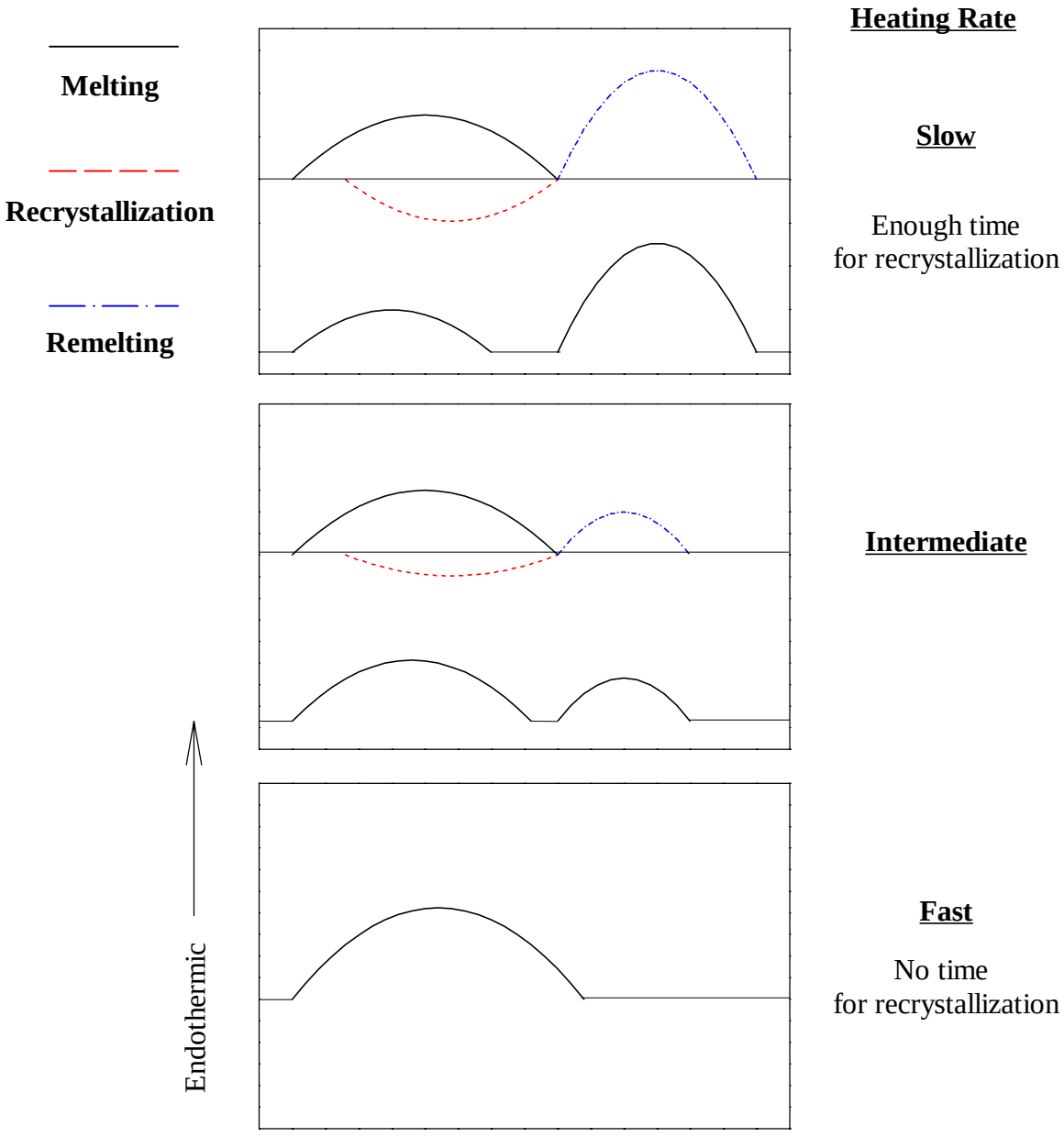

Figure 4.1 A schematic diagram of reorganization (melting-recrystallization-remelting) process as a function of heating rate.

melting of initially present crystals and subsequent recrystallization during the heating scan. In this case, the lower endotherm is the net result of the superposition of the melting endotherm of initial crystals (i.e., crystals present before the heating scan) and the recrystallization exotherm of the just-molten material. The higher endotherm is then observed at temperatures where recrystallization effects are no longer significant and the melting of crystals formed during the heating scan becomes dominant. At the fastest heating rate (c), initially present crystals melt during the heating scan but recrystallization cannot take place since the residence time at temperatures where recrystallization could take place is too short. Consequently, in this case, a single, possibly broad, melting endotherm is observed. At a moderate heating rate (b), the crystals will have less time to reorganize, thus the recrystallization exotherm and consequently the remelting endotherm will decrease in magnitude and peak temperature. Considering all these qualitative features of reorganization, an increase in heating rate should lead to a shift of the high endotherm to lower temperatures and a decrease in the relative magnitude of the high endotherm via that of the low endotherm.

4.3 Experimental

4.3.1 *Materials*

Two of the commercial bisphenol-A polycarbonate, PC-19K and PC-28K and the lowest molar mass fraction, PC-4K, were used for this study. Commercial sample purification and fractionation procedures are described in Chapter 3. These samples were originally crystallized according to the conditions depicted in Tables 4.1. These samples achieved their maximum degree of heat of fusion under each crystallization condition. The effect of heating rates on the melting behavior was examined on 1) completely

Sample	M_w (g. mol^{-1})	M_w / M_n	Crystallization Conditions	ΔH_m^{total} (J/g)
PC-4K	4,300	*1.02*	165°C, 38 hours	34.4
PC-19K	18,800	*1.99*	170°C, 384 hours	27.2
PC-28K	28,400	*2.05*	185°C, 202 hours	25.9

Table 4.1 Molecular characteristics and crystallization conditions of bisphenol-A polycarbonate samples.

crystallized, 2) partially melted, and 3) partially melted and subsequently further crystallized samples.

4.3.2 *Differential Scanning Calorimetry*

The thermal behavior of the samples was monitored using differential scanning calorimetry (DSC). Indium and tin standards were used to calibrate the temperature scale. Heating and cooling scans were performed at different rates, β, from 0.3 to 40^{o}C/min. The temperature calibration during cooling was achieved, as described in Chapter 3, using the isotropic-to-nematic phase transition of *p*-azoxyanisole ($T_{I\text{-}N}$ = 136^{o}C). In all cases, DSC traces were presented after subtraction of a baseline that approximates the heat capacity of the semicrystalline sample over the temperature range considered. Use of a linear baseline in the melting region was mandated by the lack of availability of heat capacity data for the crystal phase of bisphenol-A polycarbonate. Therefore, the heating traces presented in this chapter provide information only on enthalpic contributions associated with the melting process. As a result, apparent heat capacities (dq/dT) will vanish above and below the melting transition. Details of sample preparation and DSC experimental procedures are given in Chapter 3.

4.3.3 *Thermal Lag Corrections*

When a polymer has been crystallized before the heating scan, it may experience the additional transformation of less stable crystals into more stable crystals (reorganization process) upon heating. To avoid this reorganization effect during heating, a higher heating rate will be necessary to minimize the residence time at temperatures where the molten material transforms into more stable crystals (see the previous section of reorganization process, in detail). Unfortunately, under these

conditions, thermal lag effect becomes prominent, leading not only to a shifting of melting peak temperatures but also to a broadening of the melting endotherms[27].

Commonly, metal standards are used to calibrate the temperature scale at a given heating rate. However, it is not accurate to calibrate the actual temperature inside the sample, because the thermal conductivity of organic materials is much lower than that of metals. The use of metal standards for sample temperature calibration, therefore, invokes an inadequate temperature calibration and more importantly, does not allow for corrections of the shape of the melting endotherm due to the effect of temperature gradients within the sample. We, therefore, carried out the temperature calibration using an indium standard sandwiched between two amorphous PC films. For the correction of peak broadening, Gray's method has been applied[28,29], as a first approximation. A typical example of these corrections is shown in Figure 4.2 in which the melting traces ($\beta = 10^{o}C/min.$) of PC-28K crystallized at $185^{o}C$ for 202 hours were corrected by these calibrations: 1) temperature correction by In-sandwiched sample, 2) peak broadening correction by Gray's model. Temperature scale calibration using In-sandwiched sample were previously described in Chapter 3 (see Figure 3.4 (a)). Gray's model correction is only applicable for the heating rates less than *ca*. $40^{o}C/min$[28,29]. A brief review of Gray's method is presented in Appendix A.2.

4.4 Results

In this section, the nature of multiple melting behavior of PC and heating rate dependence of the low endotherm will be presented. First, the results of heating rate experiments performed on the as-crystallized and partially melted samples of various molar masses will be offered. Next, the results of secondary crystallization experiments

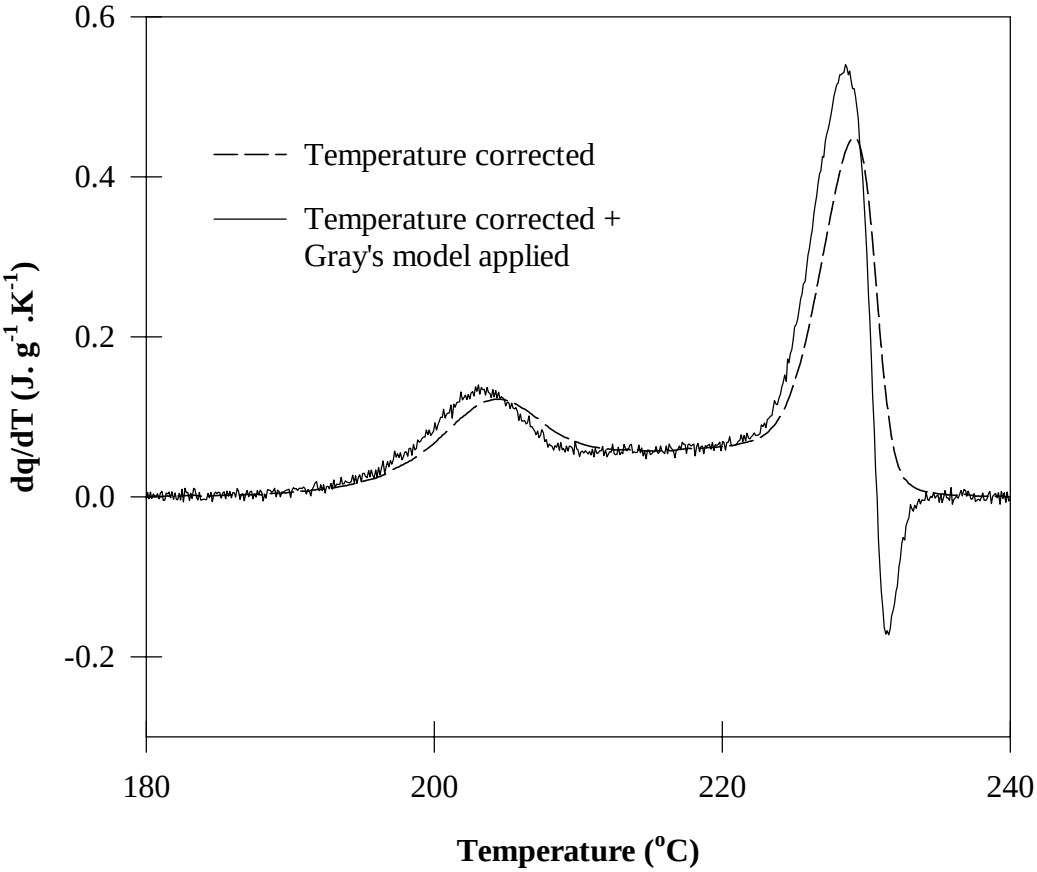

Figure 4.2 A typical example of thermal lag correction considering both temperature shift and peak broadening. PC-28K sample was initially crystallized at 185^{o}C for 202 hours, partially melted at 220^{o}C and exposed to secondary crystallization at 185^{o}C for 2 hours. Temperature scale has been properly corrected using In-sandwiched sample (for detail, see the text). Heating rate was 10^{o}C/min.

performed on partially melted sample at different temperature and time will be presented.

4.4.1 *The Nature of the Multiple Melting Behavior in PC*

As-crystallized samples

In Figure 4.3, the corrected heating traces of PC-28K crystallized from the glassy state at 185°C for 202 hours are displayed at heating rates ranging from 2.5 to 20°C/min. The heating of PC subsequent to the above crystallization process gives rise to a low, an intermediate, and a high melting endotherm. The intermediate endotherm spreads over a wide temperature range, and under this particular crystallization condition, overlaps with both low and high melting endotherms. In the case of PC-19K, however, this intermediate endotherm is relatively less overlapped mainly due to the well-separated peak positions of low and high endotherms (see Figure 2.5, for instance). Table 4.2 presents the melting temperatures of PC-28K original and partially melted samples. As can be observed in Figure 4.3 and Table 4.2, the location of the high endotherm is found to be almost independent of heating rate ($\beta > 2$°C/min). On the other hand, the position of the low endotherm depicts strong heating rate dependence and shifts systematically towards higher values with increasing heating rate. The total heat of fusion of the sample (25.9 J/g) is heating rate independent. Qualitatively, PC-19K showed similar heating rate dependent behavior to PC-28K.

Figure 4.4 shows the results of similar experiments performed on PC-4K, the lowest molar mass fraction, which has been crystallized at 165^{o}C for 38 hours. Three different scan rates, 5, 10, and 20^{o}C/min, were used. In each case, three endotherms are observed. The lower endotherm is observed slightly above the crystallization temperature and, similarly to PC-19K and PC-28K, shifts to higher temperatures with

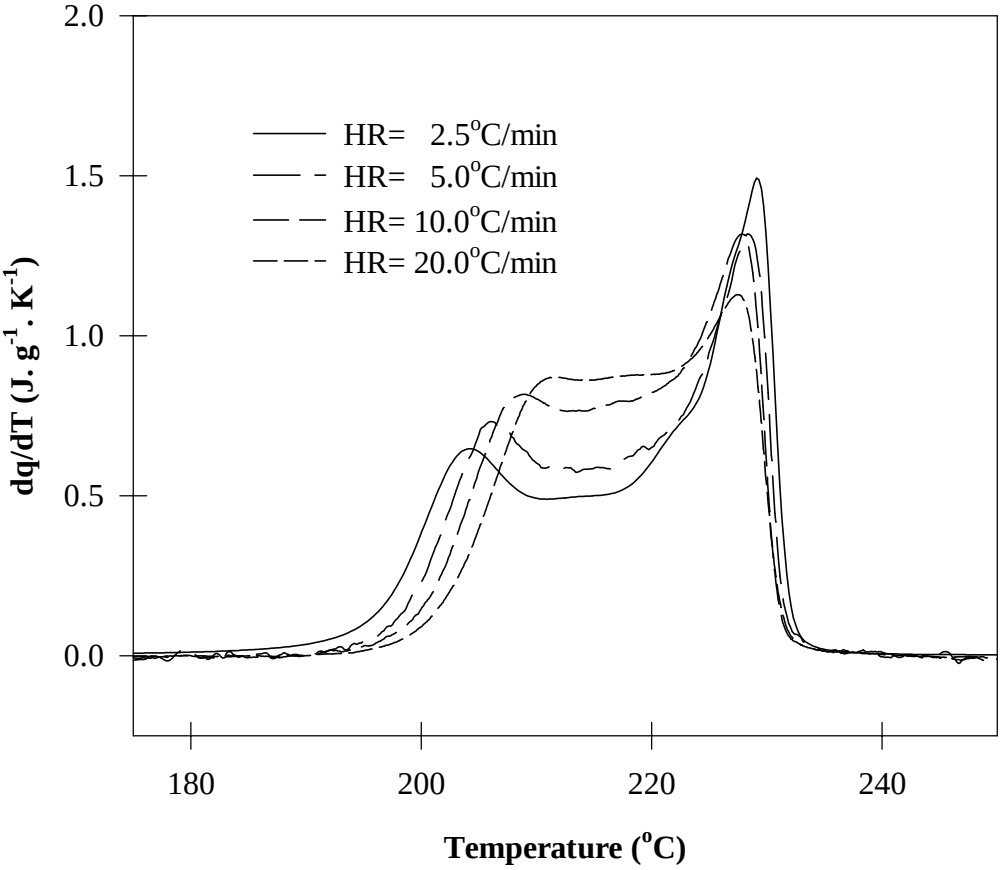

Figure 4.3 Effect of heating rate on the melting behavior of PC-28K crystallized at 185°C from the glassy state for 202 hours and quenched to 100°C

Heating Rate (°C/min)	**PC-28K (original)** ***Crystallized at 185°C for 202 hours***		**PM;PC-28K** ***Partially Melted at 220°C***
	T_m^{low} (°C)	T_m^{high} (°C)	T_m^{high} (°C)
2.5	204.0	229.1	228.9
5.0	205.6	228.5	228.2
10.0	207.2	227.8	228.6
20.0	208.9	228.4	228.7

Table 4.2 Melting temperatures of PC-28K before and after partial melting.

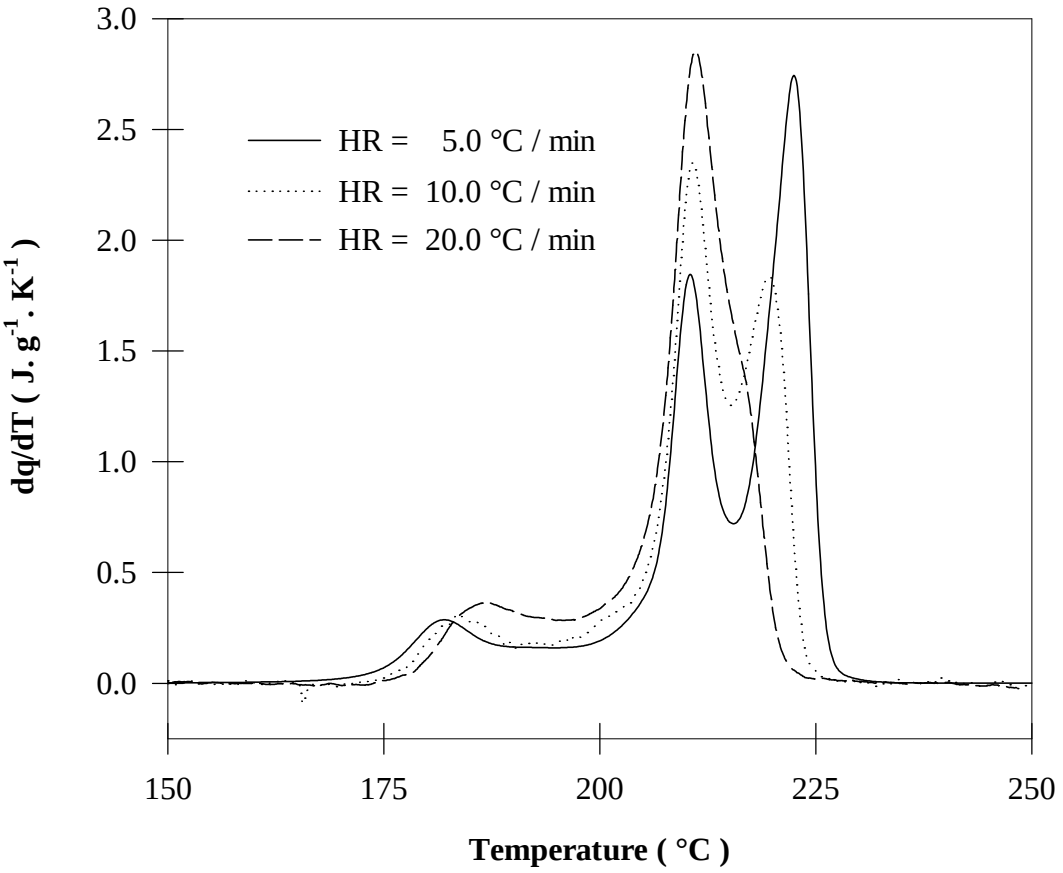

Figure 4.4 Effect of heating rate on the melting behavior of PC-4K crystallized from the glassy state at 165°C for 38 hours, and quenched to 80°C.

increasing heating rates. The upper endothermic region shows the trend expected for a melting-recrystallization-remelting phenomenon. The enthalpy of fusion of the intermediate endotherm increases and that of the highest endotherm decreases with heating rate. Furthermore, the intermediate endotherm shifts to higher temperatures while the highest endotherm shifts to lower temperatures with heating rate. A similar observation of an increase in the rate of reorganization upon heating with decreasing molar mass has been reported for poly(vinylidene fluoride), nylon-12 and poly(phenylene sulfide) by Judovits *et al.*[30].

Partially Melted Sample

This section will present a series of experiments that were performed to investigate, independently, the high endotherm for PC-28K. In addition, the effect of cooling rate after partial melting will be considered.

Partial melting was carried out by heating ($\beta = 20^{o}C/min$) PC-28K samples crystallized at $185^{o}C$ for 202 hours up to $220^{o}C$, which is approximately in the middle of low and high endotherm peak melting temperatures. Upon reaching $220^{o}C$, these samples were rapidly cooled to $100^{o}C$ ($\beta = -40^{o}C/min$) and subsequently reheated at various heating rates to record their melting behavior. The corrected heating traces of partially melted PC-28K samples (PM; PC-28K) for heating rates ranging from 2.5 to $20^{o}C/min$ are shown in Figure 4.5. Partially melted samples solely exhibit a high endotherm whose corresponding peak melting temperature and heat of fusion are found to be heating rate independent (see Table 4.2). The average heat of fusion of the partially melted sample is equal to 8.4 J/g. The high endotherm melting temperature, T_m^{high}, of the partially melted sample (fourth column in Table 4.2) is found to be identical, within an

experimental uncertainty, to that of the original sample for all heating rates (third column in Table 4.2).

Cooling Rate Effect

Many crystallizable polymers often exhibit non-isothermal crystallization upon either heating or cooling. PC, as shown in Figure 4.3 and in the literature[31-33], does not crystallize either upon heating or upon cooling, even at a very slow scan rate, due to its extremely slow crystallization kinetics (recall that PC-28K requires 40 to 50 hours of induction time at maximum growth rate temperature before the detectable heat of fusion: see Chapter 5). These observations, nonetheless, does not rule out the possibility that PC may crystallize upon cooling *in the presence of pre-existing crystals*. This is a very important question that needs to be properly addressed because in order to investigate the melting characteristics of secondary crystals, it is important to ensure that there is no morphological evolution during cooling between the upper temperature used for partial melting and the temperature at which secondary crystallization is performed (see below).

In the previous set of experiments, the characteristics of the high and low endotherms were investigated separately by direct comparison of heating traces of as-crystallized and partially melted PC samples. This comparison is based on the assumption that partial melting and subsequent cooling of the samples do not affect the population and the size of the most stable primary crystals. The observation of identical peak melting temperatures for as-crystallized and partially melted samples indicates that the heating rate and the upper temperature used for partial melting were properly chosen to avoid reorganization of the primary crystals. We therefore need to discuss the

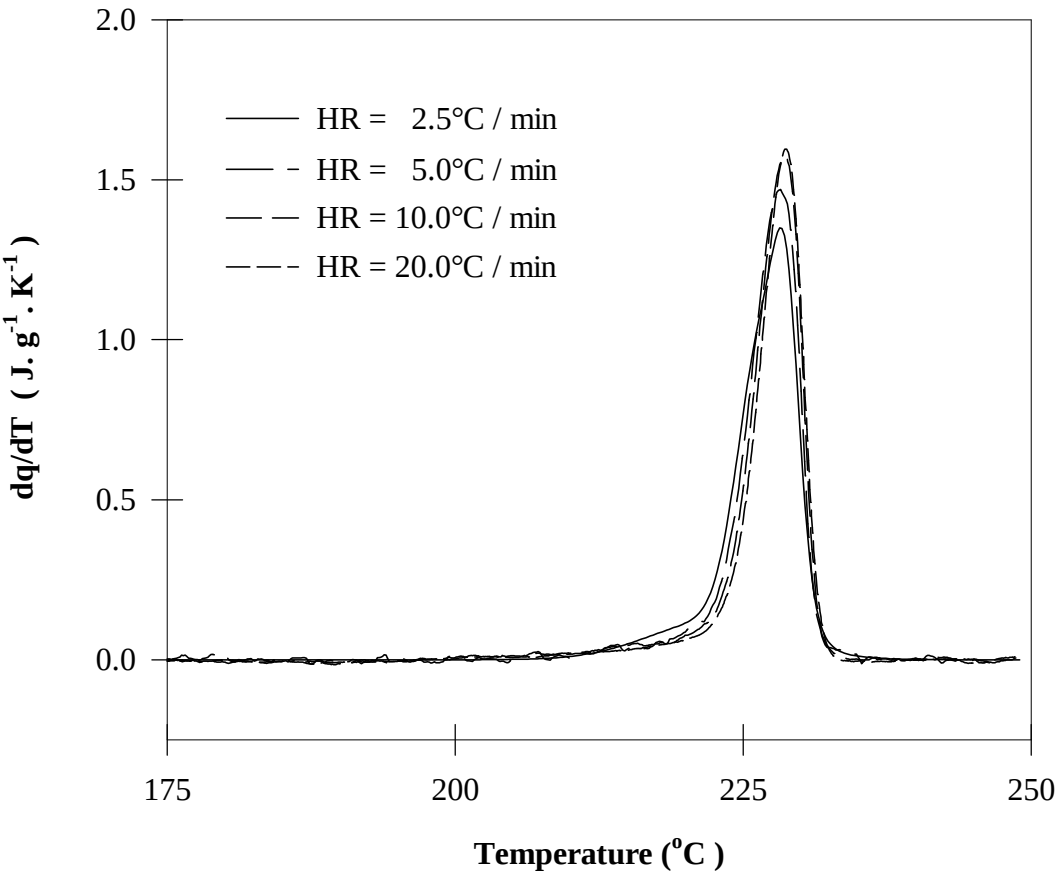

Figure 4.5 Effect of heating rate on the melting behavior of PC-28K crystallized at 185°C from the glassy state for 202 hours, partially melted at 220°C, and subsequently cooled to 100°C.

influence of the rate of cooling from 220 °C to 100 °C on the subsequent melting behavior.

To provide the proper answer to this question, a series of cooling rate experiments was conducted on partially melted samples at 220^{o}C at the scan rates ranging from – 0.3 to – 40^{o}C/min, and each melting endotherm was subsequently recorded from 100^{o}C to 260^{o}C at 10^{o}C/min heating rate. Figure 4.6 shows the melting traces of a series of samples (PM; PC-28K) with different cooling rates. Figure 4.7 depicts the analysis of the above melting endotherms in various aspects, in which the melting peak position variation (a), change of heat of fusion (b), and amount of rigid amorphous fraction (RAF) change (c) are plotted as a function of cooling rate. RAF, the fraction of amorphous that does not relax at normal T_g, was discussed briefly in Chapter 2, and will be discussed again in Chapter 7. Briefly speaking an increase of RAF shows the increase of constraints; for example, small crystals developed upon cooling will exert constraints on the amorphous phase thus decrease the relaxation intensity at T_g. This can be effectively visualized from the development of RAF upon cooling.

The melting traces of partially melted sample are independent of the cooling rate unless the rate is equal to or smaller than -2.5^{o}C/min. However, for cooling rates below -2.5^{o}C/min., the enthalpy of fusion and the peak melting temperature increase with decreasing cooling rate. The analysis of RAF in Figure 4.7 (c) also supports this conclusion. It has been demonstrated, therefore, that the heat of fusion after partial melting (8.4 J/g) comes solely from the heat of fusion of crystals survived after partial melting, not from the crystals formed upon cooling, unless the cooling rate is sufficiently slow ($\beta \leq$ -2.5^{o}C/min). This conclusion also ensures that as long as the cooling rate

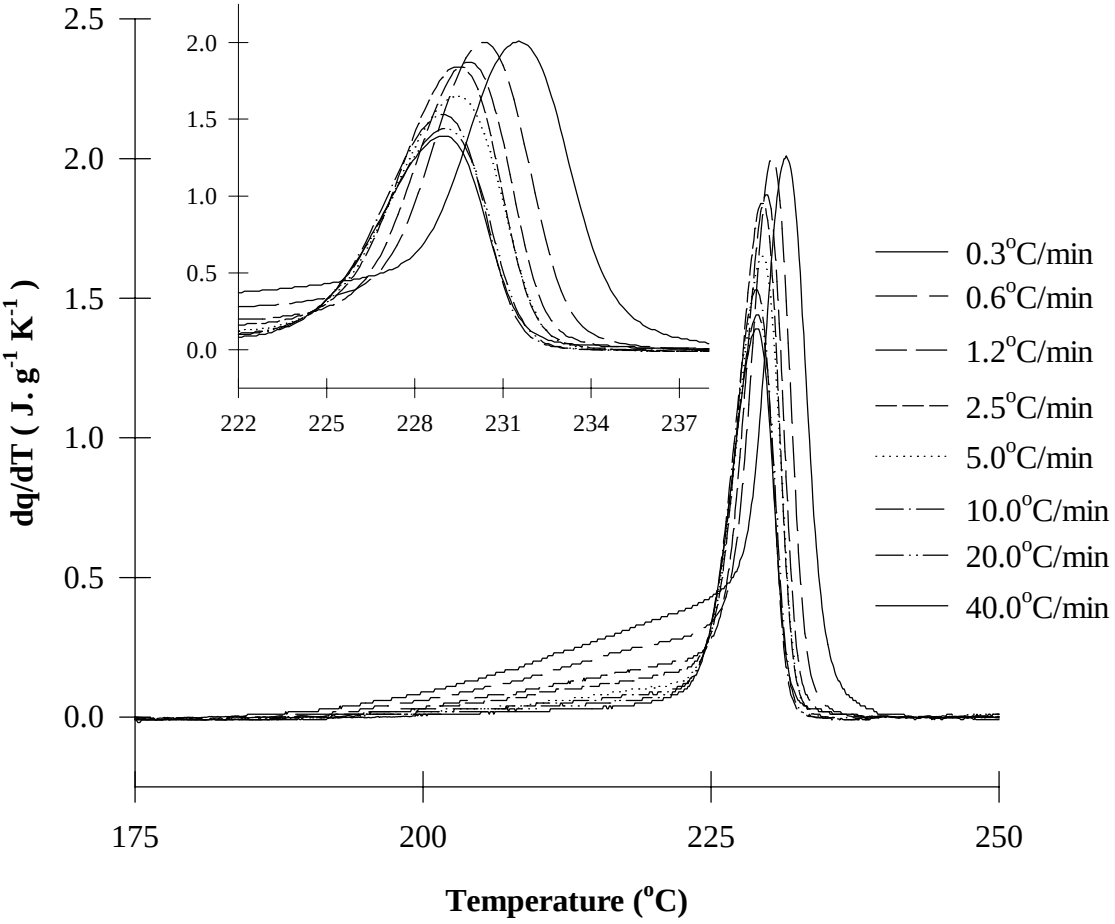

Figure 4.6 Effect of cooling rate on the melting behavior of PC-28K crystallized at 185°C from the glassy state for 202 hours, partially melted at 220°C, and subsequently cooled to 100°C at different rates.

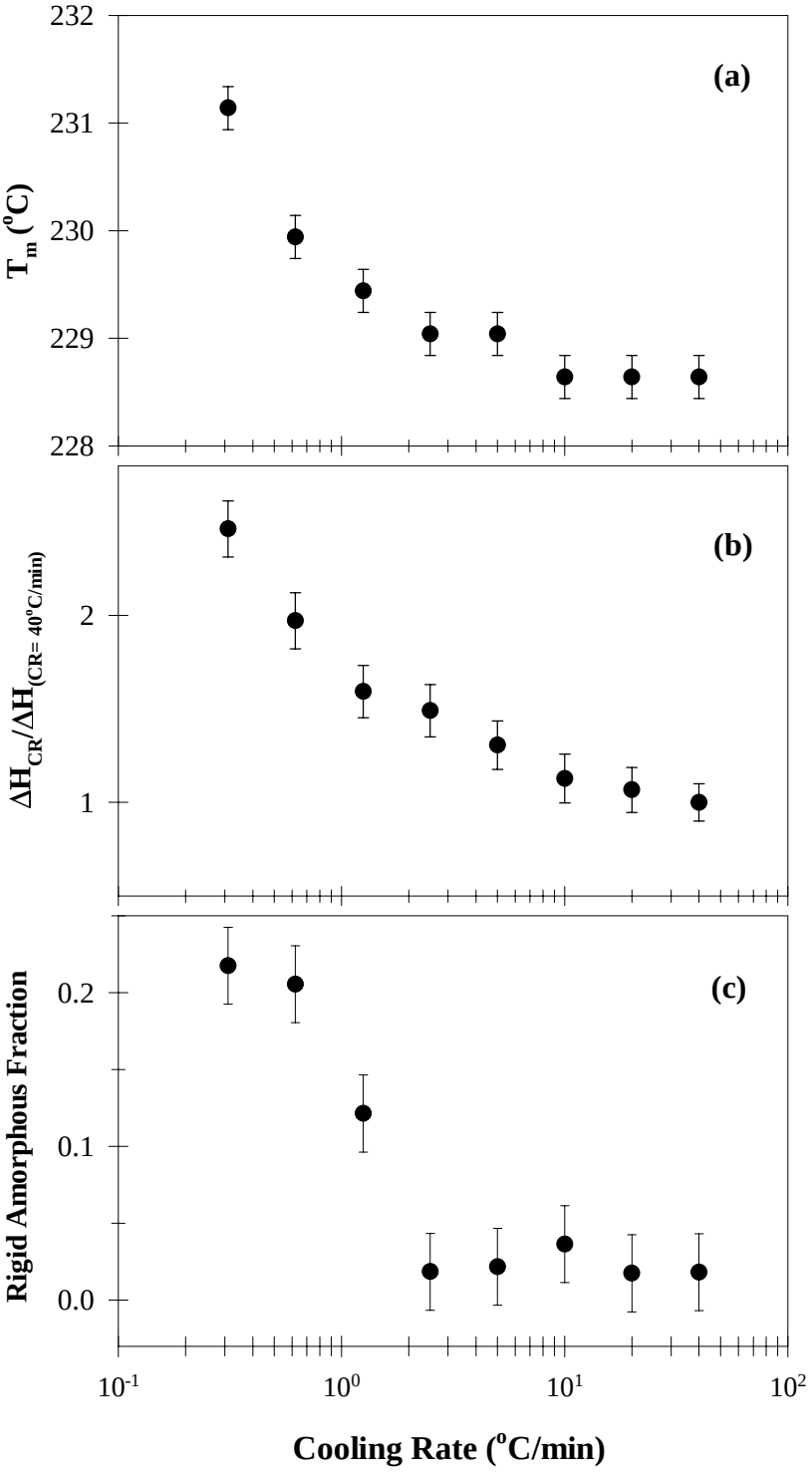

Figure 4.7 Analysis of cooling rate effect on the melting behavior of PC-28K, in terms of, a) peak melting temperature; b) heat of fusion; c) rigid amorphous fraction, all as a function of cooling rate (for detailed description of each analysis, see the text).

exceeds 2.5°C/min, the population of most stable lamellae does not change by partial melting at 220°C.

4.4.2 *Heating Rate Dependence of the Low Endotherm*

Secondary crystallization experiments were conducted on a series of partially melted PCs at different temperatures and times. After partial melting at 220°C, the samples were immediately fast cooled to a temperature T_x, where further secondary crystallization was allowed for a given time, t_x. The various experimental conditions for this secondary crystallization stage are detailed in Table 4.3. Note that in all cases, the temperature, T_x, associated with this second crystallization stage is below or equal to the original crystallization temperature. After partial melting at 220°C and subsequent quenching to secondary crystallization temperature (T_x) at or below the original crystallization temperature, the high endotherm does not change within the experimental time frame (see section 4.4.1 and Chapter 5). At T_x = 185°C, for example, up to 200 minutes, the high endotherm does not change appreciably (see Chapter 5). It can be, therefore, safely stated that *the morphological characteristics exhibited by primary crystals are not to be affected by the secondary crystallization process*. Upon reaching the desired time of secondary crystallization, the sample has been rapidly cooled to 100°C and subsequently reheated at different heating rates ranging from 5 to 20°C/min.

Figure 4.8 illustrates the melting traces of samples exposed to secondary crystallization at 175°C for 120 minutes (a), at 185°C for 40 minutes (b), and at 185°C for 120 minutes (c). As a base line before secondary crystallization, the melting endotherm of partially melted sample is plotted together (β= 10°C/min) for each sample. A comparison between samples with and without secondary crystallization (i.e., the melting

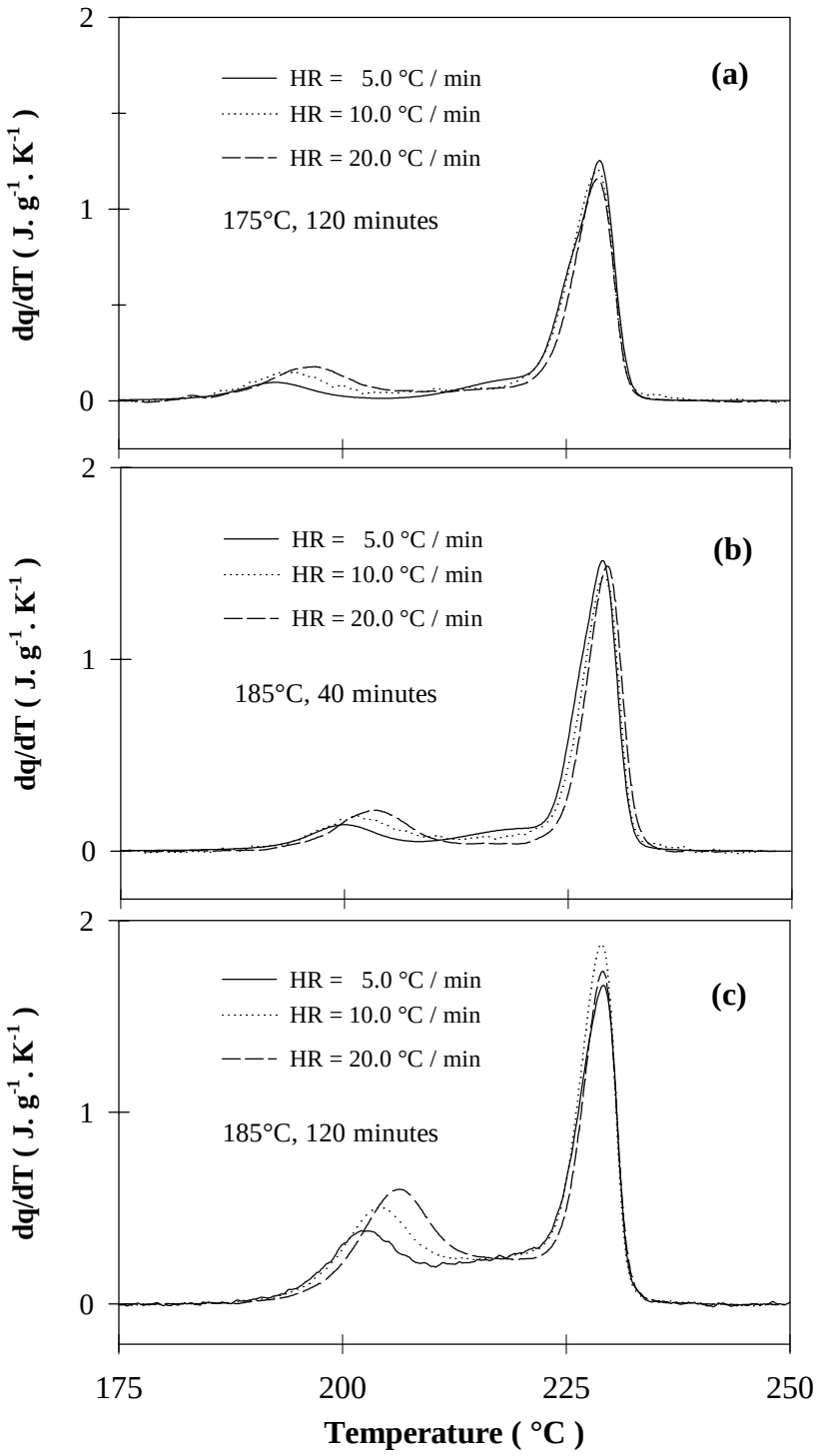

Figure 4.8 Effect of heating rate on the melting behavior of PC-28K crystallized at 185°C from the glassy state for 202 hours, partially melted at 220°C and further isothermally crystallized under various conditions: a) 175°C for 120 minutes; b) 185°C for 40 minutes; c) 185°C for 120 minutes.

Samples	Crystallization Conditions	$T_m^{low} = (T_m^{low})° + K\beta^{1/2}$	
		$(T_m^{low})°$	*K (±0.03)*
PC-28K	185°C, 202 hours	202.2	1.52
PM; PC-28K	SC:175°C, 120 minutes	189.7	1.50
	SC:185°C, 40 minutes	196.7	1.49
	SC:185°C, 120 minutes	199.2	1.56
PC-19K	170°C, 384 hours	189.9	1.50
PM; PC-19K	SC:170°C, 120 minutes	181.5	1.49
PC-4K	165°C, 38 hours	176.5	2.18

Table 4.3 Heating rate parameters for secondary crystallization under different conditions (PM: partial melting at 220°C for PC-28K and at 217°C for PC-19K; SC: secondary crystallization at the indicated temperature; β: heating rate in °C/min).

traces of partially melted sample) confirmed that both the location and the heat of fusion of the high endotherm are not affected by the second thermal treatment at or below original crystallization temperature, 185^{o}C, for a given time frame. However, secondary crystallization leads to the development of a low endotherm observed just above T_x. Furthermore, the low endotherm melting temperature increases continuously with heating rate.

In Figure 4.9, the low endotherm melting temperature, T_m^{low}, is plotted as a function of the square root of heating rate, $\beta^{½}$, for different secondary crystallization conditions. The use of this particular graphic representation is justified in the discussion section. In Figure 4.9, the data corresponding to the original sample crystallized at 185^{o}C for 202 hours are also included. In all cases T_m^{low} is found to increase linearly with $\beta^{½}$. Of more interest is that the slopes of the various T_m^{low} vs $\beta^{½}$ line are identical within experimental uncertainty (see Table 4.3, PC-28K exhibits an average slope of 1.52±0.03).

4.5 Discussion

Figures 4.3 and 4.4 contrast the effect of molar mass on the viability of the reorganization process. Low molar mass sample, most likely due to the increased chain mobility, exhibits a melting-recrystallization-remelting phenomenon, while higher molar mass sample does not. Of more importance, however, is that despite this possibility of reorganization in the neighborhood of high endotherm (i. e., melting of lamellar type crystals), low endotherm (i. e., melting of bundle-like crystals) exists independently. For example, in Figure 4.4, even when two higher endotherms are merged into a single peak due to a strong reorganization process, the low endotherm independently exists. This strongly suggests that the multiple melting behavior can not be entirely explained by the

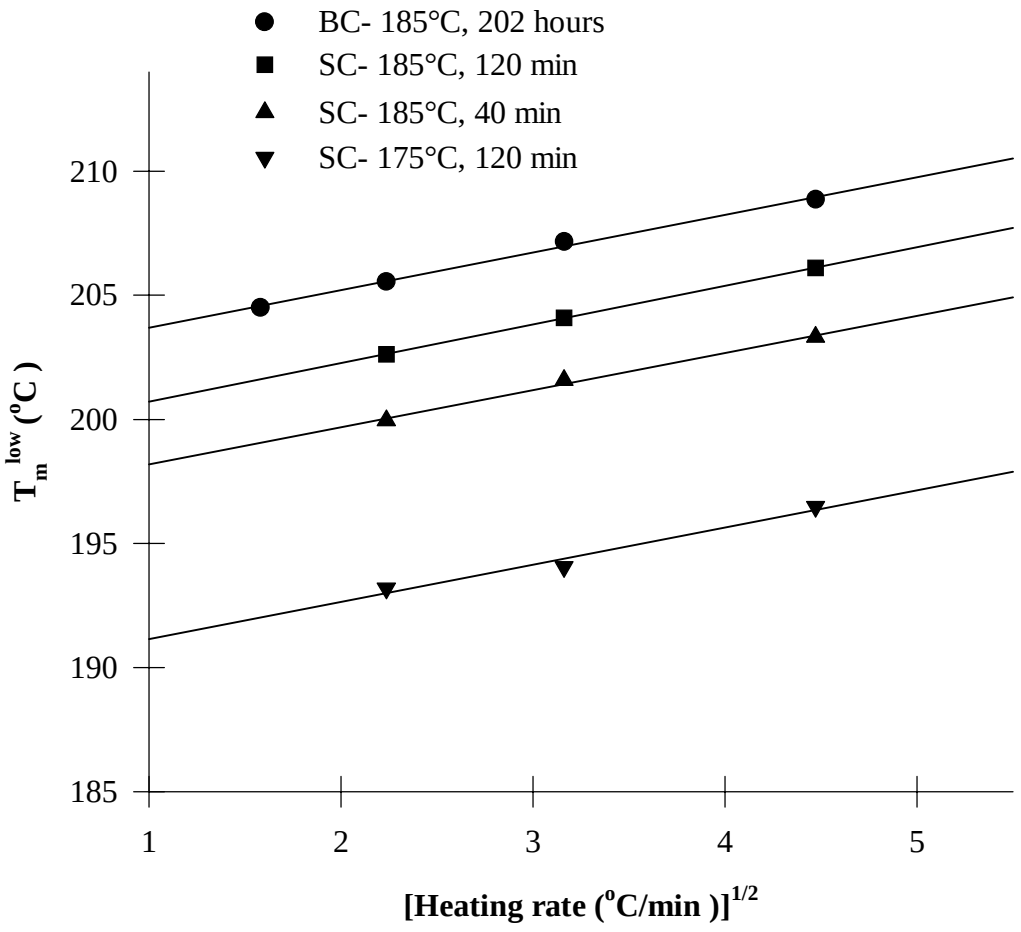

Figure 4.9 Effect of heating rate on the low endotherm location of PC-28K crystallized under various conditions (for detail, see Table 4.3).
(BC stands for bulk crystallization and SC, for secondary crystallization).
Temperature accuracy was better than 0.2°C

reorganization process, but the presence of a second type of crystals before the heating scan must be included for the proper interpretation.

The concept of the reorganization process is based on the thermal stability of preexisting crystals. After partial melting, only high endotherm is present and does not exhibit the characteristics of reorganization, mainly because these crystals have already achieved their maximum thermal stability* under a given crystallization condition. Comparing Figure 4.3 and 4.5, one can tell that the shoulder, located in between the high- and low endotherm, more than likely suffers reorganization, which can be understood from the viewpoint that these crystals will have a lower degree of perfection and thus be more vulnerable to reorganization upon heating.

However, the observations for higher molar mass PC materials– that partially melted samples exclusively exhibit the higher endothermic transition, and that identical peak temperatures are obtained for the high endotherm in the original and partially melted samples– lead to the conclusion that the multiple melting behavior is associated with the fusion of crystals exhibiting different morphologies and thermal stabilities. For high molar mass PC samples, the high endotherm does not arise from reorganization processes taking place during heating but is associated with the melting of primary (lamellar) crystals. For both high and low molar mass samples, the low endotherm is associated with the melting of crystals formed during secondary crystallization.

From Figure 4.6 and the analyses (Figure 4.7) of peak position (a), heat of fusion (b), and rigid amorphous fraction (c), it is clearly shown that cooling rate (β) is a crucial

---

* This maximum thermal stability does not mean they are the most stable crystals. In Chapter 6 an isothermal lamellar thickening will be presented and it will be shown that these crystals can also thicken if annealed at higher temperatures (> 208^{o}C) for relatively longer times (> 10 minutes).

variable in non-isothermal crystallization upon cooling: when β is equal to or greater than 2.5°C/min, crystallization during cooling can be virtually prevented, yet when β is smaller than that, non-isothermal crystallization occurs.

A close inspection of Figure 4.6 reveals that there exist at least two different types of recrystallization processes upon cooling. The first type is inferred from the long tail of the slowly cooled sample. The melting process of rapidly cooled samples after partial melting ($|\beta| \geq 10^{o}$C/min) occurs in a relatively narrow temperature range. In contrast, the onset of melting in samples cooled more slowly between 220°C and 100°C is observed at much lower temperatures. These observations indicate that during slow cooling ($|\beta| \leq 2.5^{o}$C/min) some of the PC chain segments are able to recrystallize and thus possibly form small relatively unstable crystals. Note that upon cooling an initially amorphous PC from the melt, even at cooling rates much lower than those used here, no perceptible crystallization occurs. This is due to the large induction period associated with the crystallization of PC from the free melt. However, in the presence of preexisting crystals (i.e., those left after partial melting), and possibly as a consequence of conformational constraints present in the residual amorphous fraction, the crystallization rate is noticeably enhanced. For these reasons, upon cooling small crystals may form at lower temperatures, a phenomenon that has been reported in the literature[35]. As noted earlier, these small crystals will impose constraints on the neighboring amorphous, which may be manifested by the increase of RAF with the decrease of cooling rates.

The second type of recrystallization upon cooling can be revealed in the shift of melting endotherm to higher temperatures with decreasing cooling rate. This may suggest either that isothermal lamellar thickening may be operative at temperatures in the

vicinity of 220°C or that some crystals form during cooling between 220°C and 185°C*. These crystals would be expected to be more stable than those formed during the initial crystallization at 185°C. However, in this case, the melting endotherm might be expected to exhibit multiple peaks or at least a high temperature shoulder. The observation of a single, relatively narrow endotherm may suggest that both processes (lamellar thickening and new crystal formation) may be at play. The occurrence of isothermal lamellar thickening will be further discussed in Chapter 6. Largely speaking, longer residence at temperature in the range 220°C-185°C during cooling leads to an increase in crystallinity and melting temperature. It needs to be emphasized, however, that such effects are only observed for very low cooling rates ($|\beta| \leq 2.5$°C/min).

The viability of reorganization processes in the high endotherm region is therefore a function of 1) *molar mass*, 2) *heating rate*, and 3) *cooling rate* in the presence of pre existing crystals. It has been mentioned earlier that the induction period for the crystallization of PC chain segments is much shorter when crystals are already present than when crystallization occurs from the pure melt. Studies of the effect of cooling rate after partial melting indicate that recrystallization can occur if sufficient time is allotted for this process ($|\beta| \leq 2.5$°C/min). This suggests that the rate of formation of new crystals is enhanced either first, when other crystals are already present or second, when previous melting has not led to a totally relaxed amorphous fraction. The reason for the second explanation is that during partial melting, chain segments in secondary crystals lose

---

* In Chapter 5, for the first detectable evolution of low endotherm upon secondary crystallization, which is in a sense melting of new crystals, it takes 5 and 1 minutes at 185°C and 195°C, respectively. The residence times between 220°C and 185°C and between 220°C and 195°C, at cooling rate of 2.5°C/min, are 14 and 10 minutes, respectively. These simple calculations may indicate that upon cooling there is indeed an ample time for the evolution of new crystals that are more stable than those formed by crystallization at 185°C between these temperature ranges.

crystallographic registration but cannot return to the random conformational state characteristic of the unconstrained melt. This is a direct consequence of both the rigid backbone structures of PC and the constraints exerted by the surrounding primary crystals. This lower conformational entropy, either from the preexisting crystals or from the constrained melt, is at the origin of both non-isothermal crystallization upon cooling and the much shorter induction time for secondary crystallization. Under both circumstances the energy barrier for crystal nucleation appears to be reduced. In the following chapter, where the kinetics of low endotherm is discussed, it is shown that the induction periods for the primary and secondary crystallization of PC-28K at 185^{o}C differ by more than two orders of magnitude (40 hours and 5 minutes, respectively).

On closer examination of Figure 4.8, it can be seen that at the lowest heating rate (5 °C/min), a small shoulder develops between the low and high endotherms. The overall enthalpy of fusion associated with the low endotherm and shoulder appears to remain independent of heating rate. This observation suggests that secondary crystals may undergo a small extent of reorganization by melting-recrystallization-remelting during slow heating. However, we emphasize that the extent of reorganization, as indicated by the enthalpy of fusion associated with the shoulder, is small and will not significantly affect the location of the low endotherm peak melting temperature. It needs to be also underlined that reorganization processes in the low endothermic region are not present for heating rates exceeding 10 °C/min. These latter observations provide additional and strong support for the claim that the low and high endotherms are associated with the melting of two different morphological entities. These results also suggest that temperature modulated DSC may not be the most appropriate tool to investigate the

melting behavior of as-formed secondary crystals since this technique relies on the use of very low heating rates, at which reorganization processes can become significant.

In Figure 4.9, it needs to be acknowledged that the upward shift of the low endotherm with increasing heating rate is consistent with the occurrence of the reorganization process during heating. It is important, however, to recognize that a constant value for the slopes of T_m^{low} vs $\beta^{½}$ lines is incompatible with the account of the multiple melting behavior by a melting-recrystallization-remelting process. This, the same dependence of melting temperature on heating rate, is displayed for crystals exhibiting intrinsically different thermal stabilities. For instance, the same slope of T_m^{low} vs $\beta^{½}$ is observed for crystals formed at 185^{o}C over the period of 202 hours (more stable), and for crystals formed at 175^{o}C for 2 hours (less stable). Such behavior is, once again, inconsistent with expectations for the melting-recrystallization-remelting phenomenon.

A clue for the origin of the heating rate dependence of the low endotherm melting temperature is obtained from the linearity of T_m^{low} vs $\beta^{½}$ plots after thermal lag correction. This observed behavior has been shown to be a characteristic of superheated crystals[27]. Superheating is a term used to describe the melting of a crystal at temperatures above that expected from equilibrium considerations. To obtain the linear dependence between T_m^{low} and $\beta^{½}$, the rate of melting is assumed to be a linear function of the degree of superheating. Using temperature modulated differential scanning calorimetry, Toda *et al.*[40] recently showed that the hypothesis of a linear dependence of the rate of melting on superheating maybe oversimplified. According to Toda *et al.*[40], a rate of melting proportional to ΔT^{y} leads to a linear variation of the degree of superheating with $\beta^{1/(1+y)}$.

At this point, it is not possible for us to accurately determine the value of y. However, a value of y in the vicinity of 0.5 yields an acceptable fit to our experimental data.

In polymeric materials, two types of crystal morphologies lend themselves to superheating[27]. First, large crystals, such as polyethylene or polytetrafluoroethylene extended chain crystals, exhibit superheating due to the slow kinetics of melting from the surface to core. Second, metastable crystals with conformationally constrained interfacial chains, such as tie chains or loose loops, will also reduce the entropy of fusion upon melting (i.e., superheating). The increase in the melting temperature of secondary crystals with heating rate, in this study, is most likely associated with the latter case- the reduction of entropy of fusion upon melting*. Such reduction in entropy of fusion has already been discussed by Wunderlich[27] and Zachmann[34] in the context of fringed micellar structures.

As will be further discussed in the following chapter and as has been discussed in the previous publications[38,39], the low endotherm in many semicrystalline polymers, including PC, is associated with the melting of bundle-like or fringed micellar secondary crystals. The profound effect of these bundle-like small crystals is to increase the level of conformational constraints, thus leading to a reduction in the conformational entropy of the remaining amorphous phase. In support of this point of view, both the glass

---

* Thermodynamically equilibrium melting temperature, T_m^o, is defined as $T_m^o = \Delta H_m^o / \Delta S_m^o$, where ΔH_m^o and ΔS_m^o are the equilibrium heat of fusion and entropy change upon melting, respectively. This simple equation tells us that for the increase of melting temperature, any material system can take two different routes: first the *increase of heat of fusion* by either large crystal formation or crystal perfectioning, and second, *the decrease of conformational entropy*. In the particular case of bundle-like crystal formation, for the explanation of the increase of low endotherm melting temperature with heating rate (Chapter 4), time (Chapter 5) or possibly with frequency, the second mechanism seems more feasible, at least partly, considering the constrained environments. Nonetheless, the first possibility can not be completely ruled out. This will be further discussed in Chapter 7.

transition and the low endotherm melting temperatures are found to shift to higher temperatures with increasing secondary crystallization time. This will be further discussed in Chapter 7. Theoretical support for this idea has recently been obtained from thermodynamic correlation between the temporal evolution of the melting temperature of secondary crystals and that of the glass transition temperature of the residual amorphous fraction[41]. This thermodynamic model was successfully applied to experimental data on it-PS, PEEK and PET. The above arguments suggest that the shift of the low endotherm to a higher temperature with increasing heating rate is compatible with superheating of metastable fringed-micellar crystals.

As a last discussion supporting the applicability of superheating concepts in the case of secondary crystals, one can compare the degree of superheating, defined as the difference between the melting temperature at that heating rate, T_m^{low}, and the equilibrium or zero entropy production melting temperature of that crystal, $(T_m^{low})^o$, thus $T_m^{low}-(T_m^{low})^o$. Examination of Table 4.3 indicates that the slope K, which is directly related to the degree of superheating, is considerably larger for PC-4K than for the other two samples. In a parallel study, it has been found that the rate of shift of the low endotherm with secondary crystallization time is significantly larger for PC-4K than for PC-19K and PC-28K[39]. Studies of narrow molar mass fractions indicate that this difference is not associated with the broader molar mass distribution. These results will be further discussed in the next chapter. The increase in both the superheating effects and the rate of shift of low endotherm melting temperature with secondary crystallization time for low molar mass materials is likely explained by the increase in crystallinity and the increase of conformational constraints in the residual amorphous fraction with

decreasing molar mass. In support of this interpretation, in this study, the rigid amorphous fraction (RAF) has been calculated for different molar mass semicrystalline PC samples (see Chapter 7). The interesting result is that low molar mass fraction clearly has a higher degree of RAF compared with higher molar mass samples. A similar conclusion has been drawn by Cebe *et al.*, in the study of poly(phenylene sulfide)[42].

4.6 Conclusions

Studies of the heating rate dependence of the melting behavior of semicrystalline bisphenol-A polycarbonate of various molar mass indicate that the high and low endothermic regions are associated with the melting of primary (chain folded lamellae) and secondary crystals (bundle-like or fringed micellar type), respectively. No reorganization effects during heating are observed for PC-19K and PC-28K in the usual range of heating rate ($\beta \geq 2.5^{o}$C/min). In contrast, the lower molar mass material, PC-4K, exhibits a melting-recrystallization-remelting process during heating. This reorganization process, which is mediated by the higher mobility, and thus higher recrystallization rate of the shorter chain length polymer, however, only affects the shape of the high endothermic region. The observed upward shift of the low endotherm with increasing heating rate is explained by superheating effects and is fully consistent with the notion that amorphous chains in the vicinity of secondary crystals are conformationally constrained and these constraints cannot fully relax upon melting of the secondary crystals.

References

1. G. Groeninckx, H. Reynaers, H. Berghmans, G. Smets, *J. Polym. Sci. Polym Phys*., **1980**, *18*, 1311; G. Groeninckx, H. Reynaers, *J. Polym. Sci. Polym Phys*., **1980**, *18*, 1325.
2. P. J. Holdsworth, A. Tuner-Jones, *Polymer*, **1971**, *12*, 195.
3. C. Zhou, S. B. Clough, *Polym. Eng. Sci*., **1988**, *28*, 65.
4. S. B. Lin, J. L. Koenig, , *J. Polym Sci. Polym. Symp*., **1984**, *71*, 121.
5. S. Z. D. Cheng, R. Pan, B. Wunderlich, *Macromol. Chem*., **1988**, *189*, 2443.
6. S. Z. D. Cheng, M. Y. Cao, B. Wunderlich, *Macromolecules*, **1986**, *19*, 1868.
7. P. Cebe, S.-D. Hong, *Polymer*, **1986**, *27*, 1183.
8. M. P. Lattimer, J. K. Hobs, M. J. Hill, P. J. Barham, *Polymer*, **1992**, *33*, 3971.
9. B. S. Hsiao, K. H. Gardner, D. Q. Wu, B. Chu, *Polymer*, **1993**, *34*, 3986; B. S. Hsiao, K. H. Gardner, D. Q. Wu, B. Chu, *Polymer*, **1993**, *34*, 3996.
10. D. J. Blundell, B. N. Osborn, *Polymer*, **1983**, *24*, 953.
11. Y. Lee, R. S. Porter, *Macromolecules*, **1992**, *25*, 1731.
12. A. J. Lovinger, S. D. Hudson, D. D. Davis, *Macromolecules*, **1992**, *25*, 1752.
13. H. Marand, A. Prasad, *Macromolecules*, **1992**, *25*, 1731; H. Marand, A. Alizadeh, R. Farmer, R. Desai, V. Velikov, *Macromolecules*, in press
14. S. Z. D. Cheng, Z. Q. Wu, B. Wunderlich, *Macromolecules*, **1987**, *20*, 2802.
15. S. X. Lu, P. Cebe, M. Capel, *Macromolecules*, **1997**, *30*, 6243.
16. S. X. Lu, P. Cebe, *Polymer*, **1996**, *37*, 4857.
17. J. S. Chung, P. Cebe, *Polymer*, **1992**, *33*, 2325.
18. P. J. Lemstra, T. Kooistra, G. Challa, *J. Polym. Sci*. Part A-2, **1972**, *10*, 823; P. J. Lemstra, A. J. Schouten, G. Challa, *J. Polym. Sci*. *Polym Phys*., **1974**, *12*, 1565.
19. Z. Pelzbauer, R. St. J. Manley, *J. Macromol. Sci- Phys*, **1973**, *B7*, 345.
20. J. Vivirito, H. D. Iler, H. Marand, unpublished results.
21. P. Weigel, R. Hirte, C. Ruscher, *Faserforsch. Textiletech*., **1974**, *25*, 283.
22. J. P. Bell, P. E. Slade,J. H. Dumbleton, *J. Polym. Sci*. Part A-2, **1968**, *6*, 1773.
23. F. Shuren, Z. Guanguha, T Qun, Y. Yuqin, *J. Thermal Anal*., **1993**, *39*, 875.
24. A. Alizadeh,L. Richardson, S. McCartney, H. Marand, *Macromolecules*, **1999**, *32*, 6221; *Bull.Am. Phys. Soc*., **1999**, *44*(1), 1562.

25. R. Bonart, *Makromol. Chem*., **1966**, *92*, 149.
26. P. B. Rim, J. P. Runt, *Macromolecules*, **1984**, *17*, 1520.
27. B. Wunderlich, " Macromolecular Physics", **1976**, Academic Press, New York, Vol3.
28. A. Gray, "Analytical Chemistry", **1963**, Plenum Press, New York, Vol. 1, p 322,.
29. V. Berstein, V. M. Ergov, in "Differential Scanning Calorimetry of Polymers: Physics, Chemistry, Analysis, Technology", **1994**, Ellis Horwood, U. K.
30. L. Judovits, J. D. Menczel, A. G. Leray, *J. Thermal Anal*., **1998**, *54*, 605.
31. B. Falkai, W. Rellensmann, *Makromolekular Chem*., **1964**, *75*, 112.
32. G. Kämpf, *Kolloid-Zeitschrift*, **1960**, *172*, 50.
33. Hermann Schnell, "Chemistry and Physics of Polycarbonates", **1964**, John Wiley & Sons, Inc.
34. H. G. Zachmann, A. Peterlin, *J. Macromol. Sci. Phys*., **1969**, *B3(3)*, 495.
35. G. Mendez, A. J. Müller, *J. Thermal Anal*., **1997**, *50*, 593.
36. S. Sohn, A. Alizadeh, H. Marand, *Polymer* in print.
37. J. E. K. Schawe, G. R. Strobl, *Polymer*, **1998**, *39*, 3745.
38. S. Sohn, A. Alizadeh, H. Marand, L. C. Shank, H. D. Iler, *American Chemical Soc. Polym. Preprint*, **1999**, *81*, 250.
39. A. Alizadeh, S. Sohn, L. C. Shank, H. D. Iler, H. Marand, submitted to *Macromolecules*.
40. A. Toda, T. Oda, C. Tomita, M. Hikosaka, T. Arita, Y. Saruyama, *Proc. Am. Chem. Soc. Polym. Div*., **1999**, *81*, 236.
41. H. Marand, A. Alizadeh, in preparation
42. S. X. Lu, P. Cebe, M. Capel, *Macromolecules*, **1997**, *30*, 6243.

Chapter 5

Primary and Secondary Crystallization Kinetics of PC

5.1 Introduction

The origin of multiple melting behavior in PC was discussed in the previous chapter. In summary, the high endotherm could not be explained solely by the reorganization process (melting-recrystallization-remelting) of pre-existing crystals, but required the existence of two different crystal populations with different thermal stabilities. More specifically, at moderate heating rate ($\beta > 2.5^{o}C$/min), the multiple melting endotherm could be explained by the melting of primary chain-folded lamellar crystals and secondary bundle-like crystals, which correspond to the high and low melting endotherms, respectively.

The distinct advantage offered by PC is the absence of crystallization during sufficiently fast cooling after partial melting (see Figures 4.6 and 4.7). Therefore, partially melted samples exhibiting solely high endotherm can be used to study the secondary crystallization behavior, *independently*. This unique feature of semicrystalline PC provides an excellent opportunity to pursue the precise secondary crystallization kinetics without further complications arising from the non-isothermal crystallization upon cooling. This potential problem has been noted in the previous study of PEEK[1].

An understanding of overall crystallization kinetics of PC crystallized from the glassy state is necessary for the study of secondary crystallization kinetics. However, to our knowledge, only very few publications have addressed the kinetics of crystallization of PC from the bulk [2-5]; furthermore, studies of the effect of molar mass on the kinetics of bulk crystallization of PC are even more scarce[5]. To address these issues properly, the

overall crystallization kinetics of PC crystallized from the glassy state as a function of temperature and molar mass will be presented before the secondary crystallization kinetics study. In addition, a morphology study in the stage of primary crystallization will also be offered.

The results and the discussion sections are presented in two main parts that cover the effects of molar mass, molar mass distribution, and temperature on 1) the overall kinetics of crystallization, and 2) the secondary crystallization kinetics. In the discussion section, the results are examined in the context of the conceptual secondary crystallization model that has been proposed from the studies of PEEK[1] and ethylene/octene copolymer[6].

5.2 Experimental

The purified commercial bisphenol-A polycarbonate samples and some fractions were used for this study. Details of experimental procedures for purification and fractionation processes and molecular characterizations are given in Chapter 3. Sample preparation and a general description of DSC experiments are described in Chapter 3 and 4. However, when necessary, specific experimental procedures are given before presenting the results. This section offers, first, the description of quantitative analysis of DSC melting traces upon secondary crystallization, and second, the detailed experimental methods for the morphology study using atomic force microscopy (AFM) and polarizing optical microscopy (OM). For general descriptions of AFM and OM, refer to Chapter 3.

5.2.1 *Quantitative Analysis of DSC Melting Traces*

For the study of secondary crystallization kinetics, the peak melting temperature and the heat of fusion associated with the low endotherm must be quantitatively

determined. For this purpose, peak-fitting method (peak fit software, Jandel Scientific Co.) was used to analyze the low endotherm in the DSC melting traces. In Figure 5.1, a typical example is illustrated. In this particular case, PC-28K sample was cold-crystallized at 185^{o}C for 202 hours, partially melted at 220^{o}C, and subsequently exposed to secondary crystallization at 185^{o}C for 40 minutes.

To achieve reliable and consistent results, the following criteria have been applied. The overall multiple melting endotherms are divided into three parts: high, intermediate (shoulder), and low endotherms. To fit each of these endotherms, a total of five curves was necessary; among those, three were for the high endotherm, and one for the intermediate endotherm. For the fitting of low endotherm, which is the main interest of this analysis, a single curve was used. Symmetric Gaussian function was used to generate these curves, and, more importantly, the mathematical shape of each curve was not changed throughout the analysis. In the analysis of the evolution of low endotherm with different secondary crystallization time and temperature, the position, height, and width of low- and intermediate endotherm fitting curves were changed but not those for high endotherms. This was possible because 1) *upon cooling after partial melting, no further crystallization occurs*, and thus the shape and the magnitude of high endotherm do not change; and 2*) upon secondary crystallization performed at or below the primary crystallization temperature, the growth of the high endotherm was significantly slow*, and thus further modification of fitting curves for the high endotherm was not necessary. These distinct advantages of PC provided us with reliable and reproducible low endotherm analysis, especially when the development of shoulder is insignificant. At either longer crystallization times or high temperature due to the broad overlap of low

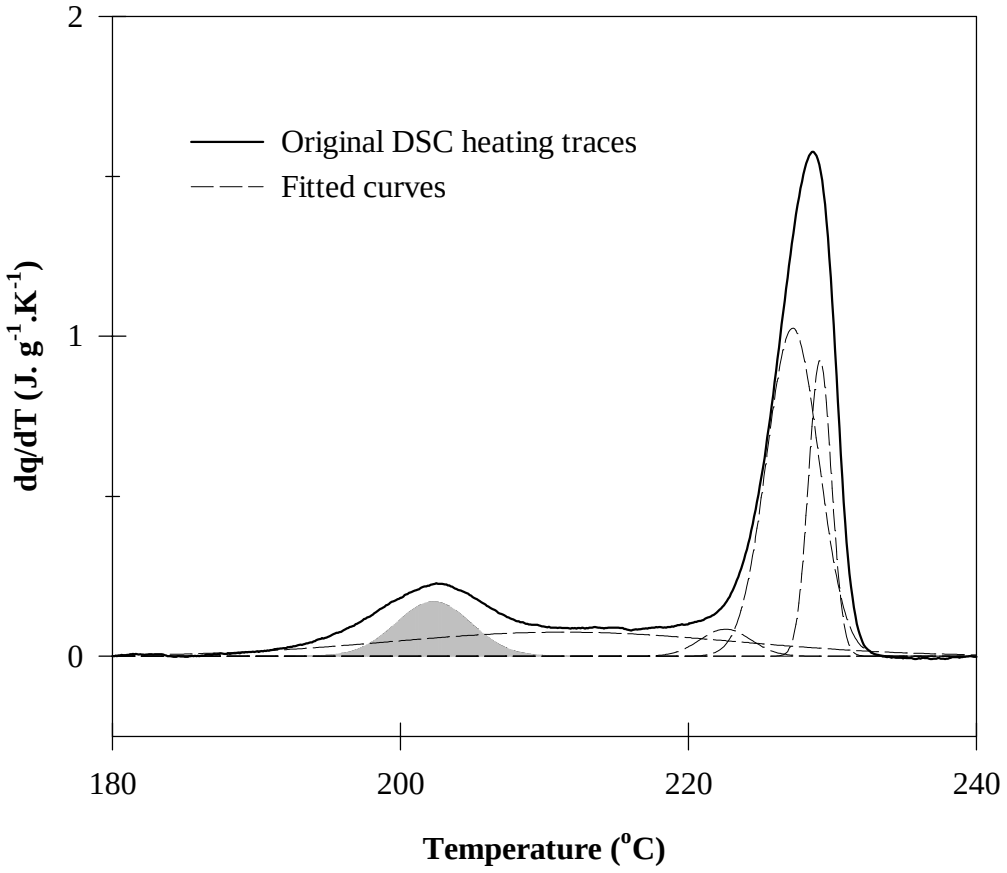

Figure 5.1 A typical example of curve fitting in DSC melting traces. The dark area designates the low endotherm developed during the secondary crystallization. PC-28K sample was initially crystallized at 185°C for 202 hours, partially melted at 220°C and exposed to secondary crystallization at 185°C for 40 minutes.

endotherm with shoulder, the analysis was inevitably subjected to relatively large uncertainty. Nonetheless, in the determination of the early stage low endotherm heat of fusion, this uncertainty was insignificant because the low endotherms could be clearly resolved. Lastly, the melting peak position of low endotherm was determined from the fitted curve.

5.2.2 *Atomic Force Microscopy*

An atomic force microscope (AFM: Digital Instrument, Dimension 3000) was operated in tapping mode at room temperature using nanosensor TESP (tapping etched silicon probe) type single beam cantilevers. Compression moulded PC samples were crystallized from the bulk inside the oven (temperature fluctuation $< \pm 0.3^{o}C$) for different conditions: PC-28K at $185^{o}C$ for 96 hours, and PC-4K at $165^{o}C$ for 6 hours. Before crystallization, all samples were preheated at $310^{o}C$ for 5 minutes to remove potential nuclei. The free surfaces of crystallized samples were examined under AFM. Images were collected in both height and phase modes.

5.2.3 *Optical Microscopy*

As will be discussed in the results section, AFM images clearly show the spherulitic structure of PC upon crystallization. However, the macroscopic size of those spherulites are in the range of 5 to 10 microns, which is too small to resolve clearly under a conventional optical microscope. To enhance the visibility of spherulites, thin film (~1 μm) was solvent cast on a glass substrate and crystallized. Although solvent (HPLC grade $CHCl_3$) must be used to cast thin film, the method of crystallization used in this study is different from the widely used solvent induced crystallization (SINC) technique because of the following procedures. After solvent casting on clean glass, the film was

subsequently dried at 150°C, slightly above the glass transition of PC and well above the boiling point of chloroform (61-62°C) for a period of 24 hours to remove the residual solvent. It needs to be noted that at this drying stage, no crystallization was induced. This completely "dry" thin film was first preheated at 310°C for 5 minutes to remove potential nuclei, and then further crystallized at 185°C for 250 hours inside an oven in a dry nitrogen atmosphere. Subsequently, the morphology of this sample was examined using the polarizing optical microscope.

5.3 Results

5.3.1 *Overall Kinetics of Crystallization*

5.3.1.1 *The Effect of Molar mass*

In Figure 5.2, the melting traces of PC-28K crystallized at 185°C for different periods of time are displayed. PC-28K exhibits a multiple melting behavior upon heating subsequent to isothermal crystallization at 185°C. While the location of the higher melting endotherm is independent of crystallization time, the melting temperature associated with the lower endotherm continuously shifts to higher values with increasing crystallization time. The total enthalpy of fusion (including both the low and the high endotherms), ΔH_m^{total}, was determined for each crystallization time from the area under the DSC curve between the fixed limits of 160°C and 250°C. The insert in Figure 5.2 shows the variation of ΔH_m^{total} with time for PC-28K crystallized at 185°C. Note that a significant induction period (≈ 40-50 hours) is required for the detection of the first sign of crystallinity at this temperature (see the footnote in page 119).

To see the effect of molar mass on the overall crystallization kinetics, the above crystallization procedures were repeated for several PC fractions, and the result is

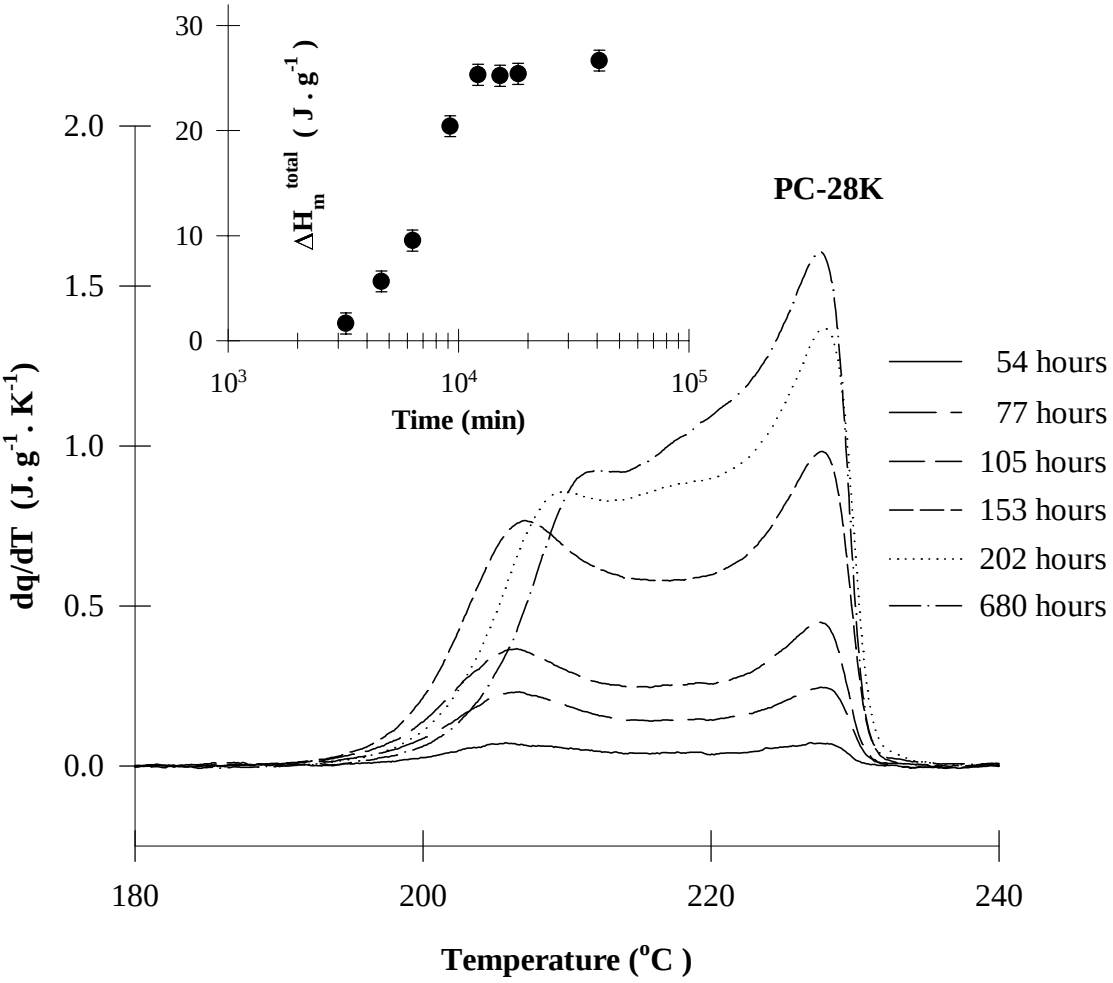

Figure 5.2 Heating traces (HR = 10°C/min) of PC-28K crystallized at 185°C for various times. Inset shows the corresponding temporal evolution of total heat of fusion.

depicted in Figure 5.4. For brevity reason, DSC melting traces are omitted for these fractions; however, the general features are strikingly similar: time independent peak position of high endotherms and strong time dependent shift of low endotherms (for instance, in case of PC-4K, see Figure 4.4, HR = 10^{o}C/min). Note that all samples were crystallized at the same undercooling ($\Delta T = T_m^{o}-T_x$), assuming the variation of equilibrium melting temperature,T_m^{o}, is not significant with molar mass distribution. It is clearly shown that the induction period dramatically increases and the maximum apparent heat of fusion decreases, with molar mass.

From Figure 5.4, we can define the half-time of crystallization ($t_{½}$), the time elapsed to reach 50% of the maximum apparent heat of fusion for a given temperature. The result is presented in Figure 5.5, in which available literature data are also included[2,5,7,8]. The literature data were carefully selected only for PCs crystallized from the bulk at the same temperature as used in the present study. $t_{½}$ exhibits a strong molar mass dependence showing more than two orders of magnitude change for a range of molar masses between *ca*. 4,300 and 67,000 g.mol^{-1}. It is also noteworthy that molar mass distribution strongly affects the $t_{½}$. Fractions crystallize slower than commercial materials for a similar molar mass. For instance PC-30K fraction, even after crystallization for 450 hours at 190^{o}C, only showed *ca*. 1% crystallinity, whereas similar molar mass commercial sample already reached their apparent maximum heat of fusion at

---

Due to the necessity of long time annealing at relatively high temperature, thermal degradation might occur during crystallization, although throughout the experiments samples were crystallized in an inert atmosphere. The variation of molar mass distribution in PC-28K samples was regularly checked during crystallization at 185^{o}C, and the results are summarized in Figure 5.3. In Figure 5.3, GPC traces of previous thermal treatments are included for a comparison reason. As clearly seen, within experimental uncertainty, the variation of molar mass distribution was insignificant during crystallization at 185^{o}C up to 300 hours.

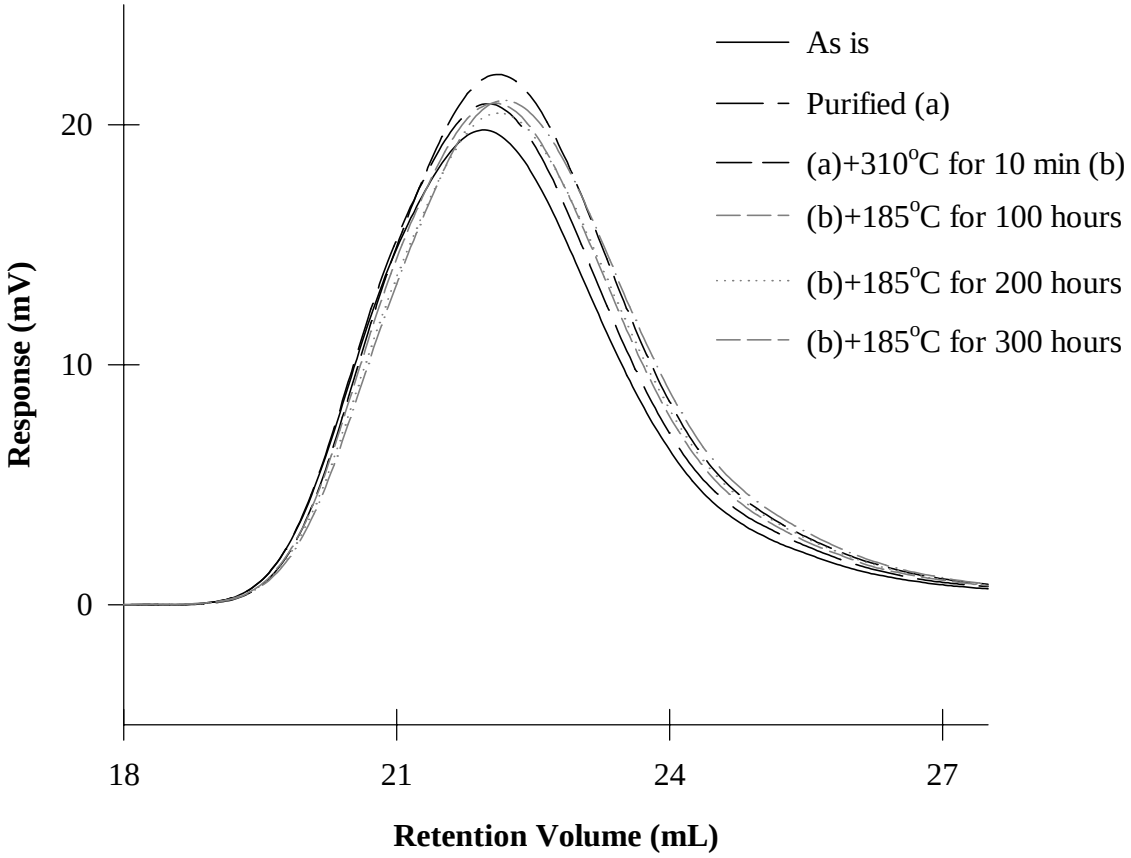

Figure 5.3 GPC traces of PC-28K samples after crystallization at 185°C for various times. For comparison reason GPC traces of previous thermal treatments are included.
(see the footnote in previous page)

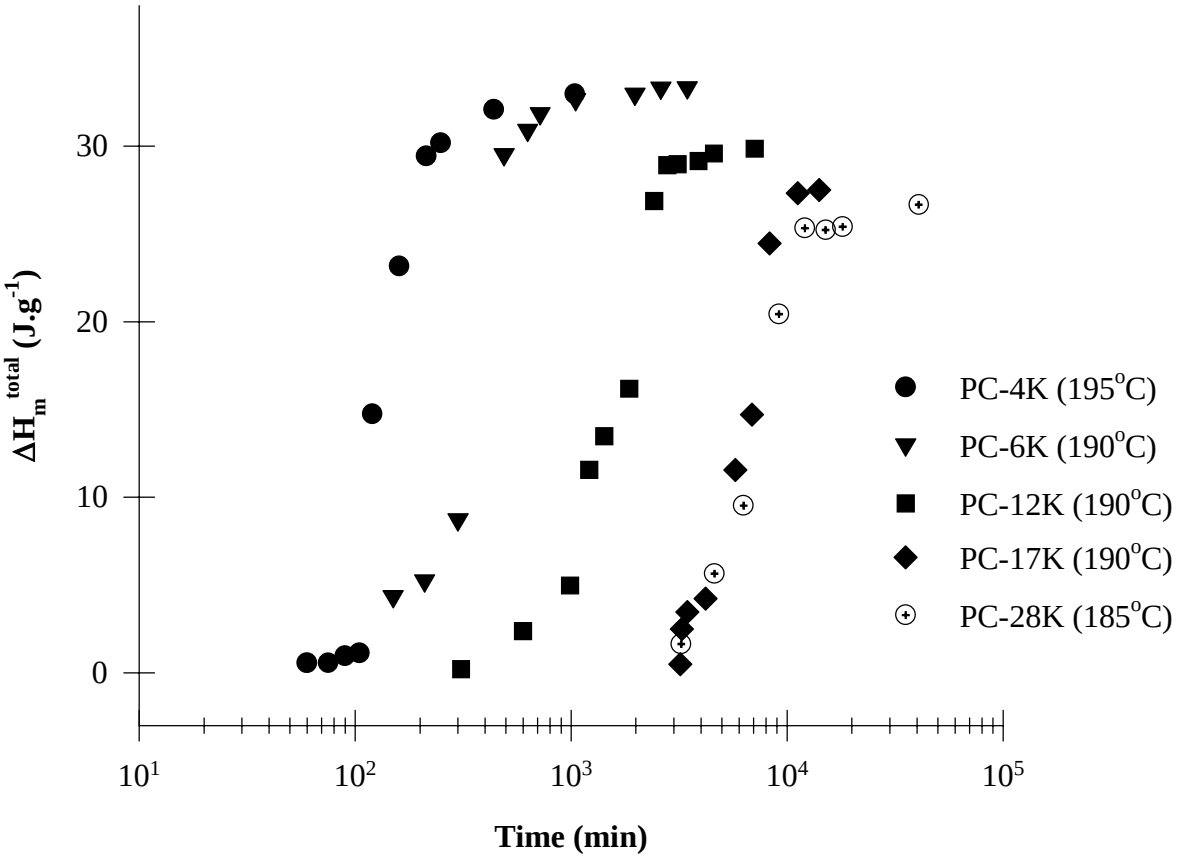

Figure 5.4 Temporal evolution of the total heat of fusion of fractions (filled symbols) and commercial (crossed symbol) PC samples of varying molar mass.

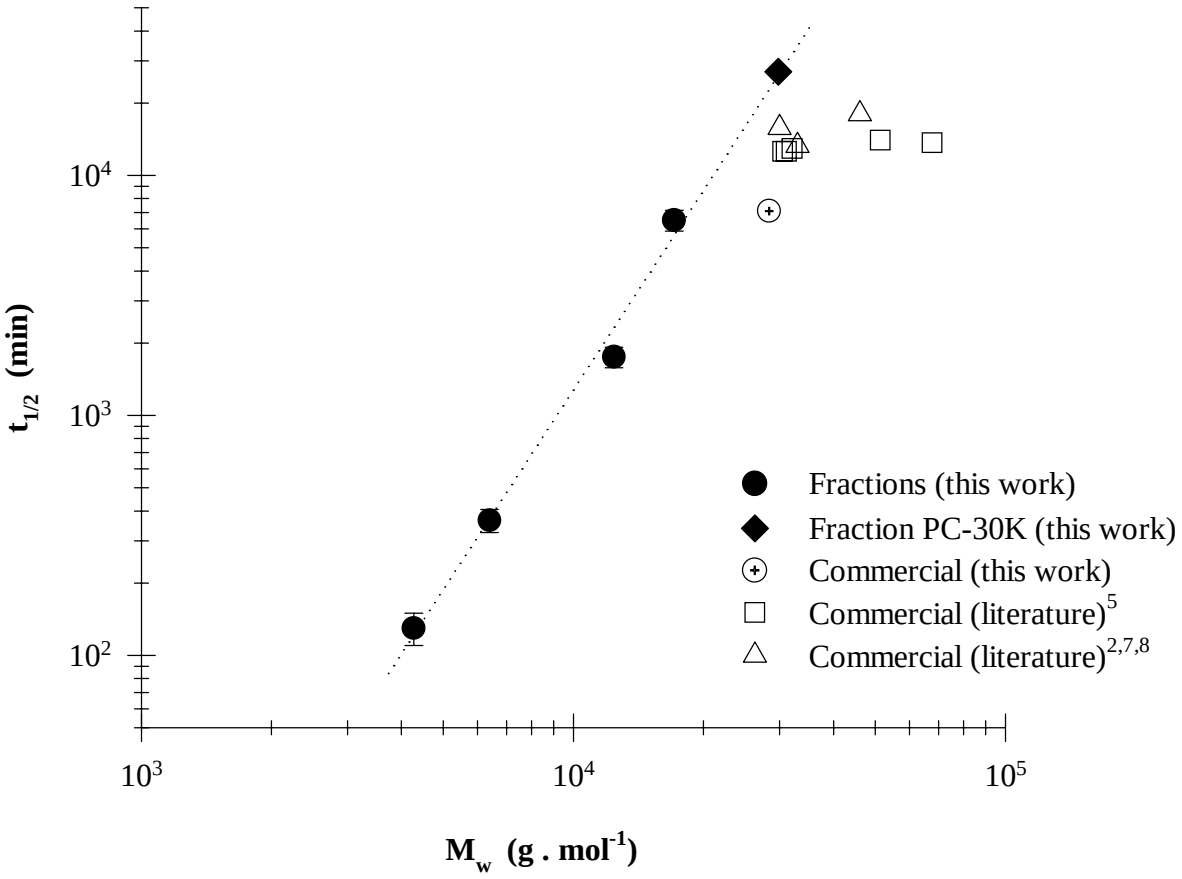

Figure 5.5 Variation of the half-time of crystallization of fractions and commercial PC samples as a function of weight average molar mass. Closed diamond symbol shows the time elapsed to develop *ca*. 1% crystallinity in case of PC-30K fraction crystallized at 190^{o}C.

this temperature and time.

5.3.1.2 *The Effect of Crystallization Temperature*

We first address the effect of temperature on the crystallization kinetics of PC-4K. This fraction was crystallized at five different temperatures between 155°C and 210°C for different times. Figure 5.6 shows the temporal evolution of ΔH_m^{total} for PC-4K at these crystallization temperatures. As expected, ΔH_m^{total} increases steeply after some induction period and finally reaches an apparent plateau at the longest crystallization times. In the range of temperatures investigated, this plateau is virtually independent of crystallization temperature.

The above procedures were repeated for other fractions, and the results were analyzed in terms of the variation of $t_{½}$ as functions of both crystallization temperature and molar mass (see Figure 5.7). PC of M_w = 46,000 g.mol^{-1} (PC-46K) using volumetric data reported in the literature[8] was included in Figure 5.7. We note that $t_{1/2}$'s differ by more than two orders of magnitude between PC-4K and PC-46K, as similarly seen Figure 5.5. Of more interest, we also note that $t_{½}$ exhibits a minimum around T_x = 186°C for the low molar mass fraction (PC-4K), and in the vicinity of 190°C for PC-46K commercial sample. This observation may lead to the conclusion that in the case of bulk-crystallized PC, regardless of molar mass the maximum crystallization rate occurs approximately at 190^{o}C. Similar conclusions have been drawn from the studies of PPS[9] and PEEK[10,11] fractions. Due to the limited amount of material for each fraction, except for PC-4K, the exact shape of the variation of $t_{½}$ for other fractions can not be rigorously determined, although it is apparent that crystallization around 190^{o}C occurs faster than crystallization

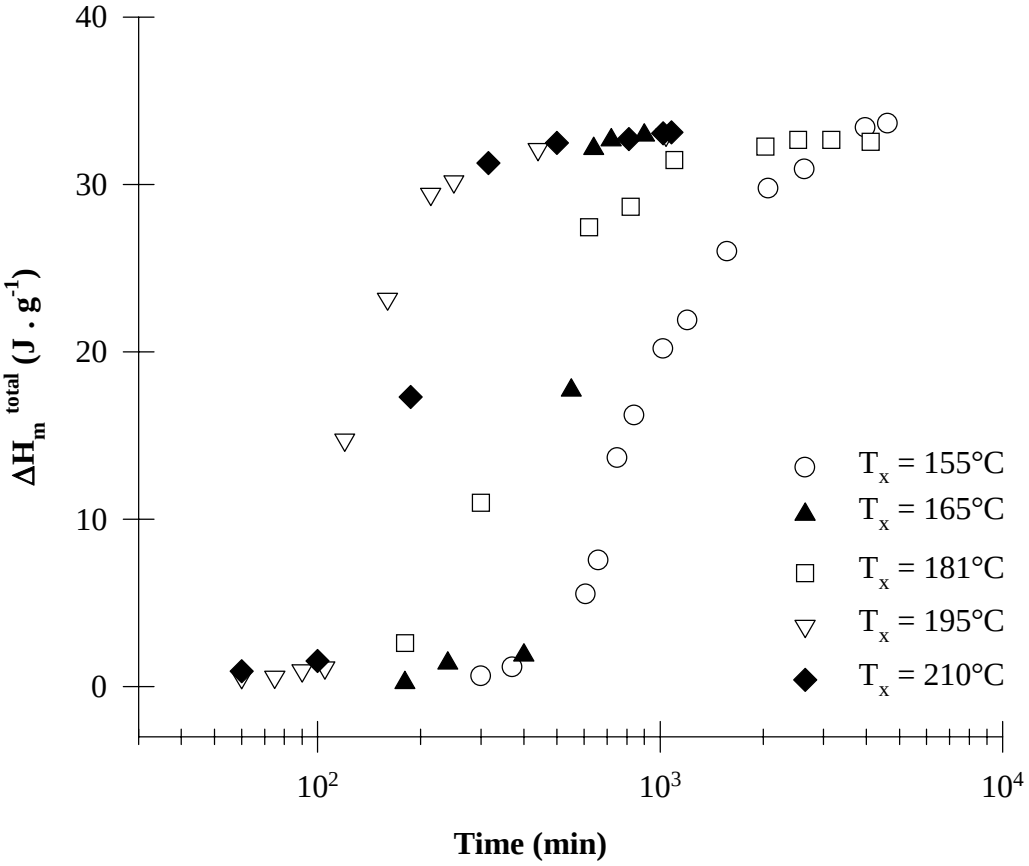

Figure 5.6 Temporal evolution of the total heat of fusion of PC-4K for different crystallization temperatures.

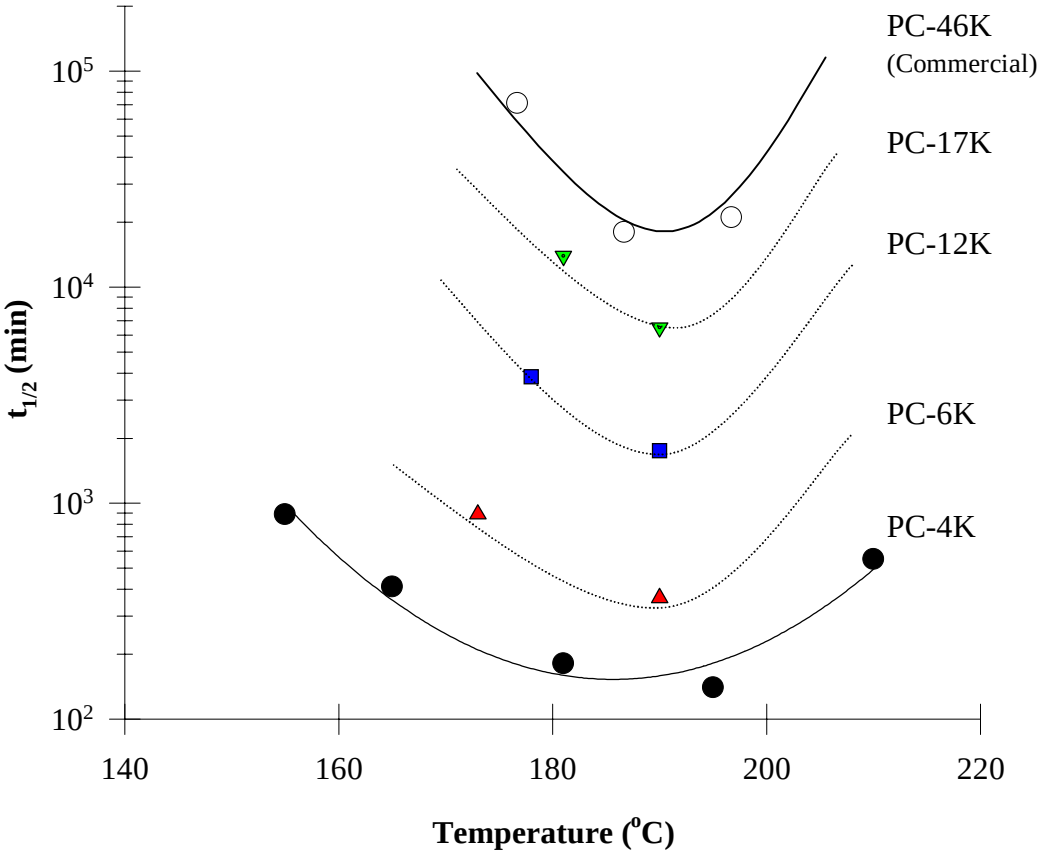

Figure 5.7 The variation of the half-time of crystallization of varying molar mass PC samples as a function of crystallization temperature. Open symbol shows a commercial PC sample (M_w = 46,000 g.mol^{-1}) from the literature[8]. The dotted lines are only for the visual guide.

at lower temperatures. In this plot, therefore, the dotted lines must be used only as visual guide.

5.3.2 *Morphology*

Micrographs 5.1 and 5.2 show, respectively, the early and later stages of spherulite formation in PC-28K cold-crystallized at 185^{o}C for 96 hours. Although the size of spherulite is small, due to the high resolution of the AFM, the phase images clearly show that PC forms spherulitic structure. Micrograph 5.1 seems to be close to a sheaf like structure observed by MacNulty under the optical microscope[12]. Micrograph 5.2 depicts the formation of branches and the spherulitic impingement upon growth. The morphology of PC-28K thin film crystallized at 185^{o}C for 250 hours is shown in Micrograph 5.3. Relatively big spherulite (50 to 75μm size) could be clearly resolved.

To study the effect of molar mass on the morphology, the lowest molar mass fraction, PC-4K, was cold-crystallized at 165^{o}C for 6 hours. In Micrograph 5.4, the height image indicates the spherulitic structure for this low molar mass PC. Similarly, Fryer[13] observed spherulites in PC-9K crystallized from solution. These studies show that in the whole range of molar masses of PC, the principal morphology of semicrystalline PC is a spherulitic structure.

5.3.3 *Secondary Crystallization Kinetics*

This section will present the results of secondary crystallization studies performed in the DSC cell for PC samples of different molar masses. In these experiments, we varied the 1) initial degree of crystallinity prior to secondary crystallization, 2) both the secondary crystallization temperature and time, 3) the partial melting temperature, and 4) primary crystallization temperature. The reproducibility of the temporal evolution of the

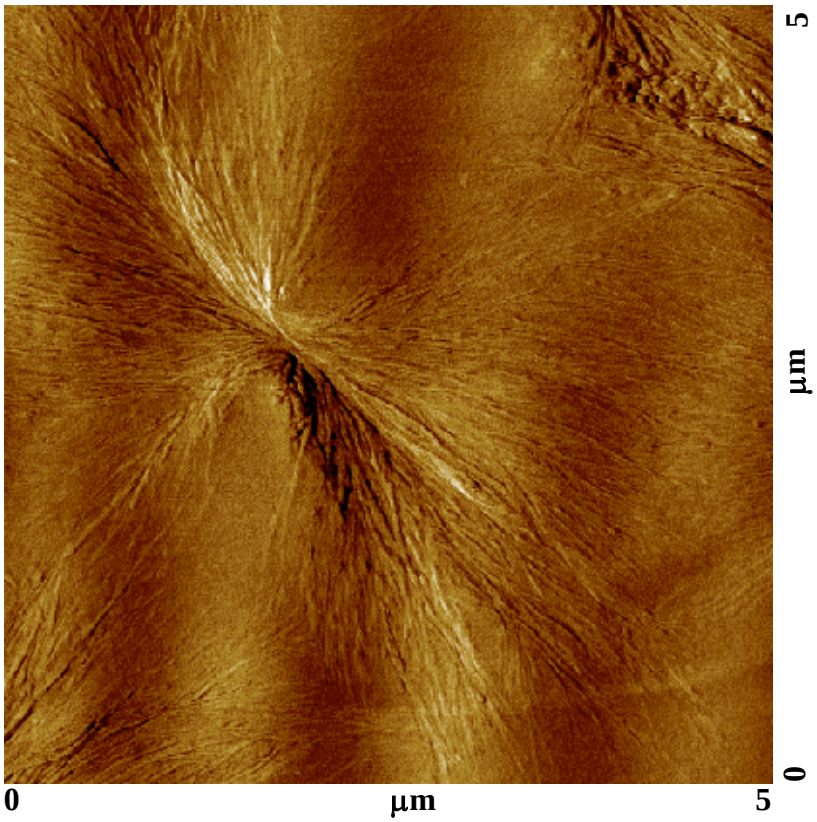

Micrograph 5.1 AFM phase image of the early stage of spherulite formation. PC-28K was bulk crystallized at 185^{o}C for 95 hours. (for detail, see the text)

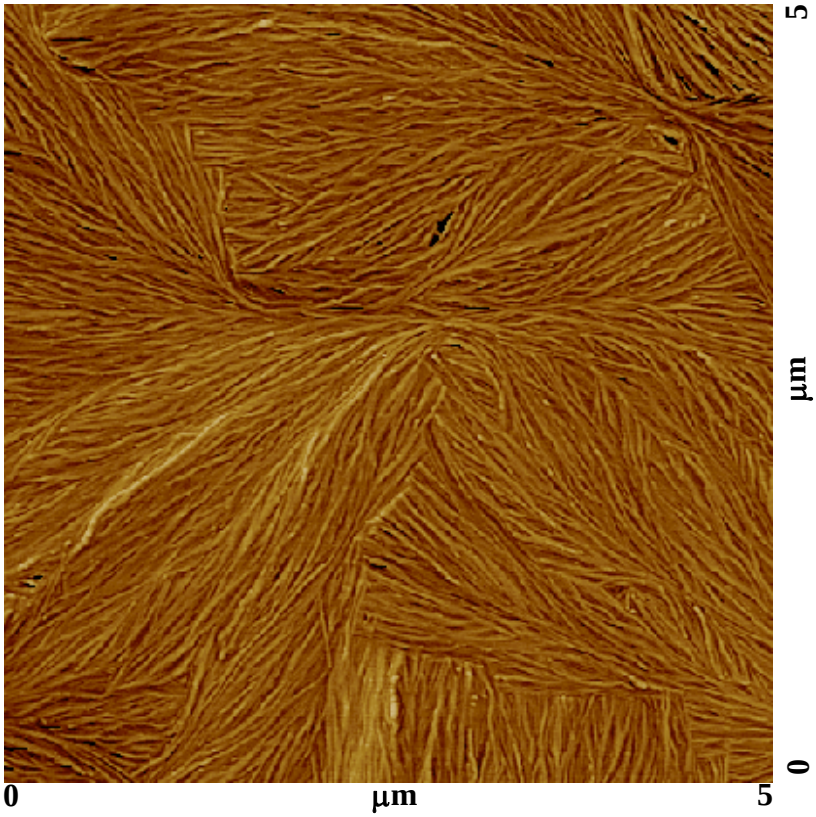

Micrograph 5.2 AFM phase image of the structure of well-developed PC spherulites. PC-28K was bulk crystallized at 185^{o}C for 95 hours. (for detail, see the text)

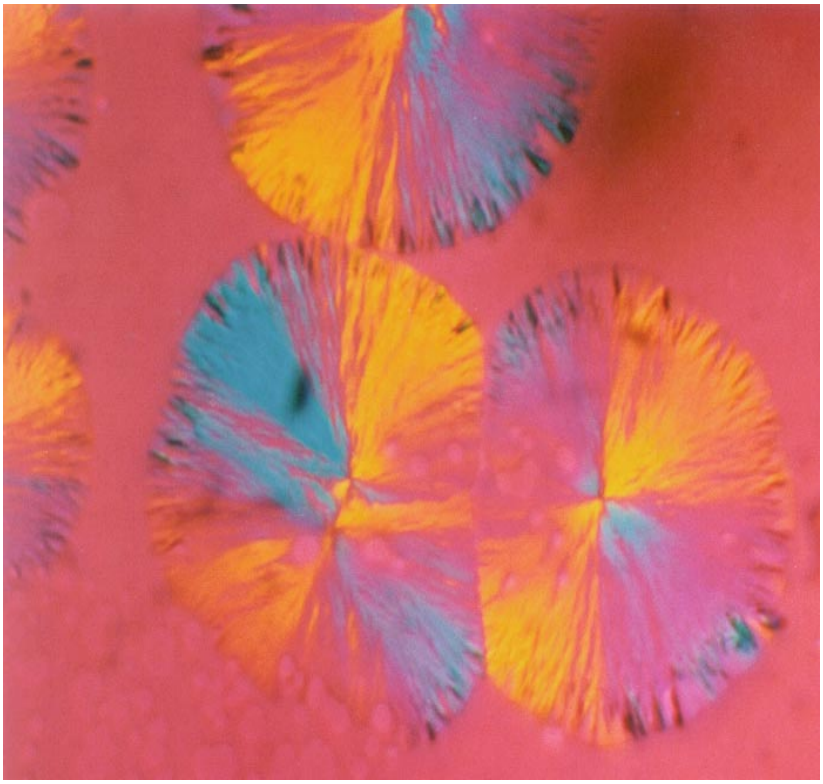

Micrograph 5.3 Spherulitic structure in semicrystalline PC-28K crystallized at 185^{o}C for 250 hours. The scale bar shows approximately 50 microns. (for detailed crystallization conditions, see the text)

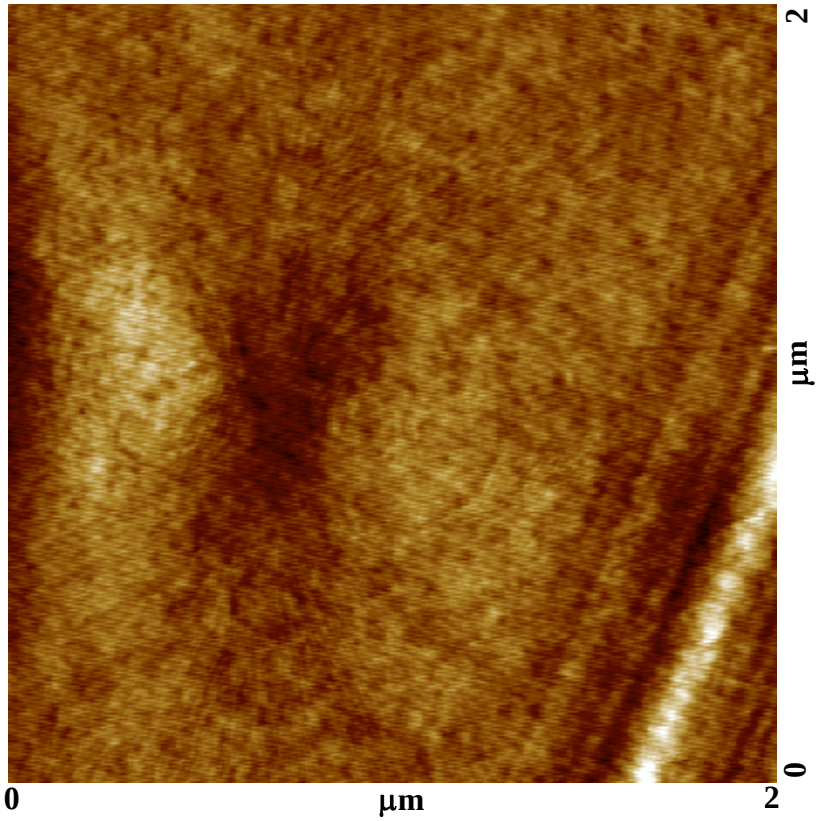

Micrograph 5.4 AFM height image of the early stage of PC-4K spherulites. PC-4K was bulk crystallized at 165^{o}C for 6 hours. (for detail, see the text)

low endotherm will also be discussed. The results will be presented in this order. Detailed crystallization conditions of PC samples used for the study of secondary crystallization kinetics are listed in Table 5.1.

5.3.3.1 *The Effect of the Initial Degree of Crystallinity*

Secondary crystallization experiments were performed under isothermal condition after partial melting for samples that were cold-crystallized for different periods of time. The choice of the crystallization temperature and times was based on the study of the overall kinetics of crystallization presented in the preceding section. Since similar experiments were carried out for PC-19K and PC-28K, the details of the thermal treatments are given only for PC-28K.

PC-28K was crystallized by annealing from the glass at a temperature of 185°C for a period of 202 hours (PC-28K; 202h). This sample was then partially melted (PM) by heating it at a rate of 40°C/min to a temperature above the low endotherm (T_{PM} = 220°C) and keeping it at that temperature for 1 minute. Note that the choice of the partial melting temperature (T_{PM}) depends slightly on the sample molar mass (see Table 5.1). The heats of fusion of the original and partially melted samples are 25.4 and 8.3 J/g, respectively. Subsequent to partial melting, the sample was quenched at the maximum cooling rate available to the secondary crystallization temperature, T_x = 185°C, and maintained at that temperature for a given period of time, t_x. The sample was then quenched to room temperature, and its heating trace was subsequently recorded at a rate of 10°C/min. This procedure was repeated for different secondary crystallization times. Figure 5.8 shows typical heating curves for this set of samples for times ranging from 5 to 900 minutes. Also plotted in this figure is the melting trace of a partially melted

Sample Designation	M_w (g. mol^{-1})	M_w / M_n	Crystallization Conditions in the Oven	Partial Melting (PM), ^oC
***PC-4K**	4,270	1.02	At 165°C, for 38 hours	216
***PC-6K**	6,110	1.05	At 173°C, for 49 hours	215
***PC-12K**	12,400	1.10	At 178°C, for 160 hours	220
***PC-17K**	17,100	1.10	At 181°C, for 382 hours	-
PC-19K	18,800	1.99	At 170°C, for 384 hours	217
PC-28K	28,400	2.07	At 185°C, for 202 hours	220

Table 5.1 Molecular characteristics and crystallization conditions for bisphenol-A polycarbonate samples (Asterisk shows the fractions).

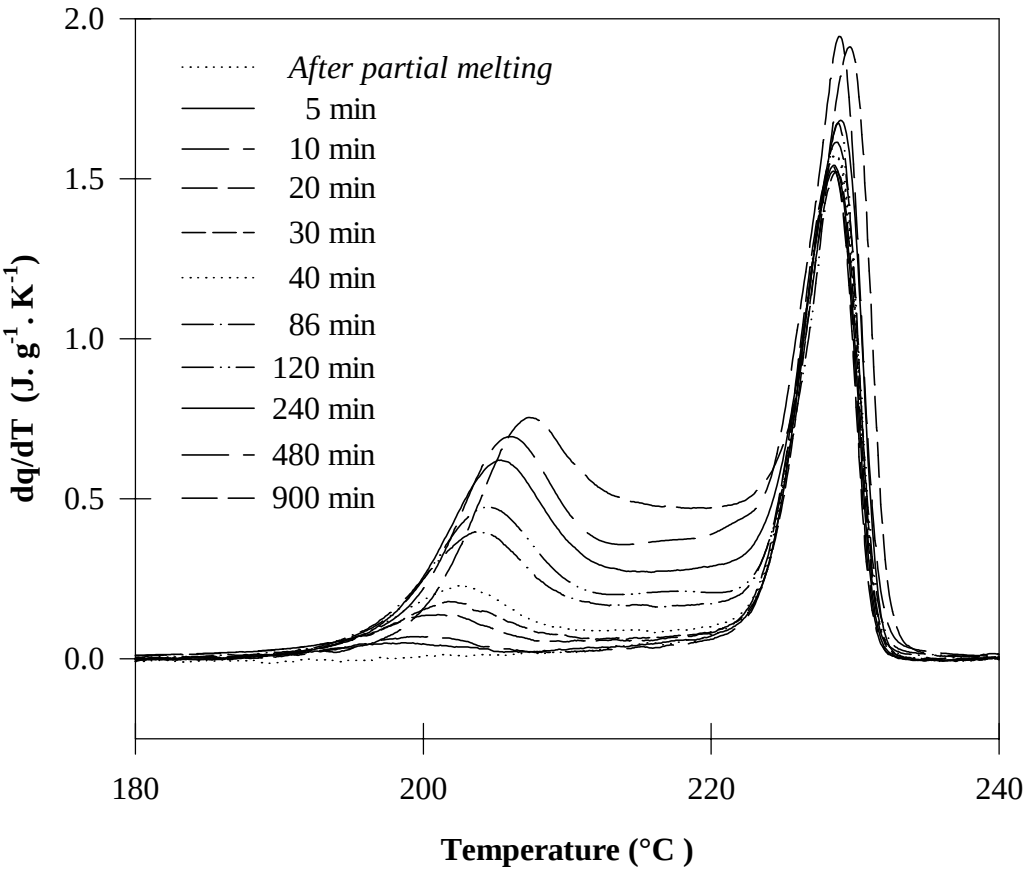

Figure 5.8 Heating traces (HR = 10°C/min) of PC-28K, crystallized at 185°C for 202 hours, partially melted at 220°C, and further isothermally crystallized at 185°C for various times ranging from 5 min to 900 min.

sample that was not subjected to further crystallization at 185°C. As a result of the second isothermal crystallization at 185°C, a low endothermic peak develops just above the crystallization temperature during subsequent heating.

The above procedure was repeated for two other PC-28K samples that were cold crystallized at 185°C for shorter times (105 and 153 hours, respectively). These samples, designated (PC-28K; 105h) and (PC-28K; 153h) exhibited overall heats of fusion of 9.5 and 20.4 $J.g^{-1}$, respectively. After partial melting at T_{PM} = 220°C, their heats of fusion decreased to 2.7 $J.g^{-1}$ and to 5.9 $J.g^{-1}$, respectively. DSC melting traces of these two samples upon secondary crystallization are shown in Figures 5.9 and 5.10. In all cases, the presence of the low endotherm was detected.

In Figure 5.11, ΔH_m^{total} is plotted as a function of log (t_x) for the three PC-28K samples. In this figure, the filled symbols represent the heats of fusion of the original and the partially melted samples, while the open symbols are associated with samples subjected to the second crystallization stage at 185°C. Note that as a result of secondary crystallization, ΔH_m^{total} increases continuously with time and, at later stages, reaches the value characteristic for the original sample (i.e. before partial melting). A deviation from this behavior is observed at the latest stages of secondary crystallization for (PC-28K; 105h). This is mainly because sample (PC-28K; 105h) is far from completing its primary crystallization.

We now focus on the time dependence of the melting temperature, T_m^{low}, and the heat of fusion, ΔH_m^{low}, associated with the low endotherm for samples (PC-28K; 105h), (PC-28K; 153h), and (PC-28K; 202h), resulting from secondary crystallization at 185°C. On Figure 5.12, T_m^{low} is found to increase linearly with log (t_x - t_0) over more than three

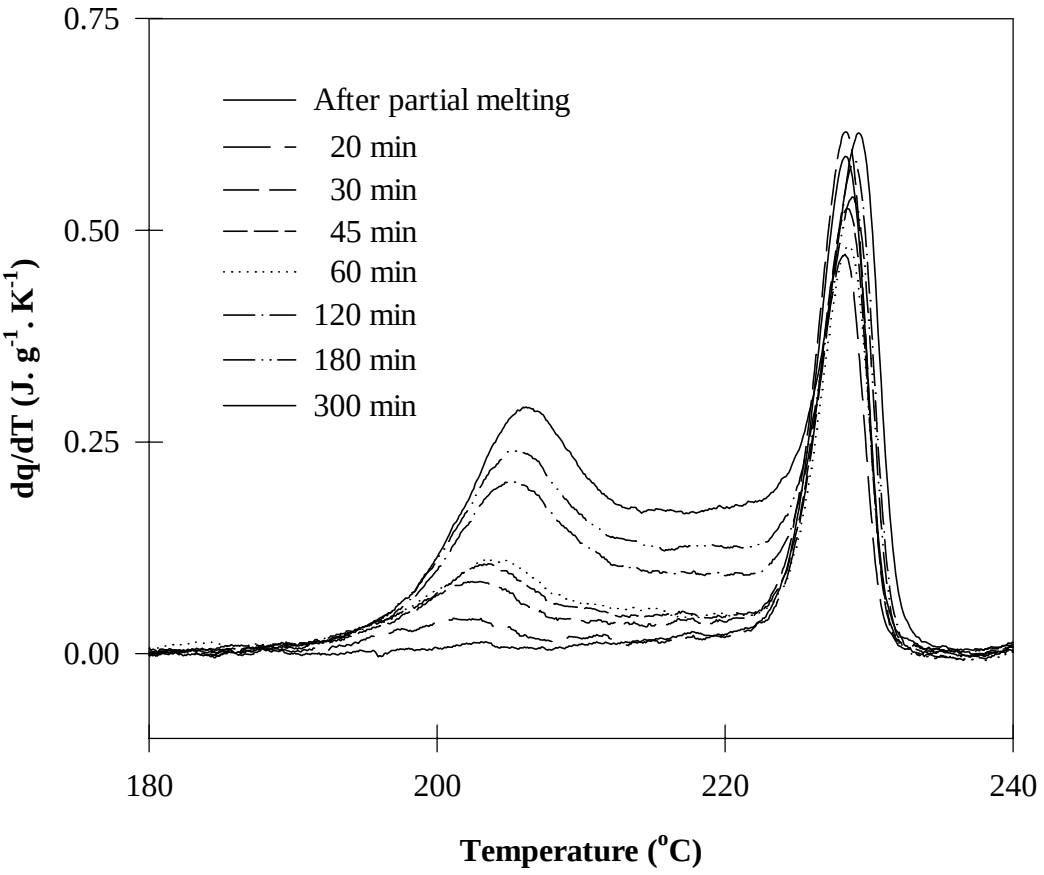

Figure 5.9 Heating traces (HR = 10°C/min) of PC-28K, crystallized at 185°C for 105 hours, partially melted at 220°C, and further isothermally crystallized at 185°C for various times ranging from 20 min to 300 min.

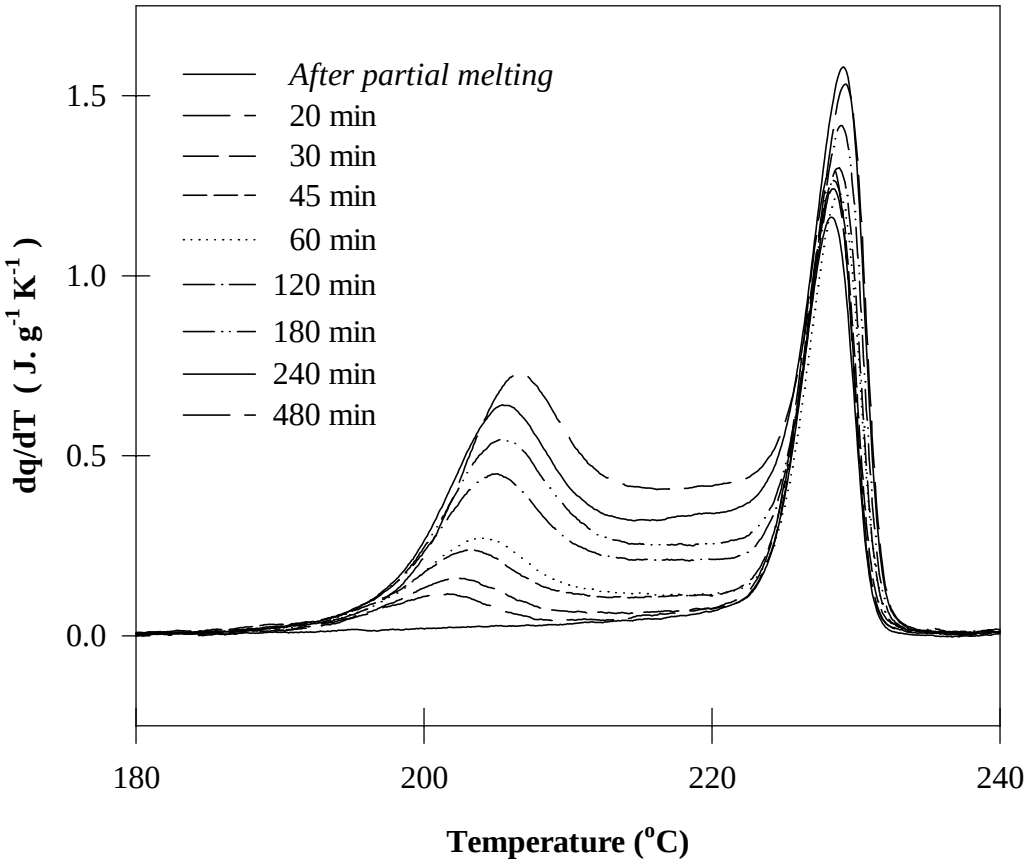

Figure 5.10 Heating traces (HR = 10°C/min) of PC-28K, crystallized at 185°C for 153 hours, partially melted at 220°C, and further isothermally crystallized at 185°C for various times ranging from 20 min to 480 min.

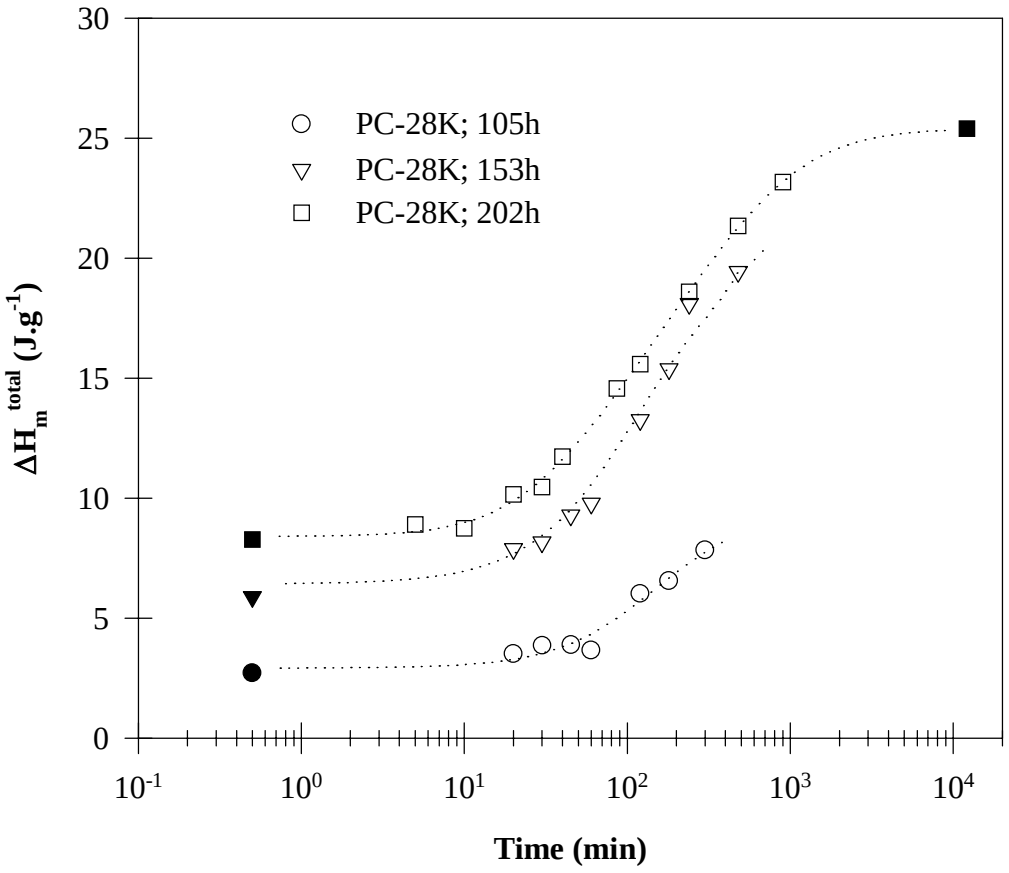

Figure 5.11 Effect of the initial level of crystallinity on the temporal evolution of the total heat of fusion of PC-28K, following partial melting at 220^{o}C, and further crystallization at 185^{o}C. Open symbols show intermediate total heats of fusion during the secondary crystallization, and closed symbols represent initial (after partial melting) and the final total heat of fusion. The accuracy of the determination of the experimental heat of fusion was better than 0.2 J.g^{-1}.

decades, where t_o is the induction period, which is defined as the time required to detect a measurable heat of fusion ($\geq 0.4\ J.g^{-1}$) for the low endotherm. Under these conditions, the induction periods for (PC-28K; 105h), (PC-28K; 153h) and (PC-28K; 202h) are reproducibly found to be 7, 3, and 2 minutes, respectively. The filled symbols in Figure 5.12 correspond to the low endotherm peak temperature for the original samples at different stages of crystallization. Note that the data scatter is larger in this case than for samples undergoing secondary crystallization after partial melting. Such scatter is a result of the overlap between the low and the high endotherms at very long crystallization times (see the heating traces of original samples in Figure 4.3 at HR = 10^oC/min). As mentioned earlier, an induction period of about 45 hours is required to detect any trace of crystallinity during the cold-crystallization of PC-28K. Once this induction time is accounted for, it is found that the same T_m^{low} *vs* log (t_x) dependence is exhibited by all samples (see Figure 5.12). Following the formalism used in the previous studies,[1,6] the variation of T_m^{low} with log (t_x) is expressed empirically by:

$$T_m^{low} = T_x + A(T_x) + B(T_x) \log (t_x) \qquad [5.1]$$

Where $A(T_x)$ and $B(T_x)$ are the fitting parameters , and in case of PC-28K ($T_x = 185^oC$), these values are noted in Figure 5.12.

Adopting the free-growth approximation[14],

$$\Delta H_m^{low} = K \cdot t_x^{\ n} \qquad [5.2]$$

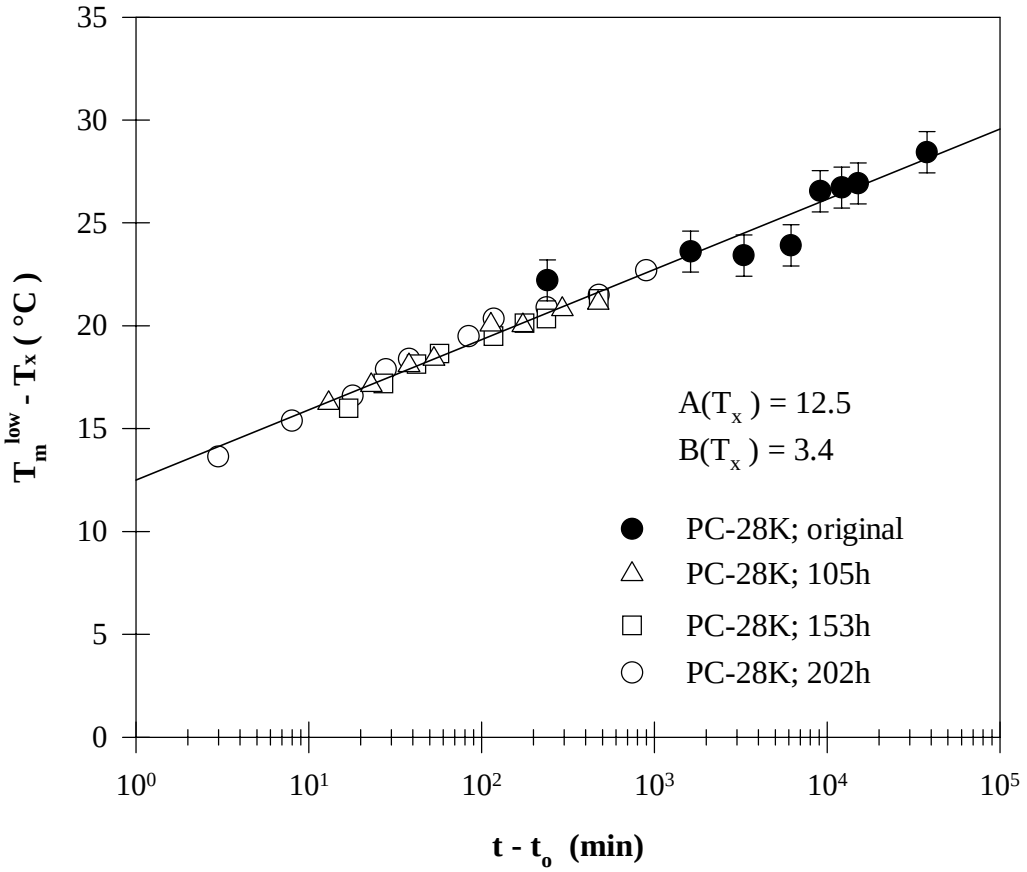

Figure 5.12 Evolution of the low endotherm melting peak temperature with time during the secondary crystallization at $T_x = 185^oC$ performed for samples with different levels of initial crystallinity.

log (ΔH_m^{low}) is plotted as a function of log (t_x) for (PC-28K; 105h), (PC-28K; 153h) and (PC-28K; 202h) in Figure 5.13. Since log (ΔH_m^{low}) increases linearly with log (t_x) at the early stage of secondary crystallization, the Avrami exponent, *n*, is identified as the slope at short crystallization times. The Avrami exponent, *n*, characterizes the geometry and the mechanism of growth, while *K* describes the rate of secondary crystallization at the early stage. Data in Figure 5.13 indicate that the initial stage of secondary crystallization is characterized by an Avrami exponent of 1/2. At later stages of secondary crystallization, *ca*. 100 -200 minutes, a deviation from linearity is observed, indicating that ΔH_m^{low} continues to increase with time but at a much slower rate. Note also that the absolute magnitude of ΔH_m^{low} depends on the initial degree of crystallinity of the sample. Note that due to the strong overlap of the low and the high endotherms in the case of the original samples, the calculation of ΔH_m^{low} is subjected to a large uncertainty; therefore, these samples are not included in Figure 5.13.

Similar experiments were conducted for the PC-19K sample. In this case, the cold crystallization was performed at 170°C for 192 and 384 hours. Partial melting was carried out at T_{PM} = 215°C, and further isothermal crystallization was also performed at 170°C for times ranging from 1 to 1000 minutes. The temporal evolutions of T_m^{low} and ΔH_m^{low} are displayed in Figures 5.14 (a) and (b) for this series of samples. These plots once more demonstrate the linear variation of T_m^{low} *vs* log (t_x) and an Avrami exponent of 1/2 for the initial stage of secondary crystallization.

5.3.3.2 *The Effect of Secondary Crystallization Temperature*

In this series of experiments, amorphous samples were again cold-crystallized under the conditions given in Table 5.1 to ensure spherulitic impingement. These

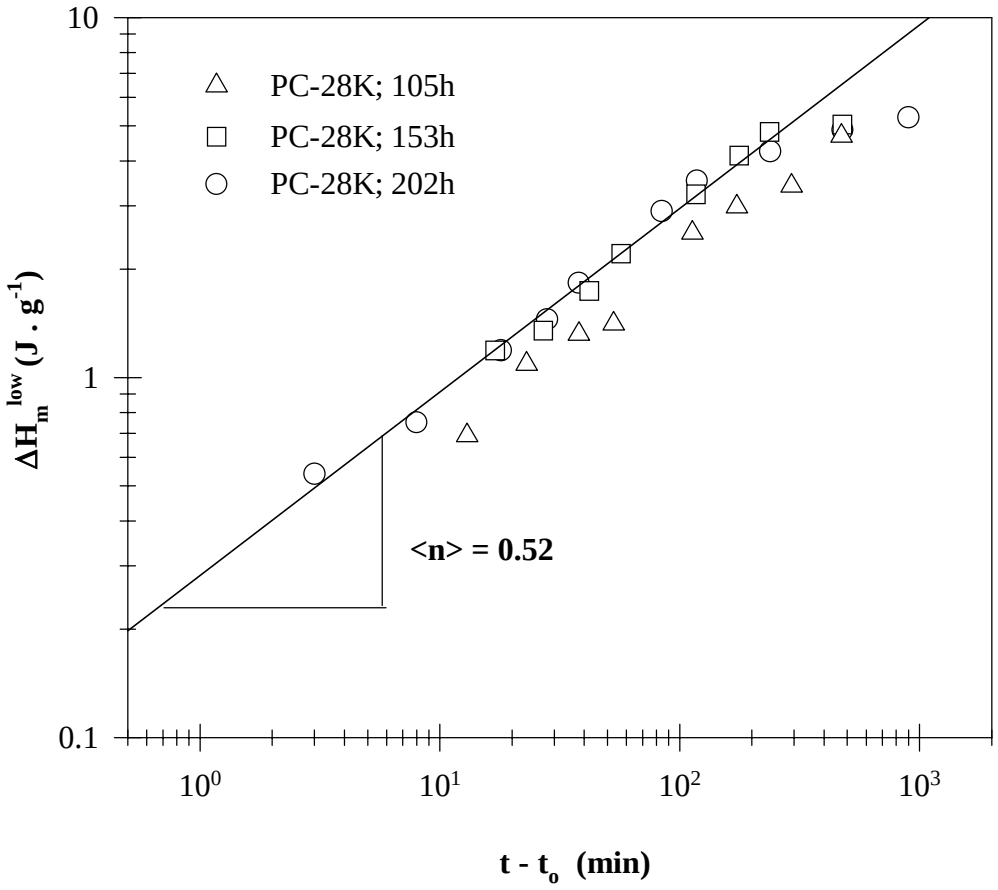

Figure 5.13 Evolution of the low endotherm enthalpy of fusion with secondary crystallization time at 185°C performed for samples with different levels of initial crystallinity. The solid lines is a fitted line for the data of 202 hours and the other two cases are omitted for the simplicity of data presentation. Experimental error < 0.2 J.g^{-1}.

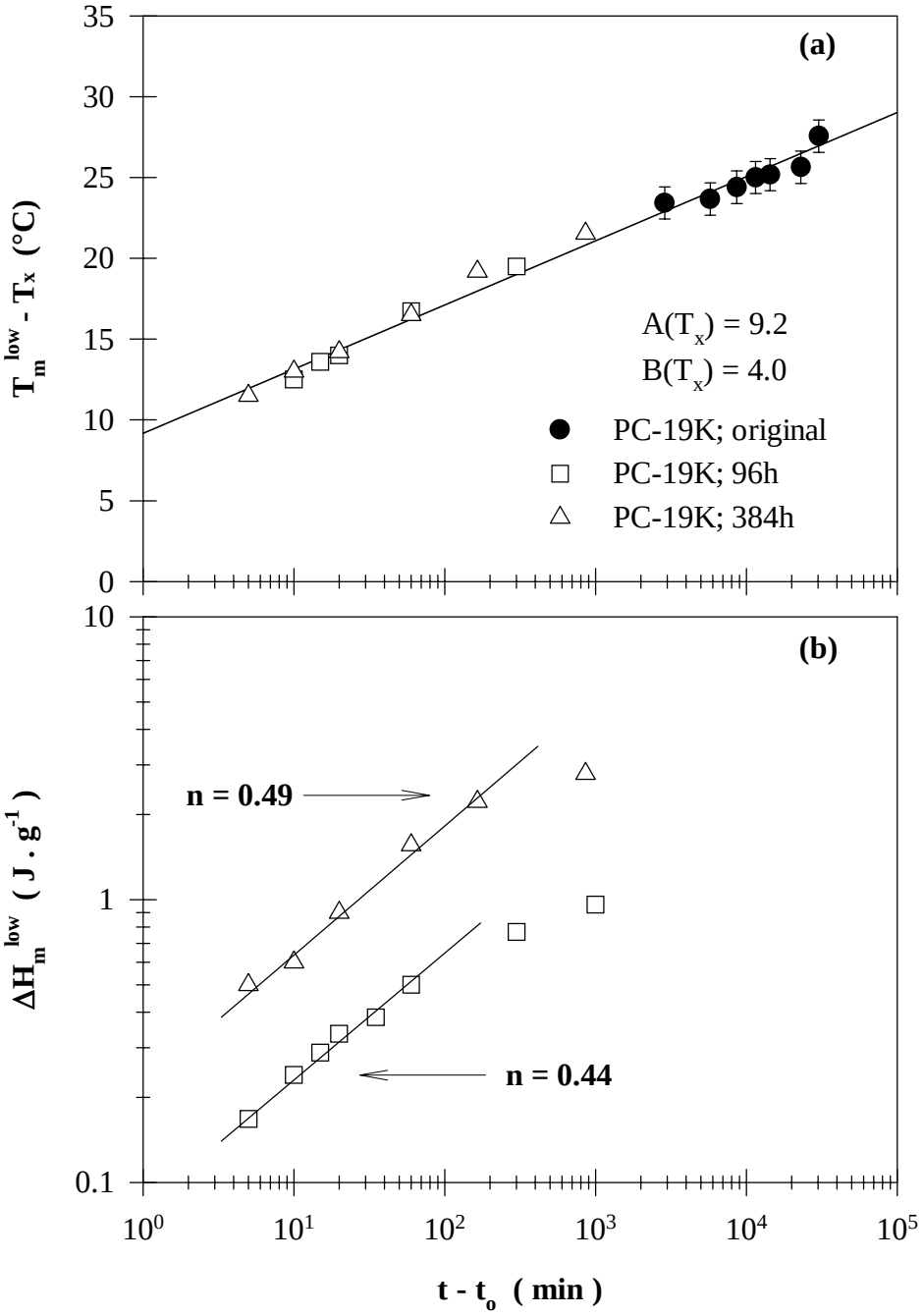

Figure 5.14 Temporal evolution of the low endotherm melting peak temperature (a), and heat of fusion (b) for PC-19K after partial melting at 217°C and secondary crystallization at T_x = 170°C for various times. The accuracies for the temperature and the heat of fusion were better than 0.2°C and 0.2 J.g^{-1}, respectively.

samples were partially melted at T_{PM} and subsequently quenched at the maximum cooling rate available to the crystallization temperature, T_x, at which they were kept for a given time, t_x. These samples were then quenched to room temperature and immediately reheated to record their melting behavior. The nomenclature (PC-XX; PM-T_{PM} ; SC-T_x) describes a given secondary crystallization experiment, where PC-XX provides identification of the sample molar mass and the initial crystallization conditions (Table 5.1), PM-T_{PM} specifies the temperature at which partial melting was carried out, and SC-T_x designates the temperature of the second crystallization stage. For instance, (PC-28K; PM-220; SC-175) implies that the sample PC-28K, initially crystallized at 185°C for 202 hours, was partially melted at 220°C and further crystallized at 175°C.

Analysis of heating traces after secondary crystallization provides an access to the crystallization time dependence of the melting point and heat of fusion associated with the low endotherm. These quantities were in turn analyzed using equations (5.1) and (5.2) to yield the parameters $A(T_x)$, $B(T_x)$, *K* and *n*. The results in case of PC-28K are presented in Figure 5.15 and Table 5.2, and all other results from the fractions are also included in Table 5.2. The values of the *K* and *n* parameters are not included for PC-4K and PC-6K, because a rigorous analysis of the enthalpy associated with the low endotherm could not be performed for short crystallization times. Indeed, low molar mass samples, which are only allowed to crystallize for short times under isothermal conditions, can develop further crystallinity during subsequent heating. The exotherm associated with crystallization during heating unfortunately overlaps the low endotherm associated with the melting of secondary crystals formed at T_x. This issue is no longer present for longer secondary crystallization times, since the rate of secondary

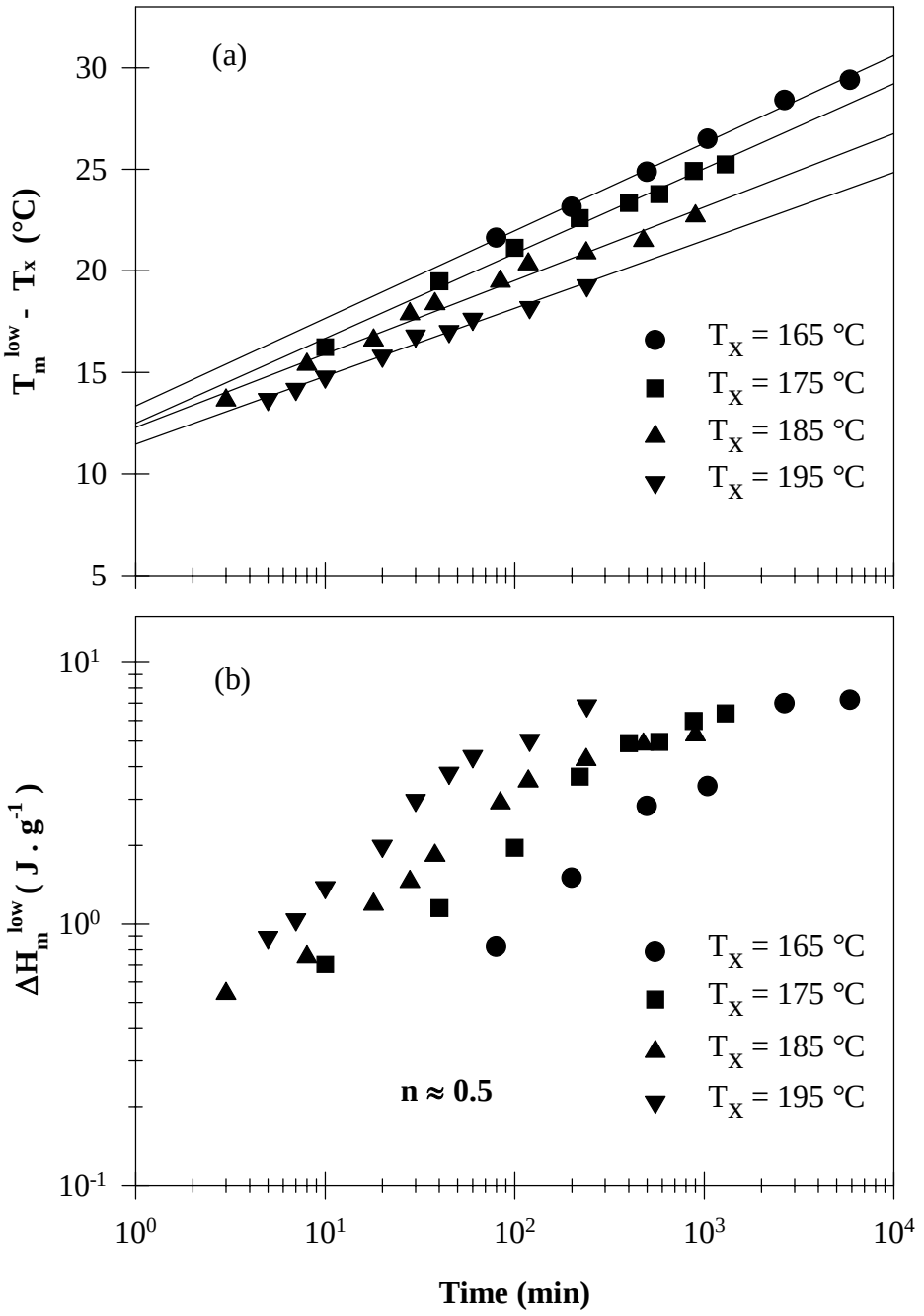

Figure 5.15 Temporal evolution of the low endotherm melting temperature (a), and heat of fusion (b) for PC-28K after partial melting at 220°C and secondary crystallization for various temperatures and times.

BAPC-28K	$A(T_x)$	$B(T_x)$	*K*	*n*
T_x = 165°C	13.35	4.32	0.064	0.59
T_x = 175°C	12.49	4.18	0.189	0.53
T_x = 185°C	12.28	3.62	0.273	0.52
T_x = 195°C	11.47	3.34	0.297	0.66

BAPC-12K	$A(T_x)$	$B(T_x)$	*K*	*n*
T_x = 168°C	9.00	4.53	–	–
T_x = 178°C	9.73	3.80	0.317	0.54
T_x = 183°C	8.41	3.90	–	–

BAPC-6K	$A(T_x)$	$B(T_x)$
T_x = 163°C	6.65	4.61
T_x = 173°C	8.64	3.04
T_x = 178°C	8.54	2.65

BAPC-4K	$A(T_x)$	$B(T_x)$
T_x = 155°C	4.94	5.70
T_x = 165°C	8.70	3.64
T_x = 170°C	8.06	3.53

Table 5.2 Parameters describing the temporal evolution of the low endotherm for various PC samples at different secondary crystallization temperatures. *Effects of crystallization temperature and molar mass*. The experimental uncertainties for the A (T_x) and B(T_x) were better than 0.5^{o}C and 0.3^{o}C, respectively.

crystallization decreases with time beyond the initial stage and the crystallinity developed during heating becomes negligible. The parameters $A(T_x)$ and $B(T_x)$ reported for samples PC-4K and PC-6K in Table 5.2 are thus derived from measurements on samples crystallized for long times. The above experimental limitations are not an issue for higher molar mass PC samples, as the rate of secondary crystallization decreases with increasing chain length. $B(T_x)$ as a function of secondary crystallization temperature is plotted in Figure 5.16. For each PC samples, an *increase* in crystallization temperature results in a *decrease* in the slope $B(T_x)$. For molar masses equal to or higher than 12,000 $g.mol^{-1}$, $B(T_x)$ decreases almost linearly with T_x. Note that commercial and fractionated samples fall on the same line. For the lowest molar mass samples, $B(T_x)$ still exhibits a quasi-linear variation with T_x, but the slope (*ca*. -0.13) is much higher than for the higher molar mass samples (-0.04).

Finally, the effect of heating rate on the magnitude of the slope $B(T_x)$ for the two extreme molar masses, i.e. samples PC-4K and PC-28K was investigated. For PC-4K, three, and for PC-28K, four, different temperatures of secondary crystallization experiments were used, and the subsequent melting behaviors were examined at heating rates ranging from 5 to 20°C/min. The results of such analyses (Table 5.3) indicate that the magnitude of $B(T_x)$ increases with heating rate. A more detailed analysis of these results will be offered in the discussion section.

5.3.3.3 *The Effect of Partial Melting Temperature*

In the previous two sections, to monitor the temporal evolution of the low endotherm, second isothermal crystallization experiments were performed on samples that had been partially melted at T_{PM}. T_{PM} is slightly different depending on the molar

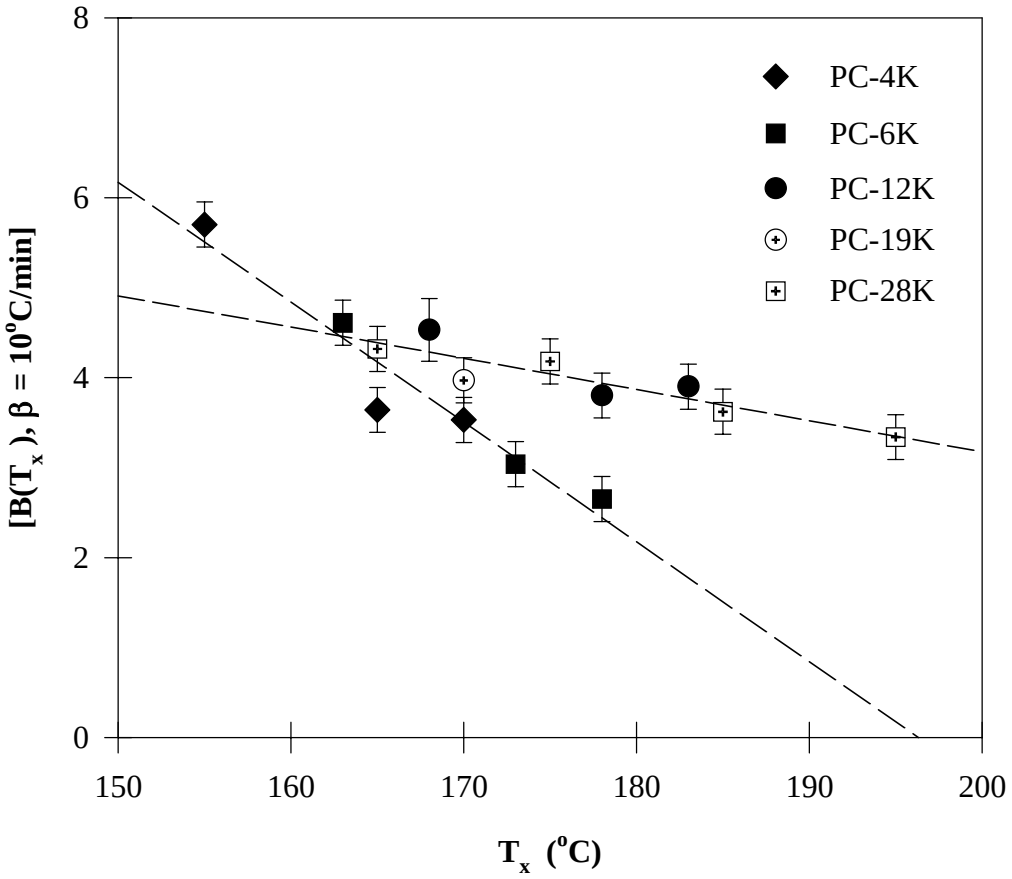

Figure 5.16 Variation of the rate of shift of the low endotherm, $B(T_x)$, as a function of secondary crystallization temperature, T_x, for various molar mass PC samples (in this plot $B(T_x)$ has been evaluated at HR $=10^{o}$C/min). Note that closed and crossed symbols represent fractions and commercial materials, respectively.

PC-4K	T_x = 155°C		T_x = 165°C		T_x = 170°C	
	$A(T_x)$	**$B(T_x)$**	**$A(T_x)$**	**$B(T_x)$**	**$A(T_x)$**	**$B(T_x)$**
β= 5°C/min	5.90	4.15	6.62	3.04	7.26	2.47
β= 10°C/min	5.80	5.38	7.05	3.64	8.06	3.53
β= 20°C/min	5.84	5.72	7.31	4.25	8.66	3.76

PC-28K	T_x = 165°C		T_x = 175°C		T_x = 185°C		T_x = 195°C	
	$A(T_x)$	**$B(T_x)$**	**$A(T_x)$**	**$B(T_x)$**	**$A(T_x)$**	**$B(T_x)$**	**$A(T_x)$**	**$B(T_x)$**
β= 5°C/min	8.00	4.30	8.55	3.63	9.30	3.01	9.8	2.80
β= 10°C/min	10.22	5.17	10.88	4.18	11.67	3.87	11.25	3.34
β= 20°C/min	10.71	5.26	11.05	4.60	10.17	3.93	11.55	4.30

Table 5.3 Parameters describing the temporal evolution of the low endotherm for various PC samples at different secondary crystallization temperatures. *Effect of heating rate*. The experimental uncertainties for the A (T_x) and B(T_x) were better than 0.5^{o}C and 0.3^{o}C, respectively.

mass of samples (see Table 5.1) since the choice of T_{PM} is to ensure the complete melting of crystals melting at the low endotherm. This partial melting temperature may affect the secondary crystallization kinetics: due to the overlapping nature of high and low endotherms, during partial melting, most of the intermediate endotherm (shoulder) and a small fraction of high endotherm have been removed.

PC-19K samples originally crystallized at 170^{o}C for 16 days were partially melted at two different temperatures (210^{o}C and 217^{o}C) for two minutes to ensure the complete removal of the low endotherm. Secondary crystallization experiments have been performed at 170^{o}C for various times. The details of the experimental procedures are similar to those described in the previous section, and will thus be omitted here. On Figure 5.17, the melting traces of the original sample, partially melted at 210^{o}C and 217^{o}C, are plotted. Obviously, a higher partial melting temperature leads to a more narrow and well-defined peak. The peak position of the sample partially melted at 217^{o}C has been shifted about 4^{o}C higher than the original sample, which could be due to the annealing effect (see Chapter 6). Figure 5.18 (a) and (b) present the heating traces for samples after secondary crystallization. The temporal behavior of the low endotherm follows the characteristics that have been observed previously. The analysis of the low endotherm in terms of peak position and heat of fusion is shown in Figure 5.19 (a) and (b), respectively. From this, it is demonstrated that regardless of the partial melting temperature, the low endotherm kinetics follows the same characteristic behavior: the peak position increases linearly with time and the initial Avrami exponent is close to 0.5. Of more interest, the peak position of the low endotherm falls on the same line, regardless of the partial melting conditions.

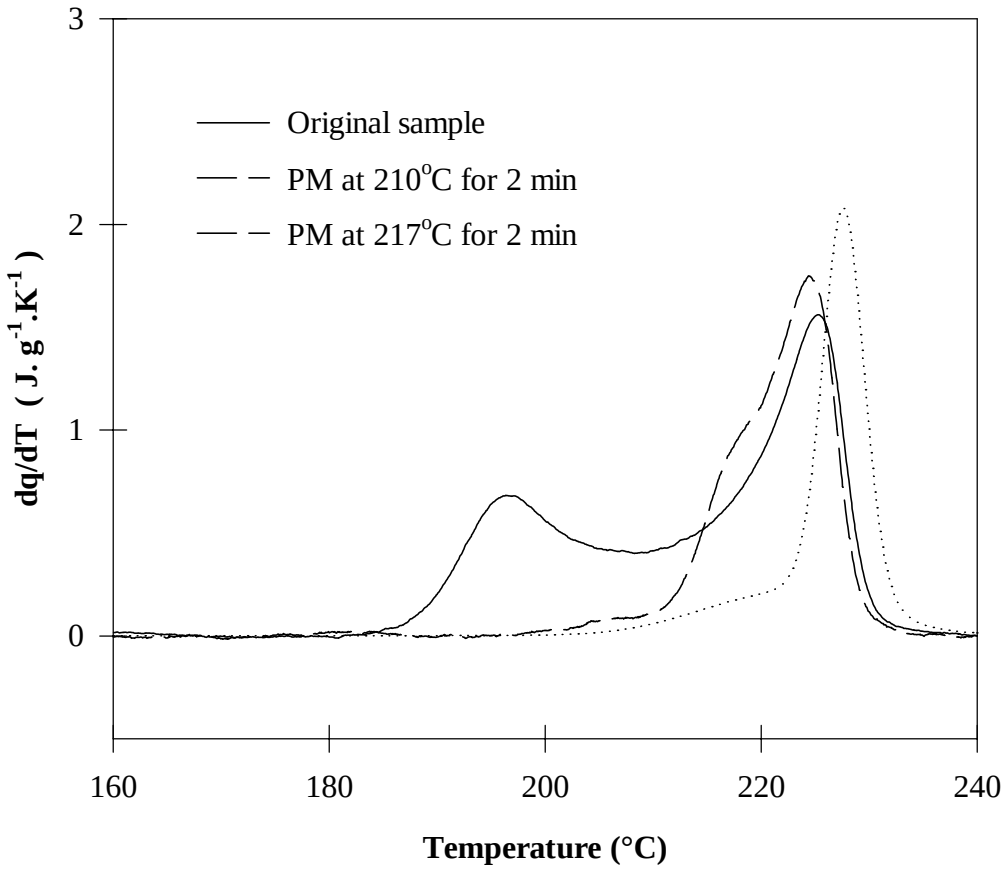

Figure 5.17 Heating traces (HR = 10°C/min) of PC-19K after partial melting (PM) at two different temperatures (210°C and 217°C). For comparison reason, the melting traces of original sample crystallized at 170°C for 16 days are plotted together.

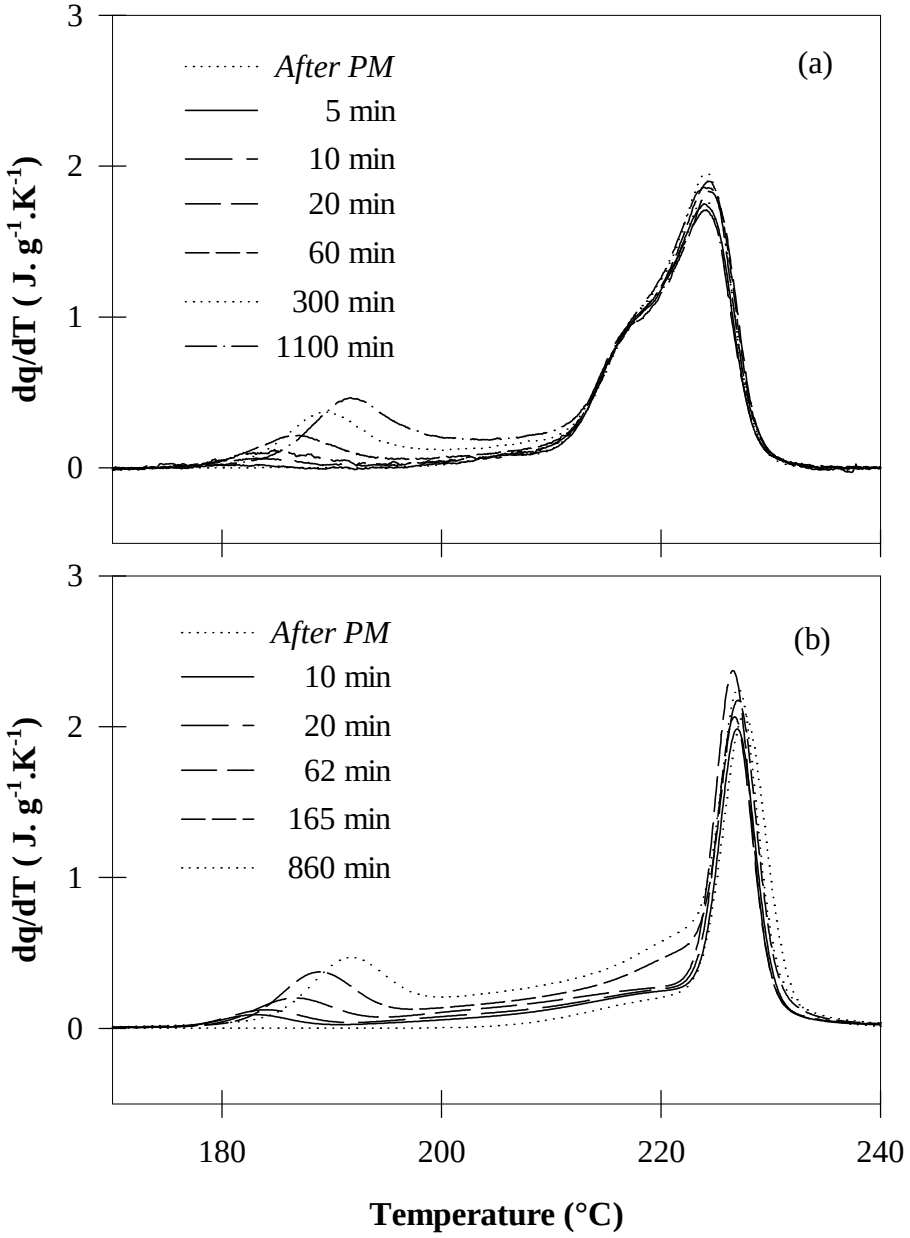

Figure 5.18 Temporal evolution of the melting endotherm for PC-19K subsequent to secondary crystallization at 170°C after partial melting at 210°C for 2 minutes (a), and 217°C for 2 minutes (b). Original sample was crystallized at 170°C for 16 days.

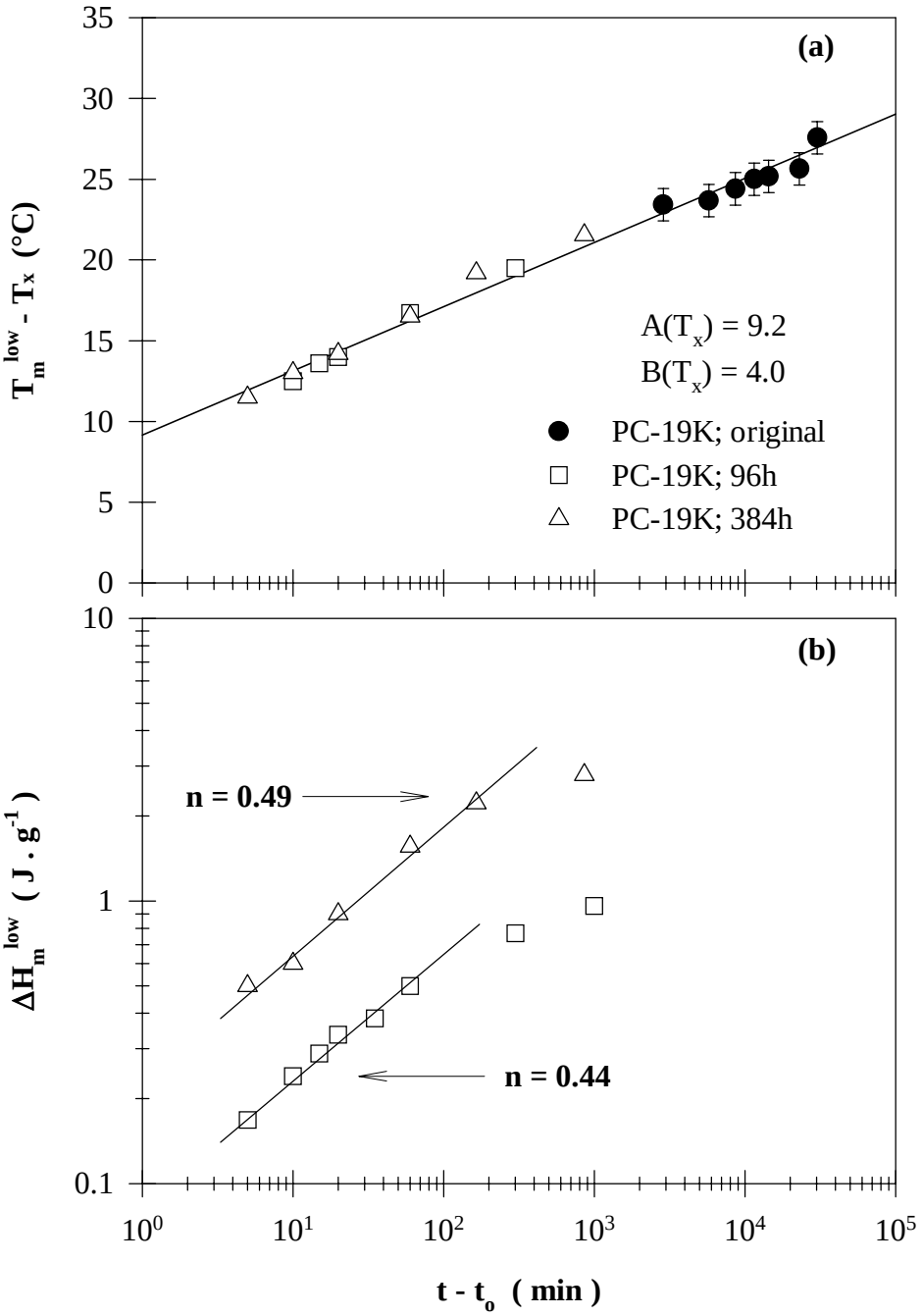

Figure 5.14 Temporal evolution of the low endotherm melting peak temperature (a), and heat of fusion (b) for PC-19K after partial melting at 217°C and secondary crystallization at T_x = 170°C for various times. The accuracies for the temperature and the heat of fusion were better than 0.2°C and 0.2 $J.g^{-1}$, respectively.

5.3.3.4 *The Effect of Primary Crystallization Temperature*

In this section, the effect of primary crystallization temperature on the secondary crystallization kinetics is presented. PC-6K samples crystallized at two different temperatures (173^{o}C and 190^{o}C) were partially melted at 216^{o}C and further crystallized at 173^{o}C for various times. Other experimental conditions were similar to previous calorimetry studies. The analysis was done only for the temporal evolution of the low endotherm peak position. This is because, as noted earlier, for this particular sample (PC-6K), the Avrami exponent, *n*, can not be determined due to the overlap of the crystallization exotherm and the melting endotherm at early times of secondary crystallization. T_m^{low} *vs* log [time] for these two sets of samples are plotted in Figure 5.20. As clearly seen, T_m^{low} exhibits a linear variation with $\log(t_x)$, and within the experimental uncertainty, the low endotherm peak position does not depend on the primary crystallization temperature.

5.3.3.5 *Reproducibility of the Temporal Evolution of Low Endotherm*

Until now, the evolution of the low endotherm has been analyzed in two ways-peak melting temperature (T_m^{low}) and heat of fusion (ΔH_m^{low}). In the preceding sections it has been clearly shown that the evolution of low endotherm exhibits a strong time and temperature dependent behavior. Time dependent behavior of the low endotherm can readily be described using equations (5.1) and (5.2). At this moment, it would be beneficial to ensure that for a given time of secondary crystallization, the melting peak position and the heat of fusion associated with the low endotherm are reproducible. To this end, PC-12K samples have been used in the following experimental procedures. PC-

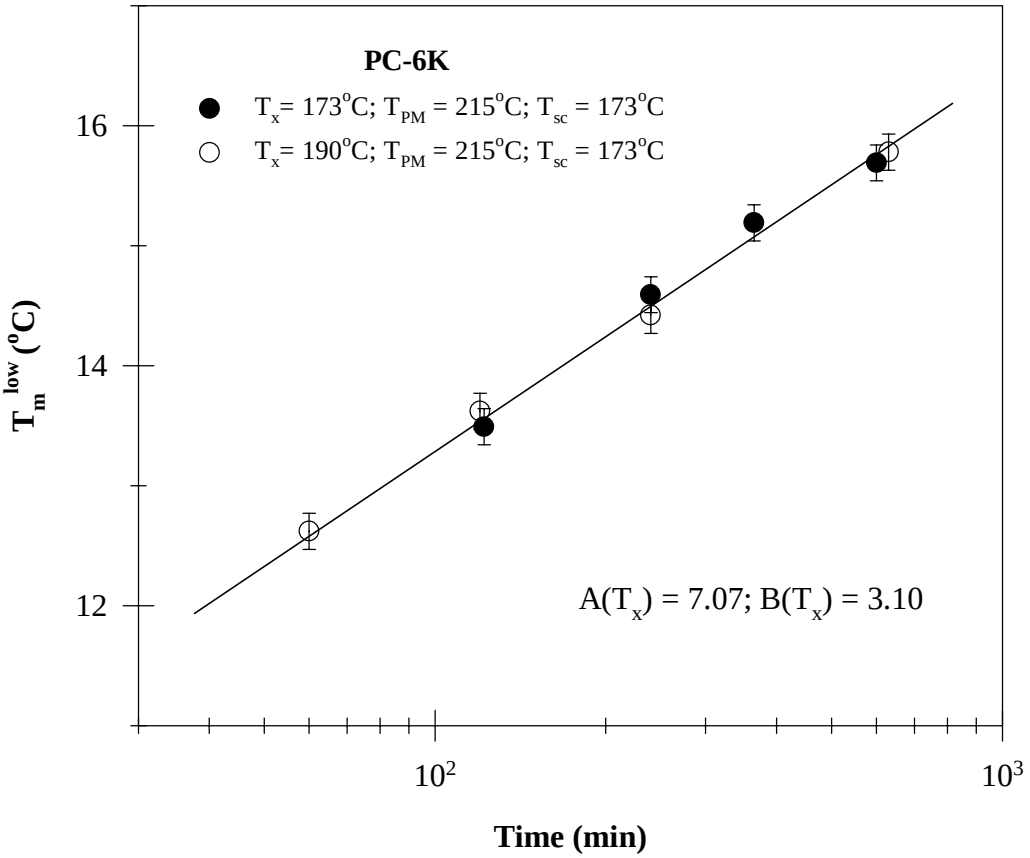

Figure 5.20 Temporal evolution of low endotherm peak position change in case of PC-6K samples initially crystallized for two different temperatures (T_x = 173 and 190°C). Only T_x has been varied and partial melting (PM) and secondary crystallization (SC) experiments have been performed at the same temperatures. Temperature scale has been corrected using In-sandwich sample. (HR = 10°C/min)

12K samples, initially crystallized at 178^{o}C for 160 hours and partially melted at 220^{o}C, were exposed to the secondary crystallization at 178^{o}C for one hour. Upon reaching the desired time, the sample was fast cooled to 100^{o}C at the maximum rate available and subsequently reheated at 10^{o}C/min up to 220^{o}C. The sample was then immediately quenched back to 178^{o}C and remained at this temperature for another hour for the second experiment. These steps were repeated four times. Note that *in each run, the preexisting high endotherm was not altered*, since the heating scan stopped at 220^{o}C, where the partial melting was performed. In doing so, the reproducibility of the low endotherm in terms of peak position and heat of fusion can be effectively checked. DSC melting traces of these four scans around the low endotherm region are shown in Figure 5.21. As clearly seen, the low endotherm resulting from secondary crystallization was highly reproducible in terms of both peak position ($\leq 0.2^{o}$C) and heat of fusion (≤ 0.05 J.g^{-1}).

5.4 Discussion

In this chapter, the bulk kinetics of crystallization is described through the temporal evolution of the enthalpy of fusion ΔH_m^{total}. The principal reason for not converting enthalpies of fusion to degrees of crystallinity stems from the rather large uncertainty associated with the theoretical enthalpy of fusion for bisphenol-A polycarbonate (110 to 140 J.g^{-1})[15,16]. Furthermore, the melting of PC crystals is generally observed over a large temperature range centered *ca*. 100 K below the reported equilibrium melting temperature (T_m = 590-600 K)[17]. It is therefore imperative to account for the temperature dependence of the molar heat capacity for both the crystal and the liquid fractions in calculations of the degree of crystallinity. More importantly, SAXS and other morphological studies indicate that PC lamellae are generally very

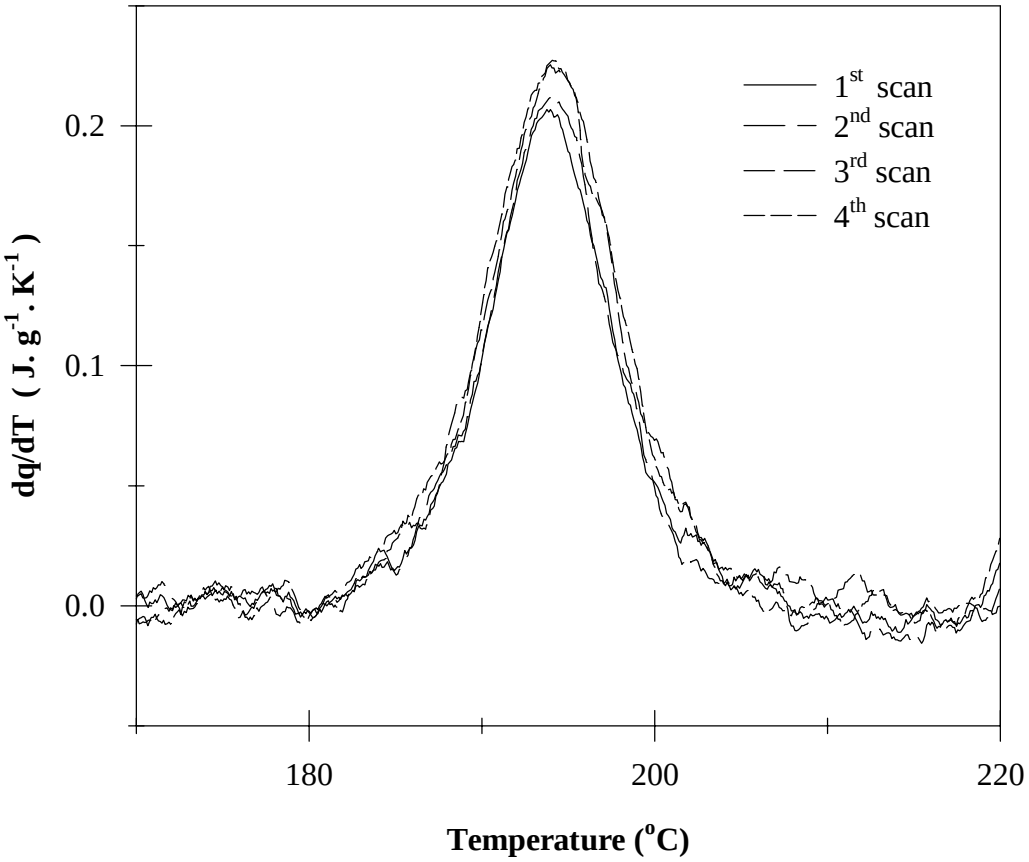

Figure 5.21 Reproducibility test of the temporal evolution of the low endotherm. PC-12K sample, crystallized at 178°C for 160 hours, partially melted at 220°C, was further isothermally crystallized at 178°C for one hour. Detail experimental conditions see the text. *Note the scale of heat flow rates.*

thin[18], suggesting that surface enthalpic contributions cannot be neglected[19]. This latter issue becomes even more critical when one considers PC samples that contain a significant fraction of small secondary crystals. These issues will be further discussed in Chapter 7.

5.4.1 *Overall Crystallization Kinetics*

5.4.1.1 *The Effect of Molar Mass Distribution*

The rates of crystallization of PC of varying molar masses are depicted in Figure 5.15, where the half-time of crystallization is plotted as a function of molar mass. Notice that $t_{1/2}$ of the fractions increases steeply with molar mass. The extremely low crystallization rates of PC, especially for higher M_w, may be related to its stiff backbone and high melt viscosity[20]. The substantially low value of the growth rate of PC mainly results from a very high free energy of fold formation (27.3 kcal per mole of fold for PC versus the corresponding value of 5.7 kcal per mole of fold for PE)[17].

In Figure 5.15, it is also noteworthy that the crystallization kinetics of commercial samples is faster than that of fractions of similar molar mass. The broader molar mass distribution of the commercial samples, when caused by the existence of the low molar mass components, might explain their faster kinetics of crystallization. In this case, the short chain molecules reduce the average relaxation time of the longer chain molecules and therefore increase the crystallizability of the material. Therefore, in commercial samples, the shorter chain molecules start the process of crystallization, and serve as nucleating sites for the longer chains. However, this sequence of crystallization is opposite to what occurs in polydisperse PE[21], where the high molar mass components initiate the crystallization. The experiments of Ergoz *et al.*[21] in fractions of low to

moderate molar mass PE clearly demonstrate this point (i.e. at a given temperature T_x, the crystallization rate of fractions of PE increases considerably with M_w). This difference is likely to be explained by the fact that diffusion effects control the rate of crystallization of PC at the temperature investigated, while nucleation effects control that of PE.

It is informative to compare the above result with other previous reports. The molar mass dependence of the total heat of fusion among different polymers after long time crystallization is illustrated in Figure 5.22[*]. In this figure, the total heats of fusion of fractions of linear PE[22,23] (triangles), PEEK[24] (squares), and PC (circles) are compared. The molar masses on the X-axis have been divided by the corresponding critical entanglement molar mass, M_c[25]. Accordingly, the values on the Y-axis have been normalized to the heat of fusion of the perfect crystal (i.e., crystallinity). It is interesting to note that for these three polymers, which have very different backbone structures, the crystallinity decreases linearly with the logarithm of M_w / M_c. The slope of each line reflects the diminishment of the crystallizability of the polymeric material with an increase in the density of the entanglements[22]. For PC fractions, over the range of molar mass investigated, the slope of crystallinity *vs* $\log\{M_w/M_c\}$ is smaller than in linear PE and PEEK. Additionally, the normalized heat of fusion of PC extrapolated to $M_w = M_c$ leads to a noticeably smaller value compared to that of linear PE or PEEK. Again this could be related to the high free energy of fold formation of PC[14] and exceedingly slow crystallization rate[2-4,26]. To elucidate the influence of the entanglements density on the final degree of crystallinity of PC, more investigations are required; for instance, it would be desirable to study *fractions* of higher molar masses.

[*] Dr. Alizadeh originally proposed this plot, and some of the arguments accompanying Figure 5.22 was constructed with her helpful discussion.

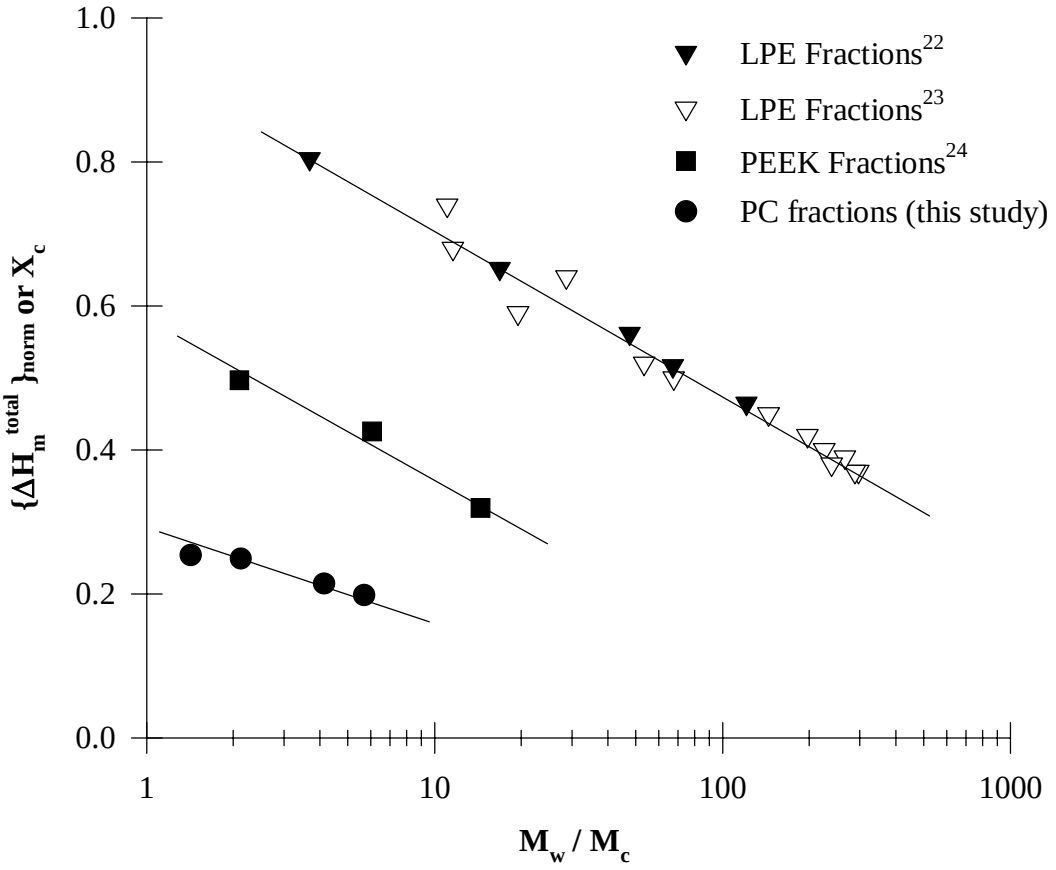

Figure 5.22 Variation of normalized total heat of fusion (or crystallinity) among different polymers after long time crystallization. The X-axis has been normalized with critical molar mass corresponding to each polymer[25].

5.4.1.2 *The Effect of Crystallization Temperature*

For a rigorous comparison of the kinetics of crystallization, the undercooling– defined as the difference between the equilibrium melting point and the crystallization temperature– of the samples should be equal. However, to our knowledge the variation of the equilibrium melting temperature of PC as a function of molar mass is not known. One should notice that the most accurate determination of the equilibrium melting temperature through the non-linear Hoffman-Weeks approach would require measuring the apparent melting temperature of the polymer at many different crystallization temperatures[27]. However, the temperature range for crystallization of PC is extremely narrow[2-4.26], thus in practice this method will be subjected to a large uncertainty.

Because of this intrinsic difficulty in PC, the conclusions from Figure 5.7 must be considered under the assumption that the equilibrium melting temperature of fractions are similar. The two important observations from Figure 5.7 are that 1) the maximum growth rate of PC appears to occur at the same temperature (around 190^{o}C) regardless of molar mass distribution; and 2) there exists a significant difference (on the order of 100 times) in the absolute time scale of $t_{1/2}$ between samples of varying molar mass. In a parallel line with the first observation, several reports claim that the maximum rate of crystallization of PC should occur around 190^{o}C[8,15,20,28,29].

5.4.1.3 *Morphology of Semicrystalline PC*

Since the first report of spherulitic structure of cold crystallized PC (M_v= 33,000 g/mol, 190^{o}C for 8 days under dry N_2) by Kämpf[4,30], many authors have studied the morphology of semicrystalline PC. Falkai and Rellensmann reported the crystallization kinetics and morphology of cold-crystallized PC (M_v= 33,000 g/mol) from the melt[2,3],

and they also showed spherulitic morphology of PC. MacNulty crystallized PC (M_w not specified) by solvent casting for periods between one and sixty hours at 180^oC[12]. The author described the sequential formation of spherulite using optical microscope starting from a roughly elliptical entity followed by a perfectly symmetrical dumb-bell shape entity. This description is very similar to a general structure of spherulite suggested by Keller[31,32]. Siegmann and Geil intensively studied the crystallization of solvent cast PC thin film either from "as is" wet film or after melting and quenching to its glassy state[33]. The authors proposed that the glassy state may have small but ordered structures, called nodules, which further grow into bigger nodules and eventually form spherulites depending on the annealing temperature and time. However, such views are highly controversial[42].

Several morphology studies of semicrystalline PC, including the above relatively earlier works, can be classified into three different types based on the methodology adopted: first, bulk crystallization either from the glassy state or from the melt[2-4]; second, solvent or vapor induced crystallization[12,30,33]; and lastly, nucleating agents and/or plasticizer assisted crystallization[17]. These very different types of crystallization studies confirm that PC forms spherulitic structure upon crystallization, regardless of sample crystallization conditions. Morphology study in the present work also supports this conclusion.

5.4.1.4 *Secondary Crystallization Kinetics*

The most striking result is that while the kinetics of crystallization of PC from a completely amorphous state is extremely slow (in the order of 10 to 100 hours), the secondary crystallization process, especially in partially melted samples, occurs at a

much faster rate (in the order of minutes). In the previous sections the remarkable influence of the molar mass on the rate of "primary" crystallization of PC was noted. In contrast, the kinetics of the low endotherm depicts two universal behaviors, regardless of the molar mass distribution, the initial stage of crystallization prior to the secondary crystallization, secondary crystallization temperature, and partial melting temperature: T_m^{low} increases linearly with the logarithm of crystallization time, and at the early stage, the Avrami exponent in $\log[\Delta H_m^{low}]$ *vs* log[time] is 0.5.

Secondary crystallization in these cases occurs in the presence of preexisting crystals and through a completely different mechanism. While the primary crystals that remain after partial melting are lamellar type, the secondary crystals most likely exhibit bundle-like or fringe-micellar type structures or possibly mosaic block crystals depending on temperature. More importantly, the formation of this specific type of secondary crystals is believed to be limited to amorphous regions within the spherulites. These amorphous regions between pre-existing lamellae are more constrained than the free melt. Thus, the formation of bundle-like crystals in these confined regions will be more favorable than chain-folded lamellae. In addition, PC chain segments could be less entangled in the interlamellar amorphous regions than in the liquid-like amorphous zones. This maybe possible because during partial melting, chain segments lose crystallographic registration but cannot return to the random conformational state characteristic of the unconstrained melt. (Again, this is a direct consequence of both the rigid backbone structure of PC and the constraints imposed by surrounding lamellae.) Therefore, during secondary crystallization subsequent to partial melting, the chain segments already have a more favorable conformational state for crystal formation. This would lead to a faster

rate of secondary crystallization, at least for the bundle-like crystals. Another viewpoint would be to consider that chains in the interlamellar amorphous region have reduced molar conformational entropy than the free melt. Thus they should exhibit a larger driving force towards crystallization.

As mentioned earlier, the kinetics of formation secondary crystals also differ from that of folded-chain lamellae. At the early stages of secondary crystallization, the logarithm of the heat of fusion of the low endotherm, $\log[\Delta H_m^{low}]$, increases linearly with log[time], the slope (i.e. Avrami exponent, *n*) being equal to 0.5. Note that the Avrami exponent of *ca*. 0.5 is observed all PC samples, either fractions or commercials, regardless of the variety of thermal treatments. An Avrami exponent of 0.5 has also been observed in our laboratory for many other semicrystalline polymers, such as PEEK[1], ethylene/octene copolymers[6], PET[34], it-PS[34], etc. We note that an Avrami exponent of 0.5 was already reported by Schultz *et al*. for the secondary crystallization of linear polyethylene at a temperature below that of the primary crystallization[35]. Such a value of the Avrami exponent was argued by these authors to be consistent with predictions for *instantaneous nucleation and diffusion-controlled one dimensional growth* and possibly linked to the observation by Keith *et al*.[36] of intercrystalline links between the edges of chain-folded lamellar crystals. One could, however, interpret this Avrami exponent in the context of the fractal growth process discussed by Mathot *et al*[37]. An Avrami exponent of a value below 0.5 was reported recently by Fu *et al*. for the secondary crystallization of ethylene/1-butene copolymers[38]. The frequently reported Avrami exponent of 0.5 for the secondary crystallization directly indicates that secondary crystallization is very different from primary crystallization in terms of kinetics, for in the

latter case, the Avrami exponent is in the range of 2 to 4 depending on the geometry and the mode of nucleation.

The remaining part of this section will be devoted to the melting behavior of secondary bundle-like crystals. In the results section, it was observed that: 1) the melting traces of PC samples after secondary crystallization reveal the presence of a low endotherm above the crystallization temperature, T_x; and 2) over more than five decades of time, the peak position of this low endotherm increases linearly with the logarithm of time. The linear variation of the low endotherm melting position with $\log[t_x]$ was depicted through equation (5.1), and the intercepts and slopes, $A(T_x)$ and $B(T_x)$ respectively, were reported in Table 5.2.

Based on previous investigations of PEEK[1] and ethylene/α-olefin copolymers[6], a series of conclusions about the physical meaning of the parameters $A(T_x)$ and $B(T_x)$ was extracted. For these polymers, it has been demonstrated that at low to intermediate secondary crystallization temperature, the extrapolation of the equation (5.1) to very short times yields the crystallization temperature, i.e. $T_m^{low} \approx T_x$. For these polymers at low to intermediate temperatures, secondary crystals were proposed to form through a non-folding process. The equality between T_m^{low} and T_x is a signature of the bundle-like crystals through a non-folding process, since the melting temperature of conventional lamellae, even at very short times, always exceeds their crystallization temperatures.

In case of PC, however, it was observed that even at short times, T_m^{low} is always 5 to 10^{o}C higher than T_x. At present this is not completely understood; however, it might be related to the rigid backbone structure of PC. Once a bundle-like crystal is formed, the environment becomes extremely constrained; thus, upon melting these small crystals

exhibit significant superheating effects, which may lead to the higher T_m^{low} than T_x even at short times. One support for this reasoning is that in Table 5.3, as the heating rate decreases, the intercept $A(T_x)$ appears to decrease (less superheating at lower heating rates).

For PEEK[1], ethylene/octene copolymer[6], PC[39], and PET[40], the rate of shift of the low endotherm to higher temperatures with time, $B(T_x)$, was proposed to be due, at least partly, to a parallel decrease in the conformational entropy of the remaining amorphous phase as a consequence of bundle-like secondary crystallization. PC exhibits only a small variation of T_g with time in the course of secondary crystallization. However, a clear broadening of the glass transition has been observed as secondary crystallization proceeds. These observations are in accordance with the explanation that, as a result of the formation of bundle-like crystals, the conformational entropy decreases, and therefore the constraints increase. These issues will be addressed in Chapter 7.

The shift of the low endotherm melting point (T_m^{low}) to higher temperatures with time could also be explained by lateral growth but not thickening of secondary crystals. If thickening was at the origin of the shift of the low endotherm, then the rate of this shift should increase with increasing crystallization temperature, because thickening is generally a thermally activated process. This is contradictory to the experimental observations, where the slope $B(T_x)$ in equation (5.1) decreases with increasing T_x (see Table 5.2). On the other hand, thickening cannot be exclusive to bundle-like crystals, and if such a mechanism is feasible, one would expect the lamellar type crystals also to thicken. Based on the time independence of the peak position of the high endotherm, this

lamellar thickening process cannot be operative at these secondary crystallization temperatures.

Finally, it should be noted that both $A(T_x)$ and $B(T_x)$ are heating rate dependent (see Table 5.3). The values reported in Table 5.2 are evaluated at a heating rate of 10°C/min. The heating rate dependence in the case of PC is very strong since the bundle-like crystals formed during secondary crystallization exhibit a significant amount of superheating[39,41]. In Figure 5.23, the temporal evolution of T_m^{low} in the case of PC-4K exposed to the secondary crystallization at T_x = 165°C is illustrated for different heating rates. T_m^{low} varies linearly with $\log(t_x)$ at all heating rates, and the slope of such lines, $B(T_x)$, becomes steeper with heating rate, β. The inset of Figure 5.23 depicts the variation of $B(T_x)$ as a function of the square root of heating rate $\beta^{0.5}$. The exponent of 0.5 for the heating-rate dependence is based on the assumption that the rate of melting is a linear function of degree of superheating (for details, see Chapter 4). Thus when polymer melting shows superheating, typically the melting point will linearly increase with the square root of heating rate. The linear extrapolation of $B(T_x)$ *vs* $\beta^{0.5}$ to zero heating rate corrects for the superheating effects, providing us with the *intrinsic rate of the shift of the low endotherm* , $[B(T_x), \beta \rightarrow 0]$, at a given crystallization temperature.

For a given polymer, the degree of superheating is a function of its molar mass, crystallization, and also melting conditions. Therefore, the determination of the intrinsic rate of the shift of the low endotherm at different crystallization temperatures and for different molar masses will be necessary. For this, samples are chosen to represent the lowest and the highest molar masses among the crystallizable specimens available, and the temperature range has been selected to be as wide as possible. In Figure 5.24, the

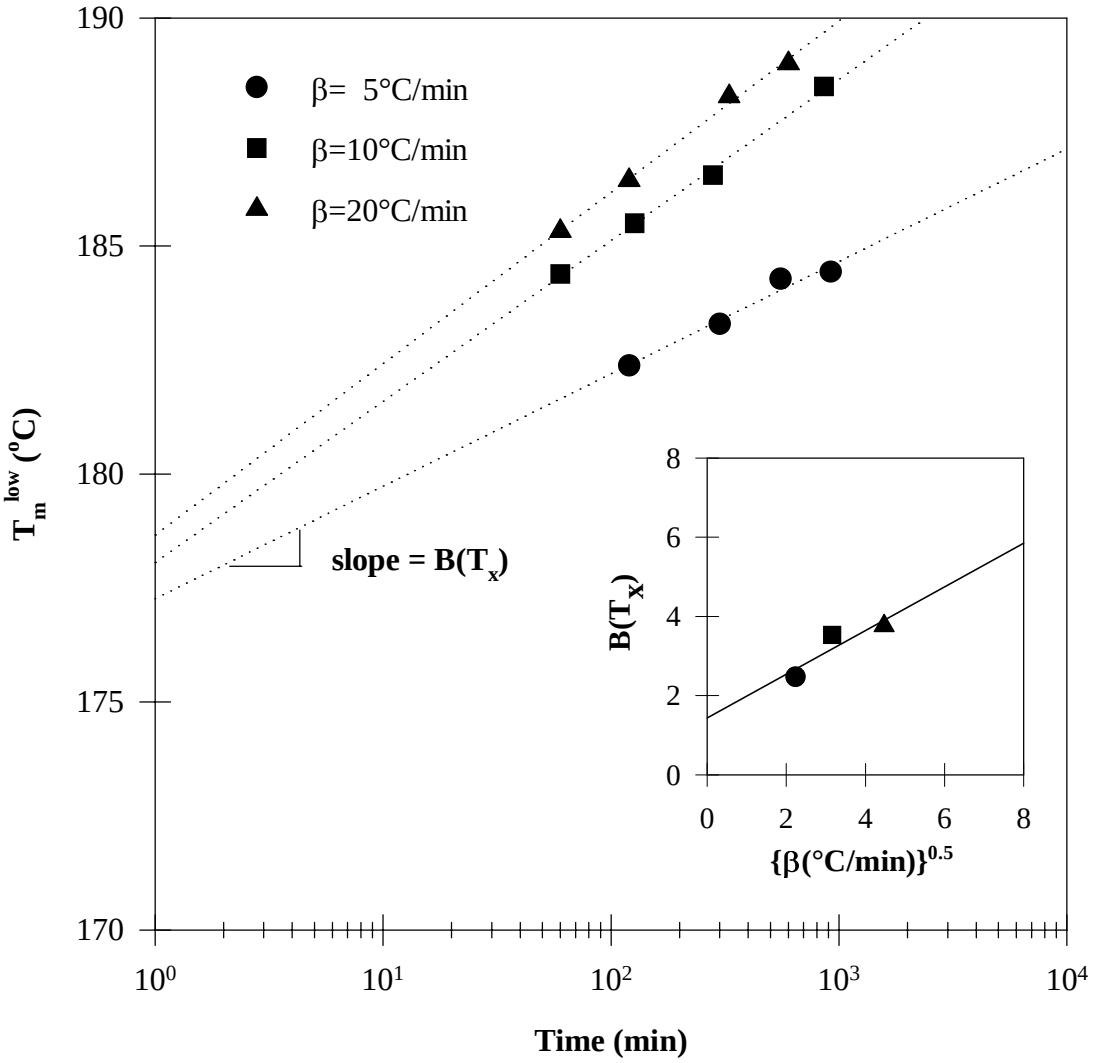

Figure 5.23 Temporal evolution of the low endotherm melting temperature in PC-4K subsequent to secondary crystallization at 165°C at different heating rates. Inset shows the rate of shift of the low endotherm, $B(T_x)$, as a function of the square root of heating rate. Samples were originally crystallized at 165°C for 38 hours and partially melted at 216°C. The accuracies for the temperature and $B(T_x)$ were better than 0.2°C and 0.3°C, respectively.

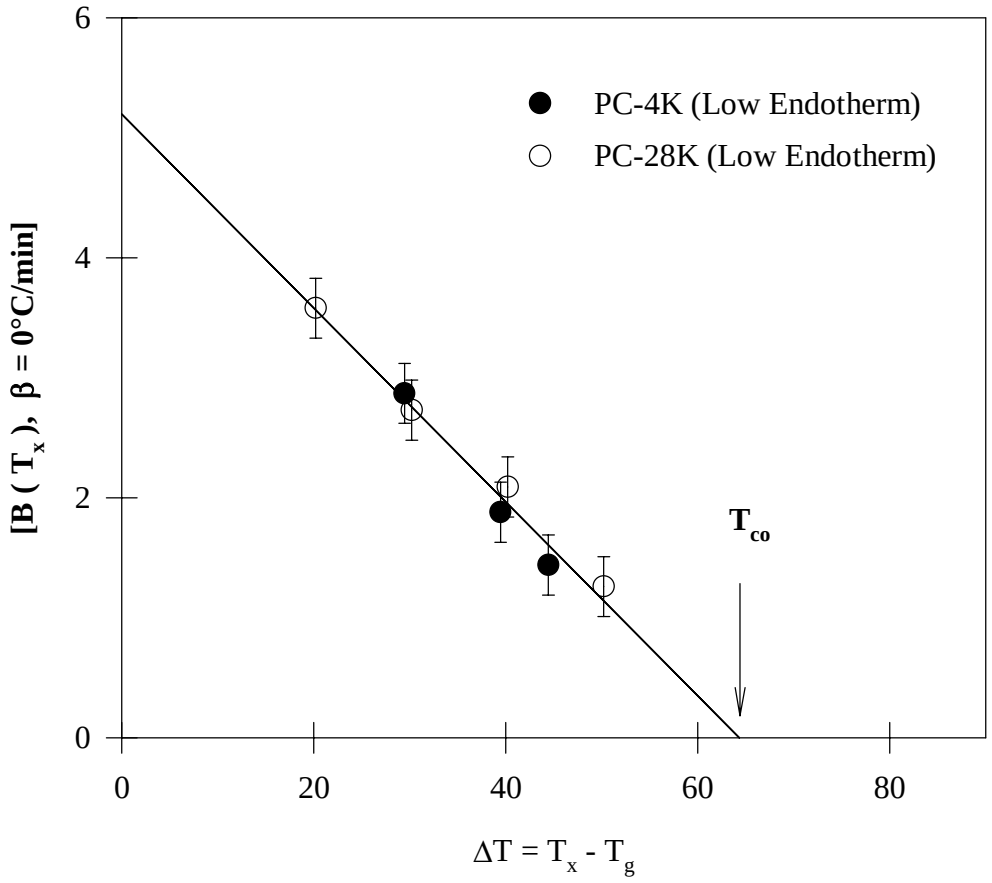

Figure 5.24 Variation of the rate of the shift of the low endotherm at zero heating rate as a function of ΔT (= T_x-T_g) for two extreme molar mass samples of PC used in this study . The arrow points the temperature at which B(T_x) becomes zero (crossover temperature, T_{co}). In Chapter 6, this figure is re-plotted with the data from isothermal annealing experiments (see Figure 6.14).

variation of [$B(T_x)$, $\beta \rightarrow 0$] with ΔT (= $T_x - T_g$) for these two samples has been plotted. [$B(T_x)$, $\beta \rightarrow 0$] decreases with increasing T_x, and more interestingly, [$B(T_x)$, $\beta \rightarrow 0$] for both samples falls on the same line and vanishes at specific crossover temperatures, T_{co}. For instance, around $T_x = 190^oC$ and 210^oC the intrinsic rate of the shift of the low endotherm for PC-4K and PC-28K, respectively, becomes zero. Therefore, possibly, low endotherm does not exist above this crossover temperature.

5.5 Conclusions

The primary crystallization kinetics shows a strong dependence on molar mass distribution. In the molar mass ranging between 4,300 and 55,000 $g.mol^{-1}$, low molar mass fraction crystallizes faster, and the overall crystallization rates differ by more than a factor of 100. It was also observed a significance influence of molar mass distribution on the overall crystallization kinetics.

In contrast, the kinetics of secondary crystallization of PC is essentially molar mass independent. Regardless of molar mass distribution, initial stage of crystallization prior to the secondary crystallization, secondary crystallization temperature, and partial melting temperature, the kinetics of the low endotherm exhibits two universal behaviors: low endotherm melting temperature, T_m^{low}, increases linearly with the logarithm of crystallization time, and at the early stage, the Avrami exponent in the logarithm of the heat of fusion associated with the low endotherm, $\log[\Delta H_m^{low}]$, as a function of the logarithm of crystallization time is 0.5. The rate of the shift of low endotherm with time, $B(T_x)$, was found to decrease with temperature.

From the heating rate correction of $B(T_x)$, it has been found that there exists a crossover temperature at which $B(T_{co}) = 0$, and below which both the low and the high

endotherm are present, and above which only the high endotherm is expected to be stable. This latter issue will be further discussed in Chapter 6.

References

1. H. Marand, A. Alizadeh, R. Farmer, R. Desai, V. Velikov, *Macromolecules* in press; *Bull. Am. Phys. Soc*., **1999**, *44(1)*, 608.
2. B. Falkai, W. Rellensmann, *Makromolekular Chem*., **1964,** *75*, 112.
3. B. Falkai, W. Rellensmann, *Makromolekular Chem*., **1965**, *88*, 38.
4. G. Kämpf, *Kolloid-Zeitschrift*, **1960**, *172*, 50.
5. E. Turska, W. Przygocki, M. Maslowski, *J. Polym Sci. Part C*, **1968**, *16*, 3373.
6. A. Alizadeh, L. Richardson, J. Xu, S, McCartney, H. Marand, W. Cheng, S. Chum, *Macromolecules*, **1999**, *32*, 6221.
7. G. E. Wissler, B. Crist. Jr, *J. Polym Sci., Polym.Phys*., **1980**, *18*, 1257.
8. F. Gallez, R. Legras, J. P. Mercier, *J. Polym Eng. Sci.*, **1976**, *16*, 276.
9. L. C. Lopez, G. L. Wilkes, *Polymer*, **1988**, *29*, 106.
10. M. Day, Y. Deslandes, J Roovers, T. Suprumchuk, *Polymer*, **1991**, *32*, 1258.
11. Y. Deslandes, F. N. Sabir, J. Roovers, *Polymer*, **1991**, *32*, 1267.
12. B. J. MacNulty, *Polymer*, **1968**, *9*, 41.
13. R. E. J. Fryer, *J. Appl. Polym. Sci*., **1974**, *18*, 2261.
14. V. F. Goler, G. Sachs, *Phys*., **1932**, *77*, 281.
15. R. Legras, J. P. Mercier, J. Polym. Sci. Polym Lett., 1970, 8, 645.
16. L. D. Jones, F. E. Karasz, J. Polym. Sci. Polym. Phys., 1966, 4, 803.
17. F. Gallez, R. Legras, J. P. Mercier, *J. Polym Sci. Polym. Phys*., **1976**, *14*, 1367; R. Legras, J. P. Mercier, *J. Polym Sci. Polym. Phys*., **1977**, *15*, 1283; R. Legras, J. P. Mercier, *J. Polym Sci. Polym. Phys*., **1979**, *17*, 1171; G. Mendez, A. J. Müller, *J. Thermal Analysis*, **1997**, *50*, 593. C. Bailly, *M. Daumerie, R. Legras, J. P. Mercier, J. Polym. Sci. Polym. Phys., **1985**,* 23, 343; C. Bailly, R. Legras, J. P. Mercier, *J. Polym. Sci. Polym. Phys*., **1985**, *23*, 355; C. Bailly, M. Daumerie, R. Legras, J. P. Mercier, *J. Polym. Sci. Polym. Phys*., **1985**, *23*, 493.
18. J. M. Jonza, R. S. Porter, *J. Polym. Sci. Polym. Phys*., **1986**, *24*, 2459.
19. L. Mandelkern, A. L. Allou, M. Golapan, J. Phys. Chem., 1968, 72, 309.
20. G. Mendez, A. J. Müller, *J. Thermal Analysis*, **1997**, *50*, 593.
21. E. Ergoz, J. M. Fatou, L. Mandelkern, *Macromolecules*, **1972**, *5*, 147.

22. A. Alizadeh, A. Munoz-Escalona, P. Lafuente, J. V. Garcia-Ramos, J. Martinez-Salazar, *Polymer*, **1999**, *40*, 4345.
23. M. Eskelinen, J. V. Seppala, *Eur. Polym. J.*, **1996**, *32*, 331.
24. V. Velikov, Ph. D. Dissertation, **1996**, Virginia Polytechnic Institute and State University.
25. L. J. Fetters, D. J. Lohse, S. Milner, W. W. Graessley, *Macromolecules*, **1999**, *32*, 6847.
26. Hermann Schnell, "Chemistry and Physics of Polycarbonates", **1964**, John Wiley & Sons, Inc.
27. H. Marand, J. Xu, S. Srinivas, Macromolecules, 1998, 31, 8219.
28. Giuseppe V. Di Filippo, Maria E. Gonzalez, Maria T. Gasiba, A.V. Müller, *J. Appl. Polym. Sci*., **1987**, *34*, 1959.
29. E. Laredo, M. Grimau, A. Muller, A. Bello, N. Suarez, *J. Polym. Sci. Polym. Phys*., **1996**, *34*, 2863.
30. G. Kämpf, *Kolloid-Zeitschrift*, **1962**, *185*, 6.
31. A. Keller, *J. Polym. Sci*., **1955**, *17*, 291,; *ibid*, **1955**, *17*, 351.
32. A. Keller, J. R. S. Waring, *J. Polym. Sci*., **1955**, *17*, 447.
33. A. Siegmann, P. H. Geil, *J. Macromol. Sci. Phys*., **197**0, *B4(2)*, 239; A. Siegmann, P. H. Geil, *J. Macromol. Sci. Phys*., **1970**, *B4(2)*, 273.
34. A. Alizadeh, S. Sohn, J. Xu, R. Farmer, S. Elkoun, H. Marand, Manuscript in preparation.
35. J. M. Schultz, R. D. Scott, *J. Polym Sci*. A-2, **1969**, *7*, 659.
36. H. D. Keith, F. J. Padden, R. G. Vadimsky, *J. Appl. Phys*., **1971**, *42*, 4585.
37. V. B. F. Mathot, R. L. Scherrenberg, T. F. J. Pijpers, *Polymer*, **1998**, *39*, 4542; V. B. F. Mathot, R. L. Scherrenberg, T. F. J. Pijpers, Y. M. T. Engelen, *New Trends Polyolefin Sci. Tech*., **1996**, 71.
38. Q. Fu, F. C. Chiu, K. McCreight, M. Guo, W. W. Tseng, S. Z. D. Cheng, M. Y. Keating, E. T. Hsieh, P. J. Deslauriers, *J. Macromol. Sci. Phys*., **1997**, *B36(1)*, 41.
39. S. Sohn, A. Alizadeh, H. Marand, *Polymer* in print.
40. H. Marand, P. Sholtz, R. Verma, V. Prabhu, V. Vivirito, *Bull. Am. Phys. Soc*., **1996**, *41(1)*, 450.

41. B. Wunderlich, in “Macromolecular Physics”, **1980**, Academic Press, N. Y. Vol 3.
42. M. Dettenmaier, H. H. Kausch, *Colloid and Polymer Sci*., **1981**, *259*, 209.

Chapter 6

Isothermal Lamellar Thickening of Semicrystalline PC

6.1 Introduction

In Chapter 5, from the heating rate effect on the shift of the low endotherm with time (see Figure 5.24), it has been proposed that around 210^{o}C, a change in secondary crystallization behavior may occur for PC-28K. In this chapter, to provide proper evidence for this hypothesis, a series of experiments was performed. First, isothermal annealing was done to follow the thermal behavior of these annealed samples. Second, the variation of lamellar thickness upon isothermal annealing was measured directly using AFM. Based on the melting temperature and lamellar thickness, a Gibbs-Thomson plot could be constructed, from which the equilibrium melting temperature (T_m^o) and the basal plane interfacial free energy (σ_e) were extracted.

6.1.1 *Isothermal Lamellar Thickening*

Polymers often crystallize in the form of spherulite composed of lamellae (see, for example, Micrographs 1 to 4 in Chapter 5). The chain folding nature of lamellae leads to anisotropic surface free energies, being higher on the chain-folded surface than on the lateral side. When lamellar thickening occurs, the ratio of surface area to total volume decreases (i.e., less surface effect), and thus overall free energy of crystals decreases.

Several polymers are known to exhibit isothermal lamellar thickening: poly(ethylene oxide) (PEO)[1-3], poly(4-methylpentene-1)[4-6], poly(ε-caprolactone)[7], and polyethylene[3,8-10]. It needs to be noted that isothermal lamellar thickening only occurs when polymer crystals exhibit an α_c relaxation; however, chain mobility inside the crystals (i.e., α_c relaxation) is necessary not a sufficient condition. All the above

polymers have been reported to possess both α_c relaxation and isothermal lamellar thickening[5]. It also needs to be emphasized that isothermal lamellar thickening is a kinetic process. Even though a certain temperature for α_c relaxation ($T\alpha_c$) exists, if sufficient time is allowed, thickening could occur at a lower temperature than known $T\alpha_c$. Therefore, $T\alpha_c$ should be understood as a range of temperatures rather than as a well-defined single temperature. Some theoretical studies explaining the mechanism of isothermal lamellar thickening have appeared. For instance, Sanchez *et al*. derived equations for the rate of thickening by treating the process using irreversible thermodynamics[11,12].

As noted earlier, α_c relaxation occurs above a certain temperature, $T\alpha_c$, and this temperature is more or less a material property, although it possesses some kinetic nature. For instance in case of PE, $T\alpha_c$ is known to be around 60^{o}C[8-10]. For PC, $T\alpha_c$ is not known, yet two reports claim that PC exhibits lamellar thickening. Jonza and Porter observed lamellar thickening by double annealing at 470K and 503K from SAXS experiments[13]. Very recently, from the DSC experiments, Mendez and Müller reported peak position shifting (3-5^{o}C) of PC by isothermal annealing at 462K[14]. They crystallized samples in the presence of acetone vapor at room temperature for 9 hours. Based on this shifting of peak position, they concluded that semicrystalline PC exhibits isothermal lamellar thickening[14].

In the previous chapter, it was proposed that a crossover phenomenon may occur around 210^{o}C in PC. Therefore, if PC crystals were annealed isothermally around this temperature, an isothermal lamellar thickening may be observed. These experiments will be of interest in that the existence of isothermal lamellar thickening in PC indeed

supports the main conclusion in Figure 5.24, that above T_{co}, low endotherm may not be stable, and thus, only the high endotherm exists. From the studies described in Chapters 4 and 5, it is known that low endotherm exists below this temperature. Isothermal annealing experiments have been conducted inside the DSC on PC-28K initially crystallized at 185^{o}C for 202 hours at five different temperatures above 208^{o}C.

It needs to be mentioned that the most direct evidence for the existence of α_c relaxation will be the measurement of chain mobility inside crystals around the proposed $T\alpha_c$ using solid state NMR or dynamic mechanical analysis (DMA). For instance, Schmidt-Rohr *et al*. recently detected the occurrence of chain flips in PE (at T_m-60K)[15,16], i-PP (at T_m-80K)[17], PEO (at T_m-100K)[17], and POM (at T_m-90K)[16]. Also using DMA, the $T\alpha_c$s of various flexible polymers such as PE[3], it-PP[18], PEO[3], and POM[3] have been reported. The debate regarding the existence of α_c relaxation in semi-flexible polymers such as PET and PEEK is not completely settled[5,15,16]; however, it is generally accepted that for these polymers, $T\alpha_c$, if it exists, should be in the proximity of the apparent melting temperature. Therefore, the most direct evidence of α_c relaxation in semi-flexible polymers using the two above mentioned techniques may not be easily achievable. This is because in solid state NMR, as noted in the parenthesis, the chain mobility is generally measured well below the apparent melting temperature, and for DMA, the relaxation peak around $T\alpha_c$ will be more than likely overlapped with the melting peak[5]. In the present work, as an alternative to provide an evidence for the existence of α_c relaxation in PC, isothermal lamellar thickening experiments were performed (recall the fact that *isothermal lamellar thickening is only possible in the*

presence of α_c relaxation, and in general the starting temperature of isothermal lamellar thickening is close to $T\alpha_c$)[5].

6.1.2 *Polymer Epitaxy*

Calorimetry study is effective in following the thermal behavior of samples that underwent isothermal annealing, and as reported recently[14], the resultant thermograms may suggest the existence of isothermal lamellar thickening based upon the change of melting peak position with time. However, the most direct evidence will be the measurement of lamellar thickness upon isothermal annealing. This, yet, is not an easy task because in general, spherulites formed upon crystallization are the mixture of lamellae grown in all orientations, so the observed morphology cannot be used for the measurement of lamellar thickness.

To resolve this issue, a special substrate will be required upon which lamellae can grow epitaxially, and preferentially in an edge-on orientation. The rigorous definition of epitaxy is the growth of one phase (guest crystal) on the surface of another phase (host crystal) in one or more strictly defined crystallographic orientations[20]. To achieve this goal, guest and host crystals must have related crystallographic structures. Although the structural analogy implies interactions at the molecular scale, such a level of understanding is seldom achieved, especially in the polymer crystallization field. Therefore, epitaxy is often defined in terms of purely geometric lattice matching; 10-15% lattice mismatch between the host and guest crystals is considered as an upper limit for an epitaxy.

Since the first observation of polymer epitaxy on alkali halide substrates[21,22] in the 1950s, several other substrates have been investigated. Among them, polymer epitaxy on

organic substrate and polymer-polymer epitaxy have been of interest. Theoretically if one can use single crystals for the substrate of the epitaxy of the same polymer, then the lattice parameter matching will be perfect, therefore, this substrate will produce perfect epitaxy. In reality, it is very challenging to grow macroscopic size single crystals. To overcome this problem, oriented polymers have been used for substrates. Various orientation techniques have been adopted, such as spinning or coextrusion[23] and uniaxial drawing[24]. References 25 and 26 are the reviews of epitaxy on low molar mass (mainly inorganic) materials, and epitaxy of polymer-organic (including polymer-polymer) systems, respectively. The use of inorganic substrate has revealed the major structural and morphological features of polymer epitaxy. As a general rule, *the guest polymer chains lie with their chain axis parallel to the substrate surface*: the lamellae that grow edge-on, i.e., are normal to that substrate.

In this study, calcite was chosen for the substrate based on the close lattice parameter matching. The morphological feature of this PC epitaxy on calcite substrate was monitored by AFM, and lamellar thickness and distribution were calculated from 100 or more measurements of lamellar thicknesses. Finally, various techniques were employed to measure the melting temperature of isothermally annealed samples. Based on the lamellar thickness and the melting temperature data, a Gibbs-Thomson plot could be constructed, from which the equilibrium melting temperature (T_m^o) and the interfacial free energy (σ_e) were determined.

6.2 Experimental

Purified bisphenol-A polycarbonate PC-28K commercial samples have been used for isothermal annealing and secondary crystallization experiments in DSC and also for

direct lamellar thickness measurements using AFM. For detailed sample molecular characteristics, see Chapter 3.

6.2.1 *Calorimetry Study*

PC-28K samples were crystallized at 185^{o}C for 202 hours, and these as-crystallized samples were exposed to isothermal annealing experiments performed inside DSC at 5 different temperatures (208, 214, 217, 220, 223^{o}C) in the time frame of 1 minute to 35 hours. Upon reaching the desired annealing time, t_x, samples were cooled at the maximum cooling rate available to 100^{o}C, and heating traces were then recorded at 10^{o}C/min. The details of procedures for DSC sample preparation and temperature calibrations were described in Chapter 3.

6.2.2 *Atomic Force Microscopy*

An atomic force microscope (Digital Instrument, Dimension 3000) was operated in tapping mode at room temperature using nanosensor TESP (tapping etched silicon probe) type single beam cantilevers. Images were collected in both height and phase modes. For the lamellar thickness measurement, at least 100 lamellae were chosen from three samples, and each individual lamellar thickness was determined from the section analysis software (see below). Lamellar thickness distribution was then constructed, from which the most probable population of lamellar thickness was designated as the mean lamellar thickness.

Figure 6.1 shows a schematic presentation of the section analysis method. After capturing the phase image of a given sample, one can draw a vertical line to the normal direction of lamellae on the image, and the software converts the phase image across the line to a near sinusoidal shape curve as shown in Figure 6.1. The upper portion of the

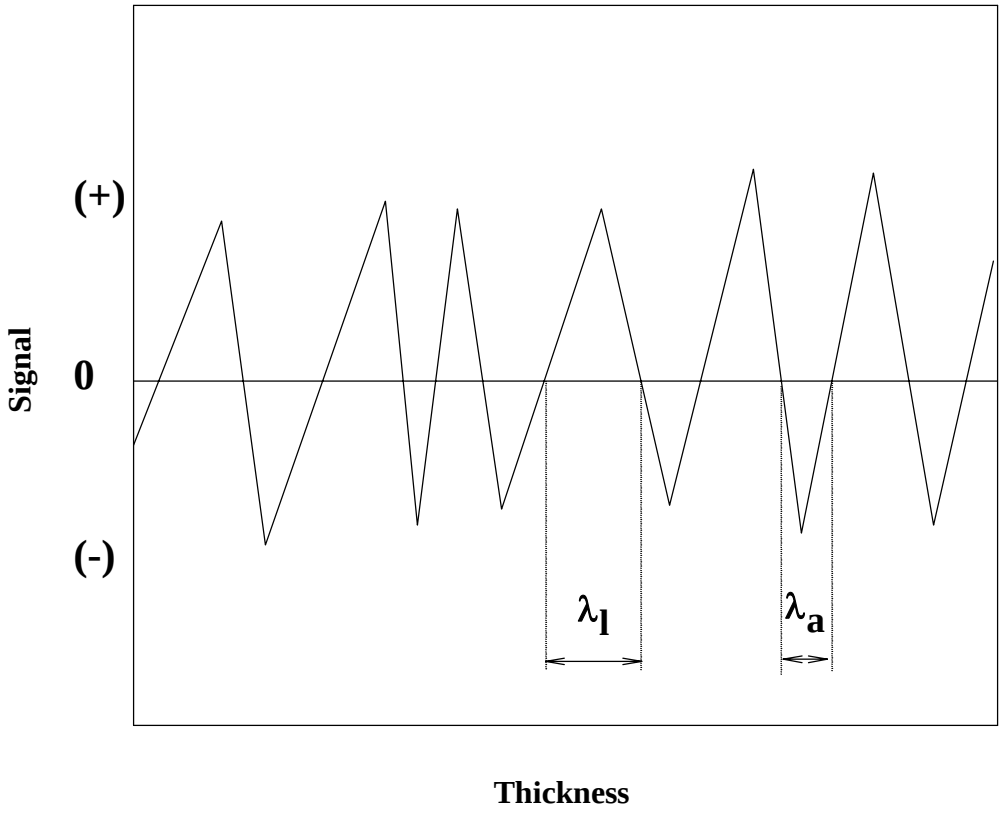

Figure 6.1 A schematic illustration of AFM phase mode signal used to determine lamellar thickness. λ_l and λ_a stand for lamellar and amorphous layer thickness, respectively (for detailed description, see the text).

sinusoidal curve depicts an individual lamella, and the lower part represents the amorphous layer between the neighboring lamellae. The lengths λ_l and λ_a shown in Figure 6.1 are the lamella and the amorphous layer thickness, respectively.

Although the above procedure provides a reliable way to measure thickness, the measured values could be overestimated. This could be because first, tip geometry and tip edge broadening may induce an overestimation of actual lamellar thickness, and second, the potential interactions between the tip and the lamellae being scanned may hinder an accurate measurement. Currently, there are no means to quantitatively correct the latter source of error. However, in tapping mode, it is more than likely that the interactions between the tip and the substrate will be much less significant than in contact mode, so in this study this effect was considered negligible. For the correction from the tip broadening and tip geometry, a standard sample (MXS 301CE, from Moxtek Co., serial number: D112805010) with a known thickness was scanned under the same conditions, and the measured lamellar thickness was calibrated according to this correction factor*. The dimensional accuracy for this particular standard sample guaranteed by the provider was better than 0.5 nm. The calculated overestimation was 10±2%, and this correction is quantitatively in good accordance with the previous report[27]. Zhou and Wilkes compared the accuracy of three different techniques– SAXS,

* The MOXTEK MXS 301 CE calibration and reference standard is fabricated using a silicon wafer substrate which is overcoated with a polymer material. To render the durability, 60nm thickness of tungsten is double coated on top of this polymer. The company certified calibration period was 288nm. In this study, the lamellar thickness was in the range of 4 to 16nm, a range that is significantly smaller than the size of calibration period. Due to the unavailability of proper standards for the comparable size with lamellar thickness, we were forced to use the above standard, and consequently a large uncertainty was inevitable. Therefore, in this study, we are more interested in the change of lamellar thickness upon isothermal lamellar thickening.

TEM, and AFM– in terms of quantitative determination of lamellar thickness[27]. They concluded that the accordance between SAXS and TEM is excellent, while the lamellar thickness from AFM was slightly overestimated in the order of 10%.

6.2.3 *Epitaxial Growth*

As noted earlier, calcite (*Iceland Spar*, origin Chihuahua, Mexico) was used as a substrate for the epitaxial growth of PC lamellae. This choice was based upon the close matching of unit cell parameters[28]. The unit cell structure of PC is monoclinic, in which unit cell parameters are: a =10.1Å, b =12.3Å, c =20.8Å and $\gamma = 84^{o}$ at room temperature[29]. The schematic structure of (014) plane (cleavage plane)[28] of calcite substrate is illustrated in Figure 6.2. From the known lattice parameters of substrate and crystalline PC, the degree of lattice mismatching in the a- and c-axis can be calculated: Δ_a = +1.2%; Δ_c = +2.7%, under the assumption of b-axis growth direction. These mismatches are well below the upper limit of 10-15% for the epitaxial growth (see above).

It is important to note that the above criterion of lattice matching for an epitaxy is only a necessary condition. To achieve a rigorous epitaxy it is necessary to know the exact surface topology of contact crystals. In other words, PC chain conformation on top of calcite is also an important criterion in epitaxial growth. Unfortunately, as far as we concerned, the epitaxy of PC has not been previously reported let alone for this particular substrate. Therefore, at present, it can not be ensured whether calcite substrate meets the latter requirement. As will be seen later, PC does not form a rigorous epitaxy for several reasons; nonetheless, at least locally, PC lamellae appear to grow edge-on under conditions of pseudo-epitaxy, which makes it possible to measure the lamellar thickness. In this context, therefore, we loosely use the term epitaxy to include this type of pseudo-

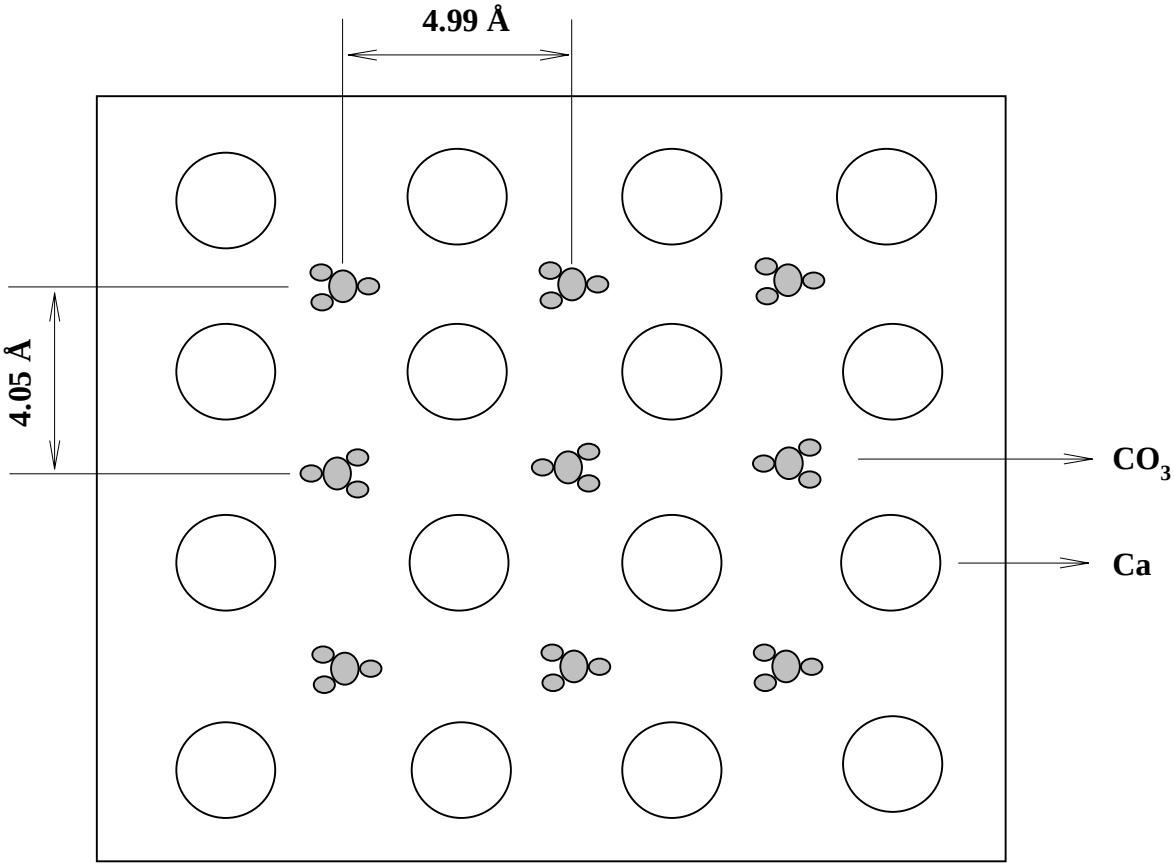

Figure 6.2 A schematic structure of (014) cleavage plane of calcite ($CaCO_3$)

epitaxy.

Each PC sample was prepared as follows. First, 0.2 wt% polymer solution was prepared by dissolving PC-28K sample in HPLC grade chloroform. A proper size of freshly cleaved calcite was placed in the solution and removed after one minute. Then the prepared sample was first dried at 150^{o}C *in vacuuo* for a period of 24 hours and subsequently crystallized at 185^{o}C in an oven for 95 hours. Upon reaching the desired crystallization time, three samples were examined by AFM to measure lamellar thickness. After these examinations, those samples were further annealed at 220^{o}C for three different time stages (5, 10, and 18 hours) to see the effect of isothermal annealing. At each stage, lamellar thickness was measured by AFM following the same procedures.

6.3 Results

6.3.1 *Isothermal Lamellar Thickening from DSC*

Figures 6.3 to 6.5 show the melting traces of isothermally annealed PC-28K for different temperatures. Figure 6.6 and 6.7 summarize the analyses in terms of melting temperature and heat of fusion change upon isothermal annealing, respectively. From the DSC melting traces, one can unambiguously tell that the melting temperature increases and the endothermic peak broadens with time for a given annealing temperature. At short times of up to 10 minutes, in this particular temperature range, melting temperature (T_m^{high}) and heat of fusion (ΔH_m^{high}) increase slowly, while at longer times, both start to increase dramatically. To explain these observations, two possible reasons are proposed. First, upon high temperature annealing, molar mass might be decreased due to the thermal degradation, and second, these annealing temperatures are above the α_c relaxation temperature ($T\alpha_c$), thus, lamellae underwent lamellar thickening possibly with

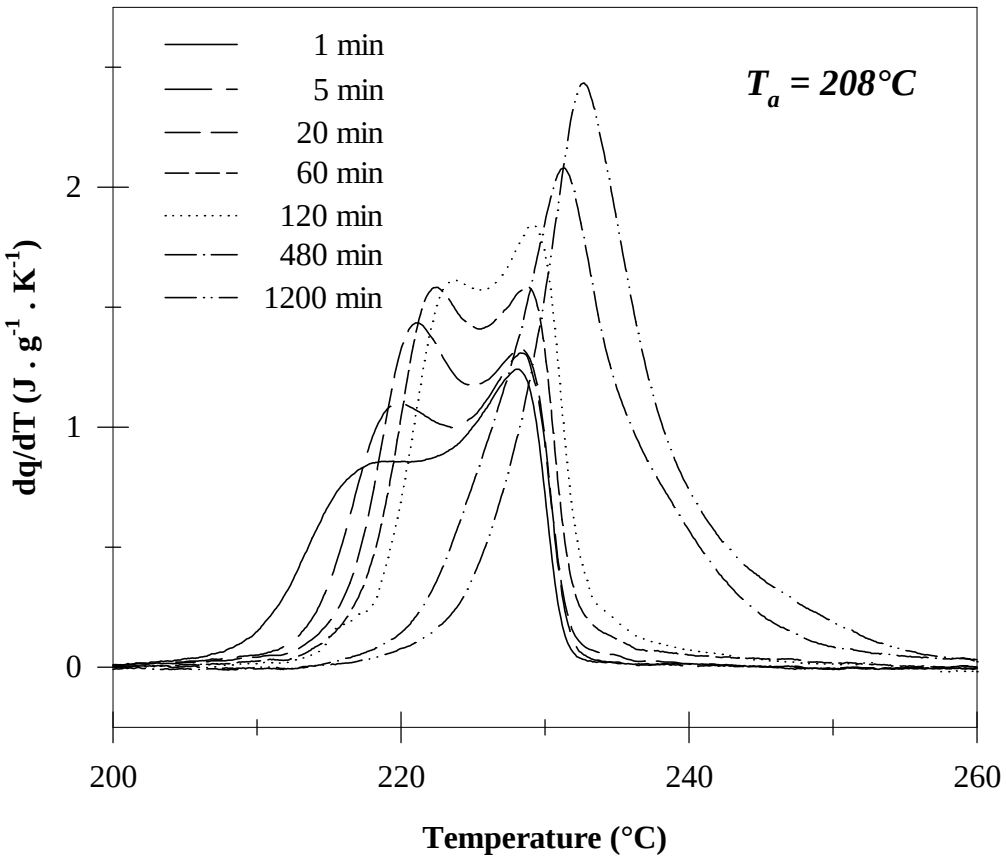

Figure 6.3 The effect of annealing above the primary crystallization temperature on the melting behavior of PC-28K. Samples were initially crystallized at 185^{o}C for 202 hours. Annealing temperature, T_a = 208^{o}C.

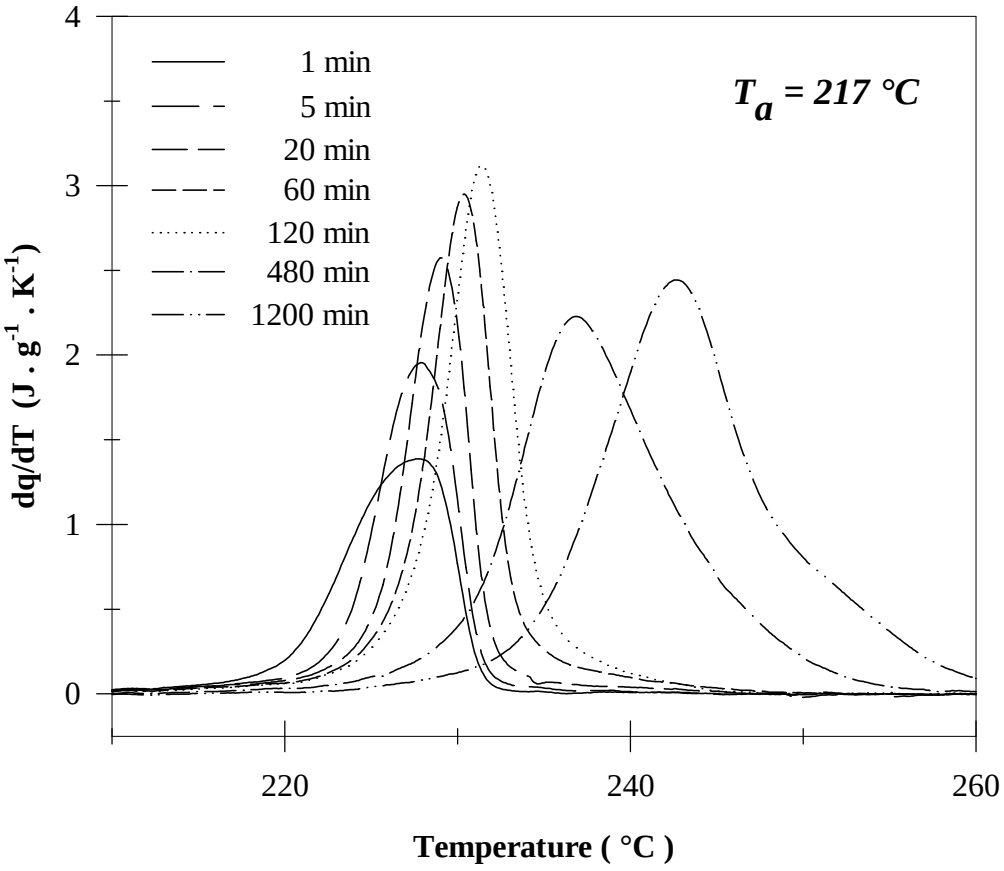

Figure 6.4 The effect of annealing above the primary crystallization temperature on the melting behavior of PC-28K. Samples were initially crystallized at 185^{o}C for 202 hours. Annealing temperature, T_a = 217^{o}C.

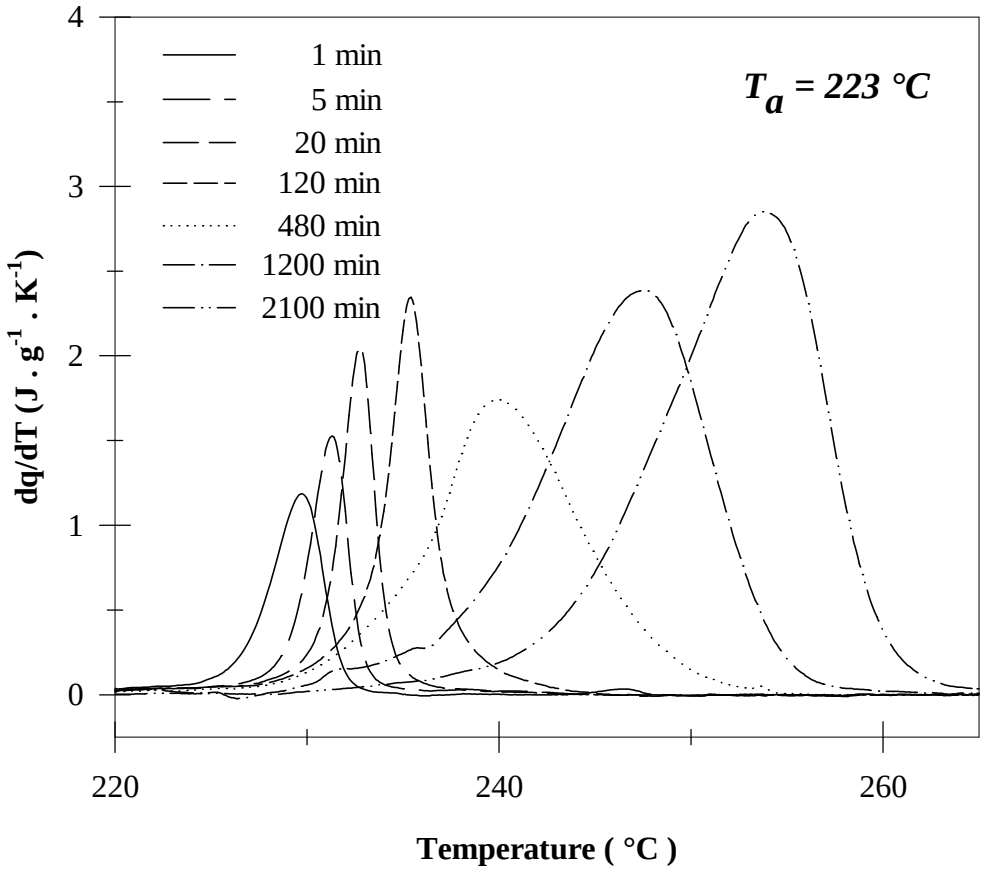

Figure 6.5 The effect of annealing above the primary crystallization temperature on the melting behavior of PC-28K. Samples were initially crystallized at 185^{o}C for 202 hours. Annealing temperature, T_a = 223^{o}C.

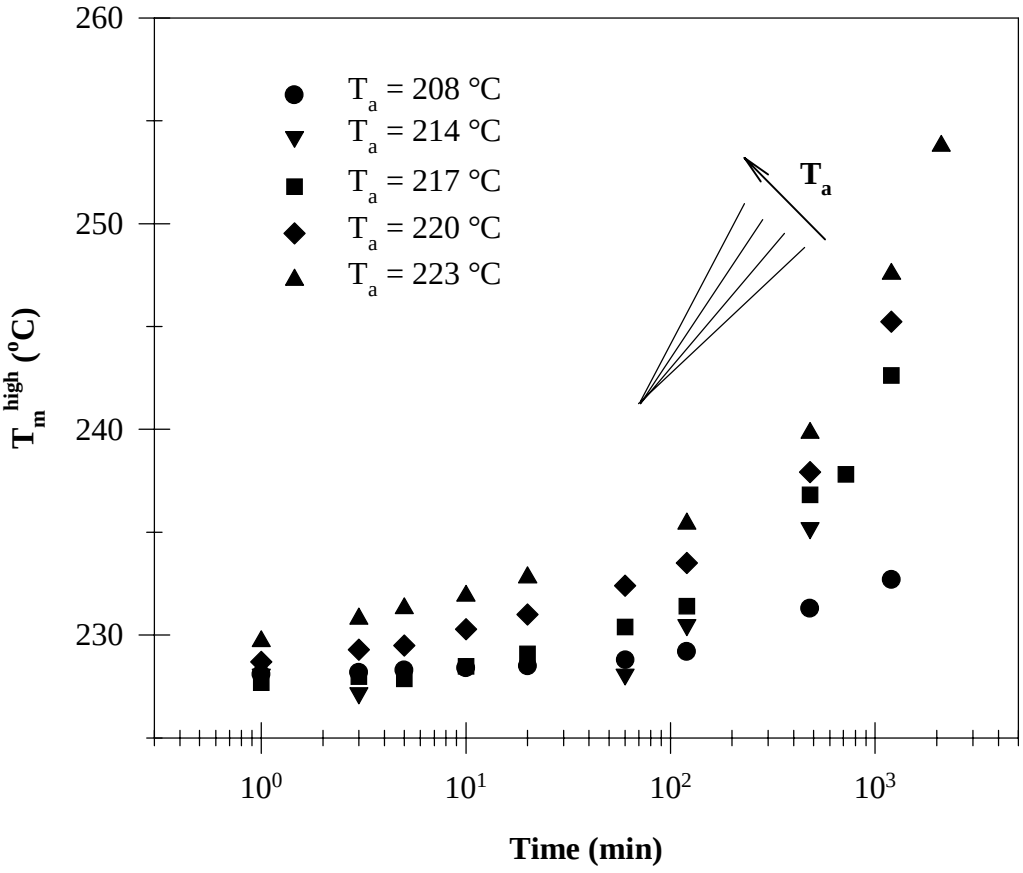

Figure 6.6 Variation of melting peak temperature as a function of annealing time for various annealing temperatures. For inset lines, see the discussion section. The accuracy of the temperature determination was better than 0.2°C.

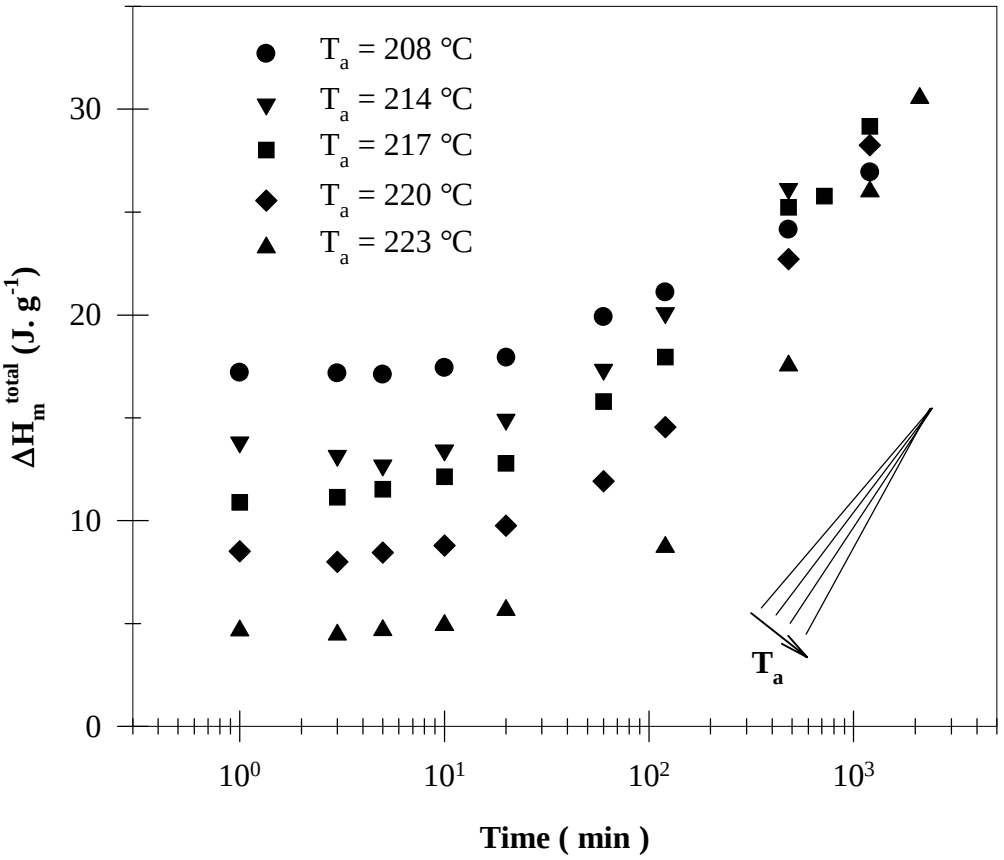

Figure 6.7 Variation of the total heat of fusion as a function of annealing time for various annealing temperatures. For inset lines, see the discussion section. The accuracy of the determination of the experimental heat of fusion was better than 0.5 $J.g^{-1}$.

crystal perfection.

To check the possibility of thermal degradation, molar masses of some of the samples, including the one annealed for the longest times at the highest temperature (i.e., 40 hours at 224^{o}C), were checked by GPC. The results are presented in Figure 6.8 and Table 6.1. Certainly, it can be stated that within experimental uncertainty, the molar mass and molar mass distribution were not adversely affected by isothermal annealing at this temperature and for the range of times. Therefore, the first hypothesis must be ruled out, leaving the second possibility that isothermal lamellar thickening, possibly with crystal perfection, is most likely at the origin of the increase of T_m^{high} and ΔH_m^{high} upon isothermal annealing.

6.3.2 *Lamellar Thickness Measurement by AFM*

From the calorimetry study, melting peak broadening and shifting to a higher temperature may indicate the consequences of isothermal lamellar thickening, yet these cannot be the direct evidences. The most direct evidence is the measurement of lamellar thickness upon isothermal annealing. To this end, AFM was utilized to measure the lamellar thickness of PC epitaxially grown on calcite substrate. In Micrographs 6.1 to 6.4, phase images of isothermally annealed specimens are presented. Micrograph 6.1 shows a PC sample before annealing (i.e., as-crystallized at 185^{o}C for 95 hours), and Micrographs 6.2, 6.3, and 6.4 show for 5, 10, and 18 hours of annealing at 220^{o}C, respectively. In each micrograph, one can observe an area of pseudo-epitaxy. Lamellae in this area were carefully analyzed to determine lamellar thickness and distribution. As mentioned earlier, at least 100 lamellae from three different samples were analyzed for each annealing time, including as-crystallized samples. One of the unique features of the

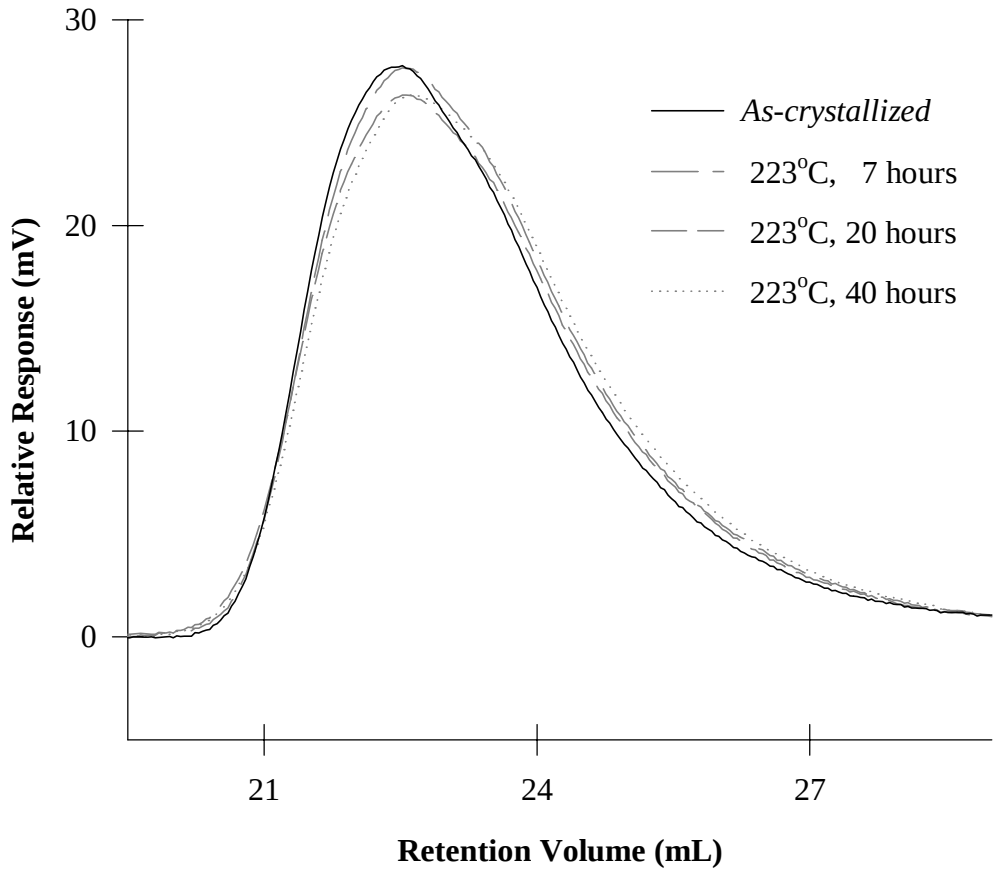

Figure 6.8 GPC traces of PC-28K samples before (as-crystallized) and after annealing at 224°C for different times. Samples were initially crystallized at 185°C for 202 hours.

Sample	**Annealing Conditions**	**M_w (g/mol)**	**M_w/M_n**
PC-28K	*As-crystallized*	29,400	*2.03*
	224^{o}C, 7 h	31,000	*2.10*
	224^{o}C, 20h	31,500	*2.08*
	224^{o}C, 40h	29,100	*2.13*

Table 6.1 GPC analysis before and after isothermal annealing at 224^{o}C.

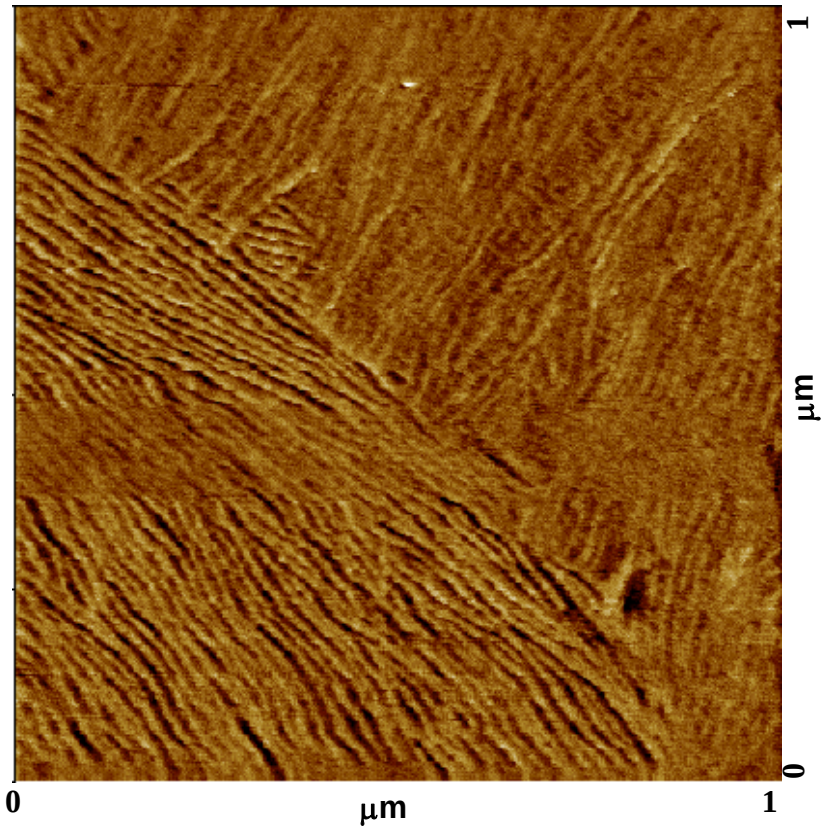

Micrograph 6.1 AFM phase image of PC lamellae on calcite. PC-28K sample was initially crystallized at 185^{o}C for 95 hours (*as-crystallized*).

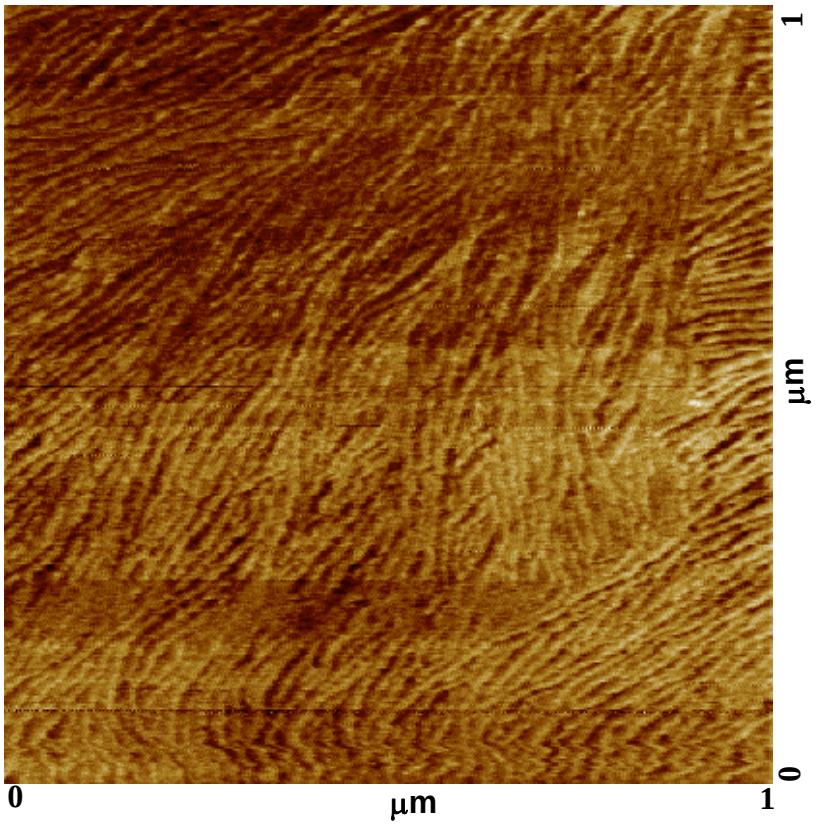

Micrograph 6.2 AFM phase image of PC lamellae on calcite. PC-28K sample was initially crystallized at 185^{o}C for 95 hours, and further annealed at 220^{o}C for *5 hours*.

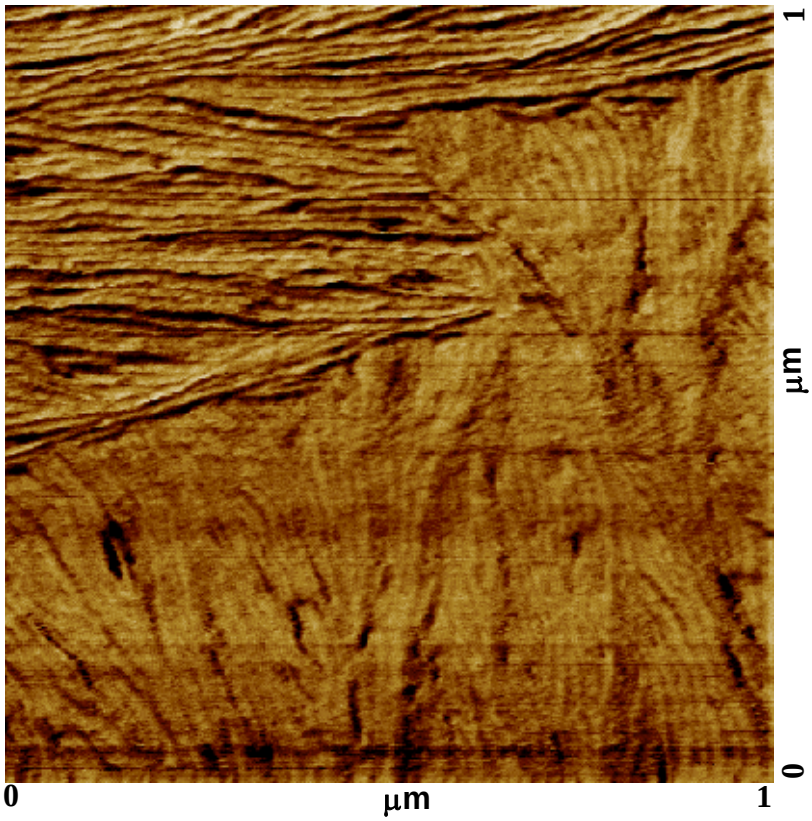

Micrograph 6.3 AFM phase image of PC lamellae on calcite. PC-28K sample was initially crystallized at 185^{o}C for 95 hours, and further annealed at 220^{o}C for *10 hours*.

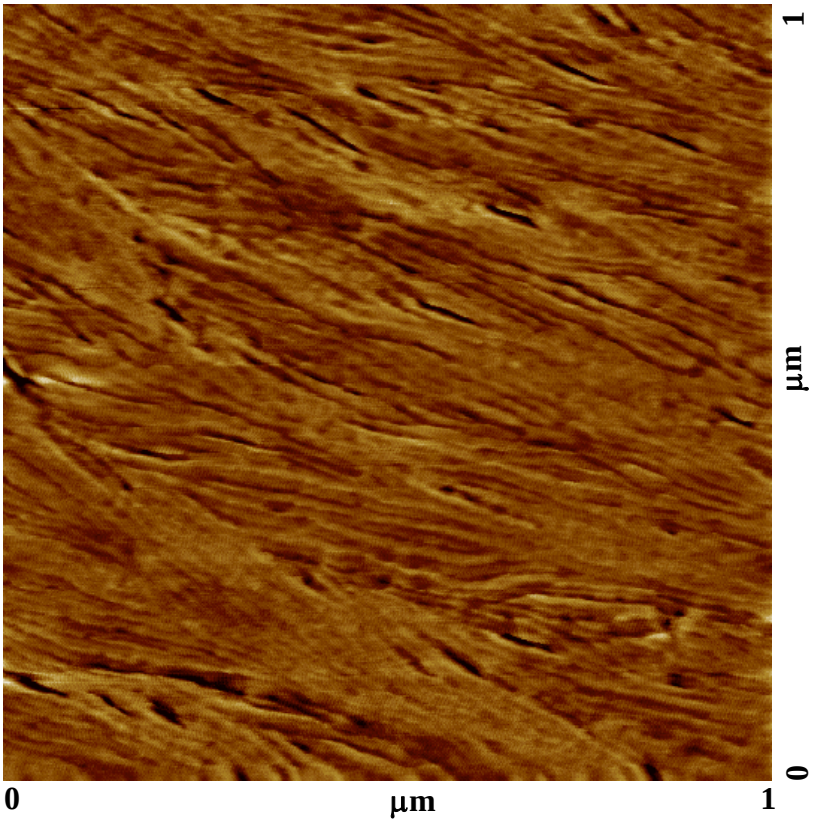

Micrograph 6.4 AFM phase image of PC lamellae on calcite. PC-28K sample was initially crystallized at 185^{o}C for 95 hours, and further annealed at 220^{o}C for *18 hours*.

AFM technique is that the surface image can be visualized under various view and light angles. This "image tilting" can be used to check the qualitative degree of epitaxy. Micrograph 6.5 shows the tilted image of Micrograph 6.1 under different angle to three-dimensionally visualize the surface structure. In the left lower diagonal, one can observe vertically oriented lamellae on top of calcite.

The analyses of lamellar thickness distribution are shown in Figures 6.9 and 6.10. In Figure 6.9, lamellar thickness distributions for each annealing temperature, including as-crystallized sample, are shown. In Figure 6.10 all these lamellar thickness distributions are plotted together to show the effect of isothermal annealing on the variation of lamellar thickness. The mean lamellar thickness and the standard deviation are also summarized in Table 6.2. Clearly, an increase in isothermal annealing time leads to an increase in the mean lamellar thickness (i.e., indicating isothermal lamellar thickening). The breadth of the lamellar thickness distribution as measured by the standard deviation also increases with annealing time. Of further interest, as seen in Figure 6.11, lamellar thickness and the standard deviation increase linearly with the logarithm of annealing time. A similar linear relationship between lamellar thickness and logarithm of isothermal annealing time has been previously reported for poly(4-methylpentene-1)[30] and poly(ε-caprolactone)[31].

6.3.3 *Construction of Gibbs-Thomson Plot*

For the construction of Gibbs-Thomson plot, melting temperature and *corresponding* lamellar thickness must be known. In the present study, peak melting temperatures of crystals were determined from the calorimetry study, and lamellar thickness from AFM. With regard to sample preparation, bulk-crystallized thick samples

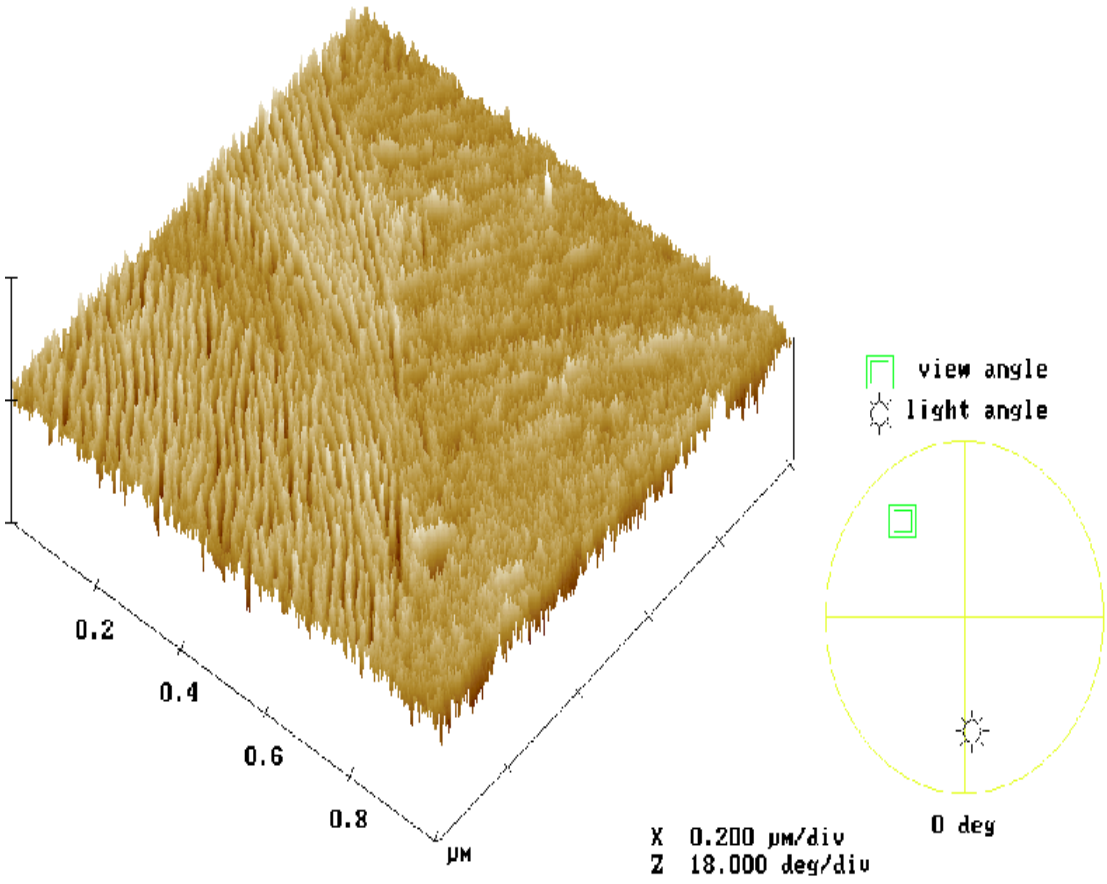

Micrograph 6.5 AFM surface image viewed from different angle of *as-crystallized* PC lamellae on calcite (i.e., tilted surface image of micrograph 6.1). PC-28K sample was initially crystallized at 185°C for 95 hours.

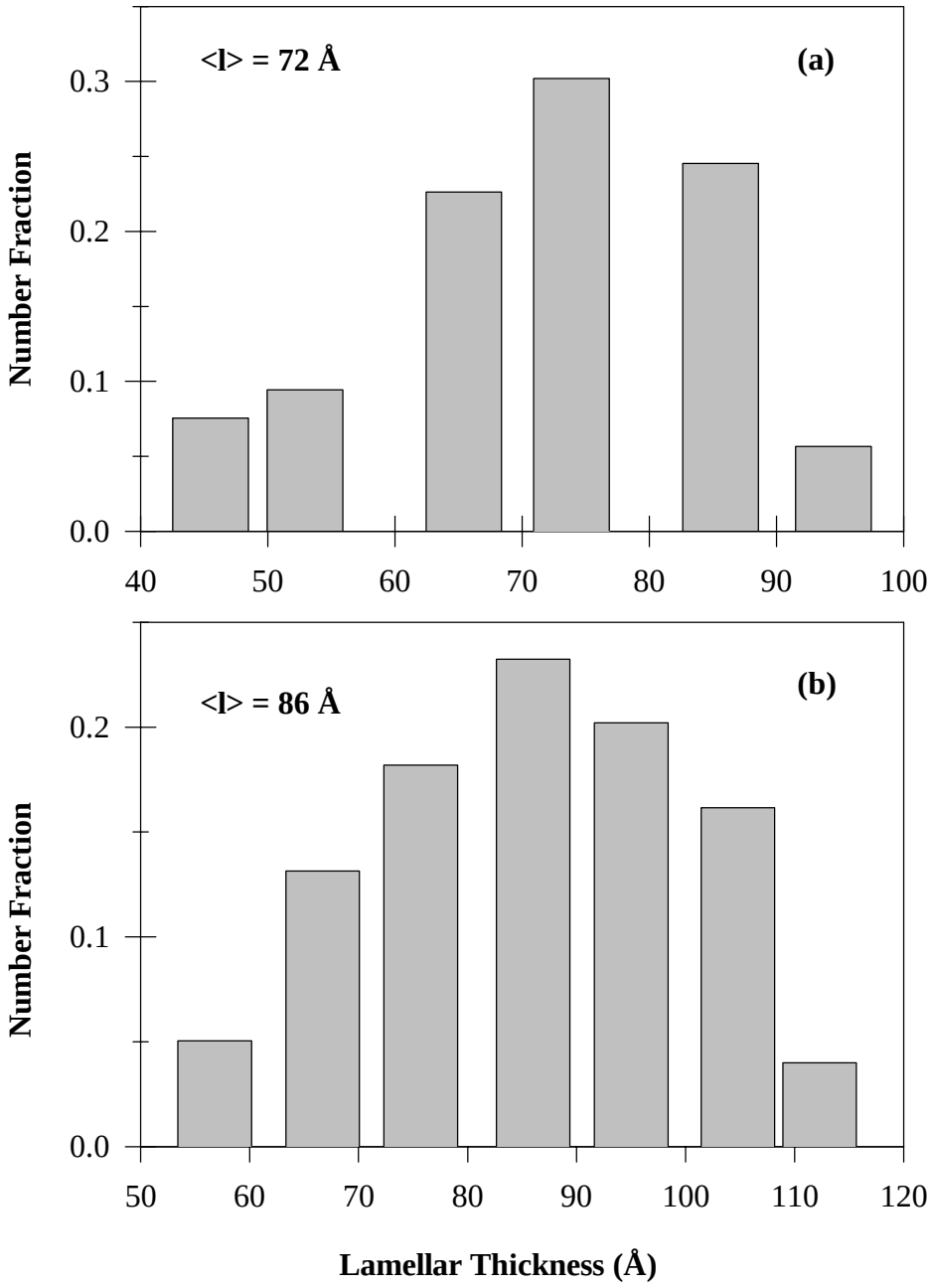

Figure 6.9 Lamellar thickness distribution upon isothermal annealing at 220^{o}C for different times. PC-28K samples were crystallized on calcite at 185^{o}C for 95 hours. a) As is; (b) 5 hours; (c) 10 hours; (d) 18 hours.

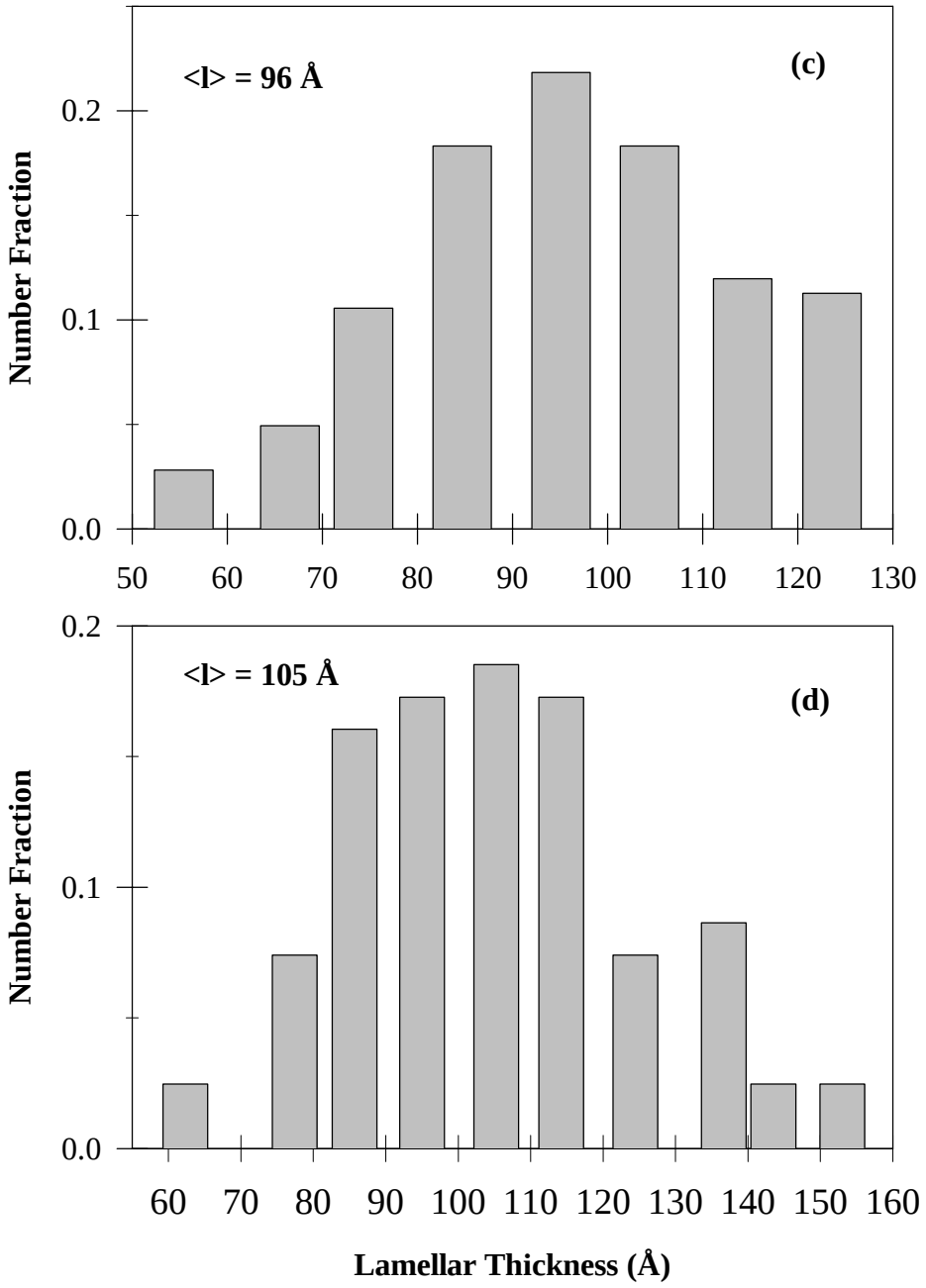

Figure 6.9 Continued

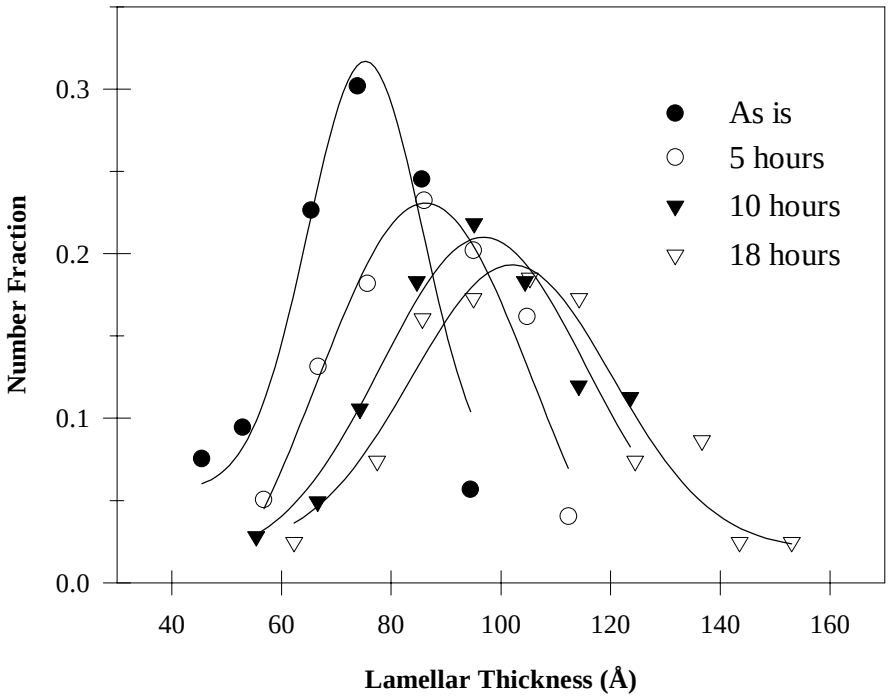

Figure 6.10 Lamellar thickness distribution upon isothermal annealing of PC-28K at 220^{o}C for various times.

Time (hrs)	$\langle l_c \rangle$ (Å)	$\langle \sigma_c \rangle$ (Å)
0	72	*14*
5	86	*15*
10	96	*18*
18	105	*21*

Table 6.2 Variations of lamellar thickness and breadth of distribution with isothermal annealing time at 220oC. PC-28K samples have been initially crystallized at 185^{o}C for 95 hours.

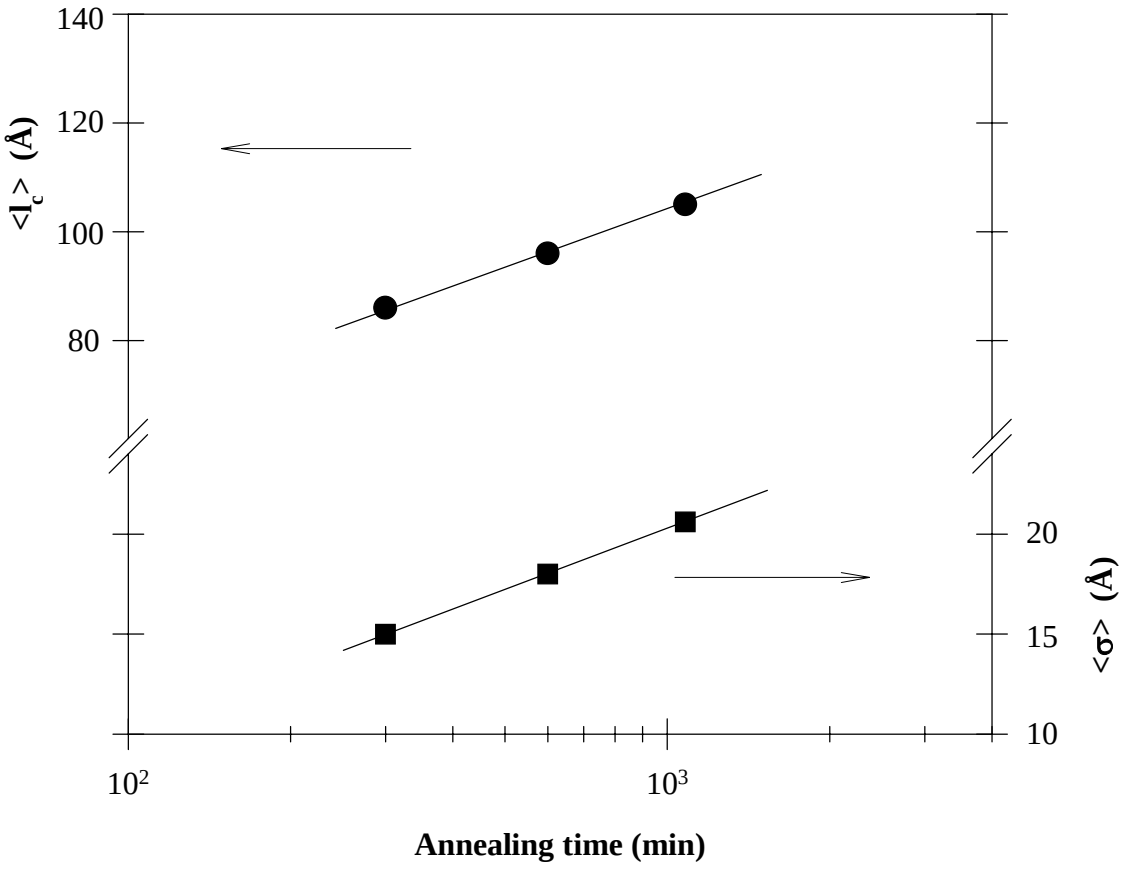

Figure 6.11 Variation of lamellar thickness (circle) and the breadth of distribution measured by standard deviation (square) as a function of the logarithm of isothermal annealing time.

(120±20 μm) were used for calorimetry experiments, while thin solvent cast films (~1 μm) were employed for AFM. Although it is widely accepted that the lamellar thickness depends only on the degree of undercooling[32,33] (i.e., $\ell \sim 1/\Delta T$, where $\Delta T = T_m^o - T_x$) for a given molar mass sample, there could be some effects from sample thickness. To compare a bulk and thin film crystallization, the effects of film thickness on crystallization behavior must be resolved. These issues will be further addressed in the discussion section.

To investigate this question properly, an attempt was made to measure the melting temperature of solvent cast thin film on glass substrate using an optical microscope equipped with a heating stage and a photodiode detector. The films were prepared following the same procedures used in the AFM sample preparation. After crystallization at 185°C for 95 hours (as-crystallized) and subsequent annealing at 220°C for 5 and 18 hours, samples were melted at 10°C/min in the heating stage. The temperature scale of the heating stage was properly calibrated by the onset melting temperature of indium standard. The polarized light intensity was monitored during the heating scan by a photo diode detector connected to a light intensity analyzer. Further details on the set up of this equipment were described in the experimental section of Chapter 3.

Figure 6.12 (a) and (b) show, respectively, the raw data and the first derivative of raw data to define the melting peak positions of as-crystallized and annealed samples. Unambiguously, in Figure 6.12, melting point systematically increases upon isothermal annealing. More importantly, the measured melting temperature of as-crystallized thin film (266°C) is considerably higher than that of thick bulk sample (228.5±0.4°C) crystallized under the same condition. This will be further discussed later.

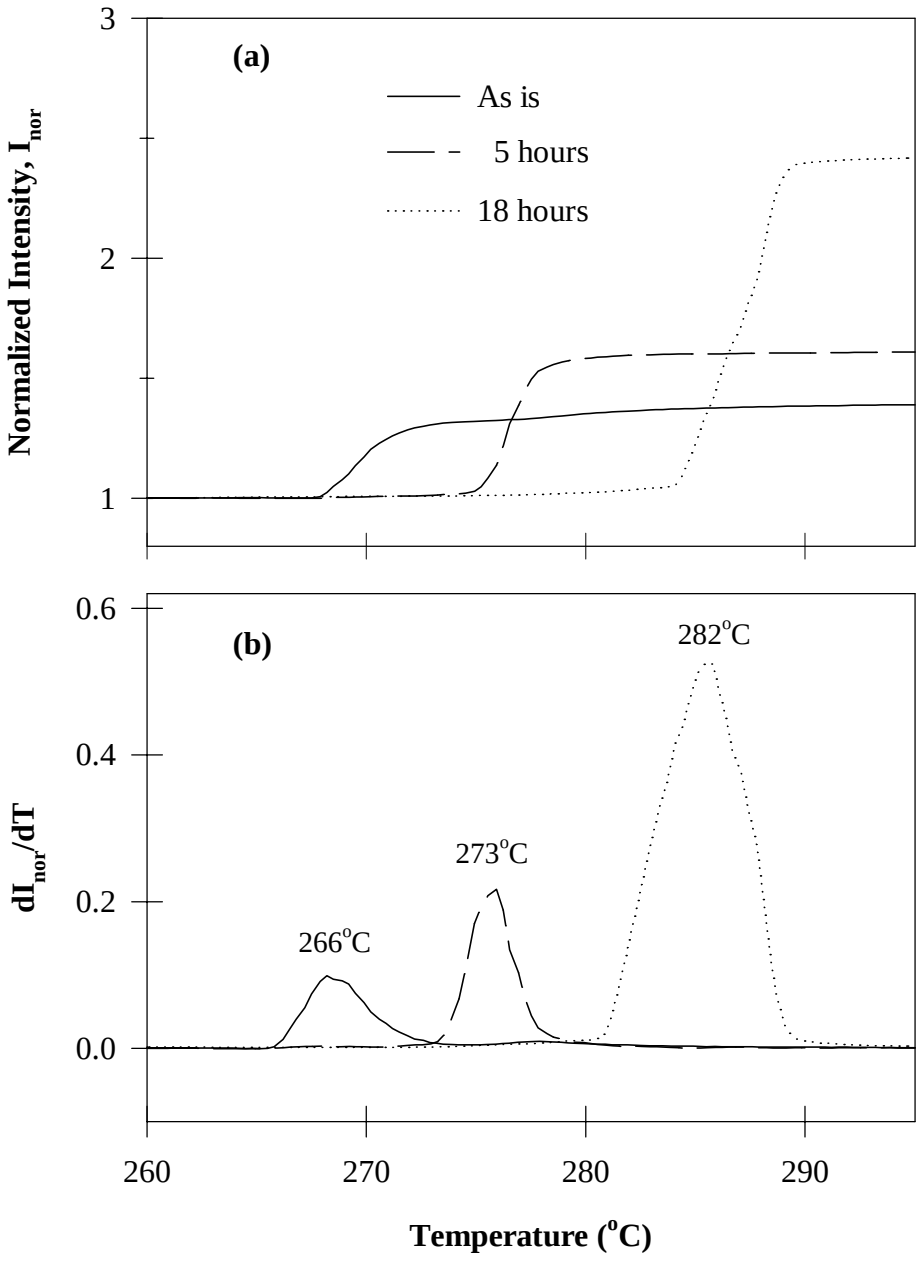

Figure 6.12 Variation of normalized light intensity during heating scan at heating rate of 10°C/min (a), and the first derivative of normalized intensity with respect to temperature, dI_{nor}/dT, to determine the peak melting temperature (b). Temperature scale has been calibrated form the onset melting temperature of In standard.

Based on the data from these two different techniques– melting temperature from the optical microscope with photo intensity detector and lamellar thickness from AFM–, a Gibbs-Thomson plot was constructed. The result is shown in Figure 6.13, in which available literature data were also included[13]. From the intercept and the slope of this plot, T_m^o and σ_e have been calculated as 597K and 52 mJ/m^2, respectively. These values are comparable to the previously reported data[13,34].

6.4 Discussion

6.4.1 *Isothermal Lamellar Thickening from DSC*

From the kinetic study of the low endotherm in the previous chapter, one of the key characteristics is that $B(T_x)$, the rate of the shift of the low endotherm melting point with time, *decreases* with increasing temperature (see Figure 5.11). In contrast, one can clearly deduce from Figures 6.6 and 6.7 that the high endotherm shows the opposite behavior, i.e., the slope– defined from either the shift of the melting temperature with time (Figure 6.6) or the shift of the heat of fusion with time (Figure 6.7)– *increases* with temperature. The inset lines in Figures 6.6 and 6.7 schematically represent the change of the slope with annealing temperature. This comparison supports the conclusion drawn in Chapters 4 and 5 that the evolution of the high and the low endotherm are quite different, possibly because these endotherms are associated with different morphological entities.

An isothermal annealing at or above 208^{o}C leads to the melting of a significant portion of preexisting crystals. Obviously, more materials is partially melted by a higher temperature annealing, and this can be readily seen in Figure 6.7, in which at 208^{o}C the heat of fusion of initial stage (1 min) is *ca*. 17.5 J.g^{-1}, while the heat of fusion decreases to 5 J.g^{-1} by 223^{o}C, after 1 min annealing. These two conditions– annealing above the

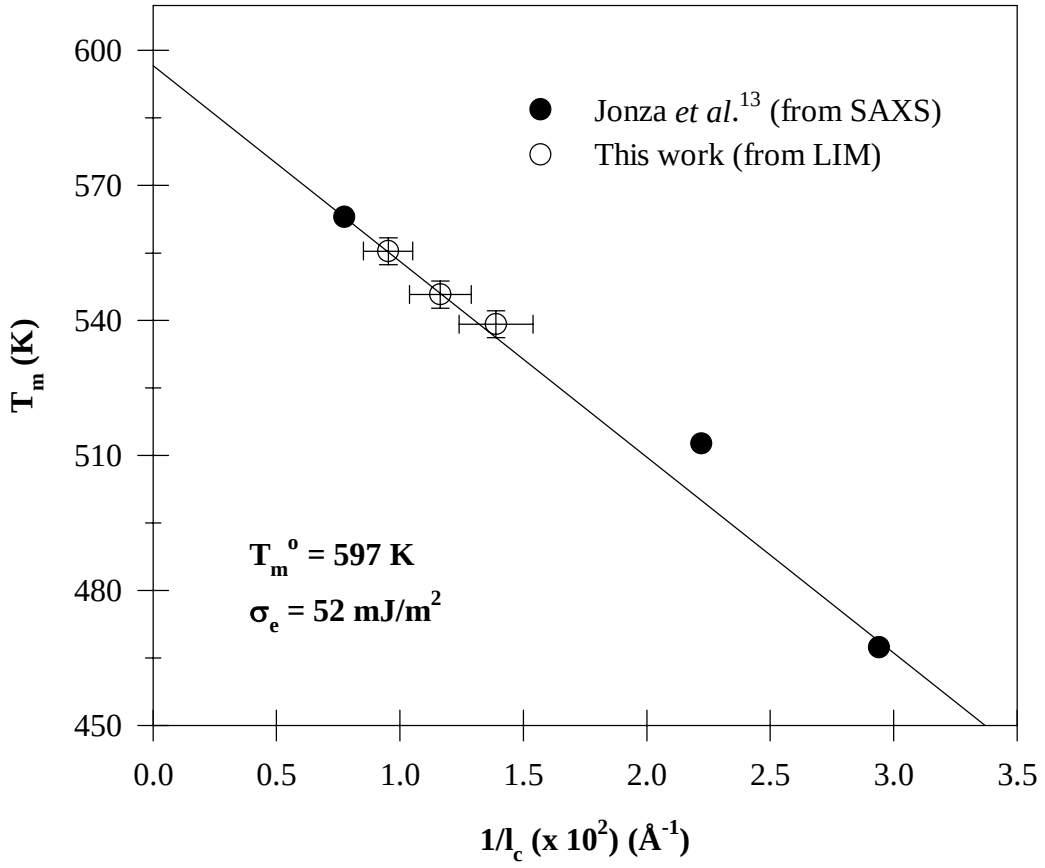

Figure 6.13 A plot of T_m *vs* inverse lamellar thickness (A Gibbs-Thomson plot). LIM stands for light intensity measurement using optical microscope. For detailed experimental conditions, see the text.

primary crystallization temperature and the presence of enough crystallizable materials created by partial melting– will drive lamellar thickening as well as recrystallization during isothermal annealing. These recrystallized lamellae will have higher melting temperatures than as-crystallized lamellae because of the higher recrystallization temperature. Overall, these two processes may both be at play for the melting endotherm broadening and shifting as seen in Figures 6.3 to 6.5.

At this moment, we can not distinguish these two processes. This is not an easy issue to address since it requires the knowledge of the kinetics of recrystallization in the presence of preexisting crystals. Nonetheless, qualitatively speaking, recrystallization alone cannot explain the results shown in Figures 6.3 to 6.5. If only recrystallization had occurred, then the endotherm would have two peaks, or at least a shoulder at higher temperature. A close examination of Figures 6.3 to 6.5 reveals that although the endotherm becomes broader, in all cases, the endotherms are single peaked. Other support comes from the observation that in Figure 6.5, the initial small and lower melting temperature endotherm *per se* has grown into a large endotherm whose melting temperature range virtually does not overlap with that of initial endotherm. Once again, if only recrystallization occurred during isothermal annealing, then the melting endotherm should not shift with annealing time. These observations strongly suggest that under high temperature isothermal annealing, lamellar thickening must occur possibly with recrystallization.

Peak broadening and peak temperature shifting as observed in Figures 6.3 to 6.5 are most likely related to α_c relaxation, the increase of chain mobility inside the crystal. However, the suggested α_c relaxation temperature around 210^{o}C (i.e., T_m – 10 ~ 20^{o}C) is

in good contrast to that in LPE, in which α_c relaxation occurs around 60°C (i.e., T_m – 60 ~ 80°C)[8-10]. As briefly explained in the introduction section, because $T\alpha_c$ is too close to the apparent melting temperature, the observation of the relaxation phenomenon using solid state NMR or dynamic mechanical analysis would not be easy, especially in the case of semi-flexible polymers. This narrow temperature window for α_c relaxation must be a direct consequence of rigid chain backbone of PC, which hinders chain mobility inside the crystal until the temperature approaches the near apparent melting temperature. A similar observation has been made for PEEK ($T_m \approx 340$°C, $T\alpha_c \approx 325$°C) by Marand *et al*[35].

From Figure 6.6, we can define the rate of the shift of the high endotherm at each temperature for short times (< 20min). This data can be combined with the data shown in Figure 5.24, and they are plotted together in Figure 6.14. Under the assumption that lamellar crystals do not show significant superheating, the rate of the shift of high endotherm also approaches to zero at very similar temperature, in the vicinity of 210°C in case of PC-28K.

Since *negative* $B(T_x)$, either for low or high endotherm, does not have any physical meaning, this temperature may be a crossover temperature for the existence of secondary crystals. One possible explanation for this phenomenon is that, as noted earlier, at this crossover temperature, α_c relaxation and isothermal lamellar thickening of PC may occur.

6.4.2 *Epitaxial Growth and Lamellar Thickness Measurement*

The selection of calcite as a substrate for epitaxial growth was entirely based on the matching of unit cell parameters on the cleavage plane (014) of host (calcite) and the

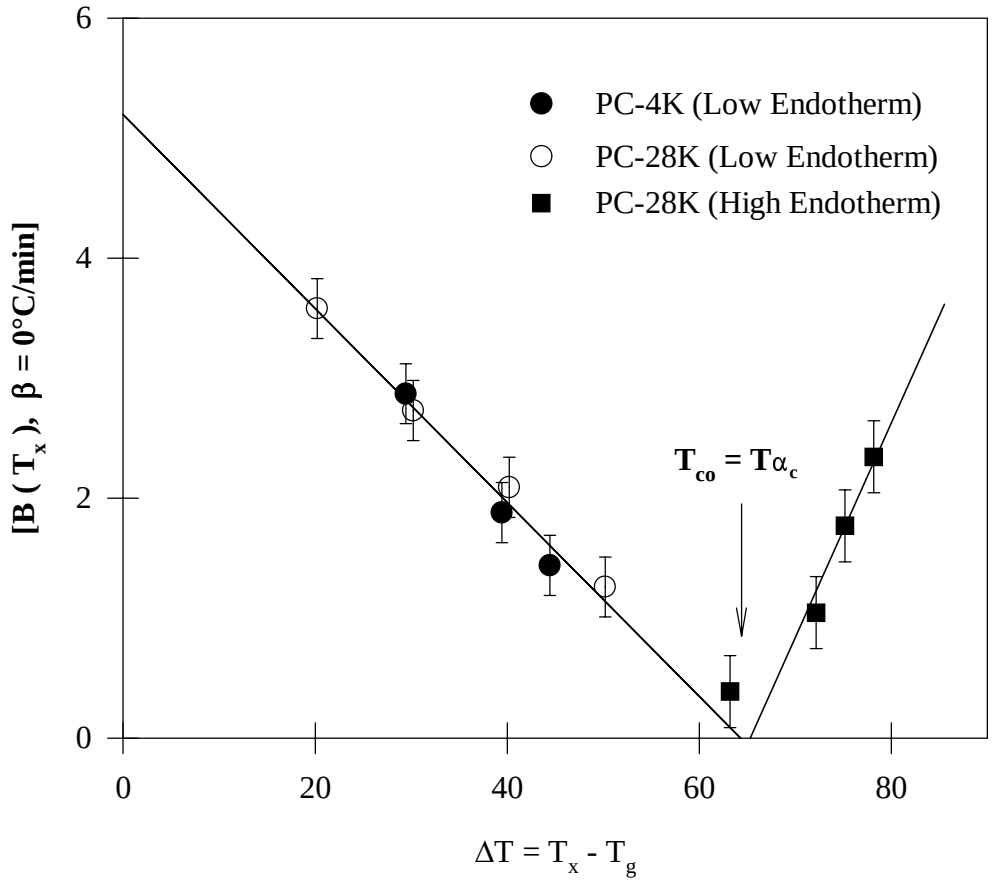

Figure 6.14 Variation of the rate of the shift of the low endotherm at zero heating rate as a function of ΔT (= T_x-T_g) for two extreme molar mass samples of PC used in this study . The arrow points the possible location of α_c-relaxation temperature in PC ($T\alpha_c$). For comparison reason, B(T_x) for high endotherm is included from the isothermal annealing experiments.
(for detail, see the text and also see Figure 5.24 in Chapter 5).

guest (PC). One caution, however, must be taken into account. The plane (014) is not the only cleavage plane. Three planes, considering the hexagonal crystal system of calcite, have been suggested as cleavage planes, i.e., (001), (011) and (014), although some authors claimed that (014) plane is the most feasible plane[28]. Because of this multiple choice of cleavage planes, even after a clean cleavage, macroscopically, the surface will be polycrystalline, containing the mixtures of all these possible cleavage planes. This will produce different orientations of pseudo-epitaxy as well as non-epitaxy, although "locally" PC may epitaxially crystallize on a proper cleavage plane, (014). For instance in Micrographs 6.1 and 6.5, the left lower diagonal shows pseudo-epitaxy, yet lower diagonal shows a change of orientation plane and also a weak tendency for the epitaxy.

Another reason for forming a pseudo-epitaxy of PC on calcite could be that, in this study, the epitaxy appears to be of a multi-layer nature rather than monolayer. The film thickness is *ca*. 1μm, and the lateral dimension of lamellae in PC crystallized at 185^{o}C seldom exceeds 200nm, so each epitaxial region in micrographs shows at least 5 or more layers of vertical stacks of lamellae, i.e., multi-layer epitaxy. Logically, the very first layer upon the substrate will have a perfect epitaxy and the next layer may be close but with some degree of misfit. Very likely, the third or higher layers will be subjected to more misfits, such as lamellar tilting in vertical and/or parallel direction.

Fortunately, this pseudo-epitaxy nature of PC on calcite, however, may not seriously affect the reliability of lamellar thickness measurement for two reasons. First, lamellar thickness is not affected by the presence of lamellar tilting in a parallel direction since it is widely accepted that lamellar thickness depends only on the inverse of the

degree of undercooling (i.e., $\ell \sim 1/\Delta T$, where $\Delta T = T_m^o - T_x$) for a given molar mass sample[32,33]. Second, the correction factor for the tilting in the vertical direction of lamellae is proportional to $\cos\theta$, where θ is the tilted angle. Based on simple calculation, even under the severe assumption of a 20^o tilting angle, the error is about 6%, so the vertical tilting, if any, will not seriously affect the results.

6.4.3 *Various Issues in the Construction of the Gibbs-Thomson Plot*

To combine the calorimetric and AFM results for the construction of Gibbs-Thomson plots, it is assumed that the melting point of AFM samples at the given annealing time is the same as that of the sample prepared for DSC experiments under the same condition. In the present study, this has been found not to be the case (see Figure 6.12). The main reason could be the difference in sample preparation methods: for calorimetry, the samples were bulk-crystallized with thickness of 120 ±20μm, yet for AFM, very thin solvent cast films (~1 μm) were used. From the measurement of thin film melting temperature, it has been shown that the melting temperature difference in these two sets of samples is not trivial: over 35^oC difference (T_m of thin film (266^oC) vs T_m of bulk crystallized sample (228 ± 0.4^oC).

Although this phenomenon is not completely understood, it appears that it must be associated with the sample thickness. The effect of film thickness on melting temperature, however, is not an easy question to address, because as film thickness approaches the size of a micron, the number of methods to measure the melting temperature of this thin film on top of a substrate is very limited. This could be the main reason why several morphology studies of PC using solvent cast film did not report the melting temperature[36-39]. Despite the experimental difficulty, logically speaking, the

glass transition temperature of a thin film could be lower than that of bulk. Siegmann and Geil claimed from the crystallization study of PC solvent cast film that the thinness of the film (up to 1μm) lowers the T_g thereby increasing chain mobility[39]. They explained this in terms of the free volume concept that surface will act as a source of excess free volume, therefore as surface to volume ratio increases, the overall free volume increases, thus T_g decreases[39].

At this moment, one may argue that there could also be a solvent effect since thin film must be prepared from the solvent. To address this question properly, the following experiment was conducted. First, a thin film was cast on the known mass of glass substrate following the same procedures used for the previous study, and subsequently the mass of sample (i.e., the total mass comes from the three contributions: glass, polymer and solvent) was measured. After complete drying of this sample at 150^{o}C *in vacuuo* for 24 hours, the sample mass was measured again. The difference in mass must be ascribed to the solvent mass removed upon drying. From the known volume and concentration of polymer on the glass substrate, the trapped solvent amount was calculated as being equal to *ca*. 0.23%. Assuming the trapped solvent depresses the glass transition temperature following a Gordon-Taylor type equation, the calculated T_g depression was less than 2^{o}C. Note that at the drying stage no crystallization was detected. This experiment clearly shows that the effect of solvent, if any, is insignificant and cannot be the main reason explaining the observed significant melting temperature difference between the bulk crystallized sample and thin film.

In Figure 6.13, for the construction of Gibb-Thomson plot, lamellar thickness and peak melting temperature were determined respectively, from AFM and optical

microscope equipped with a heating stage and a photo detector. Note that for AFM samples, a calcite substrate was utilized, while clean glass was used for the samples for optical microscopy. The reason is that the films on calcite substrate were so thin and completely transparent, even after long time crystallization, that the light intensity change upon the melting could not be detected. On the other hand, the film crystallized on a glass substrate, although thin, it formed spherulitic structures. Therefore, the light intensity can be accurately monitored during melting (see Figure 6.12). The justification of these experiments is also based on the well-known observation that the lamellar thickness depends only on the inverse of the degree of undercooling[32,33]. This seems to be a logical assumption since the measured lamellar thickness and the peak melting point are in good accordance with the reported Gibbs-Thomson plot. This, however, does not completely rule out the possibility that there could be some substrate effects on the melting temperature. To address this question properly, a fundamental study of the effect of various substrates producing different morphologies will be necessary.

The combination of the results of T_m^{high} from optical microscopy with actual lamellar thickness from AFM has led to the construction of a Gibbs-Thomson plot (Figure 6.13), in which available literature data were also included[13]. As far as the author knows, very few reports of Gibbs-Thomson plots exist in the case of PC[13,34]. Jonza and Porter[13] constructed a Gibbs-Thomson plot with three data points measured from calorimetry and small angle X-ray methods, and they concluded that T_m^o is 608K and σ_e, 70mJ/m^2. On the other hand, Legras and Mercier[34] reported that T_m^o is equal to 591K and σ_e, 94mJ/m^2 from the spherulite growth rate study of plasticized PC. The results from this study (T_m^o = 597K and σ_e = 52 mJ/m^2) seem to be comparable.

In general T_m^o can be determined either by Gibbs-Thomson equation or by a non-linear Hoffman-Weeks extrapolation[32,33], in the latter case if the polymer can be crystallized in a broad temperature range. Good examples are it-PP[33] and PEO[40]. Unfortunately, one cannot apply non-linear Hoffman-Weeks extrapolation method to PC for this purpose, since the temperature window for crystallization of PC is extremely narrow[29,41,42], thus in practice, extrapolation will be subjected to a large uncertainty. From this point of view, the Gibbs-Thomson plot will be the most appropriate method to determine T_m^o of PC.

6.5 Conclusions

In this chapter to test the hypothesis of two different mechanisms of secondary crystallization above and below T_{co}, two independent isothermal annealing experiments were performed. First, from the calorimetry study, it was observed that an increase in isothermal annealing time for a given temperature above 208^{o}C leads to an increase in peak melting temperature along with peak broadening, suggesting the presence of isothermal lamellar thickening. Second, from the direct lamellar thickness measurement using AFM, it was found a clear trend of lamellar thickness increase upon isothermal annealing performed under the same conditions as in the calorimetry study.

A Gibbs-Thomson plot was constructed from lamellar thickness and corresponding melting temperature measured by various techniques, and in this plot, T_m^o and σ_e were calculated as 597K and 52 mJ/m^2, respectively.

References

1. A. J. Kovacs, A. Gonthier, *Kolloid Z.*, **1972**, *250*, 530.
2. S. Z. D. Cheng, A. Zhang, J. Chen, D. P. Heberer, *J. Polym Sci., Part B*, **1991**, *29*, 287.
3. J. Enns, R. Simha, *J. Macromol. Sci. Phys.*, **1977**, *B13*, 11
4. D. C. Bassett, D. Patel, *Polymer*, **1994**, *35*, 1512
5. J. Rault, *J. Macromol. Sci, Rev. Macromol. Chem. Phys*., **1997**, *C37*, 335.
6. B. Wunderlich, Macromolecular Physics, **1976**, Ch. 7, Academic Press, New York.
7. P. J. Phillips, G. J. Rensch, *J. Polym Sci., Part B*, **1989**, *27*, 155.
8. C. L. Gruner, B. Wunderlich, R. C. Bopp, *J. Polym. Sci*., A-2, **1969**, *7*, 2099.
9. C.D. V. Rees, D. C. Bassett, *Natur*e, **1968**, *219*, 368.
10. D. V. Rees, D. C. Bassett, *J. Polym Sci., Part B*, **1969**, *7*, 273.
11. I. C. Sanchez, J. P. Colson, R. K. Eby, *J. Appl. Phys*., **1973**, *44*, 4332
12. I. C. Sanchez, A. Peterlin, R. K. Eby, F. L. McCrackin, *J. Appl. Phys*., **1974**, *45*, 4216.
13. J. M. Jonza, R. S. Porter, *J. Polym. Sci. Polym. Phys*., **1986**, *24*, 2459.
14. G. Mendez, A. J. Müller, *J. Thermal Analysis*, **1997**, *50*, 593
15. W. G. Hu, C. Boeffel, K. Schmidt-Rohr, *Macromolecules*, **1999**, *32*, 1611.
16. W. G. Hu, K. Schmidt-Rohr, *Acta Polym*., **1999**, *50*, 271.
17. K. Schmidt-Rohr, H. W. Spiess, Multidimensional Solid State NMR and Polymers, **1994**, Academic Press.
18. P. Tormala, *J. Macromol. Sci. Rev. Macromol. Chem*., **1970**, *C17*, 297
19. R. Boyer, *J. Macromol. Sci. Phys*., **1973**, *B8*, 503
20. I. Bonev, *Acta Crystallogr*., Section A , **1972**, *28*, 508.
21. J. Williems, *Naturwissenschaften*, **1955**, *42*, 176
22. E. W. Fischer, *Kolloid-Z.*, **1958**, *159*, 108
23. K. K. Seth, C. J. E. Kempster, *J. Polym. Sci., Polym. Symp*. **1977**, *58*, 297.
24. T. Takahashi, M. Inamura, I. Tsujimoto, *J. Polymer Sci., Polym. Lett. Ed*., **1970**, *8*, 651; T. Takahashi, F. Teraoka, I. Tsujimoto, *J. Macromolec. Sci. Phys*., **1977**, *B12(3)*, 303.
25. D. W. Pashley, *Adv. Phys*., **1965**, 14, 327.

26. J. C. Wittmann, B. Lotz, *Prog. Polym. Sci*., **1990**, 15, 909.
27. H. Zhou, G. L. Wilkes, *Polymer*, **1997**, *38*, 5735.
28. L. Addadi, S. Weiner, *Proc. Natl. Acad. Sci*. U.S.A. **1985**, *82*, 4110; L. Addadi, J. Moradian, E. Shay, N. G. Maroudas, S. Weiner, *Proc. Natl. Acad. Sci*. U.S.A. **1987**, *84*, 2732.
29. G. Kämpf, *Kolloid. Z.*, **1961**, *172*, 51
30. D. C. Bassett, D. Patel, *Polymer*, **1994**, *35*, 635.
31. P. J. Phillips, G. J. Rensch, *J. Polym. Sci. Polym. Phys*., **1989**, *27*, 155.
32. H. Marand, J. Xu, S. Srinivas, *Macromolecules*, **1998**, *31*, 8219.
33. J. Xu, S. Srinivas, H. Marand, P. Agarwal, *Macromolecules*, **1998**, *31*, 8230.
34. R. Legras, J. P. Mercier, *J. Polym. Sci. Polym. Phys*., **1979**, *17*, 1171.
35. H. Marand, A. Alizadeh, Manuscript in preparation.
36. R. E. J. Fryer, *J. Appl. Polym. Sci*., **1974**, *18*, 2261. A. Prietzschk, Kolloid. Z., 1959, 156, 8.
37. B. J. MacNulty, *Polymer*, **1968**, *9*, 41. R. Bonart, Makromol. Chemie, 1966, 92, 149.
38. H. R. Harron, R. G. Pritchard, B. C. Cope, D. T. Goddard, *J. Polym. Sci. Polym. Phys*., **1996**, *34*, 173.
39. A. Siegmann, P. H. Geil, *J. Macromol. Sci. Phys*., **1970**, *B4(2)*, 239; A. Siegmann, P. H. Geil, *J. Macromol. Sci. Phys*., **1970**, *B4(2)*, 273.
40. H. Marand, J. Xu, Manuscript in preparation.
41. F. Galez, R. Legras, J. P. Mercier, *Polym. Engr. Sci*., **1976**, *16*, 276.
42. H. Schnell, in “Chemistry and Physics of Polycarbonates”, **1964**, Interscience, N. Y.

Chapter 7

The Evolution of Rigid Amorphous Fraction and Its Correlation with the Glass Transition Behavior of Semicrystalline PC

7.1 Introduction

One of the important conclusions from the kinetics study of secondary crystallization in Chapter 5 is that the rate of the shift of the low endotherm with time, $B(T_x)$ is due, at least partly, to the reduction of the conformational entropy of the remaining amorphous phase. The observation that $B(T_x)$ decreases with the increase in secondary crystallization temperature may support this conclusion (see Chapter 5). If the above hypothesis is true, then the increase of T_g or T_g broadening during the secondary crystallization may be explained in the context of the increase of constraints imposed by bundle-like crystals. Indeed, Marand *et al*. observed almost linear relationship between the temporal evolution of T_g and $B(T_x)$ in case of PEEK, it-PS, PET; furthermore, they provided thermodynamical considerations explaining this observation[1].

In correlating the evolution of T_g with $B(T_x)$, the implicit assumption is that $B(T_x)$ is, at least qualitatively, related to the level of constraints imposed by bundle-like crystals. In this chapter the rigid amorphous fraction (RAF) is used as an alternative way of evaluating the level of constraints, and the correlation between RAF and glass transition behavior will be presented. The key assumption behind the use of the RAF as an index for the level of constraints is that the *RAF developed during crystallization is proportional to the level of constraints*. Detailed descriptions of the rigid amorphous phase (RAP) and calculations of the RAF are offered in Chapter 2.

Originally, Wunderlich *et al*.[2-4] introduced the concept of *rigid amorphous fraction* (RAF), which is defined as the fraction of amorphous phase that *does not* contribute to T_g at the normal glass transition temperature, to explain the experimental inconsistency between the measured crystallinity (X_c) and rigid fraction (f_r) (see below).

$$f_r = 1 - \Delta C_p^{sc}/\Delta C_p^{am} = f_{raf} + X_c \qquad [7.1]$$

Where f_r is *rigid fraction* representing the fraction of chain molecules that does not contribute to the heat capacity increase at normal T_g. ΔC_p^{SC} and ΔC_p^{amor} stand for the heat capacity increase at T_g in the semicrystalline and completely amorphous polymer, respectively. Equation (7.1) can be used for the quantitative determination of the RAF from the calorimetry study. Further, if X_c is known, then the difference between f_r and X_c would be the fraction of rigid amorphous phase (f_{raf}).

At this moment a caution must be taken to ensure that the level of crystallinity is determined as accurately as possible for the proper evaluation of f_{raf}. In many cases, the crystallinity is expressed as the ratio of measured value to that of 100% crystalline phase. For instance, crystallinity from the calorimetry study is often expressed as follows.

$$X_c = \Delta H_m^{exp}/\Delta H_m^{o} \qquad [7.2]$$

Where ΔH_m^{exp} and ΔH_m^{o} are the experimental and 100% crystalline phase heat of fusion, respectively. At least two corrections need to be considered for a proper use of equation (7.2). First, ΔH_m^{o} represents the enthalpy of fusion of a perfect crystal at *the equilibrium*

melting temperature, T_m^o. However, semicrystalline polymers usually melt at a lower temperature than T_m^o; therefore, ΔH_m^{exp} needs to be corrected for temperature effect. Second, ΔH_m^o assumes the infinitely large perfect crystal, yet in reality, polymer crystals are limited in size, thus the surface enthalpic contribution should be taken into account. The latter issue becomes even more critical when one considers samples that contain a significant fraction of small secondary crystals.

In this chapter, the crystallinity of all the data presented was properly corrected considering the above two effects, and based on this more accurate crystallinity, rigid amorphous fraction was evaluated. In the following experimental section, the detail procedures for these two corrections will be offered.

7.2 Experimental

In chapters 4 to 6, calorimetry studies were conducted on PC samples crystallized under various conditions, such as different 1) molar mass, 2) secondary crystallization temperature and time, and 3) isothermal annealing temperature and time. In this Chapter, approximately 200 DSC melting traces of previous experiments were analyzed, and in each DSC curve, the rigid fraction (f_r) and the experimental heat of fusion (ΔH_m^{exp}) were determined. The rigid fraction (f_r) was calculated using equation (7.1). The heat capacity changes at T_g in the amorphous state (i.e., ΔC_p^{am} in equation 7.1) for fractions and commercial PC-28K samples are presented in Figure 3.9. ΔH_m^{exp} was properly corrected to evaluate more accurate crystallinity (see below). Glass transition temperature, the heat capacity changes at T_g, and the breadth of T_g were measured following the method described by Cheng *et al*[5]. T_g was determined at the inflection point of the ΔC_p increase. T_g broadening (ΔT_g) was measured by the temperature difference in the intercepts of the

tangential line at T_g with the heat capacity lines of liquid (T_2) and glass (T_1) (i.e., $\Delta T_g = T_2 - T_1$). Detailed descriptions of these parameters are offered in Chapter 3, along with an illustration. Other experimental conditions, such as sample preparation, DSC measurements, and temperature scale calibration, were described in Chapter 2.

7.2.1 *Temperature Correction for the Experimental Heat of Fusion*

Temperature correction for the experimental heat of fusion was done using the following thermodynamic considerations. The enthalpy of fusion, ΔH_m^* at a temperature T_m will be given by:

$$H_m^*(T_m) = H_m^0(T_m^0) + \int_{T_m}^{T_m^0} C_p'(T)\, dT \qquad [7.3]$$

$$\Delta C_p'(T) = C_p^L(T) - C_p^S(T) \qquad [7.4]$$

Where $\Delta C_p'(T)$ is the difference between the heat capacities of the solid and liquid polymers at temperature T. The temperature dependencies of heat capacities of bisphenol-A polycarbonate in both liquid and glassy states are available experimentally. In addition, Wunderlich *et al*. in the ATHAS databank[6] provided the temperature dependence of the heat capacity of PC in the *crystalline state* based on theoretical considerations. In this study, a value of 608K has been used for the equilibrium melting temperature of PC[7]. Figure 7.1 shows a universal calibration curve used for the temperature correction of the experimental heat of fusion in PC. Note that PC-6K (fraction) and PC-28K (commercial), which represent two extreme molar masses used for the analysis, fall on the same line. The experimental heat of fusion in each DSC curve has been temperature corrected using the calibration factor given in Figure 7.1. After a

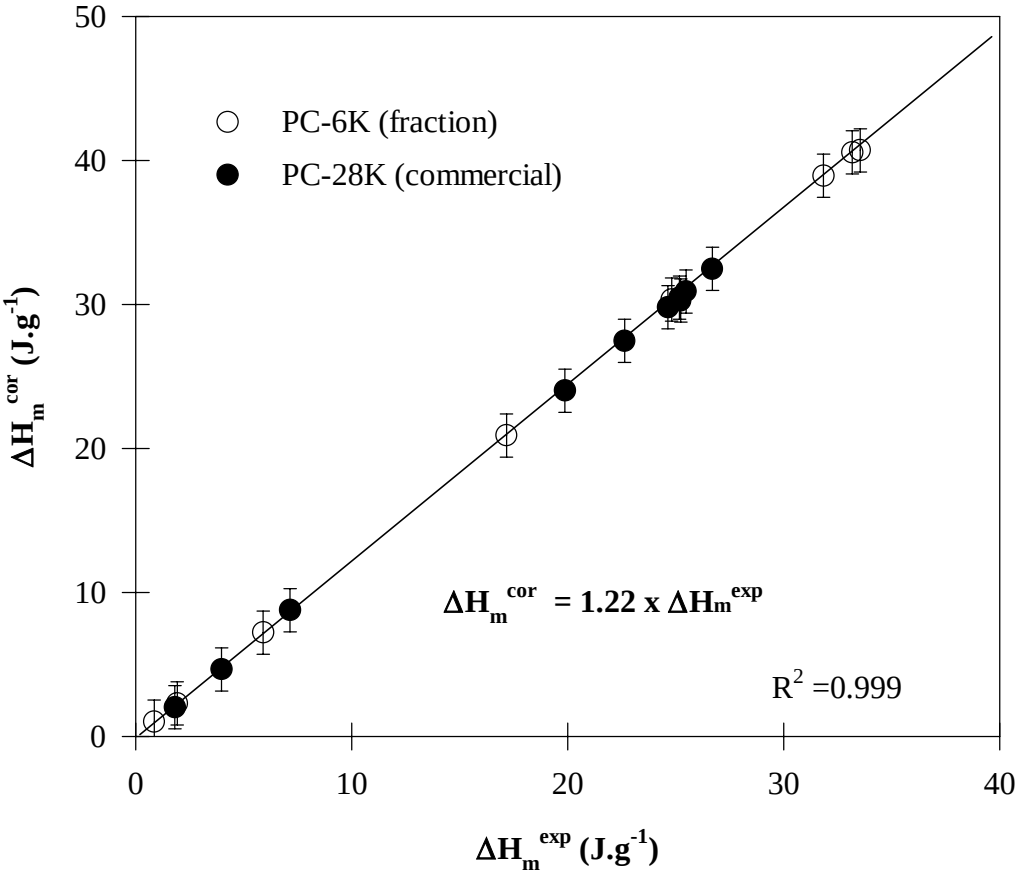

Figure 7.1 A temperature correction curve for the experimental heat of fusion of PC samples used in this study. Note that temperature corrected heat of fusion (ΔH_m^{cor}) is about 20% higher than the experimental heat of fusion (ΔH_m^{exp}).

proper temperature correction, ΔH_m^{exp} increased about 20%.

7.2.2 *Surface Enthalpic Contribution for the Equilibrium Heat of Fusion*

As noted earlier, the existence of small secondary crystals may decrease the equilibrium heat of fusion of as-crystallized samples due to a significant surface enthalpic contribution. To properly evaluate this correction, wide angle x-ray scattering (WAXS) experiments were performed on as-crystallized and partially melted PC-19K samples. From each DSC melting trace, an the experimental heats of fusion is obtained. In Figure 7.2, ΔH_m^{total} of PC-19K samples (before and after partial melting) is plotted as a function of X_{WAXS}* (crystallinity from WAXS experiments) for different crystallization times. In this plot, crystallinity from the density measurement
was also included. Note that in Figure 7.2, the heat of fusion in each line has been temperature corrected, and as-crystallized PC-19K and PC-28K fall on the same line within experimental uncertainty. One important observation in this figure is that as-

---

* The degree of crystallinity of a semicrystalline sample can be estimated from the experimental scattering profile by using the following equation:

$$X_{waxs} = I_c/(I_c + I_a)$$

where X_{WAXS} is the degree of crystallinity from WAXS, and I_c and I_a represent the integrated intensities of the crystalline and the amorphous phases, respectively. In this method, it is assumed that the total scattering within a certain region of the reciprocal space is independent of the state of segregation of polymer. The integrated intensities I_a and I_c are usually obtained by curve fitting the experimental scattering curve. For this, the scattering profiles of a 100% crystalline and a 100% amorphous specimen are prerequisites. An obvious assumption of this method is that the scattering profile of a 100% amorphous (glassy or liquid-like) specimen and that of the amorphous phase in the semicrystalline sample are proportional. This same argument is applicable to the crystalline phase, but we are deliberately discussing the amorphous phase, since in many semicrystalline polymers, such as PE, the scattering profile of the 100% amorphous specimen is not available at the same temperature as that of the semicrystalline sample. In other polymers, the scattering profile of the 100% amorphous sample, although available, is significantly different from the corresponding profile of the amorphous phase in the semicrystalline sample. Fortunately, in PC, it is easy to obtain completely amorphous films at room temperature and also due to the low levels of crystallinity (<0.30) in this material, it has been found that the amorphous-scattering profiles in the semicrystalline and 100% amorphous samples are very similar.

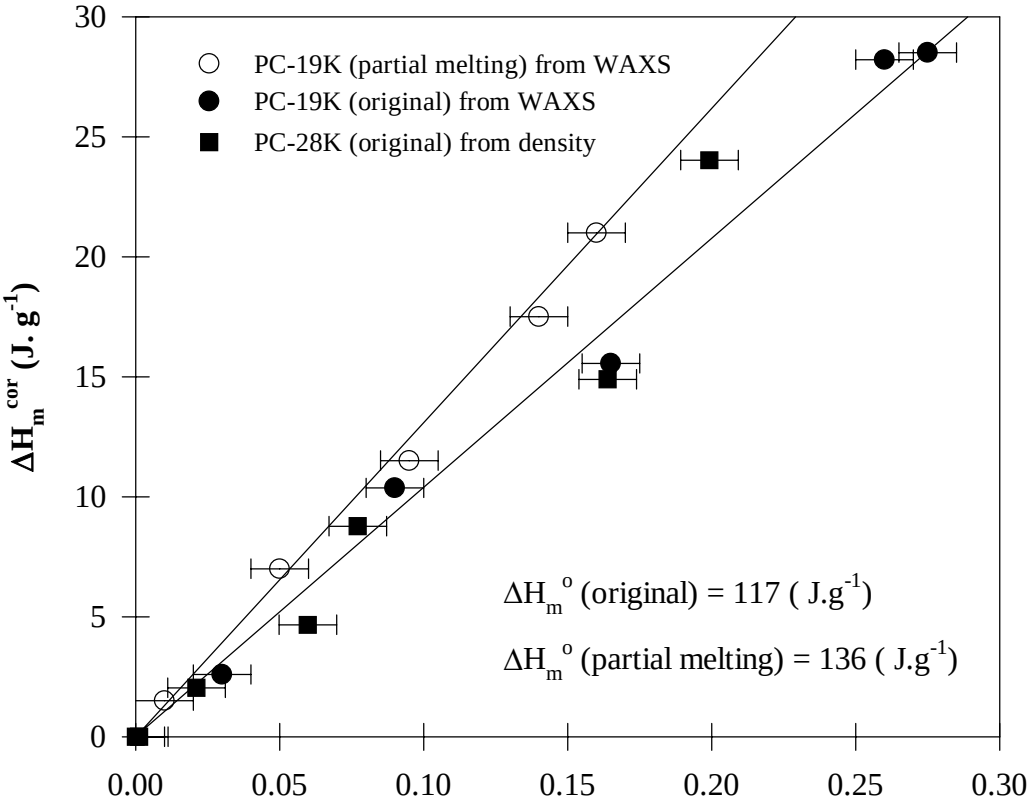

Figure 7.2 Correction for the equilibrium heat of fusion considering the surface enthalpic contribution.

crystallized and partially melted samples appear to fall onto two distinguishable lines. As-crystallized samples (i.e., containing both small secondary crystals and lamellar type crystals) follow the lower line, whereas partially melted samples (i.e., containing only lamellar type crystals) fall on the upper line. These results are consistent with the notion that the existence of small crystals will give rise to the decrease of the equilibrium heat of fusion due to a significant surface enthalpic contribution. Therefore, these two different values of the equilibrium heat of fusion was used for the calculation of crystallinity from the calorimetry study (see equation (7.2)). For instance, the upper value (136 J/g) was used for isothermally annealed samples, which exhibit the high endotherm only, and for samples possessing both the low and high endotherms, the lower value (117 J/g) was applied.

7.3 Results

Before presenting the results, we need to specify the sample nomenclature used in the following figures. All the samples were designated as (PC-XX, t_x, YY, T_x). PC-XX stands for the molar mass of PC samples; t_x, for the time of primary crystallization; YY, for the method of thermal treatment; and T_x, for the temperature of given thermal treatment. YY could be SC (secondary crystallization), IA (isothermal annealing), BC (bulk crystallization), and CL (cooling). For example (PC-28K, t_x = 202h, SC, 165^{o}C) means PC-28K sample initially crystallized at 185^{o}C for 202 hours, partially melted at 220^{o}C, and subsequently exposed to the secondary crystallization at 165^{o}C for various times. Note that primary crystallization and partial melting temperatures are slightly varied for different molar mass samples (see Table 5.1).

In Figure 7.3 the evolution of rigid fraction (f_r) as a function of corrected

crystallinity is presented. One immediate observation is that regardless of molar mass and various thermal treatment conditions, all the data fall on the same line within the limit of uncertainty. More importantly, f_r is always greater than X_c, being approximately, $f_r \approx 2X_c$. According to equation (7.1), this result indicates that rigid amorphous fraction (RAF) increases almost linearly with crystallinity; furthermore, as can be expected, the RAF becomes negligible when crystallinity approaches zero value. Another interesting observation is that clearly low molar mass sample exhibits higher level of RAF, with higher level of crystallinity.

In Figures 7.4 and 7.5, respectively, normalized T_g broadening and T_g variation as a function of RAF are shown. $[\Delta T_g]_{normalized}$ was defined as $[T_2\text{-}T_1]_{sc}/[T_2\text{-}T_1]_{am}$, in which sc and am stand for semicrystalline and amorphous phase, respectively. T_g variation was also normalized in a similar way as $[T_g]_{normalized} = [T_g^{sc}\text{-}T_g^{am}]/T_g^{am} \times 100$. Largely speaking, these two plots show a similar trend: an increase of RAF leads to the increase of T_g and T_g broadening.

7.4 Discussion

As seen in Figure 7.3, the inequality between f_r and X_c is a clear deviation from the two-phase model. In the context of the two-phase model, f_r should be the same as X_c, because this model strictly assumes two phases: amorphous (mobile) and crystalline (rigid).

Within experimental uncertainty, the observation of $f_r \approx 2X_c$ may suggest the upper limit of apparent maximum crystallinity achievable *from the bulk crystallization* of PC. Because, hypothetically, when f_r reaches 1, the corresponding crystallinity would be 0.5, and obviously, f_r can not be bigger than 1; therefore, $X_c = 0.5$ would be the upper

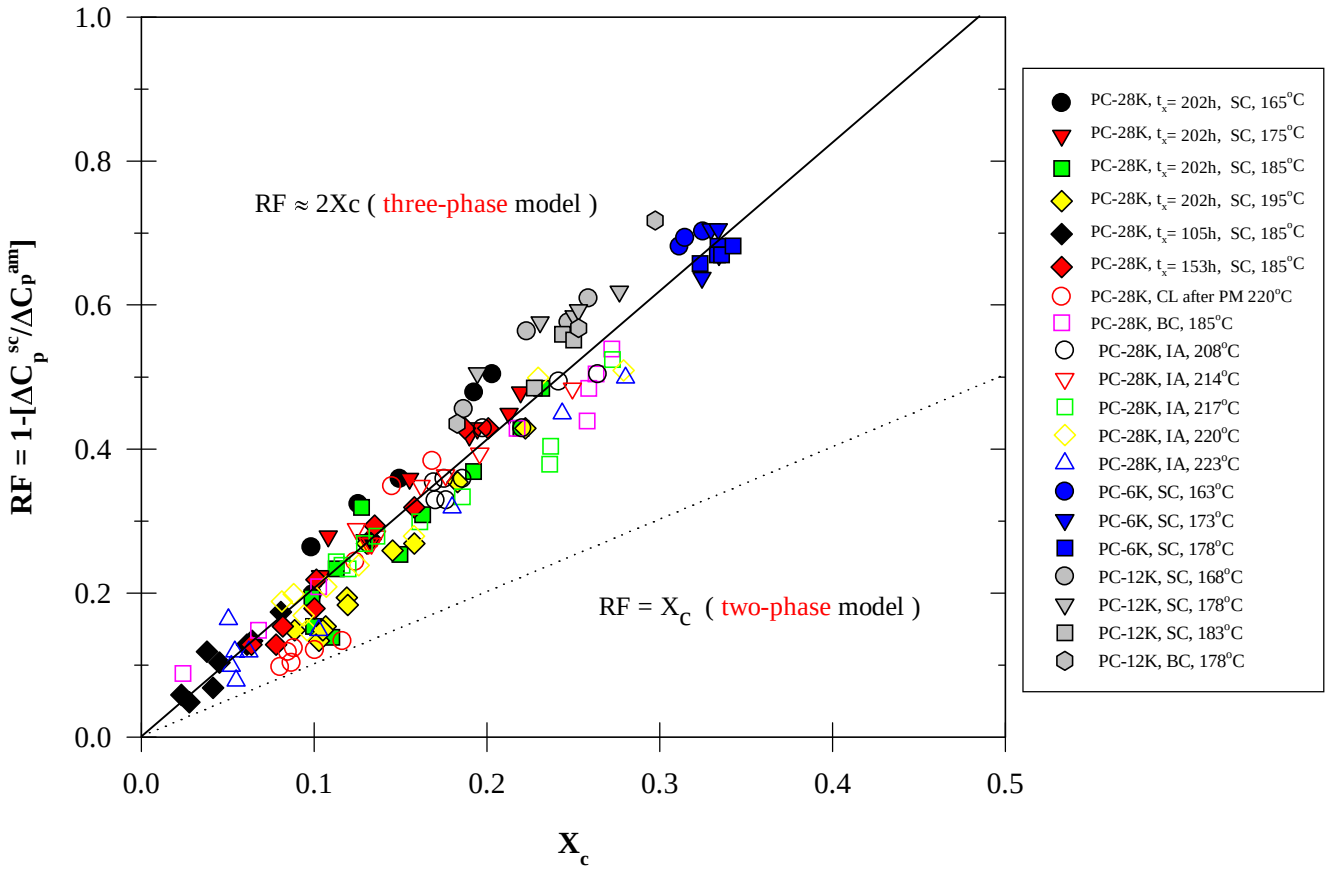

Figure 7.3 The evolution of rigid fraction (RF) as a function of crystallinity for PC samples thermally treated under various conditions. Note that crystallinity has been both temperature and surface enthalpic contribution corrected (see the text). The accuracy of the determination of RF was better than 0.03

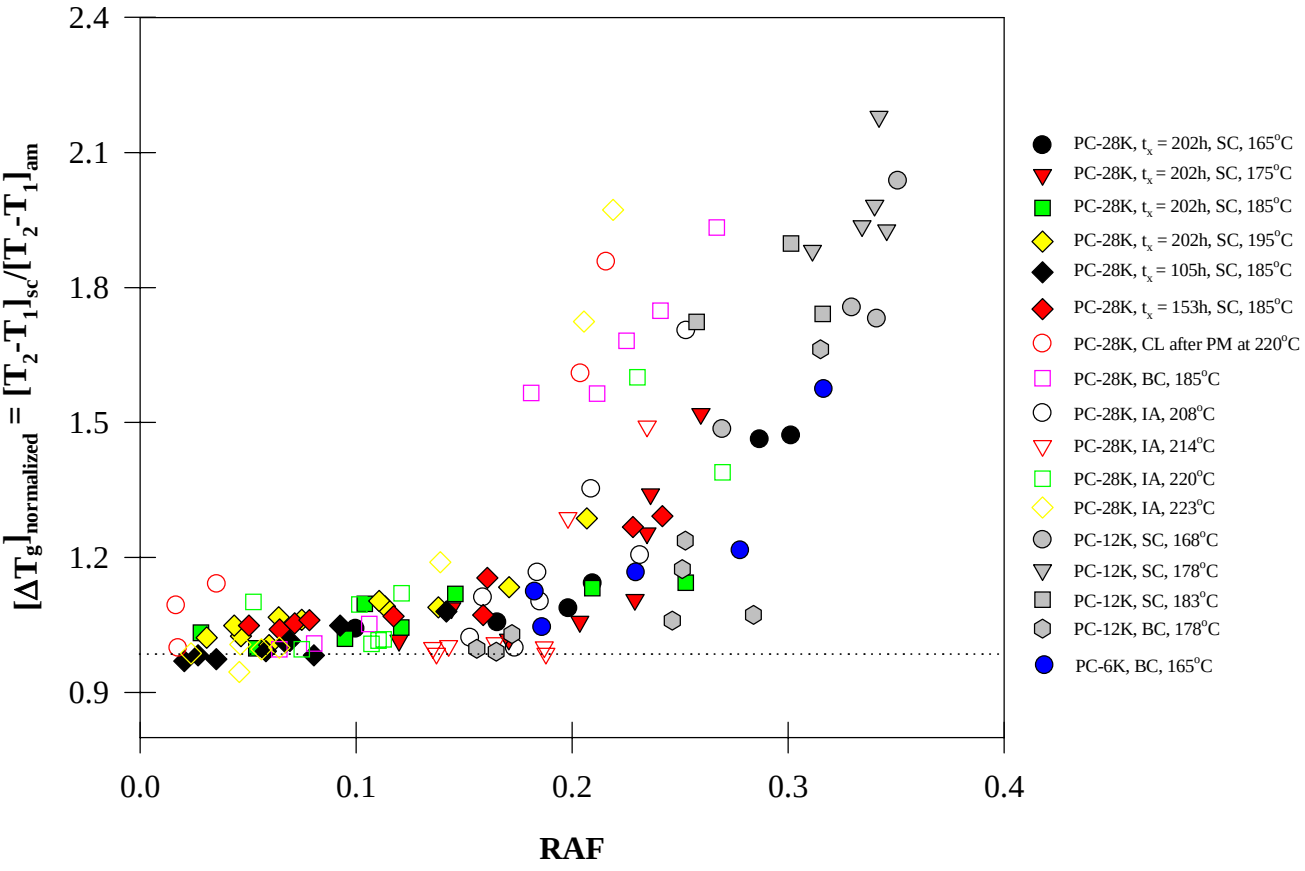

Figure 7.4 T_g broadening as a function of RAF of PC samples under various thermal treatments. The accuracy of $[\Delta T_g]_{normalized}$ determination was better than ±5%.

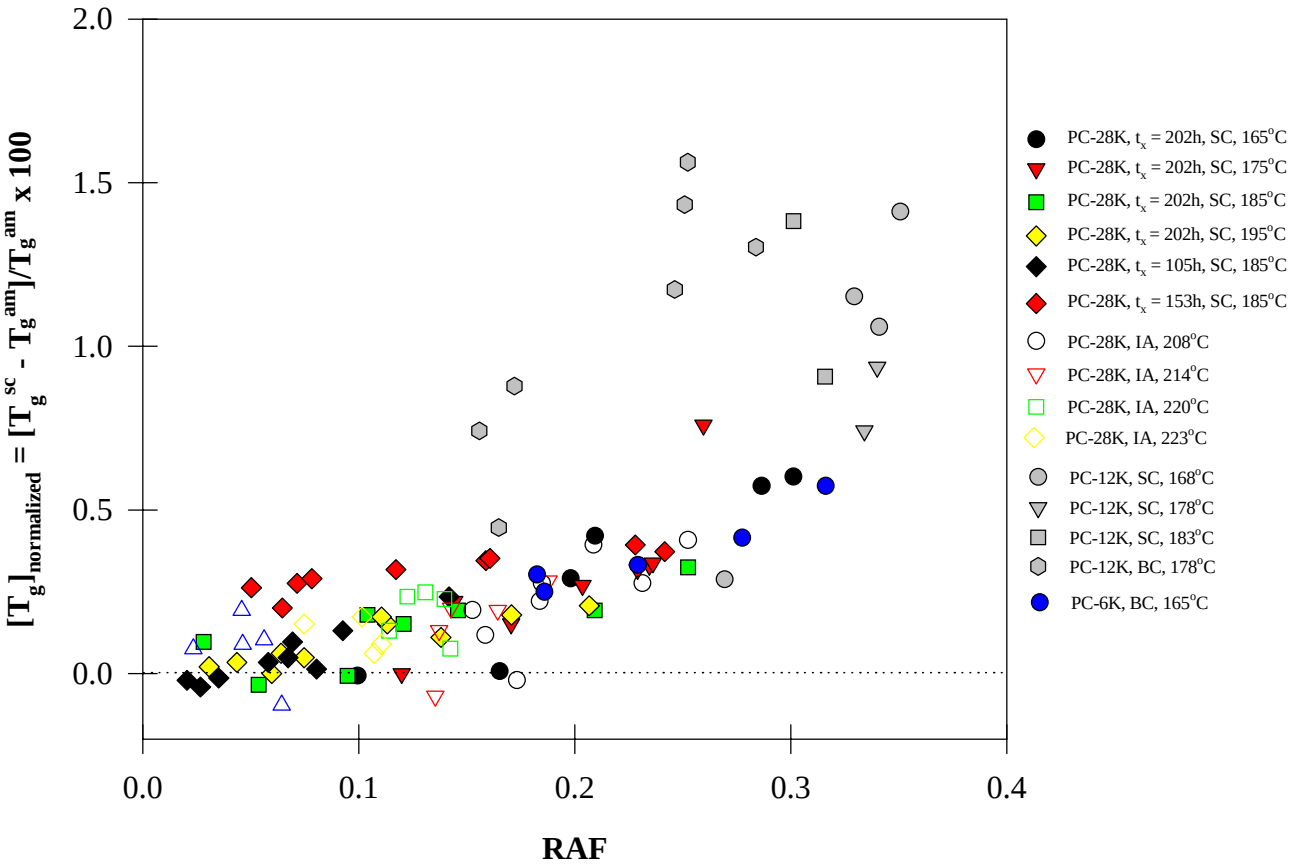

Figure 7.5 Normalized T_g increase as a function of RAF for PC samples under various thermal treatments. The accuracy of the T_g determination was better than 0.3°C

boundary. It is well known that when PC (M_w = *ca*. 30,000 to 67,000 g/mol) crystallizes from the bulk, the kinetics of crystallization are extremely slow and the maximum degree of crystallinity seldom exceeds 0.3[7-13]. In the present study, even from the isothermal annealing experiments (see the data labeled as IA in Figure 7.3), the maximum crystallinity does not exceed 0.28, being the highest value among all the PC-28K samples crystallized under various conditions. Furthermore, as depicted in Chapter 5, in the case of low molar mass fractions, the rate of primary crystallization kinetics was increased more than 100 times compared with that of PC-28K, yet surprisingly, the final level of crystallinity was always less than 0.37. According to the literature, higher crystallinity PC is only available when other methods of crystallization are employed, such as crystallization in the presence of nucleating agent and/or plasticizer[14,15]. In general, the slow crystallization kinetics and limited crystallizability of PC have been explained in terms of chain rigidity[10,16,17]. The above observation in Figure 7.3 may suggest a more specific result of chain rigidity: *rigid chain may generate the higher level of RAF (i.e., more constraints) and this will further hinder the growth of crystals*.

In this figure, it is also observed that the lower molar mass sample exhibits a higher degree of RAF. Cebe *et al*. reported a similar result from the study of cold-crystallized PPS[18]. They explained the observation in such a way that the lower molar mass sample has a greater number of taut tie molecules between the crystals resulting in a large fraction of constrained amorphous phase[18]. For PC, this could be because of the increased crystallinity of low molar mass fractions due to the increased mobility. To strictly compare RAF in different samples, the crystallinity in the samples should be the

same; however, due to the relatively fast crystallization kinetics and higher degree of crystallinity in lower molar mass PC, this condition could not be achieved.

The increase of T_g and T_g breadth with the increase of RAF in Figures 7.4 and 7.5 can be expected. The level of constraints may increase during crystallization, which leads to the increase of both the level of RAF and the degree of T_g broadening, including T_g *per se*. Of more interest, however, is that T_g increase or broadening significantly occurs only above a certain level of RAF, seemingly close to the value of 0.2. Because the data are much less scattered below this value, this upturn point can be relatively well defined. Based on the assumption that the location of the RAF could be between the lamellar crystals, possibly near the crystal/amorphous interphase, we propose a possible explanation to this observation. Before the RAF reaches this critical value, the thickness of amorphous layer is large enough not to be affected by the presence of RAF (insignificant change in T_g and T_g broadening). However, as the RAF further increases, more constrained mobile amorphous will show a retarded relaxation leading to the significant increase of T_g and T_g broadening. At this later stage, due to the large scattering, no other specific information such as the effects of molar mass and crystallization temperature could be obtained; however, qualitatively speaking, T_g and T_g broadening increase dramatically at this stage, indicating the existence of considerable constraints.

7.5 Conclusions

From the quantitative analysis of RAF in varying molar mass PC samples crystallized under various conditions, the following conclusions are drawn. Regardless of molar mass and thermal treatment conditions, semicrystalline PC exhibits a rigid

fraction (f_r) that is always greater than the corrected crystallinity (X_c). This observation strongly suggests the evolution of the rigid amorphous phase upon bulk crystallization of PC. Quantitatively, the degree of the RAF increases almost linearly with crystallinity in the range of 0 to 0.4, and the lower molar mass samples show a higher degree of RAF compared with higher molar mass samples. T_g and T_g broadening increase with the evolution of RAF, and, of more interest, it seems that there exists a critical level of RAF that initiates the significant changes in T_g and T_g broadening.

References

1. H. Marand, A. Alizadeh, in preparation.
2. J. Grebowicz, S. F. Lau, B. Wunderlich, *J. Polym. Sci.:Polym. Symp.*, **1984**, *71*, 19.
3. S. F. Lau, B. Wunderlich, *J. Polym Sci. Polym. Phys*., **1984**, *22*, 379.
4. H. Suzuki, J. Grebowicz, B. Wunderlich, *Macromol. Chem*., **1985**, *186*, 1109.
5. S. Z. D. Cheng, M. Y. Cao, B. Wunderlich, *Macromolecules*, **1986**, *19*, 1868.
6. ATHAS data Bank: http://funnelweb.utcc.utk.edu/~athas/databank/intro.html (*The heat capacity data of semicrystalline PC has been listed since 02/01/00*).
7. J. M. Jonza, R. S. Porter, *J. Polym. Sci. Polym. Phys*., **1986**, *24*, 2459.
8. E. Turska, W. Przygocki, M. Maslowski, *J. Polym Sci. Part C*, **1968**, *16*, 3373.
9. E. Laredo, M. Grimau, A. Muller, A. Bello, N. Suarez, *J. Polym. Sci. Polym. Phys*., **1996**, *34*, 2863.
10. G. Mendez, A. J. Müller, *J. Thermal Analysis*, **1997**, *50*, 593.
11. B. Falkai, W. Rellensmann, *Makromolekular Chem*., **1964**, *75*, 112.
12. G. E. Wissler, B. Crist. Jr, *J. Polym Sci., Polym.Phys*., **1980**, *18*, 1257.
13. Giuseppe V. Di Filippo, Maria E. Gonzalez, Maria T. Gasiba, A.V. Müller, *J. Appl. Polym. Sci*., **1987**, *34*, 1959.
14. C. Bailly, *M.* Daumerie, R. Legras, J. P. Mercier, *J. Polym. Sci. Polym. Phys.*, **1985**, *23*, 343; C. Bailly, R. Legras, J. P. Mercier, *J. Polym. Sci. Polym. Phys*., **1985**, *23*, 355; C. Bailly, M. Daumerie, R. Legras, J. P. Mercier, *J. Polym. Sci. Polym. Phys*., **1985**, *23*, 493.
15. R. Legras, C. Bailly, M. Daumerie, J. M. Dekoninck, J. P. Mercier, V. Zichy, E. Nield, *Polymer*, **1984**, *25*, 835.
16. Hermann Schnell, Chemistry and Physics of Polycarbonates, **1964**, John Wiley & Sons, Inc.
17. G. Kämpf, *Kolloid-Zeitschrift*, **1960**, *172*, 50.
18. S. X. Lu, P. Cebe, M. Capel, *Macromolecules*, **1997**, *30*, 6243.

Chapter 8

Summary

Crystallization and melting behavior of varying molar mass bisphenol-A polycarbonate (PC) samples were investigated using differential scanning calorimeter (DSC) for the monitoring of thermal behavior, and atomic force microscope (AFM) for the morphology study. The following is a summary of conclusions from the results of the investigations.

The glass transition temperature (T_g) of PC is strongly affected by molar mass and molar mass distribution. In the molar mass range between *ca*. 4,300 and 55,000 g.mol^{-1}, the variation of T_g is more than 25^{o}C, and near monodisperse samples show slightly lower T_gs than commercial samples. In addition, amorphous density of PC is determined as being equal to 1.1977±0.0002 g/cc.

Studies of the heating rate dependence of the melting behavior of PC indicate that the high and low endothermic regions are associated with the melting of primary (chain folded lamellae) and secondary crystals (bundle-like or fringed micellar type crystals), respectively. No reorganization effects during heating are observed for PC-19K and PC-28K in the usual range of heating rate ($\beta \geq 2.5^o$C/min). In contrast, the lower molar mass material, PC-4K, exhibits a melting-recrystallization-remelting process during heating. This reorganization process, however, affects only the shape of the high endothermic region. The observed upward shift of the low endotherm with increasing heating rate is explained by superheating effects and is fully consistent with the notion that amorphous chains in the vicinity of secondary crystals are conformationally constrained.

The primary crystallization kinetics of PC shows a strong dependence on molar mass. In the molar mass ranging between 4,300 and 28,000 $g.mol^{-1}$, low molar mass fraction crystallizes faster, and overall crystallization rates differ by more than a factor of 100. We also observed a significant influence of molar mass distribution on the overall crystallization kinetics.

In contrast, the kinetics of secondary crystallization of PC is essentially molar mass independent. Regardless of molar mass distribution, initial stages of crystallization, primary or secondary crystallization temperature, and partial melting temperature, the kinetics of the low endotherm depicts two universal behaviors: Low endotherm melting temperature, T_m^{low}, increases linearly with the logarithm of crystallization time, and at the early stage, the Avrami exponent in the logarithm of the heat of fusion associated with the low endotherm, $\log[\Delta H_m^{low}]$, as a function of the logarithm of crystallization time is 0.5. The rate of shift of the low endotherm with time, $B(T_x)$, was found to decrease with temperature, and this could be ascribed, at least partly, to a decrease of the conformational entropy upon secondary crystallization. From the heating rate correction of $B(T_x)$, we showed that there exists a crossover temperature below which both the low- and the high endotherm are present, and above which only the high endotherm is expected to be stable. It is suggested that this crossover temperature could be related to the α_c relaxation temperature in PC.

The existence of isothermal lamellar thickening in PC has been examined by two independent methods. First, from the calorimetry study, it was observed that an increase in isothermal annealing time for a given temperature above 208^oC leads to peak melting temperature increase along with peak broadening, suggesting the presence of isothermal

lamellar thickening. Second, from direct lamellar thickness measurement using AFM, a clear trend of lamellar thickness increase upon isothermal annealing performed at 220^{o}C in the time range of 5 to 18 hours was shown.

A Gibbs-Thomson plot could be constructed from lamellar thickness and corresponding melting temperature measured by various techniques. From this plot, the equilibrium melting temperature (T_m^o) and interfacial surface free energy (σ_e) of PC were determined as 597K and 52 mJ/m^2, respectively.

From the analysis of rigid fraction using corrected crystallinity, it was found that, regardless of molar mass and thermal treatment conditions, semicrystalline PC always exhibits rigid fraction larger than the corrected crystallinity. This observation strongly suggests the evolution of rigid amorphous phase upon bulk crystallization of PC. Quantitatively, the degree of rigid amorphous fraction (RAF) increases almost linearly with crystallinity in the range of 0 to 0.4. The lower molar mass samples show a higher degree of RAF compared with higher molar mass samples. T_g and T_g broadening increase with the evolution of RAF, and of more interest, it seems that there exists a critical level of RAF needed to initiate the significant changes in T_g and T_g broadening.

Future Work

Based on the results, the discussion, and the conclusions drawn from this study, the following suggestions for future work can be made:

On the effect of film thickness on crystallization

From the bulk-crystallization of some PC fractions (PC-4K, 6K, 8K, 12K, 17K) and two commercials (PC-19K and PC-28K), it was consistently shown that, regardless of the primary crystallization temperatures between 155^{o}C to 210^{o}C, the peak melting temperatures of the high endotherms of these samples are in the range of 220^{o}C to 230^{o}C. In contrast, the peak melting temperature of thin film of PC crystallized under similar conditions was significantly higher than that of the bulk-crystallized samples. We proposed that this might be due to the film thickness effect; however, at present, the exact reason could not be found. To resolve this issue, we need to crystallize several samples with different but precisely controlled thickness under the same conditions and measure the melting temperatures of those samples. These experiments may provide the information of film thickness effect on crystallization.

On the two regimes of isothermal crystallization

At the end of Chapter 5, from the heating rate studies of the rate of the shift of the low endotherm, it was found that there exists a crossover temperature, below which both the low and the high endotherm are present, and above which only the high endotherm is expected to be stable. In conjunction with this, in Chapter 6, the presence of isothermal lamellar thickening above this critical temperature was investigated using DSC and AFM, and it was suggested that this temperature is related to isothermal lamellar thickening. To provide further evidence for this hypothesis, small angle x-ray scattering (SAXS)

experiment will be of help. For instance, the measurement of the variations of long spacing below and above this critical temperature with crystallization time will provide important information.

On the epitaxy of PC

The present study used calcite as a substrate for the epitaxial growth of PC, a choice that was purely based on the lattice parameter matching. To achieve strict conditions of epitaxy, it is necessary to know the exact chain conformation of PC molecules on calcite cleavage plane. Furthermore, this information will be crucial to find better substrates of PC epitaxy. For this, computer simulation may be required.

On the evaluation of rigid amorphous fraction (RAF)

In Chapter 7, almost 200 DSC melting traces were analyzed to calculate RAF. Although qualitatively, the data show reasonable trends with other variables such as crystallinity, T_g and T_g broadening, the scattering of data is rather large, especially at later stages of crystallization. The principal reason is that each sample was thermally treated separately under different conditions, therefore, the sample to sample variations could not be eliminated. For example, in the study of the effect of time on the secondary crystallization kinetics, the following procedures were used: sample A was thermally treated by 1) crystallization at 185^{o}C for 202 hours, 2) partial melting at 220^{o}C for 1 min, and 3) secondary crystallization at 185^{o}C for t_x. The thermal treatments for the next samples were exactly the same but with a different t_x in step 3. The scattering of data shown from Figures 7.3 to 7.6 is because of these multiple steps of thermal treatments for many different samples. To resolve this issue, it may be necessary to use temperature modulated DSC (TMDSC) with a small number of samples and perform all the thermal

treatments inside the DSC. Although in the case of PC, this will be a time-consuming experiment, the results will be far less scattered, and thus we may be able to extract quantitative information.

On the bundle-like secondary crystallization model

The experimental observations that have been made in Chapters 4, 5, and 6 are qualitatively in good accordance with a newly proposed bundle-like secondary crystallization model. This model, as already pointed in Chapter 2, however, more qualitative than quantitative. To develop a quantitative model that enables us to theoretically *predict* the size, the spatial orientation, and the exact location(s) of the secondary crystals, the following information will be necessary:

1) The exact *time-dependent* variation of the concentration and the distribution of the amorphous chains, such as chain cilia and loose loops, consisting the interlamellar amorphous layers
2) The correlation between the amount of rigid amorphous fraction (RAF) and secondary crystals in addition to the exact location of RAF
3) The possible relationship between the chain rigidity and the size or the amount of secondary crystals
4) A reliable methodology of morphology study that enables us to physically *see* the secondary crystals.

Appendix A.1

Stockmayer-Fixman Plot of Bisphenol-A Polycarbonate Fractions

One can utilize different methods such as light scattering and small angle X-ray scattering to determine the unperturbed dimension ($<R_o^2>^{1/2}$) of polymer in the melt or in θ solution. If we have fractions, as an alternative, we can adopt Stockmayer-Fixman plot method to calculate $<R_o^2>^{1/2}$. The essential concept of this method is based on the known fact that as molecular weight decreases the intrinsic viscosity also decreases, and at the limiting case when $<M_w>$ approaches zero, from the intercept, one can calculate the normalized unperturbed dimension.

$$[\eta] = K_o \cdot <M>^{1/2} + 0.51 \cdot \Phi \cdot B \cdot <M> \qquad [A.1.1]$$

Where [η] is an intrinsic viscosity, <M> is molecular weight, B is a constant and Φ is a Flory universal constant of 2.5 $x10^{21}$ dL cm^{-3} mol^{-1} or 2.5 x 10^{23} $mole^{-1}$. When both sides are divided with $M^{1/2}$, equation (A.1.1) can be reformulated as follows.

$$[\eta] \cdot <M>^{-1/2} = K_o + 0.51 \cdot \Phi \cdot B \cdot <M>^{1/2} \qquad [A.1.2]$$

Equation (A.1.2) tells us that when $[\eta][<M>^{-1/2}]$ is plotted as a function of $<M>^{1/2}$, it will give rise to a linear relationship, and from the intercept, K_o, we can calculate the unperturbed dimension (more precisely normalized unperturbed dimension with molecular weight, thus $[<R_o^2>/<M>]^{1/2}$) from the following relationship.

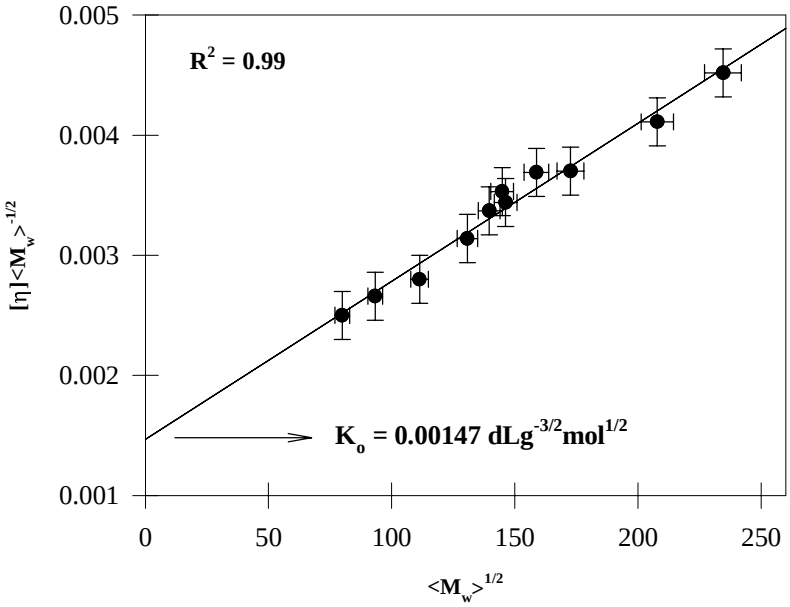

Figure A.1.1 Stockmayer-Fixman plot for the PC fractions used in this study (M_w ranges from 5,000 to 55,000 g/mol)

$$K_o = \Phi \cdot [<R_o^2>/<M>]^{3/2} \qquad [A.1.3]$$

In Figure A.1.1, the results from the analysis of PC fractions are presented. The intercept is *0.00147* dL $g^{-3/2}$ $mol^{1/2}$, which leads to the normalized unperturbed dimension, $[<R_o^2>/M]^{1/2}$ as being equal to 0.84. This value is in good agreement with the reported value, 0.93[1,2].

When the normalized unperturbed dimension is known, as a next step, the chain stiffness factor, C_∞, can be calculated.

$$C_\infty = <R_o^2>/n\ell^2 \qquad [4]$$

Where n is the number of chain backbone of length ℓ. The calculated C_∞ is 1.83, and this is close to the known value of 2.0[2].

Based on these results it can be corroborated that the measured molar masses from the GPC analysis are acceptable.

At this moment it would be informative to know the magnitude of the radius of the gyrations of PC fractions in chloroform solution at room temperature and the magnitude of the length of worm-like or Kuhn segment length of PC. The first one is in the range of 30 to 70 Å for the molar mass (M_w) between *ca*. 4,300 and 55,000 $g.mol^{-1}$. Kuhn segment for PC[3] was reported as being close to 160 Å.

References

1. A. Zang, C. Carrea, *J. Appl. Polym. Sci*., **1991**, *42*, 1965.
2. L. J. Fetters, D. J. Lohse, D. Richter, T. A. Witten, A. Zirkel, *Macromolecules*, **1994**, *27*, 4639.
3. N. Maeda, T. Norisuye, *Polymer*, **1993**, *34*, 3475.

Appendix A.2

A Brief Review of Gray's Method for Thermal Lag Correction in DSC Melting Traces

The advent of differential scanning calorimetry (DSC) has greatly facilitated an accurate and relatively convenient method of monitoring the thermal behavior of polymeric materials. One of the advantages of DSC analysis comes from the use of two separate electronic heaters for sample and reference, which is the primary difference between DSC and conventional differential thermal analysis (DTA). For an accurate measurement of temperature change during any phase change, DTA intrinsically requires higher resistance, incompatible with quick response and high resolving power; DSC does not. This advantage allows DSC to measure most accurately the heat flow with either time or temperature.

Both DSC and DTA actually measure the temperature difference between the sample and the reference, $\Delta T = T_s - T_r$, as a function of the duration of heating or temperature change. The value of ΔT is proportional to the change in enthalpy H, heat capacity C, and the total thermal resistance R to the heat flux. In both DTA and DSC, the quantity R consists of two components

$$R = R_o + R_s$$

Where R_o is the thermal resistance of the instrument appearing because of the separate arrangement of the heater and sample, and R_s is the thermal resistance determined by that of the sample itself. Largely speaking, R_s is governed by two separate factors: first, the resistance arising due to a non-ideal contact (R_{s1}) between the sample and capsule, and second, the intrinsic thermal resistance of the sample *per se* (R_{s2}). R_{s1} is strongly affected by several factors such as the shape of sample, the method of sample manipulation, and

sample mass. For example, a pre-melted metal standard, having a good electrical contact with capsule, may show an almost zero value of R_{s1}. In the case of polymeric materials, this type of "ideal" contact may not be obtainable because sometimes the aim of the study is to reveal the nature of thermal history of samples, thus pre-melting would not be allowed. Another alternative to reduce R_s is obtained by reducing the sample mass, yet sometimes this may not be desirable either, since, for instance, an accurate measurement of heat capacity change at T_g intrinsically requires higher mass of sample. Due to these reasons, the existence of R_s would be inevitable, and thus thermal lag (lagging of the sample temperature behind that of the heater) from this sample resistance needs to be corrected for the precise evaluation of temperature and peak shape. In general, this temperature correction due to thermal lag could be accomplished by using a metal standard sample sandwiched between the polymer under study. For a detailed description of this method, see Chapters 3 and 4.

Besides the necessity of temperature correction, the shape of curve also needs to be adjusted, since thermal lag not only causes temperature shifting but also invokes peak broadening. This peak broadening can be effectively corrected by Gray's method[1,2]. According to Gray[1,2], the evolution or absorption of heat by a sample per unit time, dH/dt, can be represented by the sum of the three components H_1, H_2, H_3 as schematically depicted in Figure A.2.1.

$$dH/dt = -dq/dt + (C_s - C_r)dT/dt - RC_s d^2q/dt^2 \qquad [A.2.1]$$
$$H_1 \qquad H_2 \qquad H_3$$

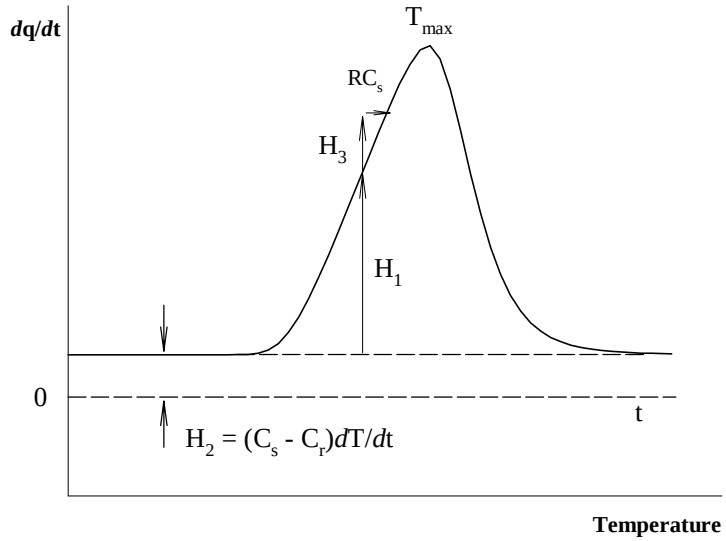

Figure A.2.1. Graphical illustration of each component in Gray's method in DSC melting traces.

Where

♦ H_1 is dq/dt, the recorded heat flux, i.e., the experimental DSC melting traces;

♦ H_2 is $(C_s-C_r)dT/dt$, the displacement of the base line from the zero level. Here C_s and C_r are the heat capacities of the sample and the reference, respectively, and dT/dt is the rate of change of temperature, such as heating rate;

♦ H_3 is $RC_s d^2q/dt^2$, the slope of the experimental curve at any point.

By finding a proper reference with a heat capacity equal or very close to that of the sample being studied, one can practically eliminate the contribution from H_2. As noted earlier, the presence of the component H_3 changes the shape of the experimental DSC melting traces. The contribution of this component is proportional to the time constant RC_s determining the resolving power of the instrument. It is impossible to eliminate component H_3; therefore, DSC melting traces require correction. This H_3 correction will be especially mandatory when a higher heating rate is used. The actual procedure is simply adding the component H_3 to the experimental melting traces using

the known value of RC_s. For instance, in the case of In standard[3], RCs is approximately 2.6s, and for polymers[4], it is in the range of 5 to 10. In case of bisphenol-A polycarbonate, from the heating rate study of In-sandwiched sample, RCs has been found to be close to 7. Figure 4.2 shows a typical example of peak broadening correction by this method. As seen, after correction, the peak width has been narrowed.

Although Gray's method is effective, it has a serious limitation. This method strictly relies on the assumption that R is a constant and does not change during heating. This is approximately valid for relatively low heating rate normally below 40^oC/min, yet above this, the onset slope of melting traces is not linear, revealing the change of R during melting. At this stage, this correction method would no longer be valid.

References

1. A. Gray, *Thermal Analysis* (4, ICTA), **1975**, Budapest: Akad, Kiado.
2. A. Gray, *Analytical Calorimetry*, **1976**, v1, New York, Plenum Press.
3. Manual of Perkin-Elmer, DSC-7 Instruction.
4. V. A. Bershtein, V. M. Egorov, *Differential Scanning Calorimetry of Polymers*, **1994**, Ellis.

Vita

Seungman Sohn was born in March 1, 1970 in Pusan, Korea. He graduated from Seoul National University with a bachelor degree in Metallurgical Engineering in 1992. He further received his Master of Science in 1994 from the same university under the guidance of Prof. Tak Kang. After spending about a year in Korea, he joined Virginia Tech in July 1995, in Materials Engineering Science program.